The Monitoring of Induction Motor Starting Transients With a View to Early Fault Detection

A thesis submitted in partial fulfilment of the requirements of the Council for National Academic Awards for the degree of Doctor of Philosophy.

STEWART ELDER
B.Sc. Honours (2:1) in Electronic and Electrical Engineering

March 13, 1992

The Robert Gordon Institute of Technology, Aberdeen in collaboration with Marathon Oil UK Ltd, Inspec and Scottish Power.

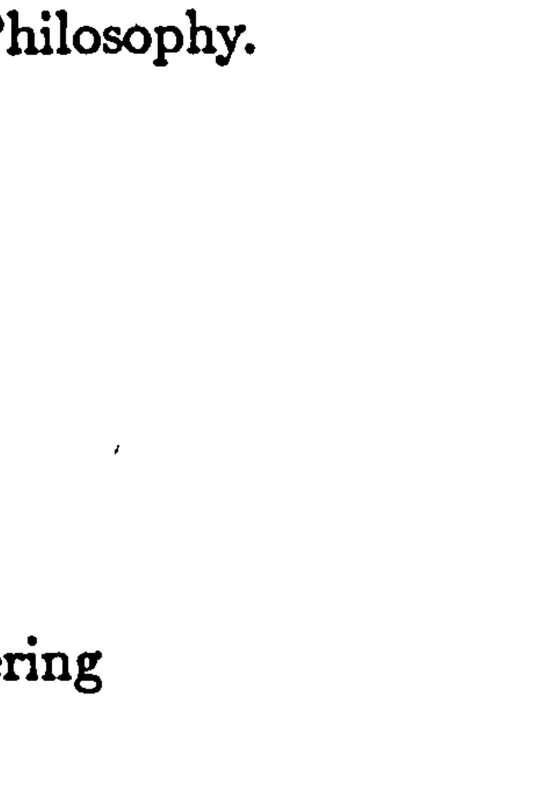

Declaration

I hereby declare that this thesis is a record of work undertaken by myself, that it has not been the subject of any previous application for a degree, and that all sources of information have been duly acknowledged.

During the course of this investigation the following courses, conferences and visits were undertaken :-

- Attended a graduate 4^{th} year level course on machine theory, RGIT.
- Presentation at the Scottish Power (formely SSEB) Research and Development Centre, East Kilbride.
- Presented a paper at the 4^{th} IEE International Conference on Electrical Machines, Savoy Place, London, Sept 1989.
- Presented a paper at the 24rd UPEC 1989 on 20-22nd September at Queen's University, Belfast.
- Attended the ICASSP conference on 23-26th May at SECC, Glasgow, 1989.
- Visit to SSEB Longannet power station May 1990.
- Three day visit to the Marathon Brae B platform, June, 1990.
- Presentation at the Technical University of Berlin, July, 1990.
- Presented a paper at the 25th UPEC 1990 on 12-14th September at RGIT, Aberdeen.

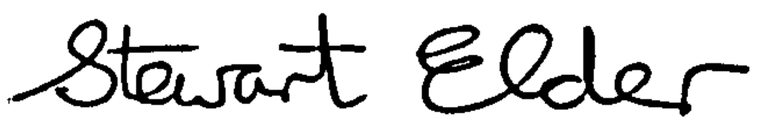

Stewart Elder

March 13, 1992

Abstract

The aim of this work is to investigate the possibility of detecting faults in a 3 phase Induction motor by monitoring and analysing the transient line current waveform during the starting period. This is a particularly onerous time for the machine and the inter-relationships between parameters such as current, torque, speed and time are very complex. As a result two parallel paths of investigation have been followed, by methods of experimentation and computer simulation.

Transient line current signals have been obtained from purpose built test rigs and these signals have been analysed in both the time and frequency domains. In order to assist with the comprehension of this data a sophisticated computer simulation of the induction motor during the starting period has also been developed. Computer simulation of the induction motor has been developed initially using the two and then three phase induction motor voltage equations which are solved by numerical integration.

Using these techniques it has been possible to detect small degrees of fault level for both wound and cage rotor machines by analysing the line current waveform during the starting period. Good agreement has been found between the real and simulated data.

A range of Digital Signal Processing techniques have been utilised to extract the components indicative of rotor faults. These techniques were at first wideband and highly numerically intensive, some originating from Speech Processing. The final processing techniques were far simpler and selected by analysis of the results from experimental data, both real and simulated.

Acknowledgements

I wish to acknowledge the following people to whom I am indebted, and without whom this project would not have been possible :

Dr. J.F. Watson, my supervisor, for his moral and academic support throughout this period of research work.

Professor W.T.Thomson and Mr. G. M. Maxwell, my second supervisors, for their advice and guidance.

Mr A.B. Dow of Scottish Power, Mr J. Hollister of Marathon Oil UK Ltd and Mr. D. Rankin of Inspec for their interest and financial support in this research project.

D. Sutherland and his staff for modifying and reconfiguring the test set on many occasions throughout the past three years.

To my Wife and Family

List of Principal Symbols

Induction Machine

s = per unit slip

f = supply frequency (Hz)

e = terminal voltage (V)

i = current (A)

I = specific phase current (A)

V = specific phase voltage (V)

$R1$ = stator resistance (Ohms)

$R2$ = rotor resistance (Ohms)

$L1$ = stator self inductance, single phase equivalent circuit (H)

$L2$ = rotor self inductance, single phase equivalent circuit (H)

$M1$ = mutual inductance, single phase equivalent circuit (H)

L = self inductance (H)

M = mutual inductance (H)

l = leakage inductance (H)

ϕ = flux linkage (Vs)

p = differential operator (d/dt)

Te = electromagnetic torque (Nm)

Tm = mechanical torque (Nm)

J = angular momentum (Kg m^2)

$\mathcal{F}_\omega$ = co-efficient of mechanical losses (Nm/rad/s)

θ = rotor electrical angle (rad)

N = turns ratio

R = number of rotor slots

B = number of broken bars

ω_r = rotational speed (rad/s)

ω_s = angular supply frequency (rad/s)

N_s = synchronous speed of supply (rpm)

N_r = speed of rotor (rpm)

n = any integer

Subscripts

a, b, c = stator phases

e, f, g = rotor phases

$d, q, 0$ = axes of two phase stationary model

$\alpha, \beta, 0$ = axes of two phase rotating model

r = rotor

s = stator

ss = stator-stator

rr = rotor-rotor

sr = stator-rotor

m = mutual, mechanical

sat = saturation

Signal Processing

t = time (s)

T = period (s)

N = number of samples

f = frequency (Hz)

n = index associated with time

k = index associated with frequency

m = sample integer

$x(n)$ = time domain sample

$X(k)$ = frequency domain sample

$y(n)$ = convolved time domain sample

$H(e^{j\omega})$ = frequency response of digital filter

$h(n)$ = co-efficients of Fourier series, Window function

$h1(n)$ = impulse response of proto-type low-pass filter

$h3(n)$ = impulse response of proto-type band-pass filter

B = normalised bandwidth

F_c = normalised centre frequency

List of Abbreviations[1]

LSB = Lower Side Band $(1-2s)f$
USB = Upper Side Band $(1+2s)f$
PSH = Principal Slot Harmonic
BBF = Broken Bar Factor
dB = deci-Bell
FIR = Finite Impulse Response (filter)
DFT = Discrete Fourier Transform
FFT = Fast Fourier Transform
IFT = Inverse Fourier Transform
STFT = Short Time Fourier Transform
AM = Amplitude Modulation
PC = Personal Computer
IBM = International Business Machines
EMF = Electro-Motive Force
MMF = Magneto-Motive Force
ADC = Analog-to-Digital-Converter

[1]Strictly, the letters of abbreviations should be separated by full stops. However, the frequent use of abbreviations with full stops can be difficult on the eye. In view of this they have been omitted from the abbreviations within this text.

Contents

Chapter 1

Introduction

The invention of the three phase induction motor is generally attributed to Nikola Tesla who demonstrated an elementary form of this machine exactly one hundred years ago. Since then many improvements to this elementary polyphase machine have been made including distributed stator windings, the cage rotor, the slip ring machine and more recently the use of variable frequency drives by utilising semi-conductor devices. The three phase induction motor is now the most common prime mover used in industry and it is generally accepted that 80% of the world's industrial a.c. motors (except fractional kilowatt machines) are plain cage rotor machines working on constant frequency supplies.

With such a reliance on this one type of machine industry finds itself heavily dependent on their availability and reliability. In view of this, considerable effort has been directed towards avoiding or predicting the sudden failure of large motors which can be very costly and potentially dangerous.

1.1 Scope of Thesis

In order to guide the reader of this thesis a brief outline of the contents of the Chapters is presented below.

Chapter 1 introduces the condition monitoring of induction motors, the development of rotor bars faults, the components indicative of rotor bar faults, application of condition monitoring, reasoning for development of starting tran-

sient monitoring and the laboratory facilities used.

Chapter 2 presents a review of the analysis of starting transient by previous researchers, highlighting aspects relevant to this work.

Chapter 3 describes early experimental work on switching transients of a single phase transformer. The spectral content of the current waveform is analysed and an attempt to model the transformers response is presented.

Chapter 4 reports on experimental work on a 3 phase induction machine with a wound rotor. Large rotor phase imbalances can be effected by means of an external resistor simulating a machine with rotor faults. Development of signal processing techniques and the selection of components indicative of the fault is described.

Chapter 5 describes the results of experimental work on a 3 phase induction machine with a cage rotor. Various degrees of faults are examined and the extraction of components indicative of the fault is further developed and simplified.

Chapter 6 reports on experimental work used to determine the induction motor's parameter values. These experimental results are used mainly for the computer model of the induction motor.

Chapter 7 presents the development of the induction motor computer simulation from the simple DQ two axis model to the full three phase model. Simulation of the faulty machine during the starting transient is undertaken and the results compared to that of the real machine.

Chapter 8 presents the conclusions of this research work and suggestions for future work.

1.2 Maintenance Schemes

Various maintenance schemes are available which aim to minimise production losses due to faults occurring and to maximise safety. Though a detailed analysis of these strategies is outwith the scope of this research work it is nevertheless of interest to consider the following four which encompass all schemes available.

- Maintain on breakdown
- Maintain at regular time intervals
- Maintain on event
- Maintain on measured condition

The first scheme has obvious disadvantages in that failure has to occur before the fault condition is dealt with. The second is common in industry with plant being shut down at periodic intervals and specific components being replaced on inspection or as a matter of course. This second strategy has the disadvantage of production loss and many components are routinely replaced whether they are in good condition or not. The third strategy is to maintain on event. For an industrial machine this may be based on the number of operations or the actual number of hours on load as opposed to the time in situ. This strategy can only be effective if a detailed knowledge of component lifetime is available. The reliability of most components is described in terms of mean time before failure (MTBF) or the mean number of operations before failure. There is of course no guarantee that a component in a critical application will not fail before the mean lifetime quoted with possible consequences for production and safety. The final strategy, often referred to as "Condition Monitoring", measures some parameter that reflects the condition of some aspect of the machine. If the change in the measured parameter suggests a developing fault then this is indicated to the operators. There are distinct advantages to this strategy in that a fault may be detected at an early stage in its development. This means the motor can be removed from service and repaired at a convenient time in order to avoid disruption to production requirements. In addition, the repair can be planned when manpower and components are available. There are however some drawbacks to the condition monitoring strategy. Firstly considerable time and effort must be directed to the identification and classification of parameters which change due to fault development. This process may take several years and may be dependent on the particular variant of the component observed. Secondly the expense of purchase, installation and commissioning of condition monitoring equipment may well exceed any possible production loss due to component failure. It may be "cost" effective to monitor a machine in a nuclear

reactor because of safety considerations whereas this may well not be the case for an identical machine in an other sector of industry.

The research work undertaken aims to develop a condition monitoring technique primarily directed at large three phase motors commonly found in offshore production platforms and power stations where production and safety are of the highest concern.

1.3 Faults within Induction Motors

A variety of faults can occur within a three phase induction motor during normal operation. Several, such as cage malfunctions, air-gap eccentricity or inter-turn insulation breakdown can result in a potentially catastrophic failure of the machine if they progress undetected [1,2,3,4].

It is of interest to consider which fault conditions are most common in industry. A comprehensive study was carried out in 1983 (by Thomson et al [5]) of offshore oil production platforms and on-shore oil production installations in which data was obtained on 84 squirrel cage induction motors (SCIM) of 500hp or above. Though this is a single study in one sector of industry which may not be totally representative of industry in general, the results are nevertheless informative. Of the total of 84 machines, 30 had never suffered a fault in their lifetime. The remaining 54 had the following faults:-

Bearing Faults	44.68%
Windings Faults	44.68%
Rotor Bar Faults	4.25%
Miscellaneous	5.39%

Bearing faults are often secondary symptoms of rotor bar faults and air-gap eccentricity problems within the machine or misalignment of the shaft. Winding faults may be caused by contamination of the insulation material by sea water or oil. Excessive vibration may also damage the insulating material. Miscellaneous faults include contamination of the bearing lubricants and foreign matter within the air-gap. Rotor bar faults are due to failure of the conductors within

the rotor which include both the bars and the end-rings. The failure of these conductors may be due to poor fabrication, or simply the operating conditions of the machine. In particular, machines which suffer frequent starts under full load tend to develop cracked and eventually broken bars/end-ring sections.

Rotor bar faults occur when one or more of the bars forming the cage of the rotor breaks resulting in an uneven current distribution. The effect of a broken bar on the rotor current distribution is represented graphically in Fig.[1.1]. The broken bar can carry no current so the current is re-distributed in the adjacent bars. A similar argument applies to high resistance bars due to cracking or poor manufacture and to the end-ring sections.

For the particular case of cage rotor faults the development of the damage to the rotor bars occurs due to thermal and mechanical stresses, which are at a maximum at starting due to the large currents flowing. The incidence of cracking is greater when the start up time is relatively long and when frequent starts are required as part of a heavy duty cycle.

The development of damage to the rotor bar after cracking of the bar has started usually progresses with the following sequence [6].

- the cracked bar overheats around the crack.
- the bar breaks and arcing occurs.
- the adjacent bars carry more current and are subject to even greater thermal and mechanical stresses during start up.
- the rotor laminations can be damaged due to the high thermal stresses.

These observations by Gaydon on the progression of a rotor bar fault suggest that indications of this fault may well be present for some time before catastrophic failure occurs.

1.4 Manifestation of Rotor Bar Faults

Previous research [1,4] has shown that when a broken bar occurs in a rotor, harmonic fluxes are produced which induce current in a stator winding at a

frequency of $(1-2s)f$, where s is the per unit slip given by :-

s=(Ns - Nr)/Ns

where

Ns - synchronous speed (r.p.m.)

Nr - speed of rotor (r.p.m)

f - supply frequency Hz.

This effect manifests itself in the form of two sidebands ($\mp 2sf$) around the supply frequency (f) if rotor asymmetry is present. A practical example of this is indicated in Fig.[1.2] which depicts the line current spectra from identical induction motors, one of which has rotor bar faults. Further work has shown that the lower sideband ($(1-2s)f$) is the better indicator of rotor imbalance and various strategies have been developed to link the number of broken bars to the amplitude of this lower sideband [2,7].

It is also known that since the air-gap flux pattern has changed the stator core vibration pattern will be altered since magnetic forces are proportional to the flux density squared [8,9]. This results in rotor slot harmonics in the core vibration spectrum being modulated at $2sf$ [10]. The axial flux spectrum also exhibits the modulation effect around the frequency component [5]. In addition the torque will fluctuate because the broken bars are unable to contribute torque which would have combined with other bar torques (with different phases) to give a steady state value [5]. A fluctuating motor torque results in a fluctuating speed.

Broken bars in the rotor can be seen to produce changes in different parameters and this means that a range of different monitoring methods can be used :-

(a) The line current can be monitored by either a current transformer or Hall effect device.

(b) The vibration of the stator core can be monitored with the use of an accelerometer.

(c) The axial flux signal can be obtained by placing a coil around the shaft of the motor.

(d) Speed fluctuations can be detected by use of a once per revolution transducer.

Only method (a) does not require access to the motor since the current measurement can take place at any point on the supply cables with the use of a clamp C.T. or Hall effect device. Method (b) requires specialist knowledge of the motor design and expertise in the analysis of the complex vibration signal. In method (c) no concise results have been published to verify that the number of broken rotor bars can be determined. Measuring the speed (d) can give an estimation of the number of broken bars but access to the motor shaft is required. Since many large induction motors do work in hazardous environments that require "hot permits" for access and in view of the convenience of simply intercepting the supply cable, line current monitoring has been used exclusively in this research work.

1.5 Objectives of Research Work

Over the last few years considerable research work has been carried out in the area of steady state condition monitoring of 3 phase induction motors. This research has shown that faults such as inter-turn winding failures, single phasing and rotor air-gap eccentricity can be detected by monitoring vibration, current and stray flux signals [1,2,3,4,7,11,12].

The vast majority of work done to date has been concerned with monitoring the machine under steady-state conditions. Many of the existing techniques require that the motor in question be under load before reliable diagnoses can be carried out. The objective of this research work was to determine whether rotor bar faults could be detected without the requirement to load the machine under test. Existing techniques are not able to detect the presence of broken bars during steady state no load operation due to the small currents flowing within the machine.

Throughout the starting transient period however (particularly if started Direct On Line), large currents flow in the motor, even under no load conditions. Not only are these starting currents usually 5 - 10 times as large as the full rated

current of the machine but due to the change in the motor's speed, contain components with a wide range in frequency variation. During this short starting period the machine is under conditions of severe electrical and mechanical stress and the purpose of this research project is to determine whether under these conditions, machine faults such as broken rotor bars could be detected.

1.6 Limitations of Steady State Analysis

Determination of the number of broken bars by steady state analysis can be accurate if the machine under test is sufficiently loaded. As the loading is decreased the amplitude of the fundamental 50Hz component and that of the lower side band (LSB) decrease and in general cause the diagnosis to underestimate the number of broken bars. This limitation can be compensated for by taking into account the amplitude of the 50Hz component and the frequency of the LSB. This type of compensation is empirically derived by persons with many years experience in machine maintenance and is understandably a commercial secret.

The benefit of a testing method that does not require the machine to be under load can be appreciated by considering a case history which is used to promote the use of steady state condition monitoring. These case histories are presented by Thomson et al of The Condition Monitoring Research Group at The RGIT, Aberdeen [13].

The particular machine in question was a 150hp single cage duty compressor based on an offshore installation. The platform operators reported that this motor was producing pulsating vibrations and an audible beating effect. Before the application of steady state monitoring this machine had been removed from service on two occasions with its bearings relaced each time. The motor had been tested at the repair workshop on no-load and on each occasion the vibration problem appeared to be cured. However when the motor was re-installed on the platform the vibration problem was still found to be present. This caused considerable speculation as to the source of the vibration. Was it broken bars, air-gap eccentricity or a vibration caused by the compressor being driven? The subsequent application of steady state analysis to the line current waveform

indicated that the machine had broken rotor bars. This case history clearly vindicated the use of steady state condition monitoring to detect broken rotor bars.

The removal, transportation, testing and re-installation of this motor from a remote offshore platform would have incurred considerable financial cost and inconvenience. Would it not have been better to have tested for broken bars during the no-load tests at the repair workshop which were primarily carried out to check the replacement of the machines bearings? Obviously the motor must have been started to perform the no-load test indicating that the facilities of an adequate power supply and starter were already available. A technique that would have detected broken rotor bars during the starting transient may well have reduced the cost and inconvenience of this whole operation.

It is clear from the above example that condition monitoring of the starting transient is not a competitor to steady state monitoring but rather a complementary technique for specific applications. In some cases, such as drives for fans in a coal power station that may operate continuously for six months or more, it is obvious that analysis of the starting transient would be of little value. However in a situation where loading of a machine is impossible or inconvenient there does seem reasonable cause to view the development of a starting transient analysis technique as benefiting some sectors of industry.

1.7 Laboratory Facilities

The major laboratory components used in this research project are shown in Fig.[1.3]. These include a custom built test rig originally constructed for steady state condition monitoring research. This test rig comprised an 11kW 3 phase induction motor connected mechanically to a D.C. generator for loading purposes. Line or phase current could be sampled through current transformers or alternatively by use of a Hall effect sensor. The machine was started by use of a star-delta starter and was always in a star configuration throughout the starting transient period. Various rotor types and fault conditions could be installed into the induction motor. The set also allowed static/dynamic air gap eccentricity to be effected and access to the stator windings, should a study of

winding faults be required.

Initially an industry standard spectrum analyser was used to monitor the current waveforms directly from the Hall effect sensor. It soon became apparent that further processing was required and this could only be achieved by recording the waveforms digitally. At this early stage of the research it was more convenient to use "off the shelf" equipment rather than design hardware for this purpose, since the specification for the hardware may have changed as the work progressed. In view of this a "Nicolet" digital oscilloscope with an RS232 serial link was interfaced to a standard IBM compatible P.C. This allowed data to be digitised and sent to the P.C. for storage on the hard disc. A further advantage of the Nicolet oscilloscope was that waveforms could be stored in its bubble memory and down loaded to the P.C. at a later date. This allowed a convenient method to collect data remote from the laboratory. The P.C. was also interfaced to a mainframe computer (HP9840) in which most of the signal processing and all of the numerical modelling was performed.

The P.C. was physically situated in the laboratory in close proximity to the test rig and in effect brought the processing power of the mainframe into the laboratory.

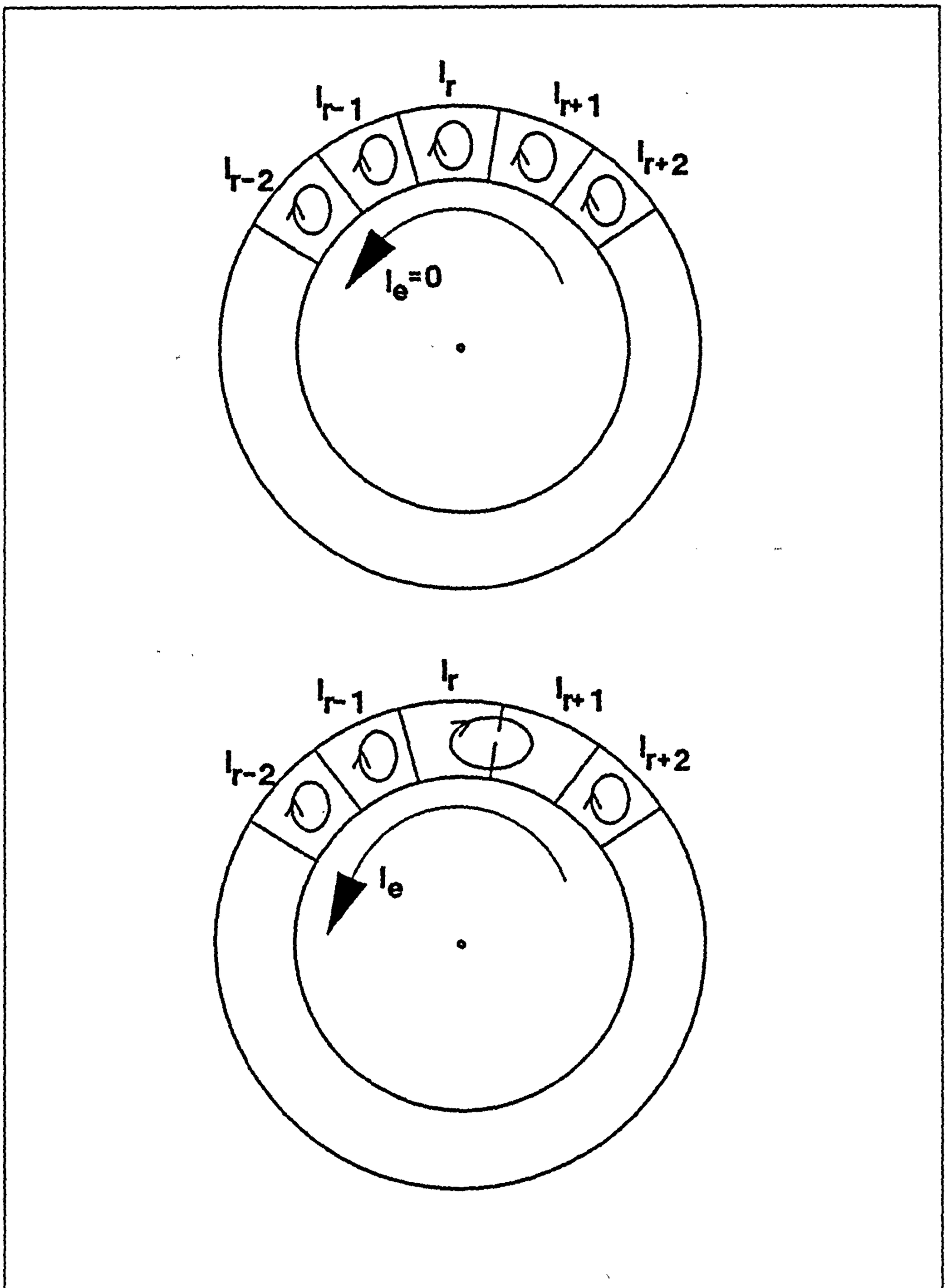

Figure 1.1: Effect of broken bar of rotor current distribution. Top : balanced rotor, Bottom : rotor with a broken bar.

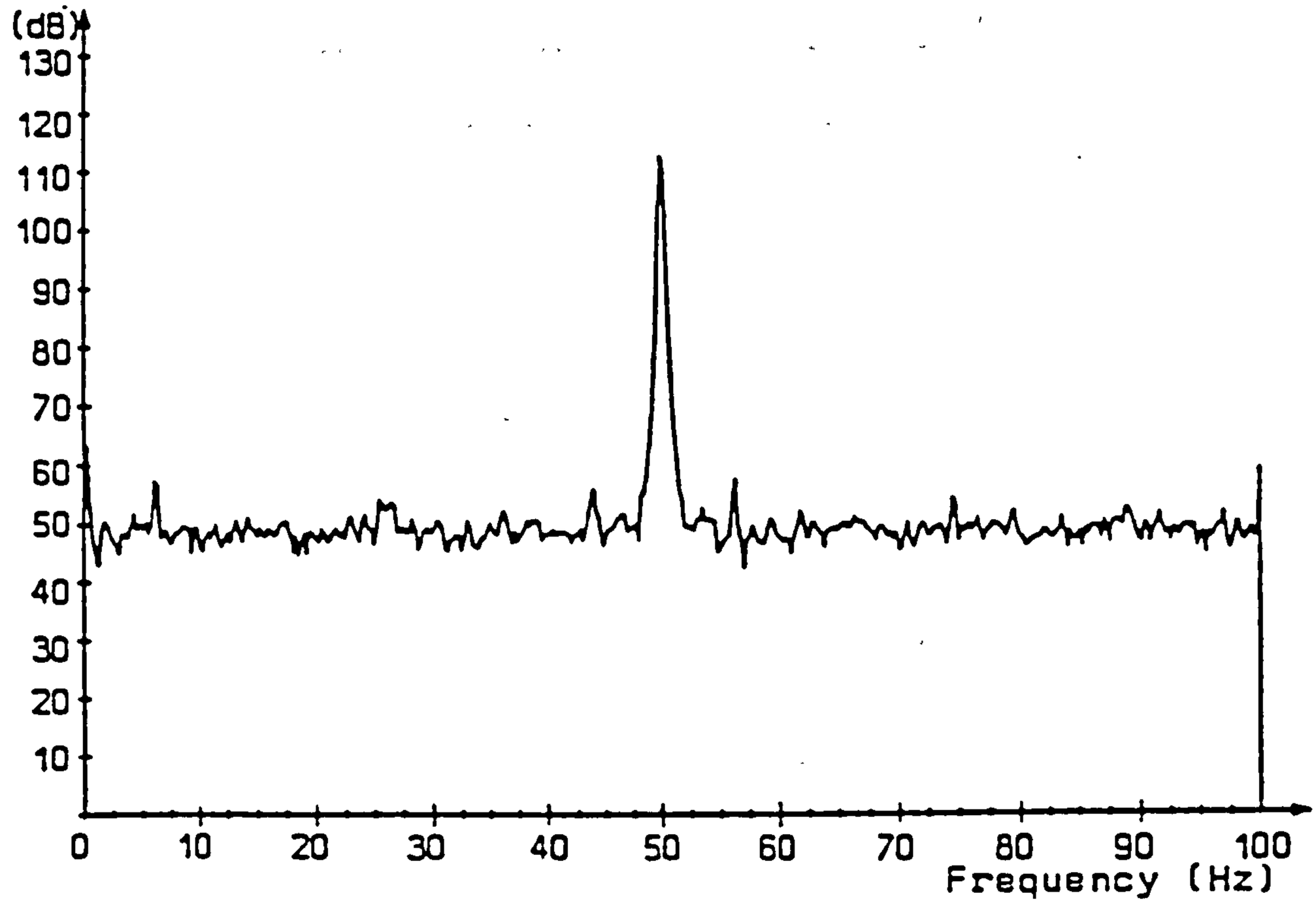

Current Spectrum-Normal Rotor

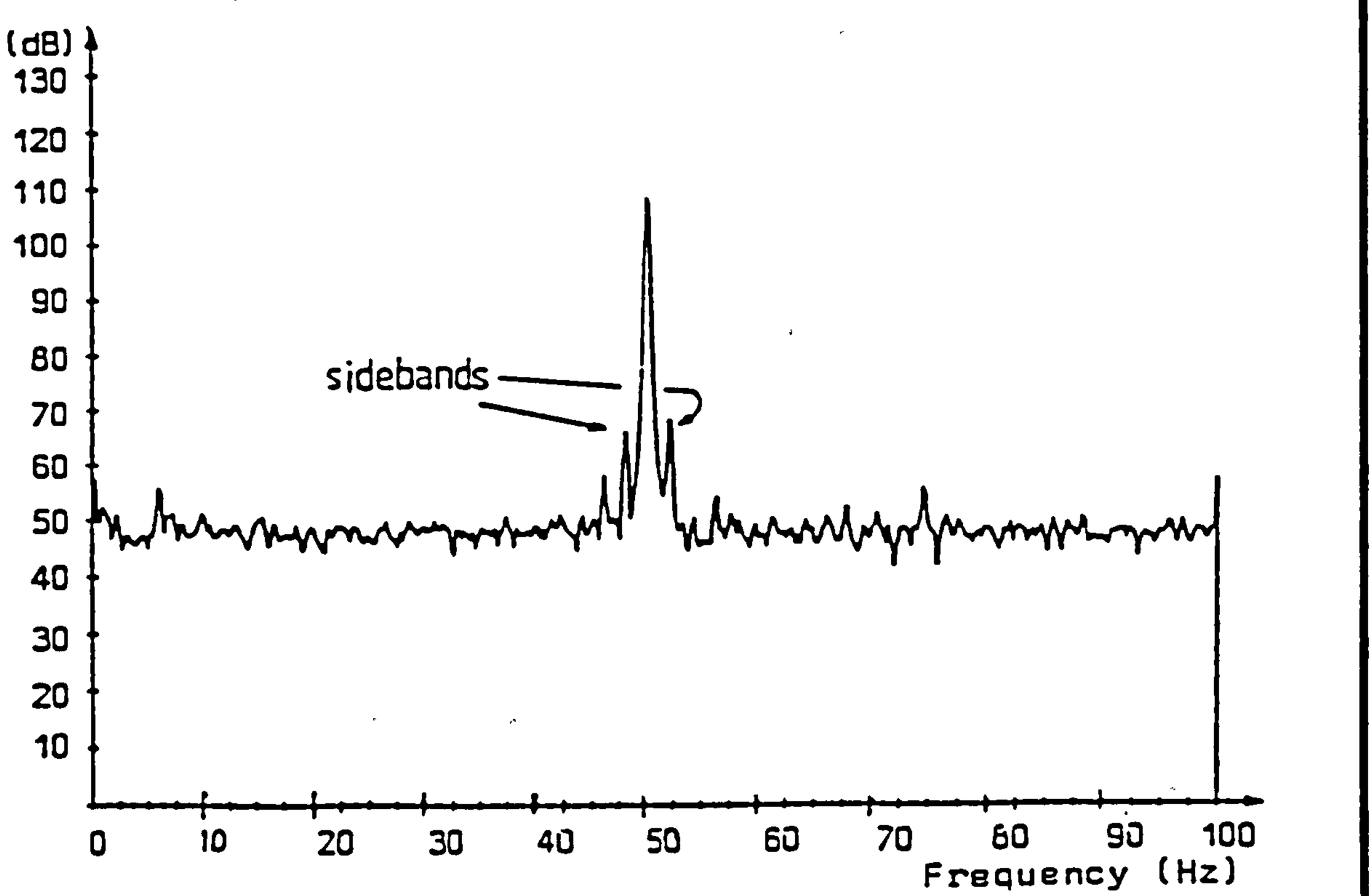

Current Spectrum-One Broken Bar

Figure 1.2: Current spectra for faulted and unfaulted machine.

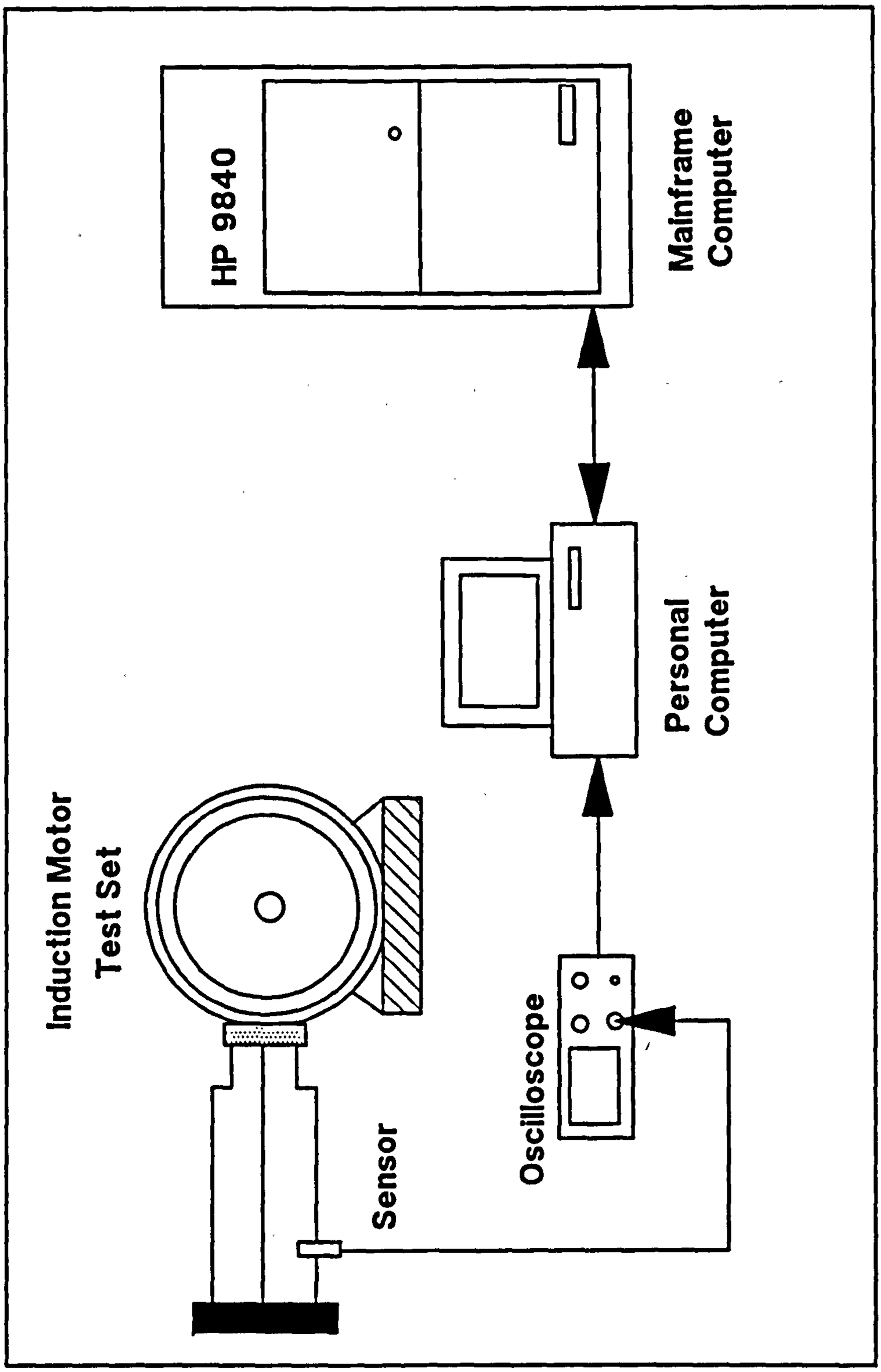

Figure 1.3: Laboratory Facilities.

Chapter 2

Review of the Analysis of Starting Transients

2.1 Introduction

One form of differential equations describing the operation of the Induction motor have been derived by H. C. Stanley [14] and are shown below.

$$\begin{pmatrix} Va \\ Vb \\ Vc \\ Ve \\ Vf \\ Vg \end{pmatrix} = \begin{pmatrix} R1+L1p & pMab & pMac & pMae & pMaf & pMag \\ pMab & R1+L1p & pMbc & pMbe & pMbf & pMbg \\ pMac & pMbc & R1+L1p & pMce & pMcf & pMcg \\ pMae & pMbe & pMce & R2+L2p & pMef & pMeg \\ pMaf & pMbf & pMcf & pMef & R2+L2p & pMfg \\ pMag & pMbg & pMcg & pMeg & pMfg & R2+L2p \end{pmatrix} \begin{pmatrix} Ia \\ Ib \\ Ic \\ Ie \\ If \\ Ig \end{pmatrix}$$

where p is the differential operator d/dt

These equations have non-constant co-efficients when the speed is a function of time or are non-linear when the speed is unknown. In these cases solutions have to use simplifying assumptions, graphical root locus methods or use a differential analyser/Analog computer. With the advent of improved digital computers in the early sixties another method for the solution of these induction motor equations was then possible, namely numerical analysis.

Considerable interest has been shown in obtaining the response of the induction motor during transient operation whether it be due to reswitching, the starting

of an electrically inert machine or the self excitation of induction generators. Though academic challenge, due to the complexity of these problems was no doubt a major driving force there were also real engineering problems that required attention. The transitory torques generated could easily exceed the maximum torques predicted by steady state theory with subsequent damage to the bearings, shaft couplings and gear boxes driven by these induction motors. Transitory current peaks could cause protection gear to trip unnecessarily and damage semi-conductor devices with ratings chosen by considering only the steady state response of these machines. Overvoltage damage to the windings of self excited induction generators and the stability of power supply systems using auxiliary induction motor drives are other examples which prompted study of the transitory response of induction machines.

In section 2.2 is presented the salient points to this research project of previous solutions for the transient response of induction motors by non-numerical methods, ie (analytical or by use of an Analog computer). The review is presented in chronological order as this clearly indicates that successive authors have increasingly exposed the complexity of the transient components, especially the torque. From Maginniss and Schultz in 1944 who found that the transient torque could be substantially larger than the steady state pull out torque indicated from the torque/speed characteristic, through to Enslin et al in 1965, who indicate that there are in fact no less than ten transient torque components during starting, with a range of frequencies of pulsation and time constants of decay. All the analytical solutions can only be derived with suitable approximations (usually constant speed) so that the differential equations that describe induction motor performance can be linearised. This, as most authors point out, means that any analytical expression for transient components will be approximate or if reasonably accurate will only hold for particular regions of speed, eg (standstill and operating speed).

Section 2.3 reviews the numerical solution of Stanley's induction motor equations which was then possible because of the improved third generation digital computers available in the mid sixties. These allowed convenient simulation of the induction motor during transient operation. In the earlier work the simpler and hence computationally less intensive d-q model of the induction machine(s) was used, though by the late sixties direct solution of the 3-phase induction

motors performance equations was utilised. A chronological review of induction motor transient simulation is presented, in which the increasing complexity of simulation can clearly be seen to develop. From Slater's study of torque transients and the sensitivity of the induction motor's parameters in 1966 through to simulation of system non-linearities such as leakage flux path saturation and deep bar effects by Lloyd in the early eighties. Despite the power and speed of modern day computers, efforts were still made to avoid the direct solution of the induction motor performance equations as indicated by Hashem and Ertem, though only the simulation of a large number of motors within a power system would justify their use.

2.2 Non-Numerical Methods

As early as 1944, Maginniss and Schultz [15] used a differential analyser (Analog Computer) to solve the induction motor equations including the rotor mechanical load and inertia. It had been usual practice to solve the induction motor transients problems either on the basis of the familiar steady state equivalent circuit or by calculations which require simplifying assumptions. These methods neglect important factors determining the response of the machine and the use of the differential analyser allowed the evaluation of these mutually interrelated phenomena. Two broad areas were considered, namely, sudden changes in mechanical load and sudden changes in the supply voltage. The changes in the supply voltage included connection to the supply, disconnection to the supply and the reversal of the phase sequence. The authors checked the analyser results against two cases which were readily solved analytically and the differences between analyser and calculated results were in both cases negligible. Several conclusions are presented in this paper, the most relevant being that large errors may be introduced by using the steady state speed torque curve for the calculations of transients. Other conclusions of particular significance are that, under transient conditions, generator torque may be developed at speeds below synchronous and that transient electric torques under shock mechanical loads or sudden electrical disturbances can be several times the steady state pull out torque. In 1946 Weygandt and Charp [16],used the differential analyser to study 2-phase induction motors primarily for the purpose of improving

the design of these small motors which found application in closed loop control systems. Various parameters were varied and the results studied to determine design rules to obtain a motor which could start and stop in an extremely short time interval. The conclusion of this work is that the induction motor may be specified completely by five parameters, namely: the stator time constant, the rotor time constant, the mechanical time constant, the coupling co-efficient and the load torque. It was noted that the large oscillations in speed during the transient were not of fundamental frequency, but are oscillations at the natural period of the system determined by the inertia and the electrical torque acting as a spring. The method of instantaneous symmetrical components was utilised by Chidambara and Ganapathy [17]in 1962 to study the transient torques developed in 3-phase induction motors during switching operations. The purpose of this investigation was to estimate the peak torque transients that may occur so that this may be considered in the mechanical design of the system. A general expression for the torque in normalised form is developed and used for the cases of starting, reconnection to the line and plugging. A comparison is made for these cases with experimental results and close agreement is obtained for the particular case of starting. It was noted that the starting torque is a fundamental frequency torque and it may be as high as seven to eight times the final steady state value. Hughes and Aldred [18] in 1964, performed analog simulation of both 2-phase and 3-phase induction motors with the purpose of predicting the transient response of each. The authors make use of the d-q-0 axes model of the induction motor where the rotor axis is considered pseudo-stationary with respect to the stator axis. The three phase machine requiring to be transformed to the equivalent 2-phase machine prior to the d-q-0 transformation. In both cases the d-q-0 equations had been derived assuming that the effects of hysteresis, eddy currents and saturation are negligible. For the case of the 2-phase servomotor, it was noted that though the mean values of the torque/time traces were similar to what was expected from the steady state torque/speed curve, the starting torque displays marked oscillations at applied frequency, which decay in amplitude as the motor speeds up. These oscillations correspond to the switching transients displayed in the stator currents, when the transients decay the torque ceases to oscillate. Two cases of unbalanced operation of the 2-phase servomotor were simulated, a stator voltage amplitude change and a stator voltage phase change. In both cases a second oscillatory

component was observed in the transient waveforms at twice the fundamental frequency. Approximate analytical expressions for the torque are derived where it can be seen that the magnitude of these oscillations are dependent on the degree of imbalance (whether amplitude or phase), and the speed of the rotor. It was noted that at no time did the torque become negative for the servomotor, though if the rotor time constant were increased portions of the torque transient could become negative. These high values of rotor time constants however, resulted in the loss of the drooping torque/speed curve which is required for a servomotor. Simulation of the 3-phase induction motor was less accurate than that for the servomotor. The authors suggest that the omission of the core effects in the initial development of the induction motors equations is the most significant contribution to this lack of accuracy. With a large machine, the amount of iron in the construction is appreciable, and some attempt to compensate for this by the addition of an extra resistance in the model does partly accommodate the core loss. One of the main points of similarity between simulated and practical results is that of the stator currents envelopes, which both display the same form of variation in d.c. level. When an alternating voltage is applied across an inductive circuit the current produced displays an exponentially decaying d.c. level, the magnitude of which depends on the switching instant. In the case of a three phase induction motor, the exponentially decaying d.c. levels of the stator currents, by transformer action, produce similar exponentially d.c. biases in the rotor. The motor acts partly as a synchronous machine, the rotor providing a decaying d.c. field rotating at rotor speed. The torque oscillation is caused by the d.c. levels of the stator fields (as with the servomotor), and in the case of the three phase motor the d.c. levels of the rotor current are much more prominent. This d.c field rotating at rotor speed causes oscillations of the torque to be at rotor frequency. Various unbalanced operations of the 3-phase induction motor were simulated namely, single stator phase operation, one stator phase open circuit, and two stator phases paralleled.

Also in 1964, Wood, Flynn and Shanmugasundaram [19] studied the transient torques of both single phase and three phase induction motors, due to the application of the supply. Extensive experimental results were obtained of the transient torque peaks for the non-simultaneous switching of the supply voltages. The authors explain the origin of the mains frequency component as arising by

interaction between the asymmetrical flux about one axis and slip-frequency currents (mains with respect to the stator) about the axis in quadrature. There is also another mains frequency component, owing to the interaction between transient speed-frequency rotor currents (direct with respect to the stator) and the alternating flux on the axis in quadrature. These transient components will tend to decay, at rates which are primarily dependent on the magnetising and leakage inductances respectively. The assumption that the speed is constant is made so that a comparison can be made between these two components. This results in two equivalent circuits from which the time constant of these components may calculated. There is also a third component of torque present due to the interaction between the transient asymmetrical flux and the transient rotor currents. The time constant of this component can be expressed in terms of the time constants for the two mains frequency components discussed above. Using practical values for the magnetising and leakage inductances this third component of torque has a time constant whose value is similar to that of the second mains frequency component discussed above. It is argued that since the ratio of magnetising inductance to leakage inductance is likely to be of the order of 20:1, this will result in the first component of transient torque at mains frequency having a time constant of approximately 40 times longer than that of the other two components. Thus the predominant component should be the transient mains frequency component associated with the transient asymmetrical flux and this in turn is associated with the transient magnetisation current. For a single phase motor, it would be expected that a transient mains frequency torque component should occur, with a magnitude dependent on the point on voltage wave at which the supply voltage is connected. Because of the high value of the ratio of magnetisation reactance/resistance, this component should be a maximum when the point is near 0°, and a minimum when it is near 90°. In the case of a polyphase motor, provided that all three phases are connected exactly simultaneously, the point on the voltage wave at which any selected reference phase is connected should have no effect on the resultant transient torques since the resultant asymmetrical flux due to all three phases will always have the same magnitude. The authors note however, that exact simultaneous switching may not occur in practice. Assuming that the alternating component of torque is almost entirely dependent on the asymmetrical magnetising current, it should be possible to almost eliminate this torque component, by

ensuring that no magnetising current asymmetry occurs in any of the three rotor phases. This was achieved in practice by connecting two of the supply lines simultaneously and the third line later after a specific delay. It was possible by suitable choice of the point on wave for connecting the two lines and then the third line to obtain a torque pattern having almost no alternating component. In a similar manner it was possible to maximise the amplitude of the torque oscillation. The authors also noted that no definite rotor position effect was observed, but in order to prevent any possible small variations due to this, the rotor was always set to the same initial position. Though the asymmetrical flux should decay exponentially for zero speed, in practice it was observed that the rate of decay increased as speed rises. The accelerated decay is explained by an "armature reaction" effect, this being due to speed frequency rotor currents caused by rotation of the rotor with respect to the asymmetrical flux.

In 1965 Rogers [20] tackled induction motor transients by using graphical root-locus method. The effect of supply frequency on the speed transients due to small voltage and torque disturbances is examined. A major disadvantage of the induction motor is that its speed is not easily variable. If a static frequency converter is to be used for speed control then the author argues that it becomes necessary to know something of its dynamic performance since the value of the base supply frequency has a marked effect on transients produced by voltage and torque disturbances. At normal supply frequencies, say 50Hz, the speed and current transients can often be considered separately. The current transients in such a case could be calculated from the equivalent circuit, and the speed transients from the steady state torque/speed curve, combined with a knowledge of the mechanical constants of the machine and load. In this paper is presented a linearised analysis of induction motor speed transients and discusses the effect of the supply frequency on these transients. Induction motor transients due to input voltage or torque disturbances are frequency dependent, and more oscillatory than their steady state performance may indicate. Rogers found that two modes of oscillation exist, one due predominantly to the rotor leakage inductance and one due to the stator resistance. At normal supply frequencies the dominant mode is that due to rotor-leakage inductance, but at low supply frequencies the dominant mode is due to stator resistance.

Also in 1965, Krause and Thomas [21] produced a paper in which the equations

for both 2-phase and 3-phase induction motors are developed for an arbitrary reference frame. In most cases, the analysis of an induction machine is carried out in either a synchronously rotating reference frame, however for an unbalanced rotor it is more convenient to use a reference frame fixed in the rotor. The authors consider several conditions of imbalance and solve these by use of an Analog computer. The induction motor equations are developed for a balanced machine in all three reference frames (fixed in rotor,stator and synchronously rotating field) by making the appropriate substitutions in the generalised equations. The authors indicate that in the case of analog simulation, it is preferable to eliminate sinusoidal quantities whenever possible and in view of this utilised the synchronously rotating reference frame for the balanced condition.

For the case of unbalanced stator voltages, sinusoidal variations will occur in the d and q quantities regardless of the choice of reference frame. For the authors it was convenient to obtain a solution in the reference frame fixed on the stator, thus retaining the stator variables. When a 3-phase machine is represented by a 2-phase equivalent, the recovery of the three line currents is obtained by use of a transformation, the choice of which is dependent on the reference in which the d q model was solved. In the case of unequal rotor resistances, time varying resistances will appear in all reference frames except for the reference frame fixed in the rotor. It is, therefore convenient to use this particular reference frame in investigating the performance of an otherwise balanced machine. The authors describe various other fault conditions and suggest the optimal (for an analog computer) choice of reference frame. Throughout this paper, individual cases of induction motor operation, have their equations derived, equivalent circuits described and finally a plot of the waveforms obtained for the variables of interest. This paper was used extensively for reference when numerically solving the d-q-0 model of the induction motor.

An analytical solution was also presented in 1965, for the solution of transient torques by Enslin, Kaplan and Davies [22]. The differential voltage equations for stator and rotor are rearranged to obtain two complex frequencies for both rotor and stator. These expressions are then simplified by approximation for the case of a machine not at or near standstill and also for a machine at standstill. The authors indicate that there are ten transient components of torque and these are produced in the following manner:-

When a magnetising current is established by the stator, a flux wave is induced which interacts to produce torque with all the current-wave components of the rotor only. Similarly a rotor flux wave interacts to produce torque with stator current-waves. There are two stator flux waves, one transient and one steady state, interacting with three rotor current-waves, two transient and one steady state, yielding six components of torque. The rotor carries one transient flux wave acting with four stator current-waves, two steady state and transient, resulting in four torque components. Expressions are derived for the amplitude, frequency of pulsation and decay for all ten components. There are three synchronous torque components and seven asynchronous components; these seven components have expressions for approximate frequency since the rotor is considered stationary for simplicity. The main distinction between these torque components can be made on the basis of duration and it is the four rotor adherent components which have the longer time constants. Grouping can also be according to frequency of pulsation and apart from the three unidirectional torques there are three frequencies of pulsation. These frequencies of pulsation can be expressed approximately by line frequency, rotor-slip frequency and the difference of the line and rotor slip frequencies. The authors conclude, that the experimental and theoretical results show that the transient torque/time characteristics of induction motors can be calculated using constants obtained from the normal short-circuit and no-load tests.

An analytical approach was also undertaken by Slater and Wood [23] in 1967, and their paper outlines the derivation of a constant speed transient torque solution for a polyphase induction motor for any switching condition. Only the early part of the torque pattern resulting from the application of the supply is examined and it is suggested that a constant-speed solution may be sufficiently accurate. The assumption of constant speed linearises the basic differential equations, and allows an algebraic solution to be obtained giving expressions for the various torque components. Such solutions have been presented before but these studies were limited to simultaneous switching conditions. The development of the torque expressions is based on the 2 axis pseudo-stationary equations of the polyphase induction machine (d-q-0 model) and depend on the assumption of no saturation, no core losses and a sinusoidal variation of the mutual inductance. When these equations are solved for currents assum-

ing constant speed and substituted into the expression for torque,six different expressions for torque components are obtained. The torque components arise, the authors argue, because each current consists of three sinusoidal components, one is the steady state component and the two others are transient components decaying exponentially. When the three phase condition is established three rotating fields are produced by the stator currents and corresponding rotating fields are set up by the rotor currents. The torque components can be considered to result from the interaction between rotor and stator fields resulting in nine torque components. As indicated previously only six of these components are different time functions, three are unidirectional and three are alternating. The frequencies of the alternating components are determined by differences in the angular velocities of the fields being considered. The exact nature of these components is discussed for the cases of zero speed, positive rotor speed and negative rotor speed where it is shown that certain torque components change their direction and nature (unidirectional or alternating) depending on the machines mode of operation. The authors conclude that the "transient" torque consists of six components, one steady state and five transient, two of which are zero for zero speed. The main transient component is lightly damped and of approximately mains frequency. This component is caused by transient asymmetrical flux associated with the transient magnetisation current, and can almost be eliminated by use of non-simultaneous switching of the supply lines.

Lipo and Consoli [24] presented, in 1981, a method for the analysis of the transients of induction machines with saturation of inductances. The equations which define the operation under this condition are arranged so that saturation of stator and rotor leakage as well as magnetising reactance can be readily modelled with an Analog computer. A new analytical method is presented for introducing leakage inductance saturation in the simulation model. The key step in this method is to separate both the stator and rotor leakage inductances into slot and end-winding portions. Although the slot portion saturates the end-winding portion is assumed constant thereby providing a means to isolate the leakage saturation effect and simplify the complexity of simulation. The simulation is achieved by implementation of the d-q-0 axes equations in the stationary reference frame on an analog computer. The saturation effects are implemented by three function generators in this case but as the authors point

out, can be programmed on a digital computer with equal facility. A subsequent paper by these authors in 1982, extends the application of this technique to asymmetrical faults on the stator, but not on the rotor.

2.3 Numerical Methods

In 1965 Humpage and Stott [25] published a paper, which discusses and compares the single step numerical integration techniques such as the Runge-Kutta routine with that of the multi-step predictor-corrector routines. At the time that this paper was written, digital computers were becoming common place and this resulted in many disciplines tackling problems described by non-linear differential equations. These digital computers were relatively slow so that any method whereby the number of calculations could be reduced was at a premium. The primary aim of this paper is to investigate the feasibility of using longer step lengths that are possible with predictor-corrector methods than are possible with single-step methods, thereby reducing the total computing time. The integration techniques are applied to a mathematical model of a power system comprising a prime mover, governor, automatic voltage regulator and transmission line. The equations describing this model have been derived in the d-q-0 axis and various integration techniques are applied for their solution. The results indicate that the length of step interval is influenced, in addition to the precise technique of integration, by the essential basis of step-by-step analysis, in which the solutions of algebraic equations always lie one step behind those of the differential equations. A method of predicting the value of non-integrable variables is also developed which allow a substantial increase in step length and hence reduction in computing time. A comparison is made between the accuracy of various integration techniques when applied to transitory phenomena on the power system model.

The added complexity of solution coupled with the speed of contemporary computers does not warrant the use of these time saving techniques, though the paper as a whole is extremely useful reading for those contemplating the numerical solution of differential equations describing a transient response.

In 1966, Slater, Wood, Flynn and Simpson [26] outlined a general approach to

the digital computation of induction motor transients in the d-q-0 axes, for a single phase capacitor motor and a three phase induction motor. In the case of the 3-phase motor, experimental results are compared with simulated results for the conditions of simultaneous and non-simultaneous switching. The numerical integration of the four d-q axes equations and single mechanical system is effected by use of the Runge-Kutta single-step technique with a fixed step length of 1ms. The authors found that there was reasonable agreement between the simulated and measured torque characteristics, both in pattern and magnitude.

Of particular interest was the investigation carried out into the sensitivity of the various induction motor parameters and it was immediately apparent that the most critical parameter is the total leakage inductance (l1+l2). Since a 10% error in the measured leakage inductance is deemed possible by the authors, it is suggested that this fact may be responsible for the differences between simulated and experimental results. It was found however that changes in the total leakage inductance which improved correlation for the starting characteristic would make it worse for the re-closing characteristic. Another source of error was the non-rigidity of the rotor and experimental evidence for this case is presented. The distribution of the total leakage inductance between stator and rotor was altered substantially and found to have little effect on the response of the simulated machine, thus confirming that it is the total leakage inductance which is most critical to induction motor performance.

Also in 1966, Smith and Sriharan [27] investigated the numerical and analytical solutions of equations describing the transient performance of the induction motor. The method of instantaneous symmetrical components is used and any phase current will be transformed into its positive, negative and zero sequence component. Since the positive and negative sequence components of any one phase are complex conjugates, the negative sequence equations contain no additional information to that given in the positive sequence equations. From considerations of the properties of an ideal induction motor a set of positive and zero sequence equations may be derived for the induction motor and these may be separated into their real and imaginary parts. The resulting equations are familiar as the set of differential equations of a cylindrical rotor machine referred to the d-q-0 axes. The method of instantaneous symmetrical components thus combines into a single operation : the transformation of a 3-phase

system to a 2-phase system, and the transformation from moving to stationary axes. The authors indicate that even under transient conditions an isolated star point of an ideal machine will remain at the same potential as the star point of the supply and no zero sequence component will exist in the stator with a balanced supply. No zero sequence components will flow in the rotor since it is short circuited. The numerical solution of these d-q axes and mechanical system equations is performed on a digital computer using the Runge-Kutta technique. The integration routine is more sophisticated than that used by Slater et al in that two estimates are made of each variable at each step. The results of these two estimates are compared and the difference (error) is used to maintain the accuracy of the solution. An analytical solution is presented for when the induction motor is switched to the supply. It is argued that because the rotor's inertia prevents a rapid change in speed that for a short time after switching (of the order of a few cycles of the supply), the rotor speed can be assumed constant. When rotor speed is assumed constant, the differential equations describing the induction motor may be linearised and thus solved by the method of Laplace transforms. An expression for the electromagnetic torque is derived which contains six components, one steady state, two which are unidirectional transient components and three which are transient components at frequencies very near the supply frequency, the slip frequency and a frequency corresponding to speed. The expressions obtained for currents and torque are extremely complicated and certain approximations are applied resulting in analytical expressions of : near zero speed, near synchronous speed and a third to cover all other speeds. Close agreement between theoretical and experimental results is observed and it is noted that the starting transient of a large machine is clearly very different from that of a small machine, where only one oscillatory term is effective after a very brief initial period. Comparison of the transient starting torques of the two machines indicates that the machine constants determine not only the magnitudes but also the form of the transients.

An all digital simulation of an induction machine and its associated control system is described by Jordan [28] in 1966. The simulation is suitable for analysing the operation either from a constant frequency, constant voltage supply, or analysing a complete control loop with variable frequency power source. The simulation is performed by solution of the d-q differential equations in the

stationary reference frame by use of a predictor-corrector algorithm which unlike many other predictor-corrector methods is self starting and therefore does not require an additional single-step method during the initial part of the solution. The solution is unusual in that the inverse of the impedance matrix is numerically calculated prior to the simulation. The d-q impedance matrix which contains eight zero elements can easily be inverted algebraically and in fact this ease in analytical inversion was a major reason for the use of d-q models over the direct solution of the induction motor equations. The direct solution requires the inversion of a 36 element impedance matrix at every step of the solution, a considerable burden to the computers of the mid sixties. This computer program has proved successful in the analysis of both induction motor transients and controlled induction motor systems, a graphical example of the numerical solution is presented for the case of starting a position regulated machine.

Another paper by Smith and Sriharan [29] in 1966, concerned the behaviour of an induction motor when disconnected from the supply and reswitched to the same or to a different supply before complete decay of the rotor currents. The computer program has three parts. The initial part of the program for the numerical solution of the induction motor's d-q equations in a similar manner to that developed in a previous paper [27] and deals with the connection of an inert machine to the supply. The next part of the program deals with the open circuit conditions in the motor, following disconnection from the supply. Since the stator voltages are now undefined, the equations are now re-arranged so that both the rotor currents and stator voltages may be found using the principle of constant flux linkage. For the final part of the program dealing with re-switching, the same equations as for the first part are used but with values determined from the open-circuit calculation. Comparisons of measured and calculated gave very good agreement for the stator voltages induced by the decaying rotor currents following disconnection. This indicates that the initial currents in the rotor required for calculation of the re-switching transients were accurately determined. Comparison between theoretical and experimental results for the transients on re-switching show reasonably good agreement, except in the case of plugging. The results from tests at reduced voltage gave reasonable agreement for the case of plugging and better agreement for all other cases. It is suggested that the mechanical system formed by the induction motor and

d.c. generator (for loading), would at rated voltage (and hence higher torque), have deviated from the simple model assumed in the calculations. This may well have introduced further discrepancies between the measured and transmitted torques.

Ramsden, Zorbas and Booth [30] in 1967, reported on the application of the d-q transformation to the induction machine equations which is used to develop a set of equations suitable for use with a digital computer in the analysis of the dynamic performance of induction machines within a power system. The method of calculation is designed to be compatible with those already in use for the analysis of synchronous-machine behaviour and makes use of a novel equivalent circuit.

The standard d-q axes equations for the induction motor are replaced by the referred equations used by Van Ness et al [31] . This results in a system of four differential equations, three of which are non-linear and from these equations, with appropriate substitutions, can be derived a steady state equivalent circuit attributed to Cooper and Howells [32]. The authors indicate that this equivalent circuit is easier to handle in comparison with the conventional circuit, since there are four quantities rather than five to be specified and the distribution of the total leakage reactance between rotor and stator is not required.

The numerical solution of the induction motor equations is effected by the use of the Runge-Kutta technique and the solution does accommodate changes in the busbar's voltage and impedance. A second version of the program neglects the transformer voltages and the variation of terms with speed and voltage of the induction motor. It is shown that this gives acceptable accuracy when studying stability of multi-machine environments including both power stations and industrial loads.

Extensive testing was performed on a variety of machines to determine the variation of the leakage reactance, magnetising reactance and rotor resistance with some or all of voltage, current, frequency and slip. The results of these tests expressed as quantities in the standard single phase model, are that the value of magnetising reactance is mainly voltage dependent. The leakage reactances are primarily load current dependent with some dependence on slip for the rotor leakage reactance. The rotor resistance increased with rotor frequency and the

rotor leakage reactance decreased with rotor frequency. Friction, windage losses and core losses were sufficiently small as to be neglected. The effect of full load temperature on the stator winding resistance was considerable giving rise to a 12% increase in one motor. All motors exhibited saturation at rated voltage to some degree.

A small digital program was developed to compute the steady state performance of the novel equivalent circuit. It appears that it is only in this program that parameter variation is modelled and no indication is given as to how the implementation of variation is achieved.

In 1967, Smith and Sriharan [33] made a study of the influence of terminal capacitors on the transient behaviour of an induction machine and differential equations are developed in which the non-linear effect of magnetic saturation is taken into account. The transients investigated are those following connection/re-connection in both modes of generating and motoring. The case of transients during capacitor and magnetic braking of the motor are also investigated. When an induction-motor/capacitor combination is disconnected or reconnected to the supply there may be large peaks in the voltage and current respectively. In the case of an induction generator the problem of overvoltage is even more severe, since the prime mover now accelerates the machine when the electrical load is removed. Capacitor and magnetic braking is effected by rapidly transferring the induction motor from the supply to a bank of uncharged capacitors and, after a suitable interval of time short circuiting the motor terminals. This method of braking has been discussed in terms of energy dissipation, but not in terms of transients produced by the switching operation.

The self-excitation of an induction machine is governed by, amongst other things, the saturation of the main flux paths, which must be taken into account in any analysis of the problem. In steady state analysis, saturation is treated as a variation in magnetising reactance, but in a transient study a more basic approach using the non-linear relationship between m.m.f. and flux density is required. For the numerical solution it is necessary to derive the machine equations in an explicit form incorporating the non-linearity. A digital computer solution of the equations is then used to investigate transient conditions in induction machines with terminal capacitors.

The induction motor equations are developed by the authors, in the d-q axes and incorporate a small cross coupling coefficient of mutual inductance between the d and q axes. The mutual inductances are made functions of the motor currents and when saturation is absent, these equations reduce to the more familiar d-q representation of the induction motor.

Saturation of the magnetising inductance was calculated by the authors by firstly performing an open circuit test on the machine and plotting the peak current against peak voltage for a range of input voltages. The experimental characteristic was extended by extrapolation to obtain the slope for large values of current. The open circuit characteristic was then represented by three cubic curves, each representing specific parts of the curve. The co-efficients of these polynomials are obtained by minimising the sum of the squares of errors. The mutual inductances now vary as a function of current, so that the inductance matrix must be evaluated at every step of the solution. The numerical inversion of this matrix was too time consuming using computers of the day, so an algebraic inversion was performed, making use of its symmetry. Algebraic expressions for the elements of the inverse matrix are evaluated at every stage of the program.

A comparison is made between the computer simulation of the induction motor with and without the non-linearity of saturation of the magnetising inductance. The authors conclude that for the motoring mode without terminal capacitors that only a small difference was found for the cases of connection/ reconnection and also for the connection of the supply to an electrically inert machine, ie (starting transient). The transient performance of an induction motor (without terminal capacitors) is not very much affected by the saturation of the main flux paths.

During the first stage of capacitor and magnetic braking of an induction motor, and following disconnection of a capacitor excited induction generator, the terminal voltage of the machine may substantially exceed the rated value. The core losses will then be much greater than during normal operation and be represented by an expression proportional to the squares of the d and q voltages. The core loss is computed at each stage of the integration and included in the torque equation as a braking torque. The core loss is regarded as an

eddy-current loss and it is suggested that this underestimates the total braking torque as many forms of loss not significant during normal operation are appreciable under conditions of high flux.

The mechanical system of both induction motor and load, include terms for the torsional constant of the coupling and a term for the damping torque, which is proportional to the relative angular velocity between the two inertias. All comparisons between measured and computed transients presented in this paper show that the theory under-estimates the transient current. The authors suggest that this must be caused by the saturation of leakage flux paths which will also produce some additional core and I^2R losses, these effects were not incorporated into the numerical modelling.

Robertson and Hebbar [34] in 1968, developed a model for the 3-phase induction machine which is particularly adapted for studying its dynamic performance when fed from an inverter.

For digital computer solutions, the d-q equations of the induction machine are usually used because they are simple and involve no time or rotor position dependent inductance terms. The equations do not deal directly with phase currents of the machine but instead they are expressed in terms of the transformed d and q axis currents. In an inverter-induction machine system, it is normally necessary to know the machine phase currents at every instant of time, in which case the d-q currents must be transformed into the phase quantities at every step.

This paper describes a system of equations for the induction machine which retains the stator variables as phase quantities, eliminates the variability of the machine inductances, and is applicable for all possible inverter modes. The development of these equations starts with non-linear differential equations of the three phase induction motor in terms of phase variables attributed to Stanley [14].

It is of interest to note that these equations are directly applicable to the machine whose rotor also has three symmetrically wound phases. A squirrel cage rotor is considered as effectively having three phases, and the equations would then relate the currents flowing in these fictitious three phase rotor windings to the fictitious voltages applied to them. These equations expressed in terms of

phase variables could be used to model the machine, however the rotor position dependence of the inductance matrix, requires that the inverse of this matrix be obtained at every step of the calculation. In order to reduce computing time the authors suggest the use of a transformation to eliminate the time dependence of the inductance matrix, similar in manner to that of the d-q transformation. However the transformation should be done with minimum change in stator variables so that these quantities be easily obtained, and so that the stator terminal constraints could be easily applied to the equations. The variable stator to rotor mutual inductances can be made constant by choosing stator and rotor reference frames stationary relative to each other. Since for this application the stator variables should not be altered, then it is obvious that the rotor quantities must be transformed to a stationary reference frame. These transformations are performed using the concept of power invariance developed by Kron [35].

The authors go on to describe in detail the application of these transformed equations to various conditions including, connection of the neutral and various combinations of open and connected stator phases. The effect of the transformation is to allow in most cases the algebraic inversion of the transformed inductance matrix. In the case where algebraic inversion is too cumbersome a single numerical inversion at the start of the program is all that is required. This of course rules out any change in inductance during the solution which may arise due to saturation or slip.

In the subsequent discussion, following the presentation of this paper, Sarkar and Berg suggest that their studies tend to indicate that for identical operating conditions, computer time requirement for the direct solution of the 3-phase induction motor performance equations does not differ much from that of the two axis equations. The repeated inversion of the inductance matrix does not appear a significant drawback with the then currently available third-generation computing systems.

The problem of solving the general 3-phase induction motor performance equations was tackled by De Sarkar and Berg [36] in 1969, and methods for the digital solution for both the three phase motor and the two axis model are described.

The development of semiconductor technology at this time extended the ap-

plication of induction motors to include variable frequency operation from an inverter. A three phase motor fed from a variable-frequency inverter may have supply voltages with a substantial harmonic content. The authors argue that, since it is inconvenient to take harmonics into account using the two axes model that a means of direct solution should be preferred.

The stator-rotor mutual inductances of the general 3-phase induction motor performance equations are dependent on the rotor angle, unlike the two axis transformed equation. Due to the presence of the rotor angle, the inductance matrix has variable co-efficients and hence the general 3-phase equations cannot be generally solved analytically. The numerical solution is achieved by use of the Runge-Kutta-Gill method which incorporates an error check at each step, based on comparing the result with normal and half normal step lengths.

The steps required to rearrange the general 3-phase induction motor performance equations into a convenient form for digital computation are presented, together with a flowchart for the digital solution. Since the co-efficients of the inductance matrix, being self and mutual inductances of the motor, are small, care must be taken to preserve the numerical accuracy of the inverted matrix. The actual error involved depends on the inversion algorithm and also on the word length of the computer being used, though no indication is given of which algorithm is used in this paper.

A comparison of the methods of solution of the two axis equations and three phase equations is presented. The two axis equations for the performance of the symmetrical induction machine are developed in the rotating reference frame of arbitrary speed. In the digital calculation, solutions are advanced in a step by step fashion assuming that no significant change of variables has occurred during a particular step. On this basis the authors found that the step in the solution of the stator fixed axes equations must be very small, whereas in the synchronously rotating axes the step length may be much longer for comparable accuracy.

An illustration of the methods discussed in this paper are given and in order to check the three phase model, start up transients of the unloaded motor were simulated. Results obtained from the two axis model and three phase model were in complete agreement.

The authors conclude that for unbalanced operating conditions including non-sinusoidal supply, the direct solution of the three phase performance equations is much more convenient and an other advantage is that the variables involved are the actual physical quantities of the motor.

Previous work on the transient performance of induction motors has paid little attention to the effect of winding parameters around their nominal values. Smith and Hamill's paper [37] of 1973, considers the severity of the transient current or torque in terms of a nominal response together with contributions derived from the parameter variations.

Predictions of the transient characteristics of an induction motor are made from the numerical solution of the d-q equations of the equivalent stationary axis machine. The mechanical system equation incorporates a non-linear expression which accounts for loss torques expressed as a function of speed.

Five machine parameters are varied from their nominal values, namely stator and rotor resistances, the stator/rotor mutual inductance, and the stator and rotor leakage inductances. The results confirm that provided that the total leakage inductance is correct, incorrect sharing between rotor and stator is not normally of great significance. However an over-estimate of the total value will lead to a serious error in the predicted response of the machine. It is also found that rotor resistance variations are by far the more significant in both the run-up and stopping times, the stator resistance has much the greater effect on the peak torque during both plugging and star/ delta starting. Mutual inductance variations are found not to be very significant except for the case of following a long period of disconnection.

This paper has demonstrated that quite noticeable differences in agreement between the computed and measured characteristics may arise if the values and distribution of parameters have relatively small errors.

Parameter variation was also described by Brown and Grantham [38] in 1975, for a 3-phase induction motor having a current displacement rotor. The method is based on the use of the Newton-Raphson procedure for the solution of two non-linear equations in two unknowns, these being the rotor resistance and leakage reactance at any particular frequency. A single assumption is made, namely that the stator and rotor leakage reactances are equal at supply frequency.

Measurements are taken to determine the resistance and the total impedance of one phase from which two non-linear equations may be derived. These two equations are solved by an iterative technique and give the variation in rotor resistance and leakage reactance as a function of the rotor currents frequency. As with results obtained from equations derived by considering the physical aspects of the rotor [39], the resistance increases and the leakage inductance decreases with increasing rotor current frequency. The assumption that the stator and rotor leakage reactances are equal at standstill is critical to this method and some discussion is presented on the results should this not be the case in the real machine.

The transient response of a group of induction motors supplied by a common transformer was simulated by Sriharan [40] in 1975. Each induction motor is represented by the differential equations referred to the d-q axes fixed in the stator and the transformer is considered an induction motor at rest. The induction motor and its load are assumed to be two rigid inertias coupled by a shaft with torsional torque proportional to the twist and a damping torque proportional to the relative angular velocity between the inertias. The windage and friction torque on the motor and the load torque are expressed as third order polynomials in speed so as to be able to represent most practical loads. A graphical plot is presented for the response of a single induction motor within the system, when another motor develops a short which is then removed from the system a short-time later.

In 1980, Smith,Stronach,Tsao and Goodman [41] developed a mathematical model for a complete marine power installation, incorporating diesel generator units and induction motor propeller and pump drives. Attention is focused on the various operational and disturbance conditions that are likely to arise and these may be summarised as follows :- a)The response to predictable disturbances, such as direct on line starting b)The response of abnormal disturbances, such as system faults c)The response to typical operational changes in demand

In the majority of marine applications, the starting of a motor is accompanied by a voltage depression and possible frequency variation dependent on the size of the motor relative to the generation.

In the formulation of the digital simulation model, the effects of non-linearities

inherent in the system are assumed to be confined to :- a)Variations in the magnetising reactances due to saturation for the synchronous machines. b)Variations in the slot leakage due to saturation and the slip dependence of the effective rotor parameters for induction machines. c)variations in the stiffness associated with shaft couplings.

The overall simulation model is obtained by combining the equations of the synchronous generators, the associated prime-movers and control systems, the induction motors and the mechanical submodels for the propeller and pump drives and arranging in 1st order differential form. The electrical system equations are computed in asynchronous rotating reference frame.

Under transient operating conditions the induction motor performance is dominated by the leakage reactance. When the currents of the machine are high i.e. under starting or heavy load conditions, the leakage paths will saturate. In this model, saturation is taken into account by the method described in reference [42]. Saturation of the main flux has less effect at starting however and this is allowed for throughout the simulation. It is usual to employ eddy currents in the cage bars of squirrel cage machines to increase the torque from the machine on starting. These eddy currents cause an increase in the effective resistance of the rotor bars as well as a decrease in the effective leakage inductance. It is the modification to the rotor resistance which is of most significance, since the change in the rotor leakage reactance is generally small compared with that due to saturation. These effects are included by the method described in reference[5].

The authors go on to describe the detail of the modelling of the transformers, diesel prime movers, mechanical system, thermodynamic system and control system. Examples are presented of the generator and motor responses to various operational and fault conditions.

Smith, Stronach and Goodman [43] used simulation to predict the starting current, torque and time to reach full speed for large motors. In order to obtain sufficient accuracy the simulation model must be capable of allowing for depressions in the supply voltage, include the facility to account for the variation of parameters due to saturation and speed changes, and be capable of representing the dominant modes of operation.

The requirements for a successful simulation of an induction motor driven process or plant essentially depends on two main considerations. The first concerns the type of system to which the motor is connected and the second concerns the degree of mathematical representation for the induction motor driven system.

If the induction motor is connected to a large power complex for which very little variation in voltage and frequency is expected subsequent to the motor starting, a single motor simulation may suffice in the assessment of the motor's overall behaviour. If however, the motor is connected to a small isolated system where for example, the run-up of a motor is accompanied by severe voltage and frequency fluctuations, it then becomes essential to take account of the system in a representative manner in addition to the drive under consideration.

For the purposes of this paper the induction motor model must be capable of accurately simulating a direct on line start condition and predicting behaviour in the forward speed region subsequent to various disturbing influences. This model must account for modification of parameters due to the deep bar effect and leakage flux path saturation. Stray loss is associated with the parasitic torques that are produced in the machine owing to harmonic fields in the airgap; caused by the distribution of the stator and rotor windings in the stator and rotor surfaces. These losses are not incorporated in the model though it may be included by assuming that this loss varies approximately as the square of the current.

The authors illustrate the accuracy of the simulation for practical systems by modelling both an induction motor driving a variable pitch propeller from a limited supply and the case of a large induction motor driven water injection pump associated with an offshore platform installation using a gas turbine generating system. Graphical plots are presented for the response of these two systems and a discussion considers the aspects of induction motor design that may be modified to obtain a better response in these small power stations.

Lloyd [44] studies the transient performance of induction motors with a view to determining the fault current contributed by the motor during various system disturbances.

The non-linearities of leakage flux path saturation and deep bar effects are incorporated into the d-q model along with mechanical non-linearities such as

gearbox backlash, shaft and coupling stiffness. The effect of eddy currents in machines with deep rotor bars, which serves to reduce the leakage reactance and increase the effective rotor resistance is discussed and two distinct methods of representing this phenomenon are indicated.

The representation of leakage inductance saturation is subject to error since the superposition principle can no longer be applied to a saturated magnetic path. The accuracy with which saturation can be assessed is related to the modelling of the BH characteristics of the core lamination material which should allow for permeability variations that can occur with large segmental stator cores.

The analysis of the simulations is used for the basis of suggesting that the fault current waveform consists of a transient and sub-transient period of different time constants. This, it is pointed out is contrary to the theory of synchronous machines where the presence of a sub-transient and transient reactance is due to two rotor windings i.e. a field winding and a damping winding. A squirrel cage machine, it is indicated has only one winding but still exhibits a sub-transient reactance. This is due to the presence of rotor deep-bar effect and saturation leakage flux paths which produce an effective second cage which produces the sub-transient phenomenon.

This line is developed further by initially assuming constant speed during the period of the fault and developing a single phase equivalent circuit containing both a transient and sub-transient reactance. It was found experimentally that the speed of an induction motor remains nearly constant during the first few cycles of a fault and that in this period the use of the constant speed solution was suffice to determine the peak currents flowing. Solutions of the decay of the fault current beyond the first few cycles requires the use of the full dynamic solution.

Buckley, Lloyd et al [45] in 1982, produced a paper directed mainly to the modelling of auxiliary drive motors in the post-fault period. Since the generator auxiliaries are often effectively supplied directly from the generator terminals their stability is of equal importance to that of the generator since failure of the motor to recover may involve shutdown of the associated generating unit. The cases of D.O.L. start, interrupted-circuit bus transfer and transient torque in an induction regulator are also considered.

The leakage inductance saturation is calculated by considering a single isolated rotor bar [46]. Extra circuit equations which represent coupled coils are included in the d-q model in the synchronously rotating axis to account for the transient eddy currents. The parameters of these coils may be calculated by modal analysis using Silvester's method [47] or if the slot has complex geometry a piece by piece field solution may be used [48]. In very large motors the bars are often rectangular and the resistance, self inductance and mutual inductance can be obtained from relatively simple expressions, however in the case of square bars more eddy current modes may be necessary to account for the variation in the field in the peripheral direction.

Godhwani et al [49] simulated the transient behaviour of two phase induction machines by use of a standard Continuous System Modelling Program (CSMP). This program in effect digitally simulates an analog computer and so avoids the requirement for extensive analog laboratory facilities. The two phase induction motor models are those developed by Krause [21] and the case of staring for both symmetrical and unsymmetrical machines is the main focus of the study. Likewise Ghani [50,51] used a static time domain model, solved by a standard circuit analysis software package, to simulate groups of induction motors within a system. The application of this analysis is mainly for determining the rating of the components used in power electronic equipment such as static power converters, conditioning or control equipment.

2.4 Discussion

Considerable interest has been shown in predicting the transient response of the induction motor during transient states, particularly the starting transient. Much of the work to date has been for the purpose of determining the amplitude of the current and torque peaks. Accurate knowledge of the extent of current and torque excursions can be invaluable in the design of the electrical supply/switching gear and the mechanical couplings between motor and load.

Much effort has been directed toward the modelling of non-linearities such as saturation, skin effect and the mechanical system. It is clear from the work reviewed that exact simulation of an induction motor over a wide operating

range such as experienced during a starting transient will always be approximate. Particularly the modelling of leakage saturation, a critical parameter in determining induction motor performance, which would require an accurate representation of the physical structure of both rotor and stator not readily applied in Stanley's equations. However, general trends in induction motor performance can be obtained by simulation which can give some insight into the machine's response that cannot be otherwise obtained by analytical means. In view of this, simulation of a faulty induction motor during the starting transient was thought to be a worthy undertaking so as to shed some light on a very complex period of operation. Unlike previous work, the purpose of the induction motor simulation in this research work was to generate line current waveforms that contained spectral components indicative of the conditions within the machine.

Chapter 3

Transformer Transients

3.1 Introduction

Before analysing the transient line current waveform of an induction motor it was thought than a preliminary investigation into a simpler though similar electromagnetic device namely, a transformer, would be beneficial. This work was primarily undertaken to study the switching transient of the open circuited single phase transformer due to "flux doubling effect" which is well documented in literature [52].

At this point in time it was still believed from the initial premise for this research work that the large currents flowing in the induction motor at switch on would be most likely to yield information about the condition of the rotor. The largest current peaks occur at the initial stage of the starting transient and any spectral components generated due to the "flux doubling effect" may well have obscured or be mistaken for components associated with broken bars in the rotor. In view of this, it was necessary to gain some insight into the nature of these spectral components using a simple single phase transformer before embarking on a study of those of the more sophisticated 3 phase induction motor. The "flux doubling" effect causes the magnetising inductance to saturate which in turn will generate a large number of harmonics in the current waveform. Modelling of the hysteresis curve was also undertaken so that this could be incorporated into a future induction motor computer model.

A number of papers concerning transient inrush currents in transformers were referred to [53,54,55,56] along with textbooks which included this subject [52,57].

3.2 Review of Previous Work

The magnitude of the inrush current in a particular instance is basically dependent on three things : the point on wave switching in the a.c. cycle, the amount of remnant magnetisation in the core and the shape of the magnetising curve of the core.

The existence of inrush was first noticed in connection with Ferranti's Deptford to London 11kV mains, when one of the transformers jumped visibly on switching, causing Fleming to investigate in 1892 [58].

Since flux cannot change instantly, the point on voltage wave at which the transformer is energised can have a substantial effect on the resulting current waveform. This phenomena is called the "doubling effect" and is documented in many well known texts [52,57,59]. A particularly informative résumé prepared by Hudson [53] collects together published information on transformer magnetisation inrush current.

Specht [54,60] developed formulae for the calculation of magnetising inrush current in a single phase transformer. In order to simplify this analytical solution, the magnetisation curve is approximated by three straight lines as indicated in Fig. [3.1]. The assumptions made were that no magnetisation current flows below saturation and that there is a constant value of saturated inductance above saturation (ϕ_s). For an analytical solution this very coarse approximation of the magnetisation curve can be accepted in view of the complexity of the subject area. For the purposes of numerical modelling and particularly if there is a requirement to perform frequency analysis on the simulated currents, a coarse piece-wise characteristic is quite unacceptable as it may cause numerical instability of the solution and will generate fictitious spectral components.

Macfadyen et al [56] analysed the transient behaviour of a transformer, taking into account the non-linearity of the magnetic material. The particular case of a 3-phase, 3-limb transformer is studied mainly for the purposes of discriminating

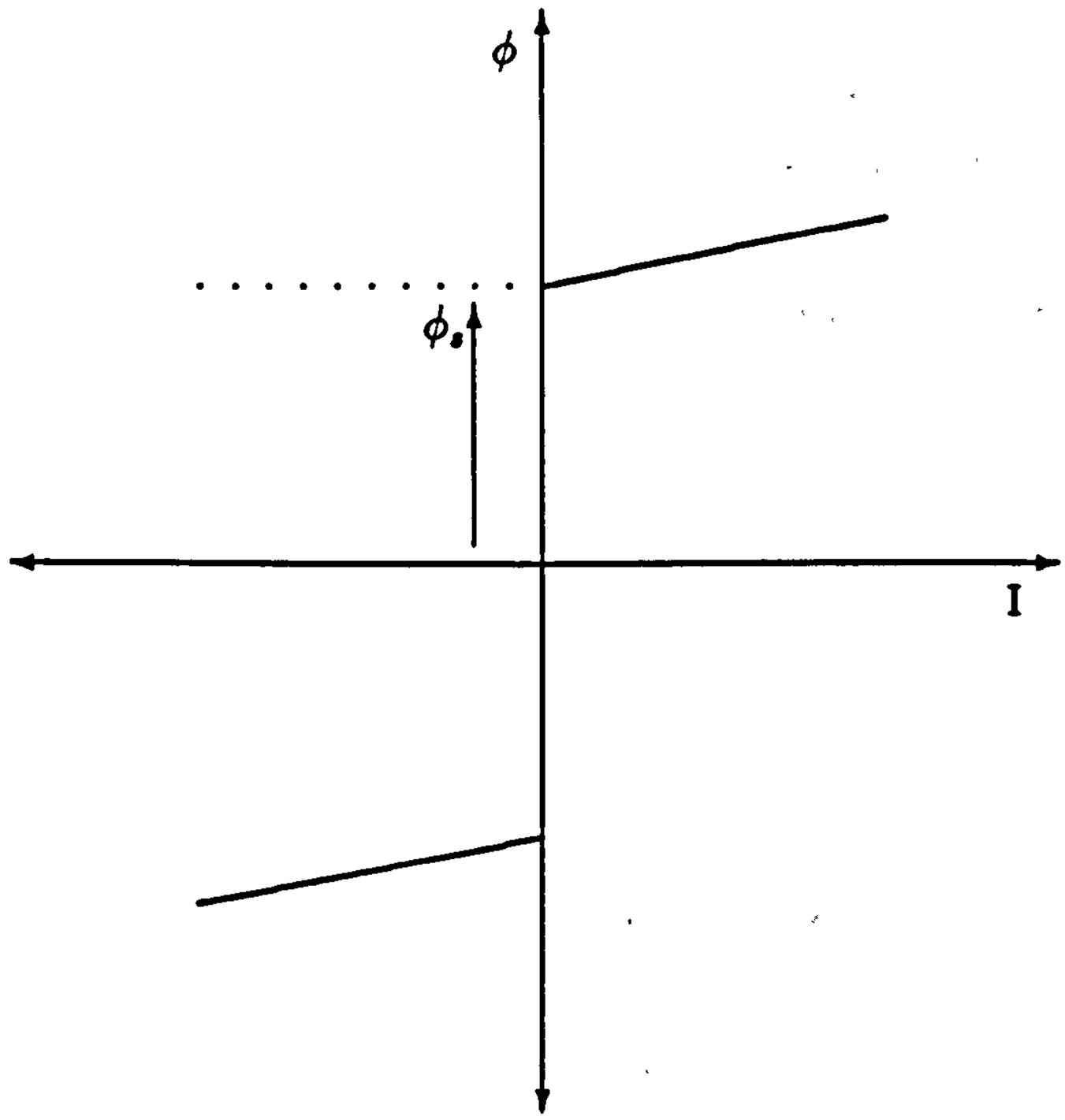

Figure 3.1: Line representation of magnetisation curve.

between transient overcurrent and any possible fault should the transformer be incorporated into a power distribution system.

The transformer is represented by nine differential equations which may be solved directly if the B/H characteristic is treated as being linear. The authors approach the B/H curve modelling by using a different method from previous work [54,61] which utilised linear approximation. Their method was to use an exponential series [62] for representing the magnetic non-linearity, the coefficients of this series may be evaluated by a simple iterative procedure applied to the experimentally obtained data.

Good agreement is obtained for the computed and experimental values of the largest current peaks, though the authors note that the error increases as the current decays. This is said to be mainly due to the fact that the single valued B/H curve (i.e. magnetisation curve) is used and hence hysteresis is neglected. The results presented are for the condition of no residual flux in the core, the core being de-magnetised before each test. The authors go on to suggest how the model could be extended to include both hysteresis and core-losses.

Yacamini [55] describes a digital technique for modelling the inrush current associated with the energisation of a single phase transformer. This technique is used mainly to investigate factors such as remnant flux and point on wave switching. The method of solution is to derive a difference equation for a lossless unloaded single phase transformer. Incorporated into this equation is the B/H characteristic or at least the magnetisation curve derived from it by ignoring hysteresis. Yacamini et al argue that this is justified since the inrush current is many times the rated current of the transformer, whereas the hysteresis phenomenon could be said to have a minor effect, even on the normal magnetisation current which is only a few percent of rated current. It is of interest to note that Macfadyen et al [56] cite neglect of hysteresis as the major source of errors in their work.

The remnant flux within a transformer is known to depend on the core material and the load power factor [63]. Results are presented which indicate that the amplitude of the first cycle of current varies linearly with the initial value of the remnant flux. The effect of the remnant flux diminishes with time though for the particular power transformer under study, has a substantial effect for some time after energisation.

Yacamini also presents a harmonic analysis in which every cycle of the first 50 cycles is subjected to Fourier analysis so that the first five harmonic amplitudes may be obtained over this period. From these results it is clear that the peak value of any harmonic during one cycle is generally different from its peak during another cycle. The second harmonic, for this transformer, is by far the dominant harmonic and the third to fifth harmonics show discontinuities where their spectral amplitude passes through zero with an inversion of phase.

Though this paper is of general interest to the study of inrush transient currents, it is the representation of the B/H curve non-linearity that is of most interest to this research project. As has already been indicated, the magnetisation curve and not the true characteristic was utilised. The authors argue that the use of sets of equations to describe the B/H curve of the core resulted in errors as the B/H curve is swept in both directions. The cumulative errors experienced in their numerical solution forced them to abandon this method in favour of a point by point representation, which in effect approximates the magnetisation curve

by a sequence of straight line segments (i.e. assumed linear between points) in the same manner as presented by Ray [64] some years later. This piece by piece representation will of course have discontinuities at the end points of each segment, the abruptness of the discontinuity will be related to the number of points used but unfortunately Yacamini et al do not indicate how many points were used in their modelling.

From the reading of all these sources it was clear that experimental work was required to :-

- determine the effect of point on wave switching
- measure the spectral components of inrush current
- use a non-piecewise model of the B/H curve
- assess the effect of remanence

3.3 Experimental Work

As a first step to observing the transient response of an unloaded single phase transformer, six transient current waveforms were obtained for the very loose conditions of small (Is), large (Il) and very large (Ivl) positive and negative initial current peaks since no point on wave switching was available at this time. The dB reference is 1μVrms developed across a 0.56Ω resistance i.e. 1.786μArms.

These six current waveforms were then plotted in both the time and frequency domains by use of an industry standard Spectrum Analyser. A comparison could then be made between their current peaks and spectral amplitudes. The current waveform in all cases settled down to steady-state in about one second and in view of Yacamini's [55] findings for the change in harmonic amplitude, the first 400ms of the current waveform was analysed separately from the second 400ms period. Figure. [3.2] shows the first 400ms for the small negative current peak case where the typical decay as time progresses can be clearly seen.

A summary of these results for the first 400ms is shown in Table [3.1] incorporating also the steady state spectral amplitudes for comparison. The steady state

DC term is thought to be due to half wave rectifiers being used on the supply lines causing a small DC bias to be developed over the resistance of the neutral line. Table [3.2] shows the change in amplitude of the spectral components between the first and second 400ms periods of the transients.

From Table [3.1], it can clearly be seen that the initial 400ms of the transient waveform for all six cases show markedly larger spectral amplitudes for both odd and even harmonics than are present in the steady-state waveform. This result would be expected in view of the nature of the abrupt discontinuity caused by energisation which will generate a wide band spectrum. It is interesting to note that the D.C. component is greatly affected by the particular transient condition.

Referring to Table [3.2], where the decrease in any one harmonic between the first and second 400ms period is tabulated. It can be seen that the even harmonics experience a substantially larger reduction in amplitude than that of the odd harmonics. Though it was not practical to analyse every cycle with the spectrum analyser, Yacamini had analytically shown that spectral components may increase in the latter portion of the transient and experimentally this can be seen for the 550Hz and 650Hz components for both the very large positive and negative transients.

No control of point on wave switching was effected in these initial tests so that the results though informative were not sufficiently repeatable to warrant further work. On obtaining a point on wave switching instrument, it was now possible to study several transients switched at the same point on wave and to observe any inherent variation in the spectral amplitudes.

3.3.1 Point on Wave Switching Control

The point on wave switching unit allowed control over the phase at which the voltage was applied to the transformer. The unit utilised a device called a magslip which had a three phase supply connected to its stator. The "rotor" of the magslip was single phase and its circuitry could be accessed externally. The rotor of the magslip did not rotate due to motoring torque but could be manually rotated. The phase of the induced voltage on the single phase winding could

then be varied as a function of the angular displacement of the rotor, which was conveniently connected to a dial calibrated in degrees. This induced voltage was then used, with some signal conditioning, to fire a thyristor and apply the supply voltage to the transformer at the desired phase.

It was only necessary to observe the time domain waveforms of the controlled point on wave switching transient currents to see that there was still a large variance in the first peak of the current waveform. This variance could be as much as 34% and it was thought that remanence in the transformer core may have been the cause. To reduce this effect the supply voltage to the transformer was slowly reduced to zero after each transient. This resulted in consistent results for any particular switching angle, for the amplitude of the first three current peaks from a suite of tests and the measured variance was reduced to 1%.

With control over the point on wave switching and steps to reduce remanence, it was now possible to investigate the transient current spectrum for a range of switching angles measured from voltage zero. As indicated by Say [52] and others the worst case switching should theoretically occur at angles of 0° and 180°, when ignoring the core loss resistance. The best case switching occurs at 90° and 270° where the current waveform should show no transient behaviour and proceed as if it were in steady state.

The results of harmonic amplitude (rounded dB), from an average of sixteen transients in any one condition are presented in Table [3.3]. At least two sets of sixteen transients were obtained for any one switching condition and were found in all cases to be in close agreement. Examining Table [3.3], it can be seen that both the cases of 0° and 180° switching have similar results, as expected from theory. In comparison the results for the 90° and 270° switching conditions do not have as close agreement, though the odd harmonics correlate well, the even harmonics, especially those below 500Hz have poor correlation.

As expected from the initial experimental work, the amplitudes of spectral components are higher for the worst case conditions of 0° and 180° switching over the 90° and 270° switching by in most cases approximately 40dB and in particular for the D.C. component by approximately 60dB or more.

Theoretically the 90° and 270° switching, should have resulted in a waveform

identical to the steady state waveform and it can be seen from Table [3.3] that there is reasonable correlation for the odd harmonics but poorer correlation for the even harmonics.

Though the angle of switching could be observed on an oscilloscope and appeared to be accurate to within one degree a set of averaged results were obtained for two degrees either side of 90°. These results are shown in Table [3.4]. All the odd harmonics have close agreement for the switching angles of 88°,89°,90°,91° and 92°, the even harmonics tend to increase in amplitude as switching angle is increased from 88° to 89°. If the 88° and 89° switching values are observed, it can be seen that a large amplitude change takes place in the even harmonics for this one degree change, far more than the other single degree changes.

It is not considered insignificant that at angles of 90° and 270°, that the input voltage is experiencing its largest rate of change (i.e. the derivative of voltage is at or near its maximum) and this must surely affect the accuracy of the point on wave control instrumentation. The type of instrument is of similar design to that used by Slater [65] and is based on the use of a magslip. The phase of the magslip output voltages with respect to their stator supplies can be varied by adjusting their rotor positions and thus selecting the desired switching angle and delay. Additional circuitry allows the firing of thyristors which supply the load. Slater claimed an accuracy of 0.18° for a 50Hz supply but also points out that the use of a mechanical dial increased the total error to 1°.

The effect of applied voltage on harmonic content was also to be examined. Supply voltages of both 200V and 230V were applied to the transformer. The applied voltage will dictate the excursion on the B/H characteristic which will result in a different current waveform in each case. From the plotted B/H loop shown on the oscilloscope it was clear that at 230V (rated voltage) that the maximum excursion reached the knee of the magnetisation characteristic and at reduced voltage the maximum excursion would remain below this knee on a more linear part of the curve.

From a set of four steady state records, each comprising a linear average of 1024 samples, obtained with a supply voltage of 200V and 230V, the following observations were made. For an increase of supply voltage all spectral components

increased, this would intuitively be expected. The increase in odd harmonics is substantially larger than that for the even harmonics. In other words the higher the level of saturation the more predominant become the odd harmonics.

There now appears to be a fundamental difference between the transient and steady state harmonic content. In the transient case, though all harmonics increase, in general even harmonics experience the largest increase over steady state values. However steady state excursion on the B/H characteristic, controlled by supply voltage clearly indicates a predominance of odd harmonics. The implication of this is that the B/H loop does not generate a large amount of even harmonics when symmetrical excursions are being undertaken, thus justifying to some extent the use of a magnetisation curve to represent a B/H loop in steady state.

The unsymmetrical excursion on the B/H loop at energisation and for a short time thereafter generates a predominance of even harmonics when compared to the steady state condition. These even harmonics reduce substantially as the transient condition subsides to a steady state condition as confirmed by the results of Table [3.2].

3.4 Synthesising a B/H Characteristic

In order to model the induction motor it was necessary to investigate the feasibility of representing non-linearities such as saturation. Subsection 3.2 summarises the approaches used by some previous researchers, although applied mainly to transformers. The introduction of a non-linearity into a system that is supplied by a voltage source of constant frequency will cause a range of harmonics to be produced in the current waveform dependent on the shape of the non-linearity's characteristic. This situation is further complicated if the voltage source itself contains harmonics.

The purpose of the Induction Motor Model was to investigate the theoretical transient analysis in parallel with the practical analysis. The simulated line currents were to be treated to the same analysis as the real line current waveforms. In view of this it was imperative not to introduce spectral components into the model that were due solely to the method of solution, since this would at best

generate fictitious spectral components and at worst cause numerical instability of the solution.

Any discontinuity in representing a characteristic will generate unwanted spectral components and on this basis the piece-wise methods used by Yacamini [55] and Ray [64] were not adopted.

Instead the B/H loop or magnetisation curve were to be represented using polynomials in a similar manner to that of Smith et al [33], except that in their case several different segments were each represented by a polynomial. This situation is better than the piece-wise straight line representation. In the case of multiple polynomials their values and that of their derivatives should be equal at the cross over point between any two segments, so as to minimise the discontinuity.

In this research work, a single polynomial was used to represent a magnetisation curve and two polynomials for each curve in the B/H loop characteristic. The use of a single polynomial was made possible by writing a computer program that could by least squares reduction generate a polynomial of any order to fit the desired data. This method and several alternative methods of polynomial approximation are discussed by Kaplan [66].

In addition to polynomial generation, the computer program could present the B/H-loop/magnetisation curve polynomial approximation in graphical form for inspection. The program was extended to allow spectral analysis using a FFT algorithm of the current waveform resulting from the application of a sinusoidal flux waveform to the characteristic curve. A graphical description is presented in Fig. [3.3] which depicts the resultant current waveform obtained from a symmetrical B/H curve subject to a sinusoidal flux.

With this program, it was now possible to obtain the magnetisation curve/BH-loop experimentally and compare the simulated spectrum to that obtained from the transformer current waveform. In order to facilitate these comparisons the magnetisation curve for the transformer was obtained by the standard O.C. test method [59,67]. This curve was then subjected to sinusoidal variations of flux linkage and the resulting current waveform analysed in the frequency domain.

The B/H loop was obtained by a method outlined by Baldwin [68] in which the primary current of an unloaded transformer is plotted against the flux linkage

obtained from the secondary. The flux linkage is obtained by integrating the secondary voltage with a series RC combination. These two signals are connected to the X and Y inputs of an oscilloscope which then displays th B/H curve. This method assumes that the laminations of the transformer core are so thin that eddy current loss is negligible. The B/H characteristic obtained could then be approximated by two polynomials. It was noticed that the B/H loop observed was not symmetrical and that the positive excursions reached higher levels of saturation than that of the negative excursions. This would have resulted in a waveform which did not exhibit half wave symmetry, which indicates a significant even harmonic content [69]. This lack of symmetry is attributed to remanence, despite steps taken to reduce this effect.

Several theoretical B/H loops from standard text books [59,67,52] were also analysed for their harmonic content when swept by a pure sinusoidal flux linkage so that some data outwith the transformer experiment could be examined.

A large amount of computing time was used to compare various orders of polynomial representation for these magnetic non-linearities with that of the experimentally obtained results. The process was in fact wholly automated for a specific range of polynomial powers (say 5th to 20th) and with a range of input flux linkages derived from voltages in the region of 200V or 230V. The program itself would measure the correlation between the theoretical and experimental harmonic amplitudes and produce a least square error value. The polynomial and input voltage which resulted in the smallest mean square error was then indicated to the user.

In summary, this work clearly indicated that the magnetisation curve would only generate odd harmonics. The B/H loop, with a different polynomial for each half cycle, would generate both even and odd harmonics, the latter being of far greater amplitude, as would be expected from a waveform which did not exhibit exact half-wave symmetry. However by far the largest generator of even harmonics was a B/H loop which was unsymmetrical as would be expected from a transformer that exhibited the phenomena of remanence.

As for the correlation between the experimental and theoretical harmonic amplitudes the best results were obtained from two 22nd order polynomials which were used to represent the B/H loop of the transformer, including the dis-

symmetry observed. The correlation was better for the odd harmonics than for the even harmonics, though in general there was not one single simulation of the transformer's steady state magnetising current which could be said to accurately model that of the real magnetisation current.

3.5 Discussion

It is clear from the research work read and the experimental work undertaken that the modelling of the magnetisation characteristic will always be an approximation. Though not perfectly representative this modelling can be useful in that the odd harmonic content will bear some similarity to the real situation and in some circumstances it may result in a more realistic representation than that obtained by ignoring this non-linearity.

For the induction motor it was latterly found, by experiment, that the optimum time to observe components indicative of rotor bar faults during the starting transient was in the region between half speed and operating speed. The "flux doubling effect" had subsided by this point in time. A slight increase in magnetising inductance saturation was experienced in this region since the current, and hence the voltage drop across both the leakage reactance and series resistance, had reduced which in effect imposed a slightly larger voltage on the magnetising inductance, driving it further into saturation.

Harmonic	-Ivl	+Ivl	+Il	-Il	-Is	+Is	S.S.
DC	117	116	103	104	82	85	54
50	121	121	112	112	101	99	97
100	114	114	107	106	93	92	63
150	112	112	105	105	93	91	85
200	108	108	103	102	89	87	85
250	108	108	101	101	87	87	80
300	102	102	97	96	84	81	53
350	100	109	93	93	82	80	70
400	95	94	88	88	78	76	49
450	92	91	84	85	76	73	64
500	80	82	78	78	72	69	38
550	79	80	73	71	68	65	53
600	67	66	67	63	64	62	34
650	79	76	72	72	62	61	55

Table 3.1: Harmonic Amplitudes during the first 400ms of transient vl:-very large, l:-large, s:-small. S.S. :- Steady State. dB re 1.786μArms.

Harmonic	-Ivl	+Ivl	+Il	-Il	-Is	+Is
DC	7.2	9.3	6.5	4.5	3.0	10
50	4.9	5.0	5.4	4.6	2.0	1.4
100	19.1	17.6	15.3	15.8	6.8	6.8
150	8.7	8.7	11.9	10.9	4.8	4.6
200	16.3	17.7	17.3	15.4	7.1	7.7
250	7.0	7.1	9.4	8.8	5.0	4.4
300	15.7	16.3	15.5	15.0	7.8	8.3
350	11.2	10.5	11.6	11.4	6.8	6.6
400	13.7	13.2	13.6	13.6	7.9	8.5
450	4.2	1.8	7.2	7.3	6.6	6.4
500	4.5	7.0	10.6	12.3	8.0	8.7
550	-0.4	-1.1	7.4	3.1	6.8	9.3
600	6.7	-4.8	**	-0.8	6.5	7.0
650	-2.8	-5.0	4.8	-0.4	3.4	3.0

Table 3.2: Change of Harmonic Amplitude between first and second 400ms periods. Component ** below noise level

Harmonic	0°	90°	180°	270°	S.S
DC	120	60	120	48	54
50	121	94	121	95	97
100	118	72	118	64	63
150	114	84	115	84	85
200	108	67	107	56	61
250	96	76	96	76	80
300	98	60	98	52	53
350	99	67	99	67	70
400	96	54	95	40	49
450	89	60	88	60	64
500	88	45	88	42	38
550	87	54	86	54	53
600	81	41	80	31	37
650	77	49	76	50	55

Table 3.3: Harmonic Amplitude for specific switching angle. dB re 1.786μArms

Harmonic	88°	89°	90°	91°	92°
DC	48	63	60	70	73
50	94	95	94	94	95
100	49	66	72	74	79
150	84	84	84	84	85
200	43	61	67	68	72
250	75	76	76	76	77
300	36	54	60	61	65
350	66	67	67	67	68
400	29	47	54	55	59
450	60	60	60	60	61
500	24	39	45	47	51
550	53	53	54	53	54
600	19	37	41	42	46
650	48	49	49	49	49

Table 3.4: Harmonic Amplitude for switching angles near 90°. dB re 1.786μArms.

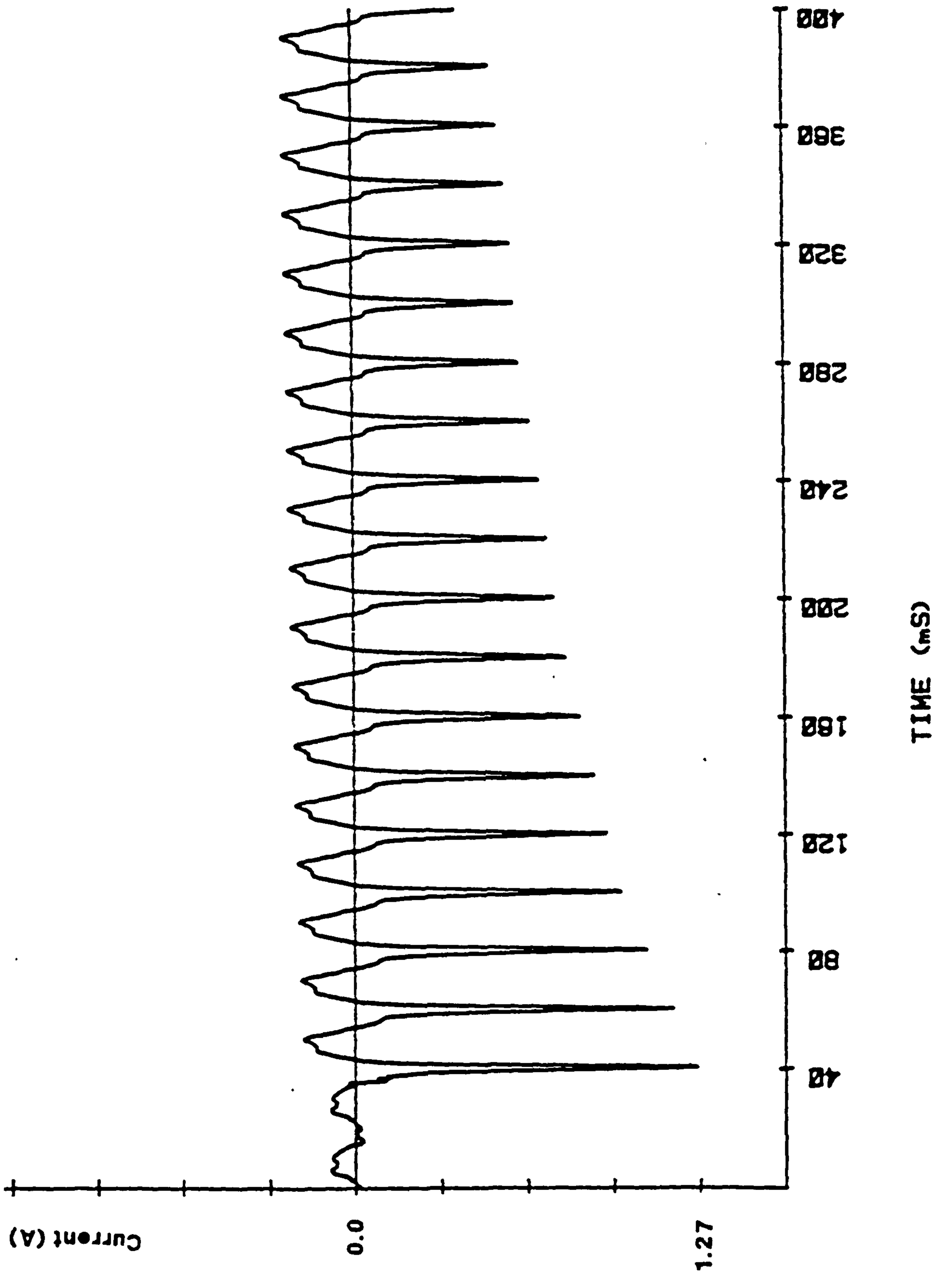

Figure 3.2: First 400ms of inrush line current for the transformer.

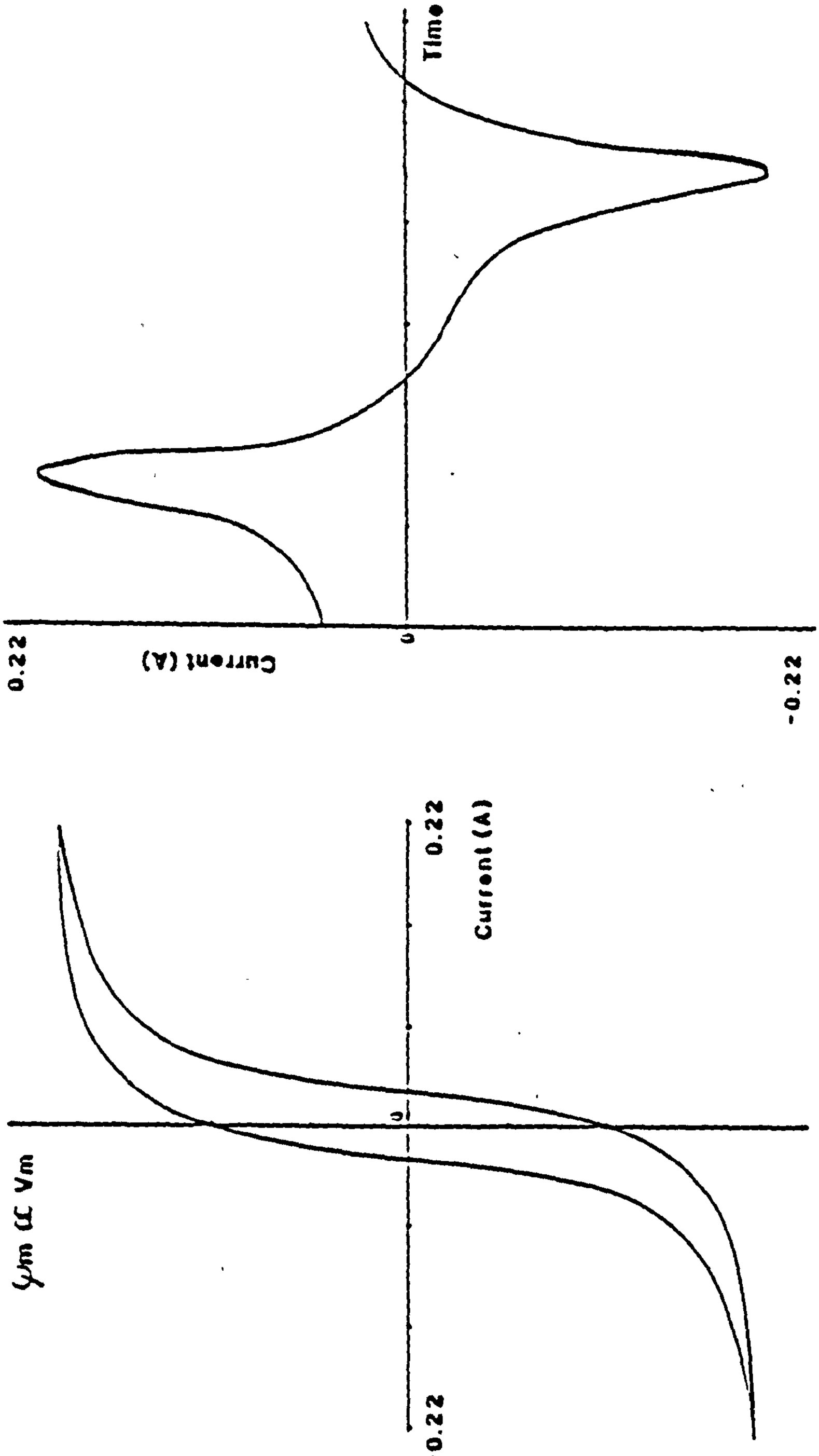

Figure 3.3: Current waveform derived from a symmetrical B/H characteristic.

Chapter 4

Wound Rotor Machine

4.1 Introduction

Initial experimental work on the detection of rotor faults within the induction motor were carried out on a test set with a wound rotor. With a wound rotor, access could easily be gained to the rotor circuit via the slip-rings. In this way, an external resistance (rheostat) could be connected to a single phase of the rotor circuit allowing an increase in the resistance of that one phase. This increase of resistance would bring about an imbalance on the rotor circuit and hence produce electrical, acoustic and magnetic frequency components indicative of that imbalance.

The test set consisted of an 11kW 3 phase induction motor connected to a D.C. generator for loading purposes and is described in more detail in section 1.7. No switching angle control was available and this is usually the case with industrial machines.

The measured rotor resistance per phase was 0.32Ω, and the external resistor could be varied between a minimum of 0.016Ω to a maximum of 0.45Ω.Measurement of resistance was made by use of a Micro-Ohmmeter. Thus large degrees of imbalance could be studied. With such large imbalances effected it was hoped to highlight frequency components which were indicative of rotor faults. These components would have been far more difficult to identify had the experimentation commenced on say, a 51 bar squirrel cage rotor with one broken bar.

The assumption of course was that a large phase imbalance on a wound rotor machine would generate similar components to that of a squirrel cage rotor with broken bars. Such relationships had been previously shown to exist in steady state analysis [2,52].

4.2 Initial Experimental Work

Line current waveforms were obtained mainly by use of a Hall effect sensor, though the output of a current transformer was available in the star-delta starter unit. Comparison of the waveforms obtained from both types of sensor for the test set in identical conditions indicated that the current transformer did generate slightly larger odd harmonics. It was later found that components indicative of rotor imbalance were best observed at the latter portion of the starting transient where current transformer saturation was minimal.

Three conditions of the wound rotor machine were studied initially with external resistances of $R_{ext} = 0.0$, 0.2 and 0.4Ω, though it was later found that the minimum resistance of the rheostat was 0.016Ω . The line current waveform from a starting transient with minimum and maximum imbalance are shown in Fig.[4.1], where differences can be readily observed. It should be borne in mind that the fault level with $R_{ext} = 0.4\Omega$ represents almost a doubling of the phase resistance, whereas to match other condition monitoring techniques any method based on transient analysis must be able to resolve one broken bar for a machine that may have 50 bars or more. It was quite evident that the results from time domain analysis at this point in time would have been extremely difficult to quantify, if at all possible.

Performing spectral analysis on these two single transients resulted in the Amplitude Spectrum shown in Fig.[4.2]. It can be clearly seen that an increase in the undulation of the plot between the frequencies of 12-50 Hz takes place with increased imbalance. Also a peak, loosely referred to as the "13Hz" peak can be seen to increase in amplitude with the level of imbalance. This peak is always observed though its frequency may differ by a few Hertz for transients obtained with the same level of imbalance.

4.3 Variance of Spectral Estimates

Referring to Fig.[4.1], the nature of these time domain waveforms is not stationary. It is known from steady state condition monitoring that components indicative of rotor faults and those indicative of static/dynamic eccentricity have frequencies that are functions of slip [3,4]. These components change in frequency as the transient progresses. The amplitude of these transient waveforms are obviously not constant and this, coupled with the possible frequency variation means that the use of the Fourier Transform for spectral analysis can produce results with a high variance [70]. This may be overcome partially by recording a number of transients and averaging their spectral amplitudes, though any rigorous analysis of the value for the minimised variance would require an accurate probability distribution of these line current waveforms to be calculated or obtained.

In view of this requirement to minimise the variance of the spectral estimate, ten spectra of transients for any one level of imbalance were recorded for a range of external resistance values of 0.05Ω through to 0.45Ω in steps of 0.05Ω. At each step in imbalance the ratio of the "13Hz" to 50Hz component was noted. These results are show graphically in Fig.[4.3]. Clearly the plot of Fig.[4.3] can be used to estimate the degree of imbalance (value of R_{ext}) from the averaged value of the "13Hz"/50Hz ratio, though in general the estimates were less accurate for values of R_{ext} greater than 0.2Ω. This was not thought to be a limitation since R_{ext}=0.2Ω represents a 67% increase in the phase resistance which would represent a very large fault. Examining the other extremity of the graph shown in Fig.[4.3], it was not possible to obtain accurate control over the resistance values of less than 0.05Ω (15% imbalance) which limited experimental work. More importantly the "13Hz" component would exhibit a variance in amplitude dependent on the point on wave of energisation. Though more transient records of the same fault condition could have been averaged, it was apparent that if ten starting transients were required to obtain a reasonably accurate estimate of a 15% level of imbalance, then a larger number may well be required to resolve say one broken bar in a 51 bar cage rotor.

The need to start a large industrial machine on numerous occasions (say twenty or more) so that this technique could be applied was thought impracticable and

in view of the duty cycle limitation of some large machines, too time consuming. Also the requirement for any point on wave control was to be avoided since most industrial machines would be switched via a star-delta starter or direct on line. The cost and impracticability of having point on wave control would have been a serious limitation to any prospective analysis technique.

It was concluded that some other method of processing the line current waveform would be necessary which required a study of signal processing methods in general so that likely techniques could be identified [71,72,73]

4.4 Wound Rotor Parameter Measurement

In parallel with the investigation of the real line current waveforms and the signal processing methods available was the development of a numerical model of the induction motor. This model would assist in the study of the very complex real machine transients. It could be used to determine the influence of individual parameter variations on the resulting line current waveforms, but perhaps more importantly it could be used to indicate particular aspects of the transient waveform of the real machine which would merit further detailed investigation.

In order to model the induction motor it was necessary to obtain the machine's electrical and mechanical parameters. The purpose of the induction motor model was to theoretically investigate the spectra of the line current waveforms for faulted conditions and use this information to assist in the diagnosis of the real machine.

The parameters required were :-

- $\alpha\beta$ electrical parameters (2 phase model)
- 3 phase model electrical parameters
- rotor moment of inertia
- magnetisation curve
- leakage saturation curve

- friction/windage losses
- core losses

A detailed presentation of experimental values and methods is given in Chapter [6].

The $\alpha\beta$ components are those electrical parameters that are required for the 2 phase model based on the dq axes representation of the induction motor. With a wound rotor, and hence access to the rotor circuit, several winding configurations are possible for the evaluation of these components [67].These parameters are also identical to those obtained from the standard running light/locked rotor tests which result in values for the standard single phase equivalent circuit. As can be seen in Chapter [6], there is close agreement for the values of $L1\alpha, L2\alpha$ and $M\alpha$ from all these tests.The values of the leakage reactances on both stator and rotor are also obtained by these various tests. Although the total leakage reactance measured have close agreement the $\alpha\beta$ tests do not give results that equally apportion this leakage reactance between the rotor and stator. It has been shown previously [26] that it is the value of the total leakage inductance that is critical to induction motor performance and not the distribution of this leakage inductance between rotor and stator. This fact was clearly evident by use of the induction motor model where little change in response was obtained for large re-distributions of this parameter.

The standstill rotor and stator resistances values R1 and R2 could be obtained by D.C. measurement and calculated from the above tests. The measurement of the rotor standstill resistance R2 proved particularly difficult since slip ring contact resistance was not constant with position.

The electrical parameters (Lss,Mss,Msr,Lrr,Mrr) were required for the 3 phase model that was to be developed, and were obtained for the wound rotor machine by having all the windings of the stator and rotor open circuited with excitation being applied to only one winding at any one time. A large amount of experimentation was performed to obtain these parameters, which is described in detail in Chapter [6]. Since access to the neutral point of the rotor was not possible, not all the parameters required could be measured directly [67]. The parameters obtained by this method, when transformed to the single phase

equivalents had close agreement to those obtained by standard RL/LR and $\alpha\beta$ methods.

The moments of inertia for several types of rotor were obtained by the method of trifiliar suspension [74]. For experimental control,the moment of inertia of a brass cylinder was also experimentally obtained, and due to its uniform density and simple geometry an analytical calculation was possible. Comparison of the two results showed that the error was less than 6%. The full test results and methodology are presented in Chapter [6].

Both the mutual saturation characteristic (magnetisation curve) and the leakage saturation curve were required so that these non-linearities could be incorporated into the I.M. model. The methods of experimentation were those reported by Jones [67]. Two problems arose in these tests. Firstly the magnetisation curve could only be obtained upto rated voltage, it was not possible to apply sufficiently high voltage to simulate the current excursions experienced by the mutual inductance during transient operation. Secondly, the leakage saturation curve could only be obtained upto 15 Amperes, the maximum current that the Variac could deliver, which is substantially less than the currents flowing in say a full load start. In both cases the experimentally obtained curves were extended intuitively by examination of similar characteristics depicted in the literature [52,67,75].

Friction and windage losses have been used in previous models [30,37] though Ramsden et al [30] neglect the term due to its small effect and Smith et al [37] use a second order approximation. To estimate these friction losses, the machine running at approximately synchronous speed was electrically disconnected and the time taken to reach a speed of zero noted. Though the run down characteristic was certainly not linear, a linear approximation was used. As found by other researchers [30] these losses are very small, being a maximum at synchronous speed demanding a torque of less than 2Nm.

Core losses are normally incorporated into I.M. models as an extra torque demand from the load [27]. The core loss was measured at no-load speed and could be approximated by an extra demand torque of less than 4Nm.

4.5 Wound Rotor Machine Modelling

The parameter values obtained were used in a 2 phase dq model of the induction motor. The development of this 2 phase model and subsequent models are discussed in detail in Chapter [7].

It was now possible to compare results from the laboratory machine to those obtained from a numerical model.

The cases of a balanced and unbalanced simulated machine have their line current spectra shown in Figs.[4.4] and should be compared to the real current spectra of Fig. [4.2]. Though there are clear differences (background noise is almost non-existent in the simulation) the change in the 0 - 50Hz region from the balanced to unbalanced case can be seen to occur in both the real and simulated data.

The simulation of the leakage saturation was achieved by altering the leakage inductance of both rotor and stator as a function of the rms d and q currents in a manner similar to that used by Lipo [24] and is described in Chapter [7].

Characteristics appeared in the line current spectra of the simulation due to leakage saturation and these could be observed in the real line current spectra. The most notable was the introduction of the notches above 100Hz when leakage saturation was modelled, these features were always present in the real data as can be seen in Fig.[4.2]. One other characteristic observed in the simulation was an increase in both the amplitude and frequency of the "13" Hz component. These low frequency components are described by Hughes [18]. When an alternating voltage is applied to an inductive circuit the current produced displays an exponential decaying d.c. level. The magnitude of this decaying d.c. level is dependent on the phase of the voltage at switch on. In the case of the 3 phase I.M. the exponentially decaying d.c. levels of the stator currents, by transformer action, produce similar exponentially decaying d.c. biases in the rotor currents. The motor then acts partly as a synchronous machine, the rotor providing a decaying d.c. field rotating at rotor speed. The stator current is influenced by this field so that it's bias becomes a decaying exponential with sinusoidal variation. This can be seen in the envelopes of the stator current as an undulation of the 50Hz component in the initial stages of the starting period.

This results in a synchronous machine action during start up which induces an increasing frequency component decaying exponentially in magnitude in the stator windings. It was therefore possible with the use of the simulation to identify two components of the real line current spectra. This is an example of how the model was expected to aid the understanding of the very complex spectra obtained from the line current of an I.M. during the starting period.

4.6 Side Band Frequency Variation

As discussed in the section [4.3], the nature of the line current waveform during start up is non-stationary [70]. This is partly due to the presence of components which have frequencies that are functions of slip s and partly due to the amplitude variation of the line current waveform as a whole.

It has been shown that the sidebands $(1+2s)f$ and $(1-2s)f$ associated with rotor bar faults in the steady state condition are also present during the starting transient, but of course they are changing in frequency with slip and hence time [1]. The origin of these sidebands is discussed in Chapter 5. At normal operating slip of say 3%, the sidebands, which are are situated at $+2sf$ and $-2sf$ around the 50Hz component, have frequencies of 47Hz and 53Hz respectively. However at the beginning of the starting transient the rotor is stationary and hence slip is unity. This places these two components at frequencies of 150Hz and -50Hz respectively. The -50Hz component is a phase shifted 50Hz component with respect to the fundamental 50Hz wave. As the rotor accelerates these two components change in amplitude and frequency. At half speed (i.e. slip=0.5) the lower sideband component (LSB) has moved upto 0Hz and the upper side band (USB) has moved down to a frequency of 100Hz. As the machine continues to accelerate from half speed to operating speed the LSB moves in frequency from 0Hz to a final value of approximately 50Hz dependent on the loading of the machine. The USB, during this same period, moves in frequency from 100Hz down to approximately 50Hz, dependent again on the loading of the machine and hence the final value of slip. The movement in frequency of the side bands is depicted in Fig.[4.5] and shows clearly the predicted frequency changes of the sidebands during the starting period as derived from the use of steady state

equations.

If the phase of the LSB is ignored, it can be seen to move from a frequency of 50Hz at starting down to 0Hz at half speed and upto approximately 50Hz at operating speed. The USB moves from 150Hz at starting down through 100Hz at half speed to approximately 50Hz at operating speed. It would be necessary to track these components and measure their amplitude to assess whether they could be used for rotor bar fault diagnosis.

The starting transient line current waveform is therefore a predominately 50Hz waveform but also contains components which vary their frequency as a function of slip and hence time. It is in this respect that these transient line current waveforms are similar to human speech which is also a non-stationary waveform. It seemed reasonable to assume that methods used to extract the frequency and amplitude content of speech as a function of time would prove useful in extracting data from these starting transient line current waveforms. Effort was now directed to the study of suitable speech analysis systems.

4.7 Phase Vocoder Analysis

After some research reading and discussion with project supervisors, a speech processing method known as the Phase Vocoder was selected as a suitable choice for the analysis of the line current transients. The Phase Vocoder developed by Flanagan and Golden at Bell Laboratories [76] has been used in speech processing for many years. The phase vocoder can be represented by a bank of bandpass filters. As components change their frequency they will pass through different filters in the bank and their amplitudes can be measured at the output of the appropriate filters. Though the original phase vocoder developed at Bell Laboratories was an analog electronic circuit, the technique can be implemented in software where it can be readily modified if required [77]. It was the latter method that was adopted in this research work in view of the ease with which filter parameters could be modified. A detailed mathematical description of the phase vocoder is presented in Appendix [B].

A software phase vocoder was developed and tested with controlled input signals (e.g. fixed amplitude swept sinewave). The output of this process may

be used to construct a three dimensional plot of frequency versus time versus amplitude and is often referred to as a Spectogram. This three dimensional representation of the line current waveform allows the amplitude of a particular frequency component at a particular time to be evaluated, which is in effect two dimensional filtering.

A large amount of data was produced by the software vocoder's filters which would eventually require interpretation. Though the number of filters in the bank was variable, it was not independent of the sampling interval and the frequency resolution. A high frequency resolution would naturally incur a long period of computation even for the mainframe computer used. A low frequency resolution would speed up computation but may not have highlighted components of interest. After some experimentation a suitable compromise was reached in which there were 64 filters in the bank, each separated by 7.8Hz and having a bandwidth of 7.8Hz. This allowed an analysis bandwidth upto 500Hz which dictated a sampling interval of 1ms or less to fulfil Nyquist's sampling theorem. It was known from steady state analysis that the amplitude of spectral components decreased markedly upwards of the fifth harmonic (250Hz) of the fundamental supply frequency.

Displaying 64 channels, each containing 1024 data points in such a manner that components which changed both their frequency and amplitude could be readily identified posed considerable problems. Several different methods of presentation were used and even with a high resolution monitor merged into a blur. Small sections of the output could be displayed clearly but this defeated the wideband nature of the phase vocoder. Though the sidebands were expected to yield information on the condition of the rotor it had not been established at this point in time whether there were components at other frequencies which may well have been more sensitive to rotor asymmetry.

It was necessary to use another dimension in the screen displays, namely colour. The combination of the human eye and brain is remarkably good at detecting differences in coloured patterns. The outputs of the phase vocoder were presented as coloured patters on the screen where differences could be readily observed. These colour graphics plots were used to display all sixty four channels at once. This enabled the change in both sidebands amplitudes and the PSH

to be observed with increasing fault level. These graphics plots encoded the channel amplitudes by colour using the psychological association of colour and heat i.e. blue - cold - low amplitude, red - hot - large amplitude. Thus all sixty four channels were plotted in a colour that was related to their amplitude at any particular point in time. A high amplitude was encoded as red, green represents an intermediate level and blue a small amplitude. This made observation of the trends in the large amount of data produced possible. Using this method of graphical representation it could clearly be seen that the lower sideband was particularly sensitive to rotor imbalance, as had been found to be the case in steady state condition monitoring [2].

Having established that the LSB was the most sensitive component to large degrees of rotor imbalance during the starting transient it was only necessary to display the vocoder data upto 50Hz. This allowed more conventional display method to be used as shown by the two spectograms in Figs [4.6,4.7]. Each spectogram displays the output of the first thirteen bandpass filters (channels) from 0Hz (d.c.) through to 100Hz in steps of 7.8Hz. Figure [4.6] is the spectogram of the line current waveform for the test rig in a nominally balanced condition, whereas Fig.[4.7] represents the rig with a 58% imbalance in one rotor phase. The amplitudes of the thirteen channels displayed can be seen to change with time as the machine runs up to speed. Clear and significant differences can be observed between the two cases shown. Using this technique it was possible to detect imbalances of 5% from a single starting transient whereas previously using standard FFT analysis, imbalances of only 20% or more could be detected from an average of ten or more spectra.

4.8 Description of Spectograms

The spectogram is a three dimensional plot of amplitude and frequency versus time. Referring to the spectograms of Figs.[4.6,4.7]. Two features not associated with fault mechanisms must firstly be explained. Due to the abrupt nature of the connection to the supply a discontinuity occurs in the line current waveform at start up. Abrupt discontinuities generate wideband spectra [70] so each channel will show some energy initially. This is indicated by the row of humps present

at the initial stages of each channel. The predominant component is of course the 50Hz supply which falls almost equally between the 46.8Hz channel and the 54.6Hz channel. Thus both channels register the component almost equally and this is depicted by the two high amplitude components which stretch across the time axis. The amplitude of each channel is normalised so that all components may be viewed otherwise the 50Hz component would swamp the picture due to its large amplitude.

The two sidebands associated with rotor imbalance can clearly be observed in Fig.[4.7]. As time progresses the sidebands change in frequency and hence move through the bank of channels. The energy associated with these sidebands can be seen as a hump progressing through the channels towards the 50Hz component as the machine accelerates. The LSB moves from -50Hz through 0Hz and finally reaches approximately 50Hz, the USB moves from 150Hz down to approximately 50Hz once operational speed is attained. In the case of the LSB the phase of the waveform is irrelevant as far as the filters (channels) are concerned so this component is seen to start at 50Hz at zero speed and progress towards 0Hz at half speed. From half speed the frequency increases from 0Hz towards 50Hz.

It is of interest to note that the amplitude of the LSB between half speed and operational speed is significantly larger than its amplitude during the zero speed to half speed interval. The only reference found from previous research work on the amplitude of the LSB during the transient component was presented by Williamson [1]. In his paper is described a steady state model for the induction motor. This model was used with a range of values of slip to produce the amplitude of the LSB during the starting period. Though there is a slight difference in the maximum amplitude in the pre-half speed region to that of the post-half speed region, the amplitudes only differ by about 2%. Furthermore, analysis of the simulated line current waveforms from the newly developed 3 phase model showed a similar difference in maximum amplitude to that found from the real line current waveforms.

The LSB between zero speed and half speed is negative sequence and this firstly suggested that the nature of the supply to the induction motor may have caused this difference in amplitude. However the three phase model, which exhibited

the same phenomenon, was supplied by an infinite bus bar as no modelling of the supply had been undertaken. This tended to suggest that this amplitude difference was a characteristic of the induction motor though no succinct explanation can yet be given. This difference of maximum amplitude of the LSB was also observed in the 28 bar double cage and 51 slot single cage rotors.

Since this phenomenon was unexpected and certainly not predicted a fictitious signal varying linearly from -50Hz to 50Hz was processed by the phase vocoder. This was performed to ensure that this effect was not due to some aspect of the signal processing. The spectogram observed showed equal amplitude in both regions confirming that the difference in maximum amplitude of the LSB was real. This amplitude difference is discussed in Chapter 5 describing the 51 bar rotor work where it can be used to differentiate between faulty bars and faulty end-rings.

The upper side band is only seen on the spectogram of Fig.[4.7] as it passes from approximately 100Hz to 50Hz due to the limitations of space. This component can be readily observed between its starting point at 150Hz at zero speed through to approximately 50Hz at operational speed.

4.9 Principal Slot Harmonics

It has been shown in previous research work [7] that when rotor impedance imbalance is present, $(\overline{+}2sf)$ sidebands appear around the Principal Slot Harmonics (PSH). The frequency of these slot harmonics is given by :-

$$Fpsh = \{(R/polepairs)\,(1-s)\overline{+}k\}\,f \quad k = 1,3,5,\cdots \tag{4.1}$$

where
R= 24 Winding slots on wound rotor
k= time harmonic of stator MMF
f= 50Hz supply frequency
polepairs= 2

The PSH will experience frequency variation during the starting transient and if we take the case of $k = 1$ will result in two components. These will start at

R_{ext}	LSB	USB
*0.016	0dB	0dB
0.016	-0.97	-0.04
0.042	6.6	5.0
0.062	11.2	8.5
0.078	14.5	11.6
0.1	17.4	14.2
0.12	20.4	15.3
0.14	22.1	17.1
0.154	23.9	18.99

Table 4.1: dB change in measured LSB and USB energies ($\propto I^2$) versus external resistance. * Rheostat unable to give resistance of zero Ω

+50Hz and -50Hz at standstill and increase to 650Hz and 550Hz at synchronous speed. Each of these harmonics will have the $\mp$2sf sidebands associated with them if there is imbalance in the rotor. Figure[4.8] depicts the frequency of the slot harmonic with sidebands as the machine accelerates to speed. Tracking the sidebands of these harmonics would be extremely difficult in view of their small amplitude and the fact that their carrier (slot harmonic) is increasing in frequency whilst the separation between sideband and slot harmonic is decreasing. In view of this measurements were made of the amplitude of each slot harmonic including the associated sidebands.

4.10 Test Results

A sequence of tests was performed on the slip-ring machine with the external resistance increased by 4% steps upto an imbalance of 40%. At each step, measurements were made of the LSB, USB and PSH. These measurements indicated that the PSH data had a high variance and was not suitable for a diagnostic technique with the present signal processing. The LSB and USB however showed better correlation between the measured energy and the value of external resistance as indicated in Table [4.1].

These measurements were performed after half speed where channels 1 to 5 were considered the LSB (7.8 - 39Hz) and channels 9 to 13 were considered the USB

(70.2 - 101.4Hz). Channels 6 and 7 (46.6 - 54.6Hz) were used to measure the energy of the 50Hz component. With this three dimensional data it was possible to ignore all events before half speed thus excluding the switching noise which was phase dependent. It was also possible to ignore the synchronous machine action which can be observed as a bulge near the beginning of the spectogram on channels 0 and 1 (0 - 7.8Hz).

The value obtained for the side band measurement, consisted of summing the square of the amplitude component for a particular channel from half speed. This value was then divided by the time between half speed and operational speed. This process was carried out for each channel associated with a side-band (e.g. channels 1 to 5 for the LSB) and the final figure obtained was the summation of all these associated channels. Various other measurements were obtained which included accounting for the energy in the 50Hz component, the ratio of the initial peak of the 50Hz component to the maximum of the side-bands, but none proved any more sensitive to imbalance than the method which resulted in the changes depicted in Table [4.1].

Polynomials were generated from the data in Table [4.1] which related the USB and LSB energies to the degree of imbalance (value of external resistance). It was thus possible to write a computer program which would examine a spectogram and produce an estimate of the external resistance. The estimated results were very close (1%) to the external resistance connected to the rotor phase indicating a degree of repeatability. It was therefore possible to determine the degree of rotor imbalance during the starting transient of the laboratory machine.

It was necessary to gain statistical information on this application of the phase vocoder such as variance and its root the standard deviation. Batches of tests were performed at specific imbalances and the results compared. It was observed that the first result in any one batch had a high accuracy for the estimated external resistance. However subsequent records in that same batch resulted in poorer estimates of the external resistance as can be seen in Table [4.2]. The external resistance was measured before and after the experiment giving values of 0.03Ω and 0.034Ω resulting in an average value of 0.032Ω.

This effect was thought to be due internal heating as more and more starts were

Filename	Rav	Re
Vsame1	3.14e-2	3.33e-2
Vsame2	3.28e-2	3.31e-2
Vsame3	2.58e-2	3.21e-2
Vsame4	2.21e-2	2.46e-2
Vsame5	2.92e-2	2.88e-2
Vsame6	2.47e-2	2.56e-2
Vsame7	2.42e-2	2.58e-2
Vsame8	2.57e-2	2.59e-2
Vsame9	1.98e-3	2.66e-2
Vsame10	2.44e-3	2.74e-2

Table 4.2: Re is the estimated external resistance using only LSB energy, Rav uses both LSB and USB energies.

performed. The external resistance was a free standing rheostat with a large surface area exposed to the air in the laboratory. It is argued that this external resistance maintains a constant temperature whereas the windings within the rotor are enclosed and therefore increase in temperature due to the sequence of starts. With an increase in winding resistance, the constant external resistance would represent a decreasing percentage of the total resistance.

Any new technique must be as good if not better than existing techniques and in view of this tests were performed to compare the steady state technique based on LSB amplitude change to that obtained from the phase vocoder during a transient start. Since this steady state technique requires that the machine be loaded, it was necessary to analyse a transient start at the same loading. In fact most of this early work was carried out on full load starts since this highlighted the components of interest, refinement to light load starts was to follow later. The machine had the external resistance changed from 4% to 10% ($0.016\Omega - 0.037\Omega$). In each case records were taken for both transient and steady state on the same loading. The results indicated that the steady state technique registered a 3dB rise in amplitude of its lower side band. The transient technique indicated a 2dB rise in sideband energy (1dB amplitude). Thus the transient technique was less sensitive to rotor imbalance than the steady state technique, though further refinement was thought possible.

4.11 Discussion

In conclusion, it was found for full load starts, that low levels of imbalance in one phase of a wound rotor could be detected by use of the phase vocoder. This data could be used to automatically predict the value of external resistance applied. This indicated that a diagnostic technique suitable for industrial use was feasible. The accuracy of the technique at that time was good only if long time intervals existed between tests, allowing the windings to cool to the ambient temperature. Several squirrel cage rotors with damaged bars were available within the department and initial work indicated that the data was independent of temperature, as anticipated. Two rotors, one with 51 bars, of which three were broken and the other, a 28 bar double cage rotor with one broken bar had spectograms of their lines currents which were very similar to that of the wound rotor. These similarities prompted the purchase of two 51 bar rotors so that experimentation could continue with a sequence of broken bars on the same rotor.

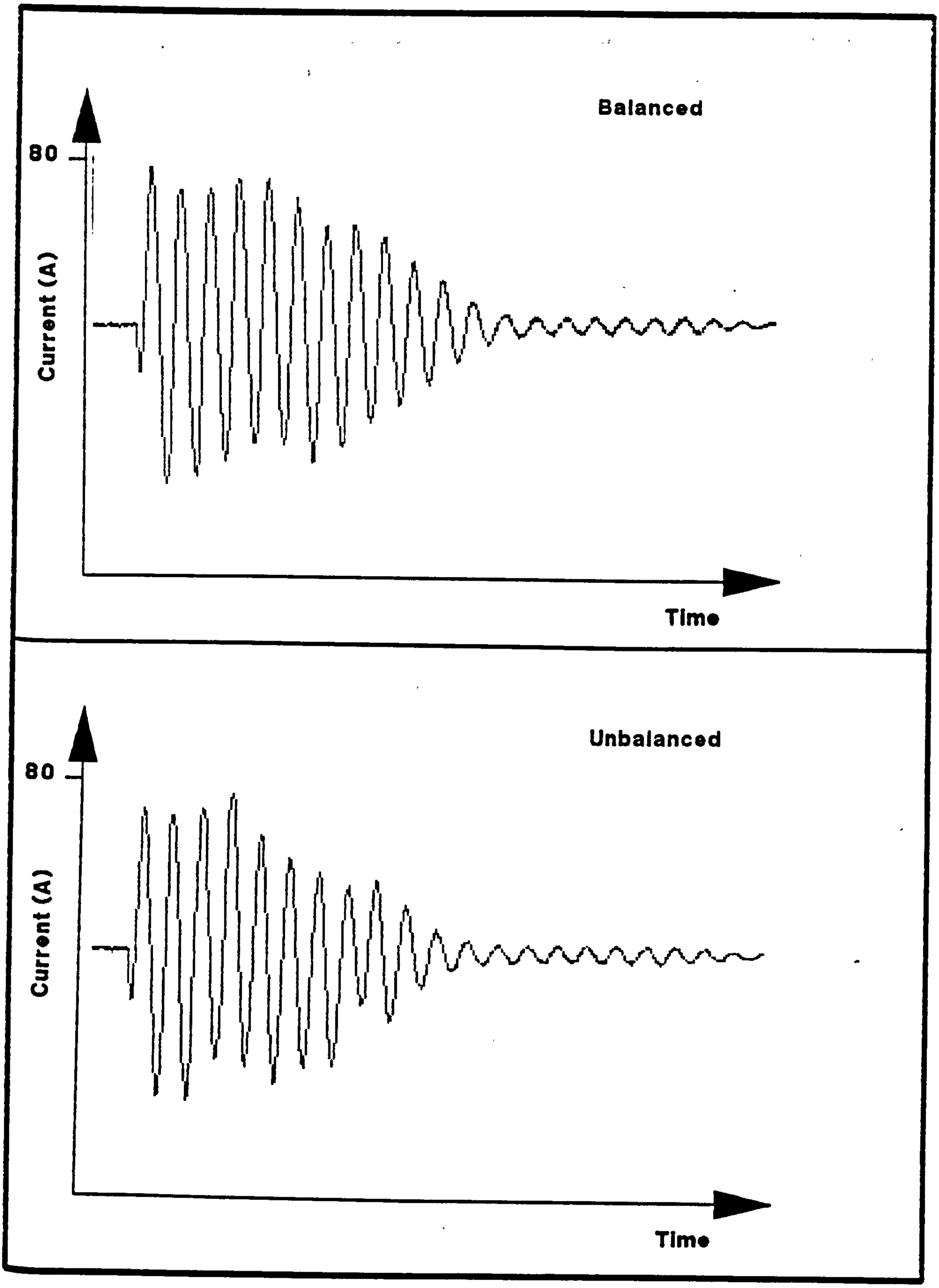

Figure 4.1: Line current waveforms of, nominally balanced and with R_{ext}=0.4Ω for wound rotor machine.

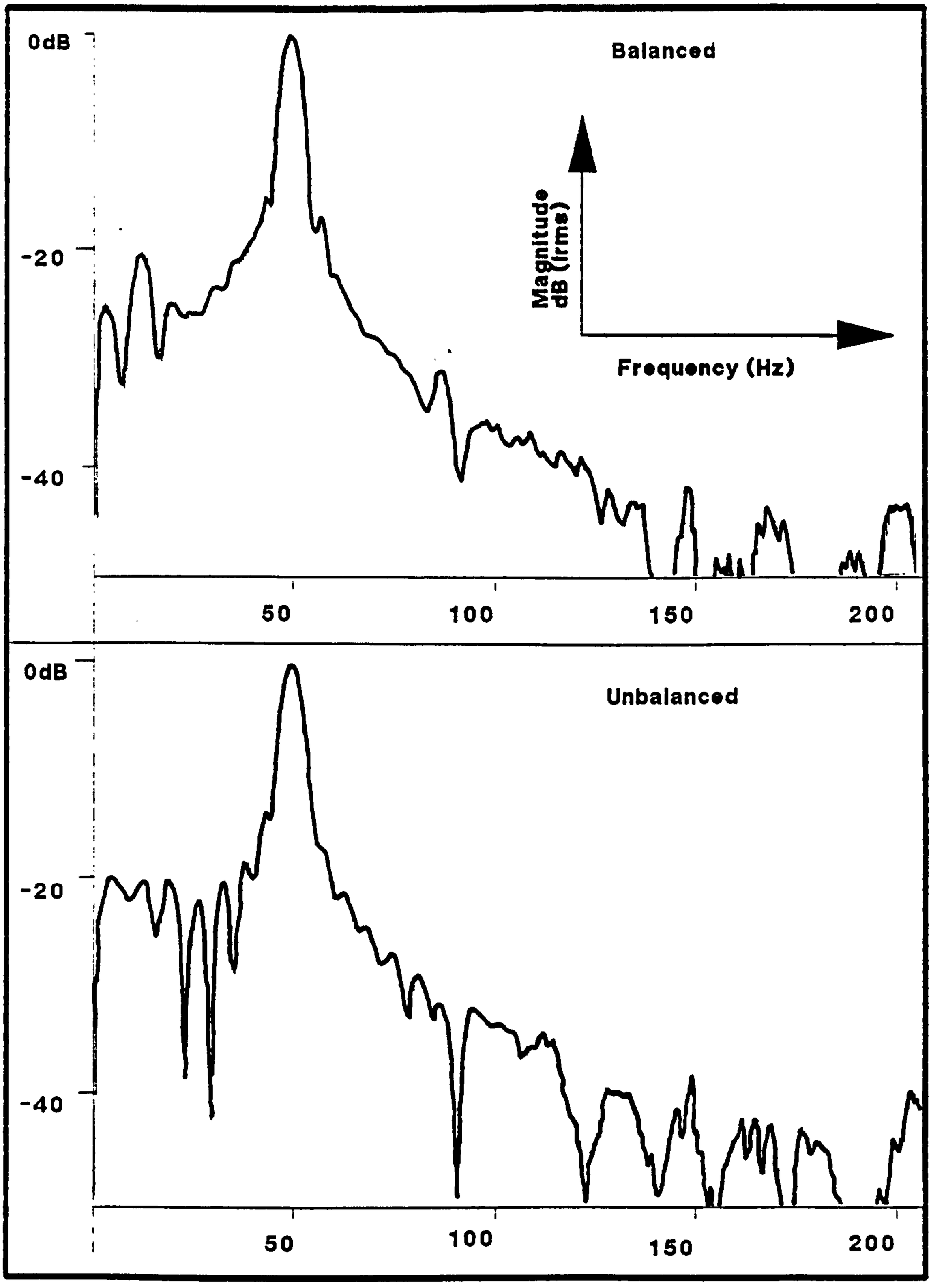

Figure 4.2: Line current spectra of, nominally balanced and with R_{ext}=0.4Ω for wound rotor machine.

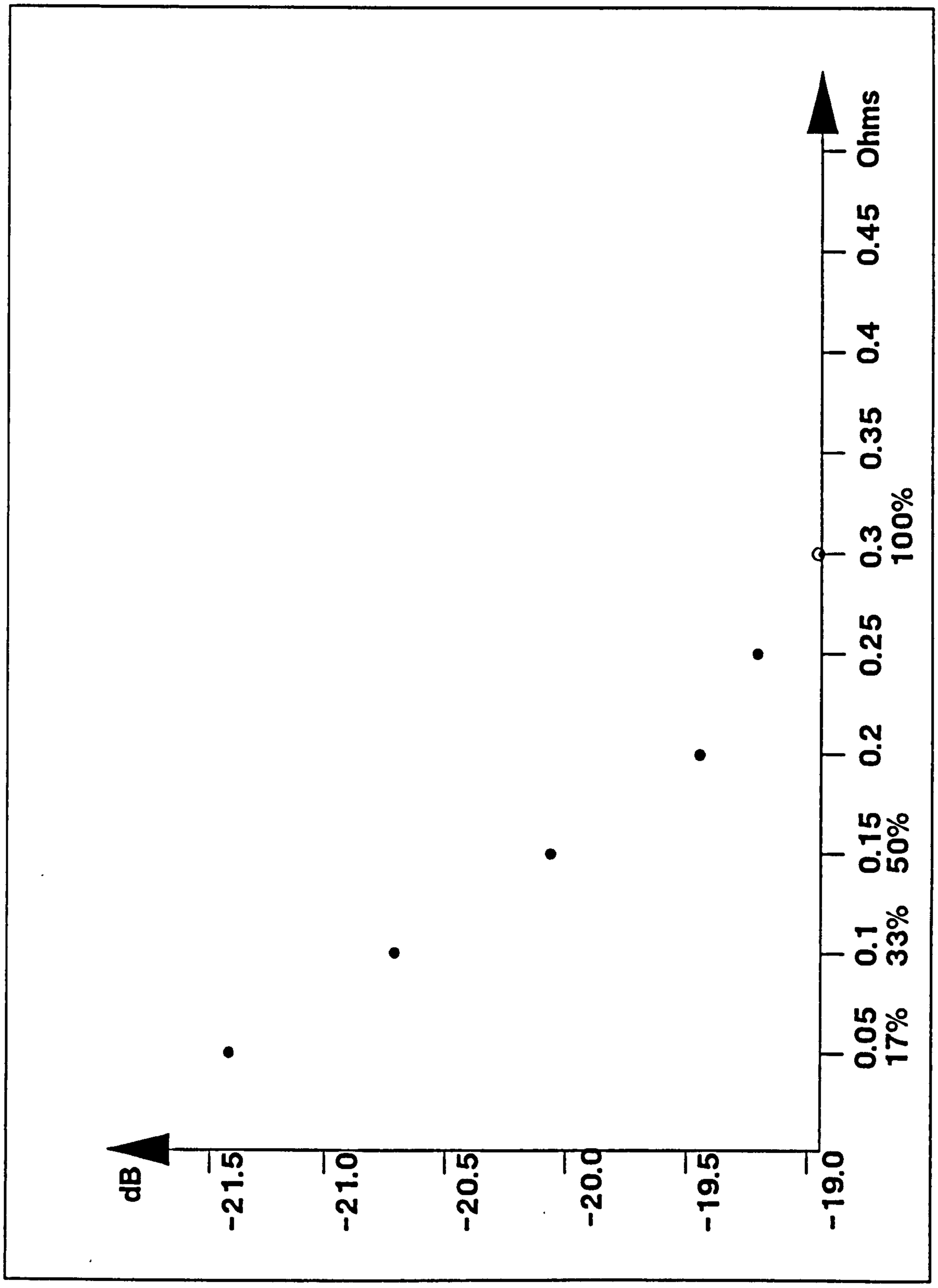

Figure 4.3: "13Hz"/50Hz amplitude ratio versus rotor imbalance.

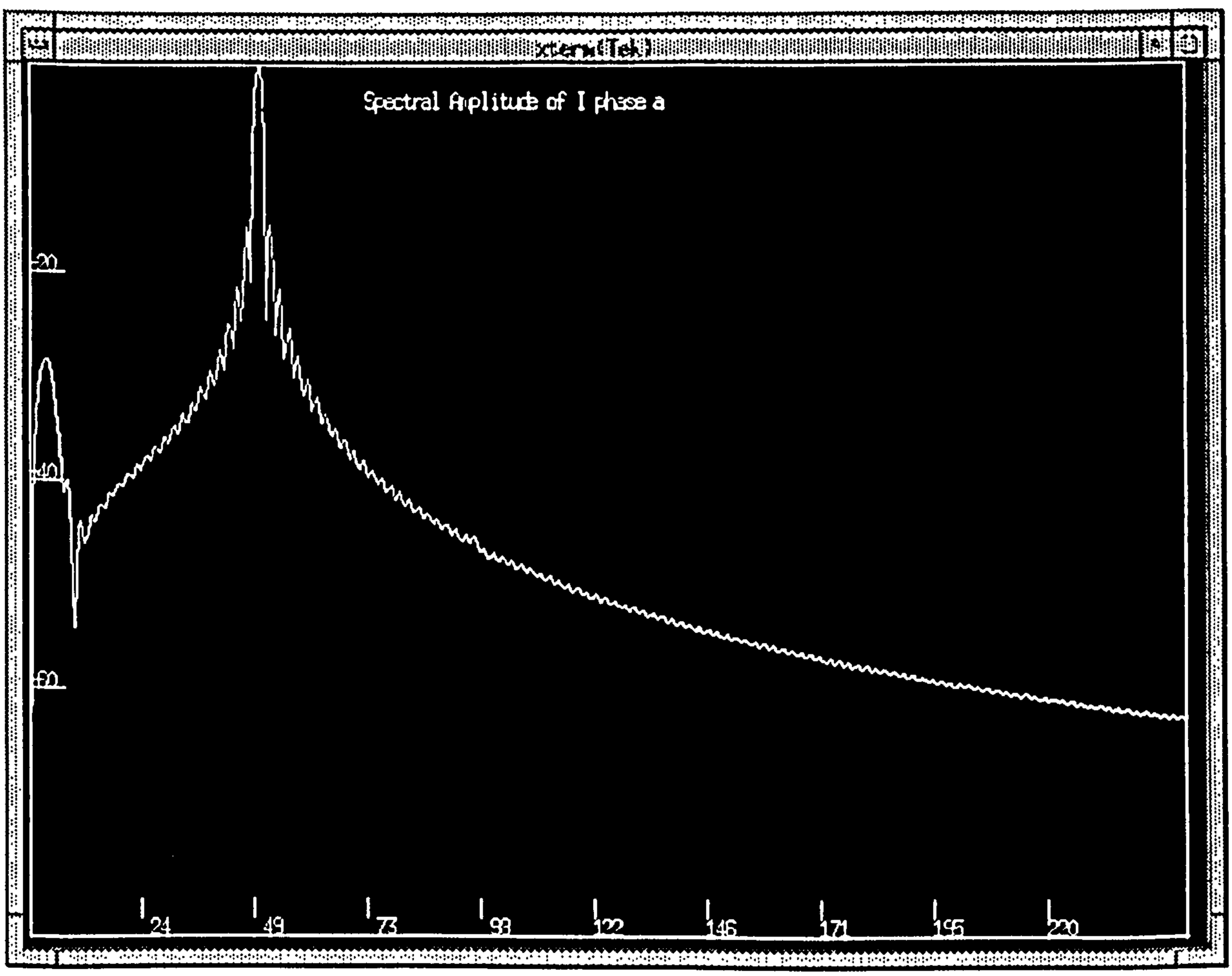

Figure 4.4: Simulated line current spectra for the balanced and unbalanced conditions.

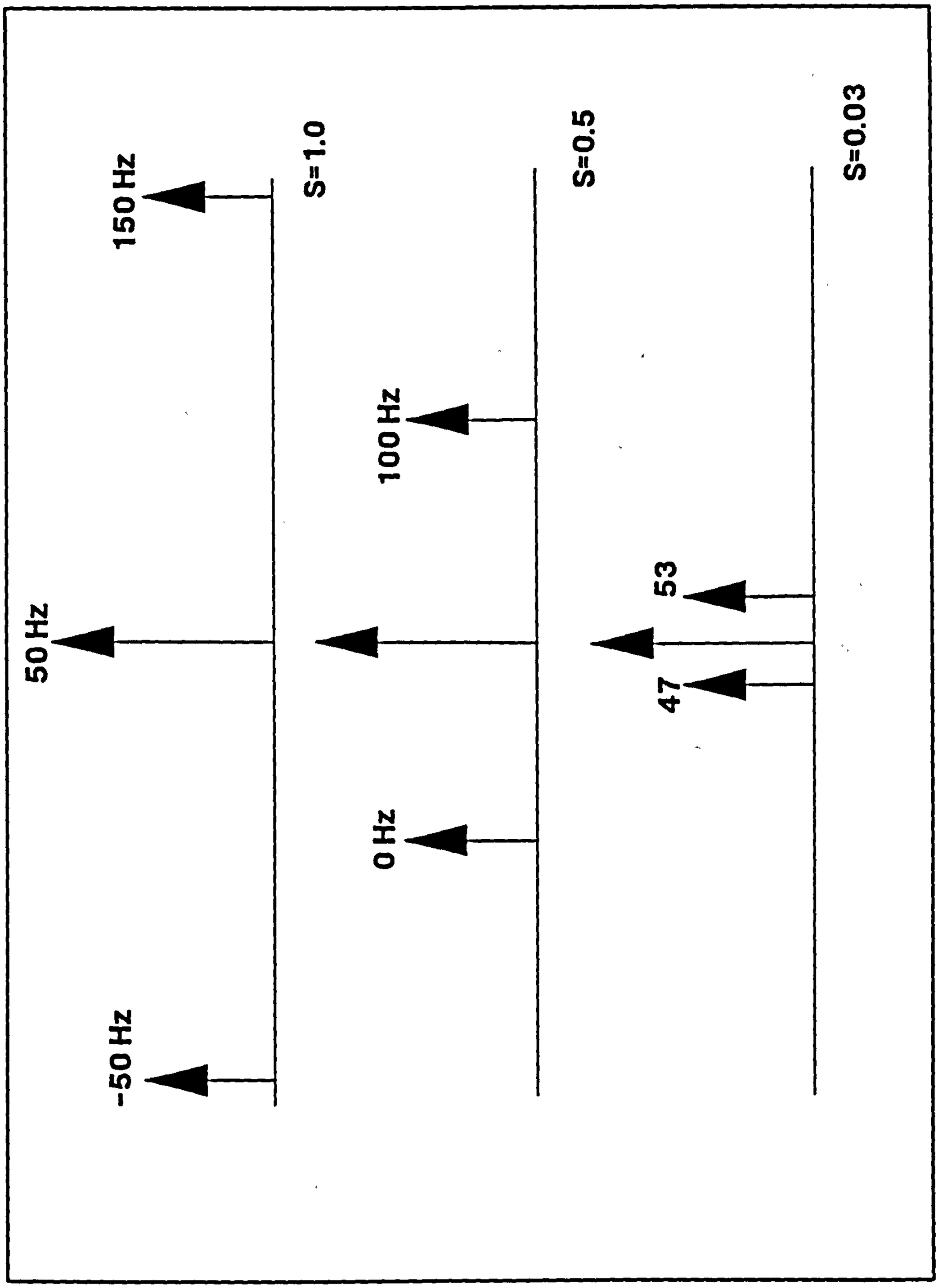

Figure 4.5: Side band variation in frequency with slip.

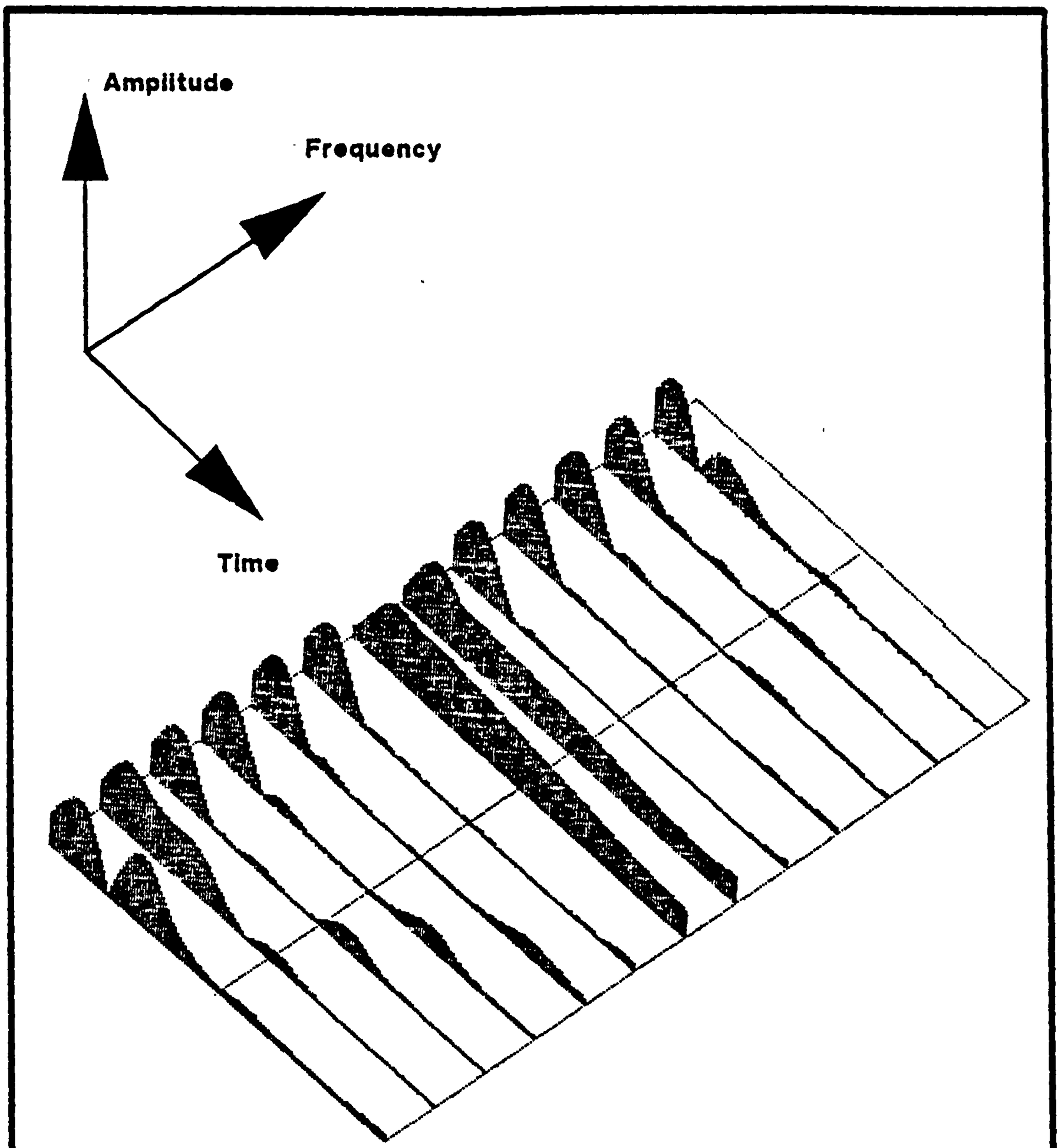

Real Machine 4% Imbalance

Figure 4.6: Vocoder spectogram of nominally balanced machine.

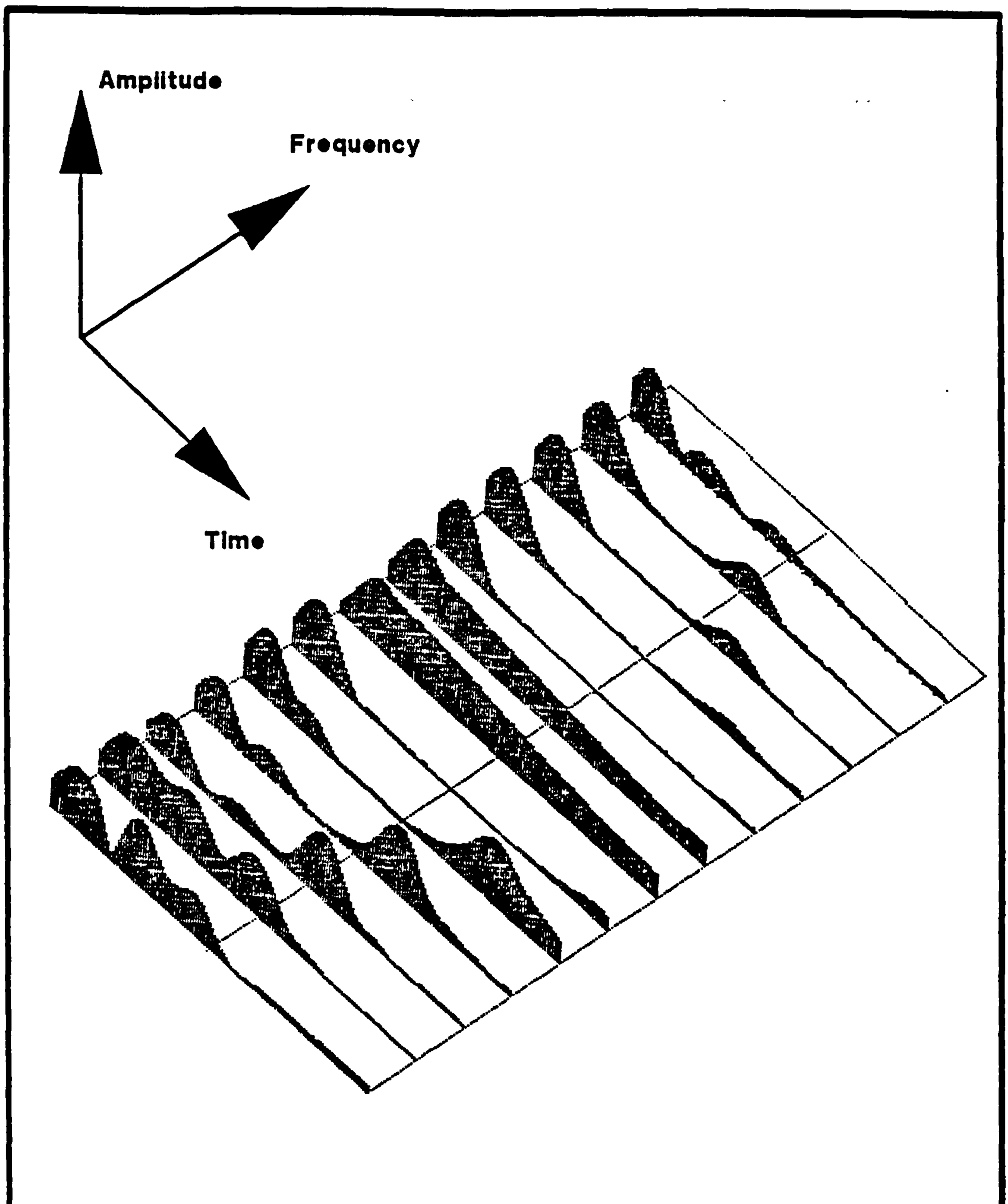

Figure 4.7: Vocoder spectogram of machine with 58% imbalance.

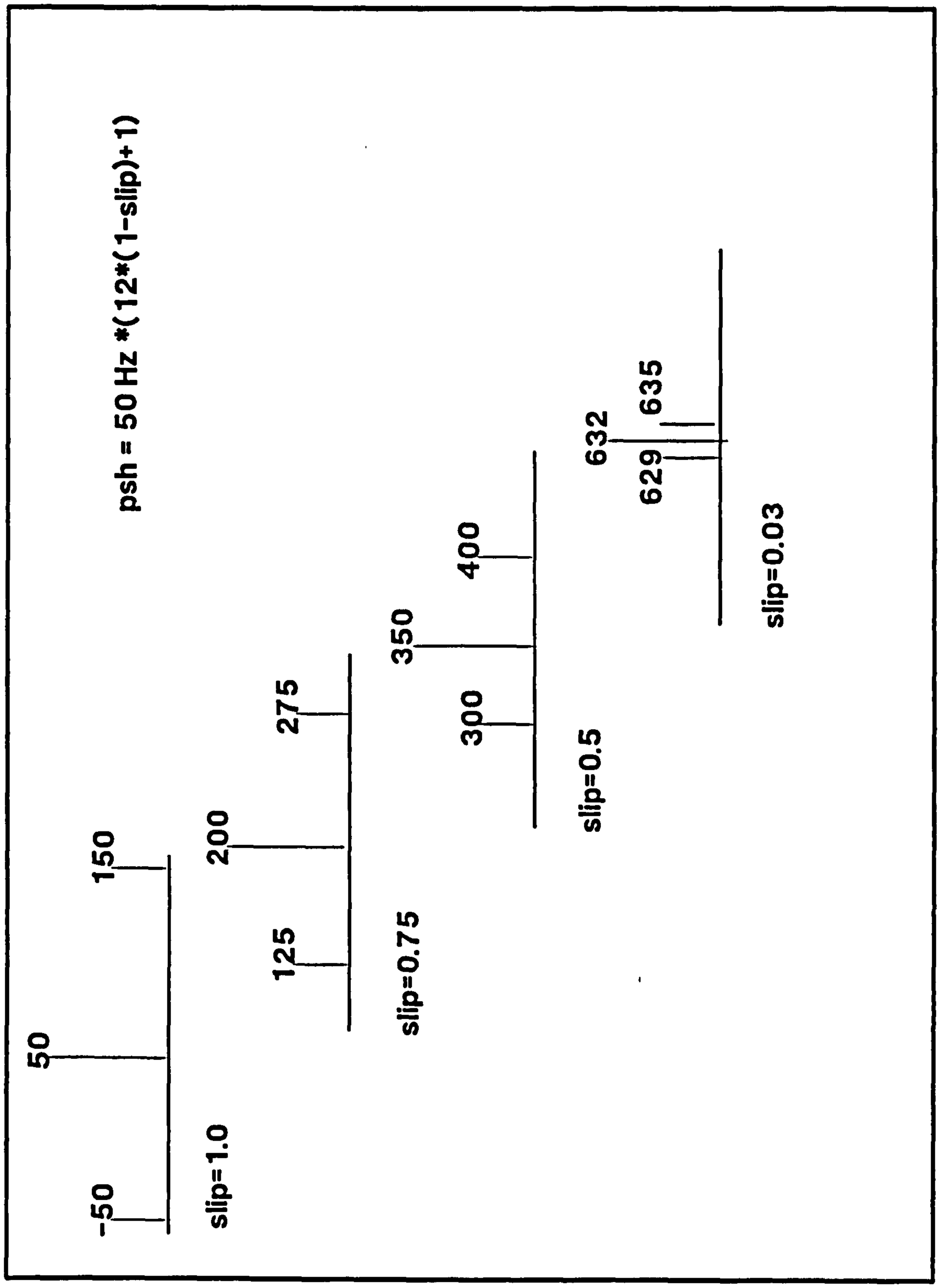

Figure 4.8: Side band of PSH during the starting transient.

Chapter 5

Squirrel Cage Rotor

5.1 51 Bar Rotor

5.1.1 Introduction

The squirrel cage rotor is the most common type of rotor found in industry. This is mainly due to the simplicity of design and hence ease of fabrication and low cost of production. For machines rated at 200kW or less, the squirrel cage rotor is usually fabricated using the die cast process using an aluminium alloy. Since the cast rotor bars and end rings are fabricated in one process the unit as a whole is not repairable. For larger machines the bars are individually fixed (brazed) onto the end ring sections of the rotor and are usually made from a copper alloy. These rotors are serviceable and damaged bars can be replaced or all the bars may be replaced at specific service intervals. This second method of fabrication however can result in bars breaking off from the rotor into the air gap with possible damage to the machine as a whole but in particular the relatively fragile and expensive stator windings. This scenario is unlikely to occur in the die cast rotor where the aluminium bars are within the laminated core and as such held by the core metal.

The squirrel cage rotors used in this research work were all die cast 51 slot single cage. The method of breaking the rotor bars was to drill a small hole out of the core material which also removed the cast bar embedded. To obtain a high

resistance bar a smaller hole was drilled removing only part of the bar section. High resistance end rings were obtained by milling out a section of the end ring between two bars.

5.1.2 Initial work

Prior to the purchase of two 51 slot squirrel cage rotors specifically for this research project, two 51 slot rotors available within the department were studied. One of these rotors was balanced and the other had three broken bars. The following cases were studied :-

- Balanced rotor full load start
- 3 broken bars full load start
- 3 broken bars no load start
- 3 broken bars full load start (high temperature)

In the first three cases the rotors were initially at room temperature, in the fourth the machine had been run on full load for an hour reaching its operating temperature quoted as 85°C.

Analysis of the spectograms indicated that the ratio of LSB energy to that of the 50Hz component increased by 21dB for the case of 3 broken bars over the balanced condition. Steady state measurements were also performed on these two rotors which resulted in an amplitude increase of the LSB by 26dB.

The relationship between the energy ($\propto V^2$) measured on the spectogram and the r.m.s. voltage measured in steady state must be taken into account before a meaningful comparison can be made. This can easily be implemented by halving the dB figures obtained for the spectogram. Thus the present analysis was 15.5dB (26 - 10.5)dB poorer that that of the steady state. i.e. its sensitivity to rotor faults was one sixth that of the steady state method. It would be necessary to improve the sensitivity of the analysis so that it was at least as good as the steady state method.

For the case of the rotor with 3 broken bars on full load start, at room temperature and at 85°C, there was no significant change in the LSB measurements. This clearly indicated independence of temperature which was a desirable feature. Two other points to note were that the "hot" rotor condition gave more consistent results for each separate transient and that the USB was of significantly less energy that that found for the wound rotor machine. In fact the USB disappeared at about half speed, in contrast with the wound rotor case where it was still clearly observable. This was due to the differences in the leakage saturation characteristic for the wound and cage machines which is discussed in Chapter 7.

In the case of the unbalanced rotor on no load start, the same general features were observed though the energy of the LSB was significantly less than that of the full load case. This result was the first experimental evidence that this technique could be applied to no load/light load testing. The ability to test machines under no load conditions suggested a possible edge over steady state techniques which required the machine under inspection to be running at least at 25% full load.

At this point it was decided to concentrate on full load starts and refine the signal processing until results comparable to that obtained from steady state analysis were obtained. No load transients would then be examined.

5.1.3 Improvement in Analysis

The nature of the analysis of the spectogram was that the energy of channels 1 to 5 (7.8Hz - 39Hz) were summed for the period over half speed. This excluded the switching noise and the synchronous machine effect occurring during the initial stages of the transient. The summation from half speed onwards however included any noise in a channel before the sideband passed through and the noise from this point until the end of the transient. This noise was reducing the sensitivity of the LSB measurement to almost a sixth that of the steady state measurements. A better method was developed whereby the computer detected the approximate half speed point by detecting a minimum in the energy of channel 2 which had been observed to occur in all spectograms. From this point the software proceeded to track the peak of the sideband as it increased

in frequency. This was relatively simple in that each channel was searched from the half speed point until a maximum was located. This maximum is of course the LSB passing through the centre frequency of that particular channel. This method eliminated much of the background noise that had previously been included in the measurements and also enabled tracking of the PSH. The frequency of the LSB was relatively easy to determine from the amplitude maximas of each channel, the centre frequencies of which were known. Having obtained the LSB frequency at any point in time during the latter part of the transient the value of slip could be determined. With this value of slip it was possible to calculate the frequency of the PSH at any point in time and thus measure its energy. Results from this improved method of processing and shown in Table [5.1].

Filename	(fe/lsb)dB	(fe/usb)dB	(fe/psh)dB
v513un1	45.8	94.7	80.2
v513un2	45.8	91.2	80.7
v513un3	46.1	88.7	83.1
v513un4	46.2	89.2	80.1
v513un5	46.5	90.5	81.0
Average	46.08	90.86	81
StndDev	0.3	2.36	1.2
v51bal1	96.8	102.7	68.7
v51bal2	97.1	101.6	67.7
v51bal3	93.7	98.8	69.2
v51bal4	96.9	96.1	68.7
v51bal5	98.9	96.8	67.8
Average	96.7	99.2	68.4
StndDev	1.9	2.9	0.6
v513h1	46.1	90.5	82.0
v513h2	45.9	90.5	82.6
v513h3	46.0	89.4	78.6
v513h4	46.0	88.3	80.6
v513h5	46.1	89.3	79.4
Average	46.0	89.6	80.6
StndDev	0.1	0.92	1.7

Table 5.1: Results of improved Vocoder processing for balanced (v51bal*), 3 broken bars (v513un*) and hot rotor with 3 broken bars (v513h*).

Halving the numbers in Table [5.1] gives results suitable for comparison with the steady state amplitude values. This results in an increase of 26dB for the LSB measurement for the transient case which agrees exactly with the increase observed in the steady state case. This is unusual as subsequent sets of tests did show that both methods gave results which would fluctuate slightly for the same fault condition giving rise to differences of about 2dB.

5.1.4 USB and PSH Components

Table [5.1] also indicates that the USB and PSH show amplitude changes of 4dB and 6dB respectively, substantially less sensitive than the LSB of 26dB. Apart from the lack of sensitivity of the USB to the rotor fault level, it has a high variance. This is thought to be a function of the switching angle which dictates the initial effect of saturation. It has been shown in steady state theory that the effect of saturation or imbalance of the supply is to generate a third harmonic of slip which contributes to the amplitude of the USB [2]. On this basis and that of the observed variance in the experimental work it was concluded that this USB component was not suitable for reliable diagnosis without considerable effort and control.

There are several factors which cause the appearance of the USB, namely, speed variation, oscillating load torque, 3^{rd} harmonics in the supply and imbalanced supply voltages. In the case of a rotor impedance imbalance, the high resistance phase or bar cannot contribute its normal torque and hence the average torque developed by the whole machine is oscillatory in nature. An oscillating torque gives rise to an oscillating speed which in turn modulates the line current. This has the effect of reducing the amplitude of the LSB and producing an USB component [6]. The USB can also be generated due to the negative sequence component of the applied voltage present if there is an imbalance in the supply allowing 3^{rd} harmonic currents to flow. Measurement of the supply voltages showed than a difference of upto 12dB could exist between the 3^{rd} harmonic content of the lines.

The PSH (k=+1) can be used to indicate rotor imbalance, however as with the USB the resolution is poor (6dB amplitude change). The PSH can only be measured accurately after the LSB had been tracked and this seemed pointless

in view of the sensitivity to imbalance of the LSB.

5.1.5 LSB Amplitude during Transient and Steady State

It is of interest to compare the amplitude of the LSB in both transient and steady state conditions. In steady state, on full load, with three broken bars on the rotor the LSB amplitude was in the region of 11mA r.m.s. (Full load current 19Amps). In the transient case the peak amplitude after half speed for the LSB as it passes through the vocoder channel number 3 (23.4Hz) is approximately 1.1 Amps peak. Thus a highly observable component exists during the starting transient period which has a large signal to noise ratio and this of course is a desirable feature. It should be borne in mind at this time that it is the change in the component of interest that dictates the fault resolution rather than its absolute magnitude.

5.1.6 Rotor Acceleration

An interesting result was observed with this refined processing method. This method detected half speed by analysis of the minimum in channel number 2 (15.6Hz) and from that point in time tracked the frequency of the LSB. As a matter of course the time taken to reach the maximum amplitude through each of channels 3 and 4 (T3,T4) was noted and from this it was clear that a machine with broken bars accelerates to speed in less time than that of a balanced rotor. The measured time included the constant delay in the vocoder channels of 256ms. Figures [5.1,5.2] show the line current waveform for full load starts with no broken bars and three broken bars. The unbalanced rotor in this case reaches operation speed in about 50ms less than the time taken by the balanced rotor. The rotational inertia of the rotor is not thought to be changed significantly by the small holes bored out to break the bars. Thus the energy required to accelerate the rotor to speed in both cases must be similar. The power dissipated in the 3 broken bar case must be increased since the time taken to reach operating speed is reduced. This will cause an increase in the I^2R losses over that of the balanced machine. It has been shown by Gaydon [4] that rotor bars tend to fail in groups and that once a bar breaks the adjacent bars are more

likely to fail. This has been indirectly observed in this research project in that a damaged rotor will cause I^2R heating to increase and presumably increase metal fatigue within the machine.

A similar trend was observed for the wound rotor machine in that a higher external resistance in one phase rotor reduced the run up time. Increasing the resistances in all three phases is a standard technique for for increasing starting torque [52]. The torque speed characteristic is moved by the inclusion of these resistors so that more torque is available in the early stages of the run up and less at operational speed. The observed effect is thought to be simply due to a phase (or apparent phase in cage rotor) having its characteristic changed so more torque is available between standstill and half speed. It is of interest to note that the induction motor models did not exhibit this response with a single high resistance rotor phase as discussed in Chapter 7.

It has also been observed that at any one fault level there is still a variation in the time taken to reach half speed and this is thought to be dependent on both switching angle and initial rotor position. These effects were to be investigated later by experimental observation and use of the newly developed 3 phase I.M. computer model.

5.2 Advanced Work on Cage Rotors

Two 51 bar squirrel cage rotors were purchased to extend the range of fault levels studied. A number of rotor conditions were investigated during both full load and no load starts. These conditions are itemised below :-

- balanced rotor
- rotor with one high resistance bar
- rotor with one broken bar
- rotor with one broken bar and rotor position control at start
- rotor with one broken bar and static airgap eccentricity
- rotor with two broken bars

- rotor with three broken bars
- balanced rotor with high resistance end-ring

Ten starting transients, on full load and no load were performed on the new 51 bar balanced rotor as were the standard running light/locked rotor tests. This data would be used as a reference for the faulty conditions to be examined later and for use in the computer model.

The first fault level to be studied was of a single high resistance bar in the rotor. Some experimental work was carried out on a "control bar" to compare the theoretical increase in resistance expected by drilling out holes in the bar with the measured increase in bar resistance. This control bar was not of the same shape nor made of the same material as the rotor bars but served to compare theoretically predicted and measured increases in resistance. It was found that small holes widely separated had better correlation between the theoretical and measured increases in bar resistance. Based on the results from the control bar experiment, four widely separated, 5.5mm diameter holes were drilled out of a single bar within the rotor. The diameter of bars was 6.985mm which meant that a substantial portion of the cross sectional area of the rotor bar had been removed, but not open circuited completely.

Ten transient starts for both full and no load were recorded and processed with the phase vocoder. Differentiation between the healthy rotor and rotor with high resistance bar was not possible for the no load start. The inherent variation (noise) obtained from the results of the healthy rotor was sufficient to mask the presence of the high resistance bar. It was quite apparent from the results that the present signal processing and extraction techniques were not suitable for small fault levels on no load starts. In view of this only the third and fourth channels (23.4 - 31.2Hz) of the vocoder were used to determine fault level. It was known from experimentation on full load starts that the LSB component reached a maximum in or around this frequency range. This was certainly observed to be the case with the initial work on a 51 bar rotor having three broken bars. The analysis had thus been simplified to observing the output of only two of the sixty four vocoder channels available. Further more, the vocoder output was changed from one proportional to the energy of a channel to one which was proportional to the amplitude. This allowed direct

comparison between steady state and transient results. The wideband nature of the phase vocoder was no longer required and in fact became an inconvenience due to its numerically intensive solution, requiring much time to perform.

The implementation of a much simpler processing technique using finite impulse response (FIR) bandpass filter was then undertaken.

In the meantime experimental work continued to be processed with the phase vocoder. The results for the balanced rotor condition are shown in Table [5.2].

Filename	T3	A3	T4	A4
Vse1nl1	596	4.1	643	3.0
Vse1nl2	640	2.9	644	3.7
Vse1nl3	596	2.4	644	4.9
Vse1nl4	620	2.4	670	3.3
Vse1nl5	539	2.7	587	2.3
Vse1nl6	552	1.8	598	1.1
Vse1nl7	*	*	641	4.7
Vse1nl8	608	2.9	*	*
Vse1nl9	654	4.2	681	2.7
Vse1nl10	585	4.1	632	3.2

Table 5.2: Time of maximum (T)ms and amplitude (A) after half speed for vocoder channels 3 and 4 for a balanced 51 bar rotor, no load start. * unobservable components.

Thus for the balanced rotor, averages and standard deviations for channels three and four are respectively 3.06, 0.87 and 3.2, 1.17. These figures relate not only to the condition of the rotor but also to the background noise and in some cases (* entries in Table [5.2]) were not of sufficient magnitude to be observable. The rotor of course cannot be perfectly balanced and the peak of the LSB could only be observed during the full load start, this inherent imbalance due to the manufacturing process can also be observed in steady state analysis.

Observing again only the third and fourth channels of the phase vocoder the results of Table [5.3] were obtained for the case of the high resistance bar condition.

Thus for the rotor with a high resistance bar, averages and standard deviations for channels three and four are respectively 8.3, 1.25 and 6.4, 1.2. The high

resistance bar in the rotor can clearly be identified from this technique from the line current waveform of a no load start.

All experimental work to this point had not exercised control over the initial position of the rotor. Twenty more records were taken with the high resistance bar fault on no load start. In each case the rotor was moved to a specific starting position before the motor was switched on. Despite the initial rotor position control, there was still a variation in the time taken to reach half speed. The angle of switching of the supply was thought to be a likely cause so the phase of switching was also noted. Two records of the twenty were switched at the same angle though there was still a difference of 10ms as to when the peak passed through the 3rd channel. Thus with similar initial rotor starting angle and phase of switching there still appeared to be other factors influencing the run up time of the machine. The sampling of the line current waveform was at 1ms and this results in a minimum phase resolution of 18°. This could certainly be a source of error, however remanence and non-simultaneous switching could also be contributory factors. It was imperative for simplicity to have a diagnosis technique which was independent of all these factors.

Computer simulation of the induction motor with variable switching angle and with a range of initial rotor starting positions is discussed in Chapter 7.

5.2.1 Rotor with One Broken Bar

The next fault condition studied was for a rotor with one broken bar. Ten records for both full load and no load starts were taken. Work presently concentrated on the no load conditions since they were more difficult to determine due to the smaller sideband component. These results are presented in Table [5.4].

The average and standard deviation for channels three and four on the vocoder are 10.7, 1.4 and 7.7, 1.38 respectively. Comparison of Tables [5.2] and [5.4] show that the maximum amplitude passing through channels three and four show a marked increase for the one broken bar condition over that of the balanced condition.

5.2.2 Static Airgap Eccentricity

It was necessary to determine if any inherent static airgap eccentricity within the machine could lead to an erroneous diagnosis. In view of this ten records for both full load and no load were taken using the rotor with a single broken bar. In addition 60% static airgap eccentricity was introduced into the machine by offsetting the position of the stator with respect to the rotor by use of calibrated metal spacers. Static airgap eccentricity has been shown to increase the amplitude of the PSH [3]. The processed results for the single broken bar plus static air gap eccentricity no load case are shown in Table [5.5].

It can be seen that the introduction of 60% static airgap eccentricity has made little difference to the results over those for the single broken bar rotor without eccentricity.

No rotor of this type was available with dynamic airgap eccentricity. It has been shown that the introduction of dynamic eccentricity generates new frequency components in the line current spectrum [3]. The frequency of these components is given by :-

$$Fpsh = \{((R \mp n_d)/polepairs)(1-s) \mp k\}\, f \tag{5.1}$$

where
R= 24 Winding slots on wound rotor
k= time harmonic of stator MMF
n_d= harmonic value of dynamic eccentricity wave
f= 50Hz supply frequency
polepairs= 2

For the case of the fundamental stator MMF harmonic (k=1) and fundamental harmonic of the dynamic eccentricity wave (n_d=1), four frequency components are generated. Two have frequency values of 50Hz for unity slip rising to 675Hz and 625Hz respectively at synchronous speed. The other two have frequency values of -50Hz for unity slip rising to 575Hz and 525Hz at synchronous speed.

5.2.3 Summary of Vocoder Results

In summary, the average results of the preceding tests are shown in Table [5.6].

From Table [5.6] it can be seen that there is an increase in the LSB amplitude of 10.8dB for the single broken bar condition over that of the balanced condition. The single broken bar case with and without static airgap eccentricity shows little difference of maximum amplitude. Since the level of eccentricity is 60%, it is assumed that the inherent levels in operating machines will normally be substantially less than this. On this basis it is clear that static airgap eccentricity should not confuse the present diagnostic method.

In the case of the high resistance bar (supposedly 10%), it is clear that the fault level is almost as severe as the single broken bar condition. This was also found to be the case in steady state analysis indicating, despite the control bar experimentation that the fault level may well be larger than a 10% increase in a bar's resistance. However the sensitivity of the LSB was later found to be largest for smaller degrees of imbalance and without further experimentation it is difficult to quantify this level of fault.

5.2.4 Application of FIR Bandpass Filter

By this time the software to implement a FIR bandpass filter by convolution had been completed. The detail of this signal processing method is presented in Appendix C. The phase vocoder was now superseded by this simpler and more versatile processing method. Some time was spent optimising the filter parameters for this study. If the bandpass filter was incremented in 1Hz steps between 0-50Hz the diagrams shown in Figs [5.3 and 5.4], which like the spectograms, display amplitude versus frequency versus time, are obtained for the waveforms of Fig.[5.1,5.2]. These diagrams show the track of the LSB as the transient progresses if a rotor fault is present. These diagrams are plotted up-ended for reasons of spacing and should be viewed with the label or page number to the left. The transient starts at the left side (standstill) and progresses to the right where operational speed is reached. Each line represents a 1Hz increase in frequency from the bottom of the diagram starting at 1Hz. Amplitude is shown in the conventional manner with a peak having a larger amplitude than a trough.

The LSB component can be seen to move in frequency from 50Hz to 0Hz and then from 0Hz up towards the 50Hz component.

Of course it was not necessary to perform all fifty filtering operations for a diagnosis, though the resulting diagrams were initially helpful in selecting appropriate areas of interest. All that is required for the purposes of diagnosis is a filter which will intercept the LSB when it peaks. There were several considerations in the selection of the filter parameters and centre frequencies, for instance, the peak amplitude of the sideband was at 15Hz. The use of a filter with a centre frequency of 15Hz however was not optimal since there was a large variance in the results. The bandwidth of the filter used could also create problems, too small a bandwidth and the filter would ring, corrupting the data. Eventually the two centre frequencies of 21Hz and 24Hz were selected for each filter. It was not imperative to observe the output of two filters, however it was thought prudent to observe the LSB at two points in case any unexpected results occurred.

A typical output from one of these filters for both the balanced and faulted rotor is shown in Fig.[5.5]. The two plots shown in Fig. [5.5] are in fact one slice of the diagrams shown in Figs. [5.3,5.4]. Referring to Fig. [5.5], the initial peaks occur at switch-on. In the case of the faulted condition two subsequent peaks can be observed. There are therefore three clearly observable peaks from the demodulated output of the 21Hz filter. The second peak is the LSB passing through 21Hz on its way from 50Hz to 0Hz at half speed. The third peak is the LSB being intercepted on its way from 0Hz to 50Hz during the post half speed region. It is the third peak of these full load starts which is used to indicate the degree of fault level.

For the case of no load starts, the LSB is smaller in amplitude and the whole transient period is shorter as shown in Fig. [5.6] for the case of one broken bar. The demodulated output of the 21Hz filter for the conditions of balanced and one broken bar are shown in Fig. [5.7] for no load starts.As with the full load start a large peak occurs at switch-on. However in the faulted case only a second peak can be observed and this is the LSB in the post half speed region. The LSB in the pre-half speed region has such a low amplitude that it is not visible. It is the second peak that is used to diagnose the fault level in the rotor

for no load starts and two typical sets of results are shown in Tables [5.7,5.8] for both the 21Hz and 24Hz filters. Averages for these results are presented in Table [5.9].

5.2.5 FIR Processing of Multi-Bar Faults

This FIR filtering method of analysing the line current waveforms detected a change of amplitude in the 21Hz filter of 11.4dB between the balanced and single broken bar conditions. This was a slight improvement over the best results that were obtained from the phase vocoder which only detected a 10.8dB change between these two same conditions. However the FIR method had a major benefit in that it required a fraction of the processing time used by the phase vocoder. The signal processing necessary had thus been substantially reduced.

All the broken bar conditions indicated at the beginning of this Chapter were now reprocessed/processed using this FIR technique plus the case of an identical type of rotor with ten broken bars. The averages for these fault conditions, for both cases of no-load and full-load start using a 21Hz bandpass filter are presented in Table [5.10] and the change of the component of interest in Table [5.11].

The results of Table [5.11] are shown diagrammatically in Fig.[5.8]. This graph shows that the change in the LSB amplitude is greater for full-load starts than that of no-load starts. The full-load conditions for both transient and steady state show similar sensitivity to imbalance upto two broken bars where they diverge slightly. It does appear from the data set that the transient analysis has a better sensitivity for full load conditions with greater than two bars broken. This is not thought to be an advantage since these numbers of broken bars are considered large faults which would ideally be detected and corrected before reaching these levels. For the no-load transient results which also have their standard deviations indicated (Fig.[5.8]), there is a clear separation between the rotor fault levels. As with steady state results, progressively more broken bars result in smaller increases in the component of interest with maximum sensitivity conveniently at the low fault level condition.

The results from the other experimental conditions studied are presented in

Table [5.12]. The rotor had a single broken bar in all cases apart from the high resistance bar experiment.

In order to asses the influence of initial rotor position, ten transients were recorded for each of the rotor starting angles indicated in Table [5.12] under no-load starting conditions. As can be seen from the results the initial rotor position does not adversely affect the diagnosis. None of the values measured fall outwith the standard deviation of the no-load, single broken bar average result obtained from Table [5.9] for a starting position of 0°. (10.25dB - 12.5dB)

5.2.6 High Resistance End-Rings

As to be discussed in Chapter 7, concern was expressed about the representation of the end-ring sections by the three phase model. This suggested that high resistance end-rings could not be simply considered as high resistance bars and as such should manifest themselves differently. Steady state techniques do not presently differentiate between bar and end-ring faults, instead a measure of the condition of the rotor called the broken bar factor (BBF) is presented. Nevertheless experimentation was carried out using an otherwise healthy rotor which had a small cross section of one end-ring removed. This resulted in a high resistance end-ring section between two bars. The subsequent signal processing gave rise to Fig.[5.9] where the sideband component can be clearly observed.

For comparison Fig.[5.10] represents the two broken bar condition. The maximum amplitude of the LSB in the post half speed region is similar to that obtained for the high resistance end-ring condition, the very reason that the two broken bar condition was chosen for comparison. However if the diagrams of Fig.[5.9] and Fig.[5.10] are compared in the pre-half speed region, it can be seen that the LSB is much more prominent for the end-ring fault. Comparison of the ratio of the two side band peaks in the pre- and post half speed regions at the frequency of 21Hz shows that the high resistance end ring condition results in a lower sideband peak that is 13% higher than the case of two broken bars.

Thus differentiation between end-ring faults and bar faults may be possible but more importantly this result clearly indicated that the rotor modelling was inadequate. Interest had been expressed by industry on the ability to

differentiate between bar and end-ring problems, since it is apparently well known that end-ring failures cause less problems than bar failures.

5.3 Discussion

In conclusion, a method has been devised to indicate the number of broken bars within a rotor by analysis of the line current waveform during the starting transient. This method has been tested for the laboratory machine having a squirrel cage rotor and shown to be independent of :-

- point on wave switching
- initial position of the rotor
- temperature of machine
- large values of static airgap eccentricity

However the present diagnostic technique only applies to the laboratory machine. With the laboratory machine faults could be introduced and components of interest measured. No theoretical prediction has been established to relate the amplitude of the LSB to the level of fault, though attempts were made using the models.

If this technique were to be applied to a wide range of machines then some method must be found to relate the LSB to fault level. This data could be obtained in two ways, either by acquiring information on a wide variety by experiment or deriving a prediction from a mathematical model. The first option would possibly take some years before sufficient information were obtained. For example, some present steady state techniques were developed from knowledge accrued over ten years comprising of data from over two thousand machines. The second option was investigated and though the 3 phase model did exhibit a similar response to rotor faults as with that of the real machine, it is not at the present time considered sufficiently developed to predict the LSB amplitude peak of an arbitrary machine with rotor bar faults.

Filename	T3	A3	T4	A4
Vse1nhi1	408	9	441	6
Vse1nhi2	424	8	472	5
Vse1nhi3	452	6	443	5
Vse1nhi4	446	7	448	7
Vse1nhi5	433	9	460	6
Vse1nhi6	438	10	456	8
Vse1nhi7	419	8	448	7
Vse1nhi8	390	8	476	8
Vse1nhi9	422	10	451	7
Vse1nhi10	416	8	436	5

Table 5.3: Time of maximum (T)ms and amplitude (A) after half speed for vocoder channels 3 and 4 for the condition of a high resistance bar, no load start.

Filename	T3	A3	T4	A4
vse1n1b1	430	10.7	448	7.6
vse1n1b2	393	9.2	424	9.4
vse1n1b3	392	8.8	433	9.5
vse1n1b4	404	9.7	440	8.8
vse1n1b5	417	11.9	460	5.6
vse1n1b6	412	10.7	454	8.0
vse1n1b7	398	12.4	425	5.9
vse1n1b8	400	9.5	433	8.3
vse1n1b9	412	13.0	459	6.5
vse1n1b0	416	10.7	422	7.3

Table 5.4: Time of maximum (T)ms and amplitude (A) after half speed for vocoder channels 3 and 4 for the condition of one broken bar, no load start.

Filename	T3	A3	T4	A4
vse1n1be1	419	10.9	448	7.6
vse1n1be2	443	10.9	452	7.6
vse1n1be3	430	10.4	451	8.3
vse1n1be4	440	11.5	451	8.5
vse1n1be5	388	14.5	460	6.5
vse1n1be6	427	10.9	451	6.5
vse1n1be7	419	11.2	459	6.8
vse1n1be8	424	10.4	459	8.0
vse1n1be9	424	11.9	454	6.5
vse1n1be0	416	10.0	441	9.2

Table 5.5: Time of maximum (T)ms and amplitude (A) after half speed for vocoder channels 3 and 4 for the condition of one broken bar and 60% static airgap eccentricity, no load start.

Condition	A3	SD3	A4	SD4	A3dB.
N.L. Balanced	3.06	0.87	3.2	1.17	0dB
N.L. Hi-Res.	8.3	1.25	6.4	1.2	8.7dB
N.L. 1 Bar	10.7	1.7	7.7	1.38	10.8dB
N.L. 1Bar+S.E.	11.26	1.3	7.6	0.96	11.3dB

Table 5.6: Comparison of channel three and four maximum amplitude for fault conditions on no load start. Column six expresses A3 changes in dB re balanced condition.

Filename	21Hz	24Hz
wse1nl1	0.0071	0.0049
wse1nl2	0.0053	0.003
wse1nl3	0.0046	0.0026
wse1nl4	0.0031	0.0037
wse1nl5	0.0028	0.0031
wse1nl6	0.0027	0.0021
wse1nl7	0.0031	0.0046
wse1nl8	0.0039	0.0030
wse1nl9	0.0038	0.0048
wse1nl0	0.0048	0.005

Table 5.7: Second peak amplitude at 21Hz and 24Hz for balanced rotor on no-load start.

Filename	21Hz	24Hz
wse1n1b1	0.0149	0.0139
wse1n1b2	0.0126	0.0118
wse1n1b3	0.0122	0.0117
wse1n1b4	0.014	0.0122
wse1n1b5	0.0169	0.0144
wse1n1b6	0.0163	0.0134
wse1n1b7	0.0178	0.0155
wse1n1b8	0.0146	0.0121
wse1n1b9	0.0175	0.0162
wse1n1b0	0.0160	0.0136

Table 5.8: Second peak amplitude at 21Hz and 24Hz for rotor with one broken bar on no-load start.

Condition	21Hz	24Hz
Balanced	0.00412, 1.37e-3	0.00368, 1.07e-3
Broken Bar	0.01528, 1.95e-3	0.01348, 1.57e-3
Ratio	11.4dB	11.3dB

Table 5.9: Average, Standard deviation and ratio for the no-load case.

Condition	Transient F.L.	Transient N.L.	Steady State
Balanced	0.0038	0.0041	-69.9dB
1 Broken Bar	0.0214	0.0153	-54.8dB
2 Broken Bars	0.0553	0.0359	-47.0dB
3 Broken Bars	0.0899	0.0596	-44.4dB
10 Broken Bars	*	0.167	-41.3dB

Table 5.10: Measured amplitude of significant component for a range of broken bar conditions. dB reference 1Vrms. * not acquired due to potential damage caused.

Condition	Transient F.L.	Transient N.L.	Steady State
Balanced	0dB	0dB	0dB
1 Broken Bar	15.0	11.5	15.1
2 Broken Bars	23.0	18.8	22.9
3 Broken Bars	27.5	23.3	25.5
10 Broken Bars	—	32.0	28.6

Table 5.11: Relative change for the component of interest with respect to the balanced condition.

Condition	Transient F.L.	Transient N.L.	Steady State
60% Static Eccentricity	14.9dB	10.5dB	—
45° Rotor Position	—	11.4	—
90° Rotor Position	—	11.4	—
180° Rotor Position	—	10.5	—
270° Rotor Position	—	10.4	—
315° Rotor Position	—	11.0	—
High Resistance Bar	12.6	8.7	12.0
Hi Res.End-Ring	23	19.5	23

Table 5.12:

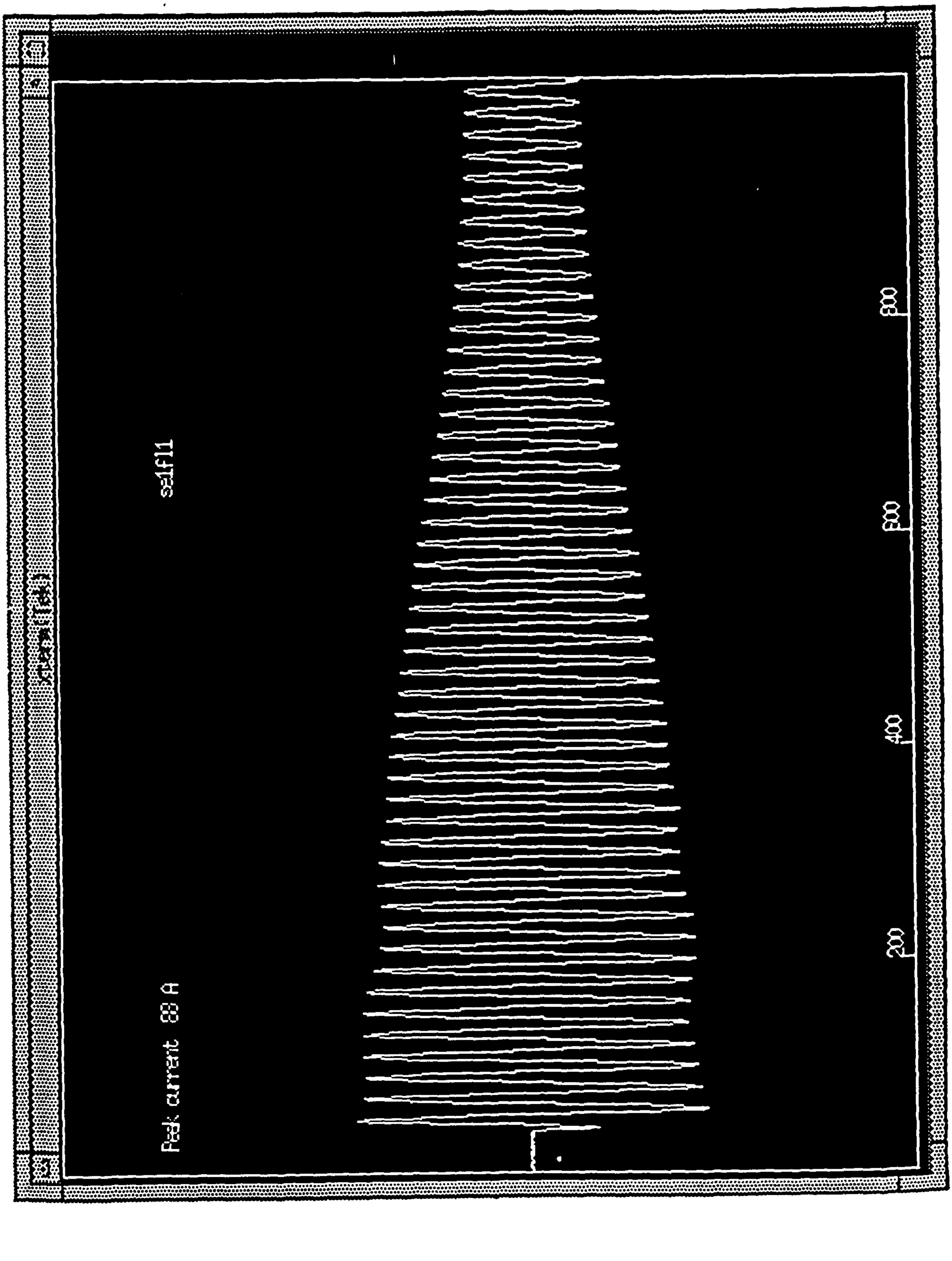

Figure 5.1: Line current waveform balanced rotor. Full load start.

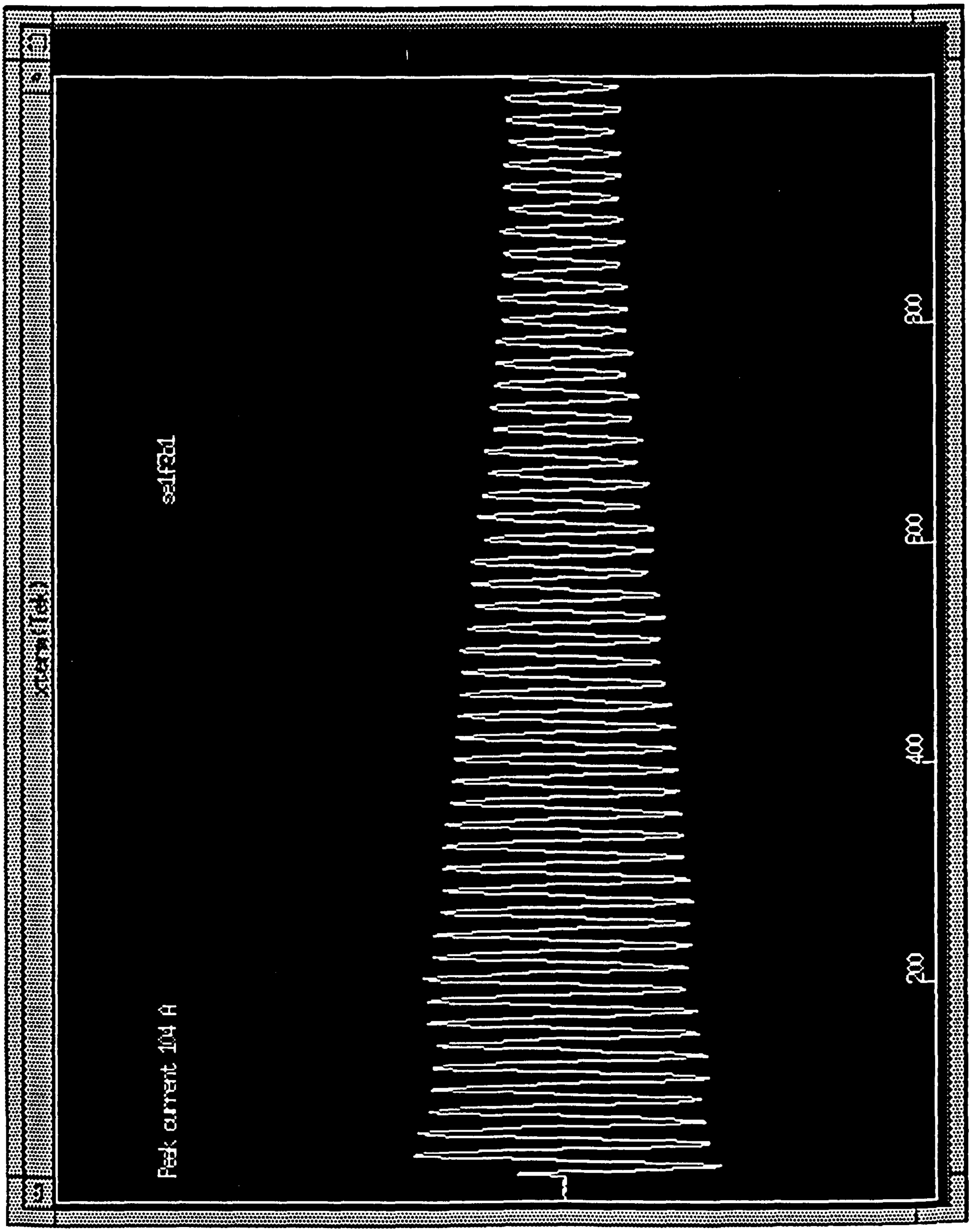

Figure 5.2: Line current waveform 3 broken bars. Full load start.

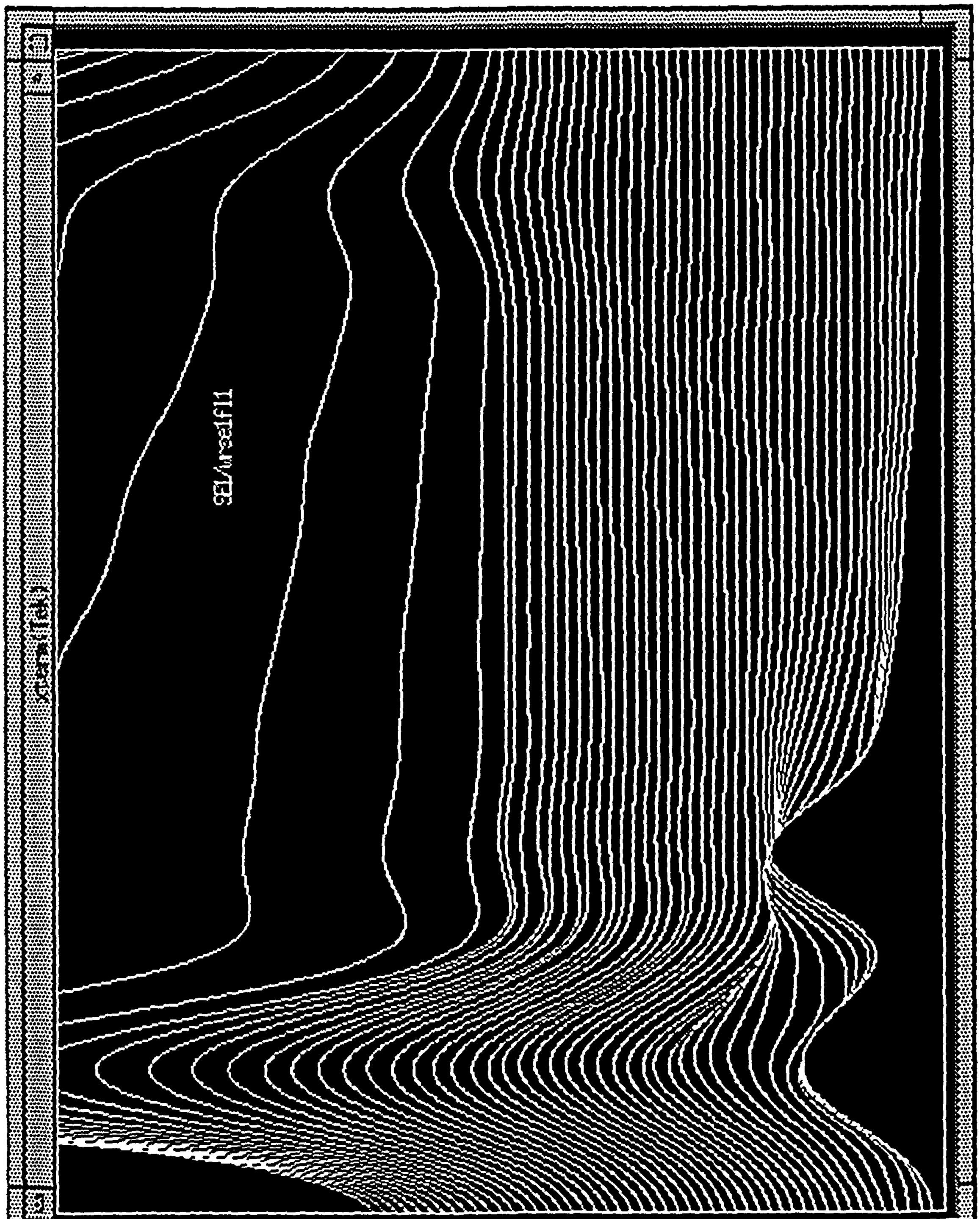

Figure 5.3: FIR plot from line current waveform with balanced rotor. Full load start.

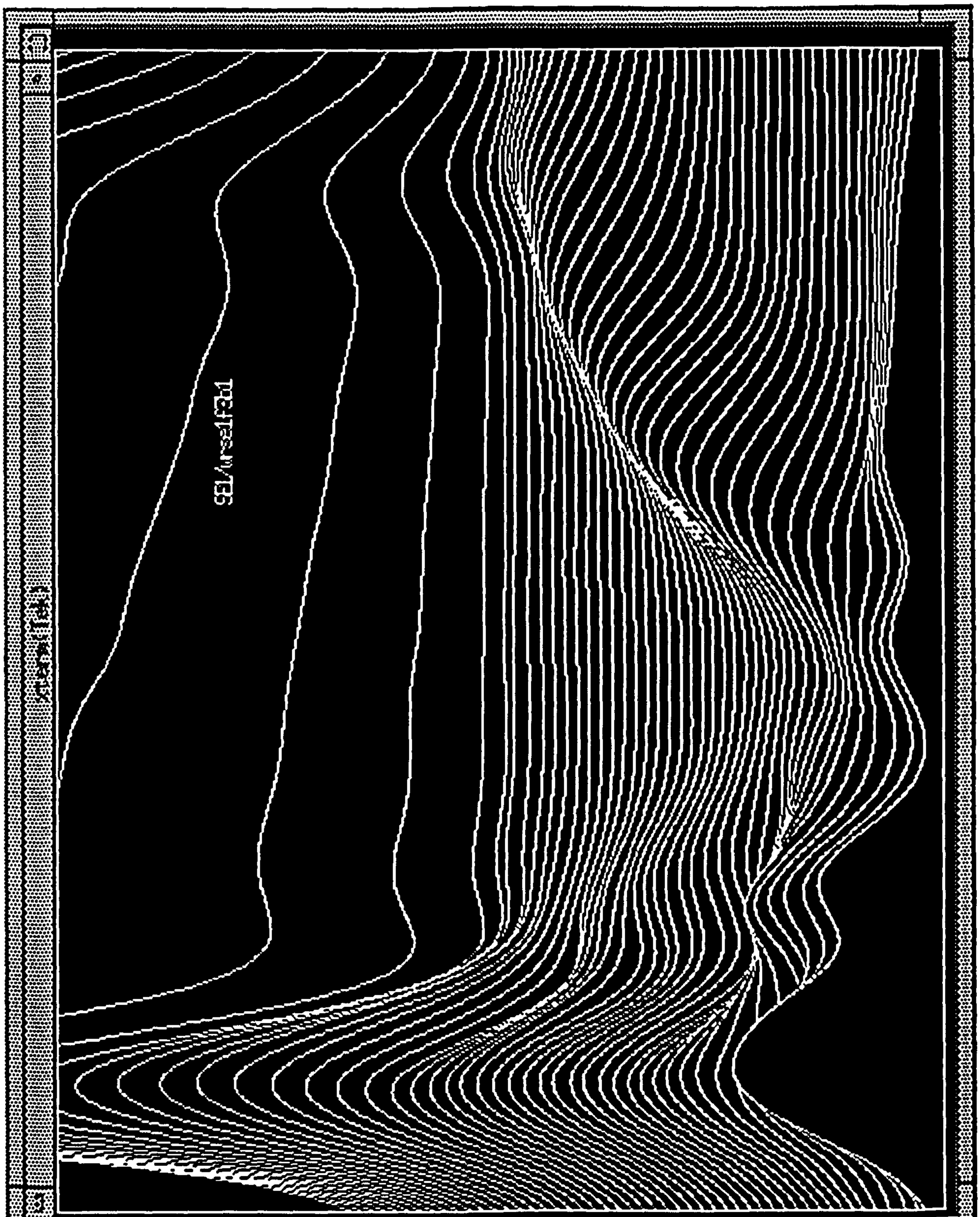

Figure 5.4: FIR plot from line current waveform for rotor with 3 broken bars. Full load start.

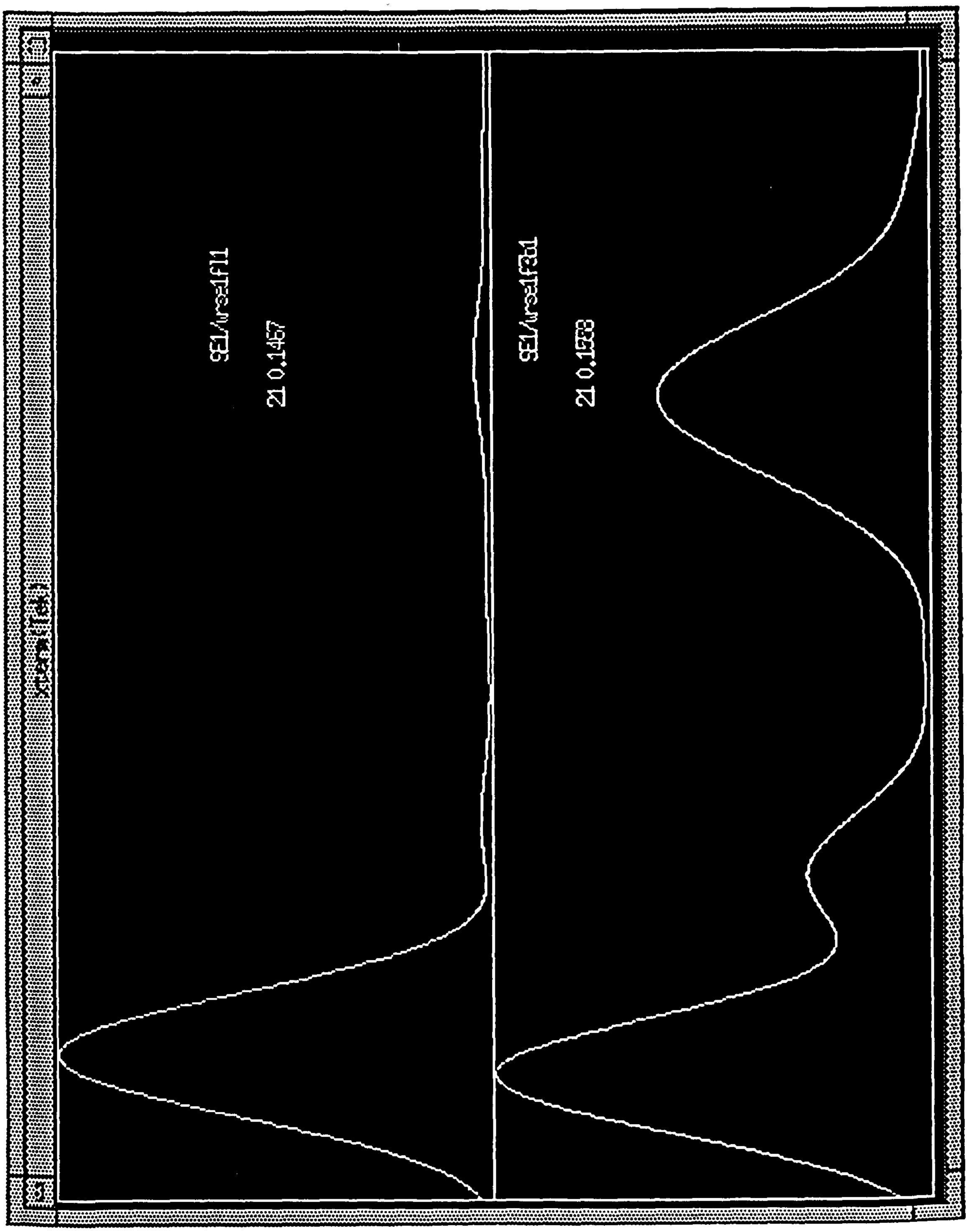

Figure 5.5: Demodulated output of the 21Hz filter for the case of balanced (top) and 3 broken bars. Full load start.

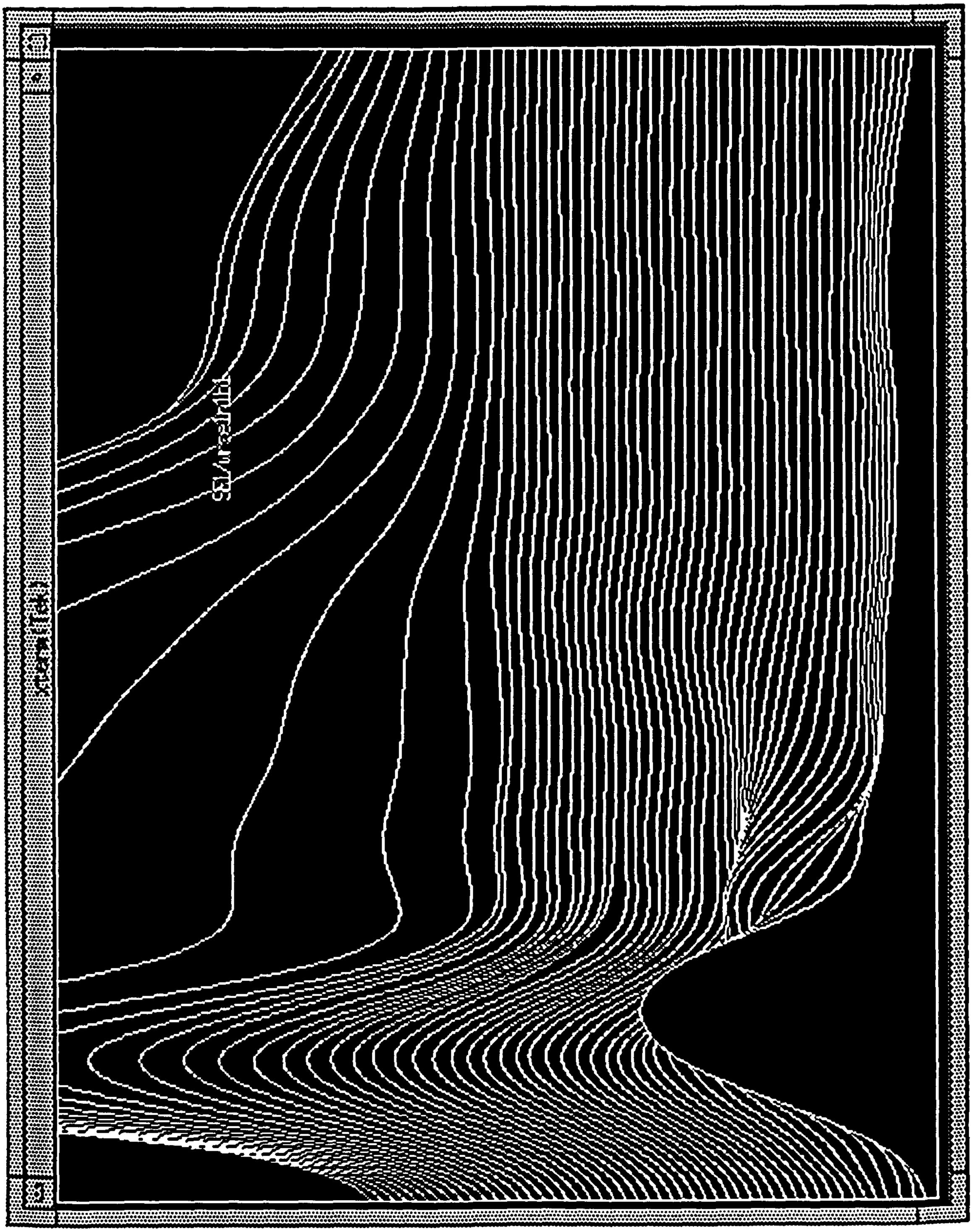

Figure 5.6: FIR plot from line current waveform for rotor with one broken bar. No load start.

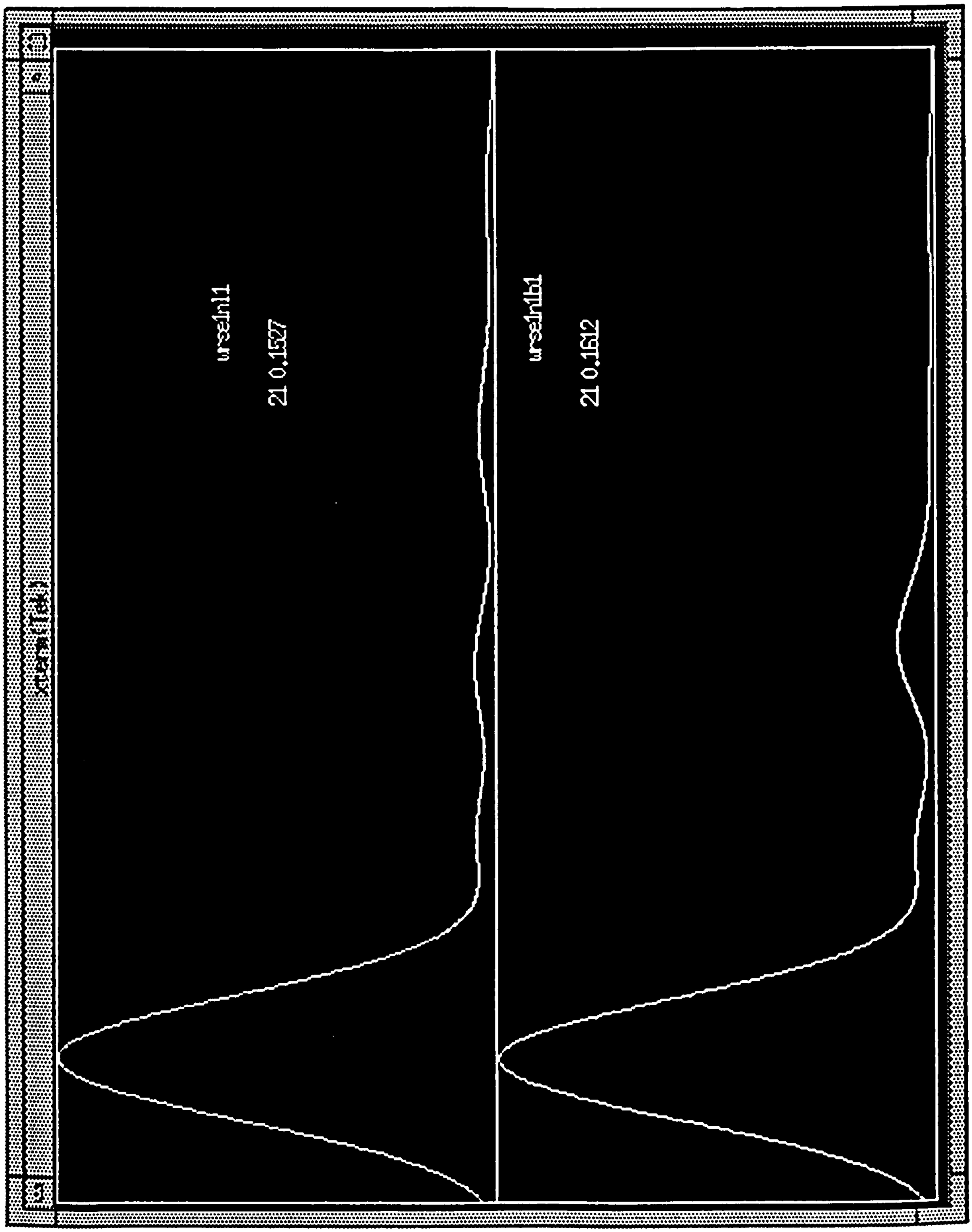

Figure 5.7: Demodulated output of the 21Hz filter for the case of balanced (top) and one broken bar. No load start.

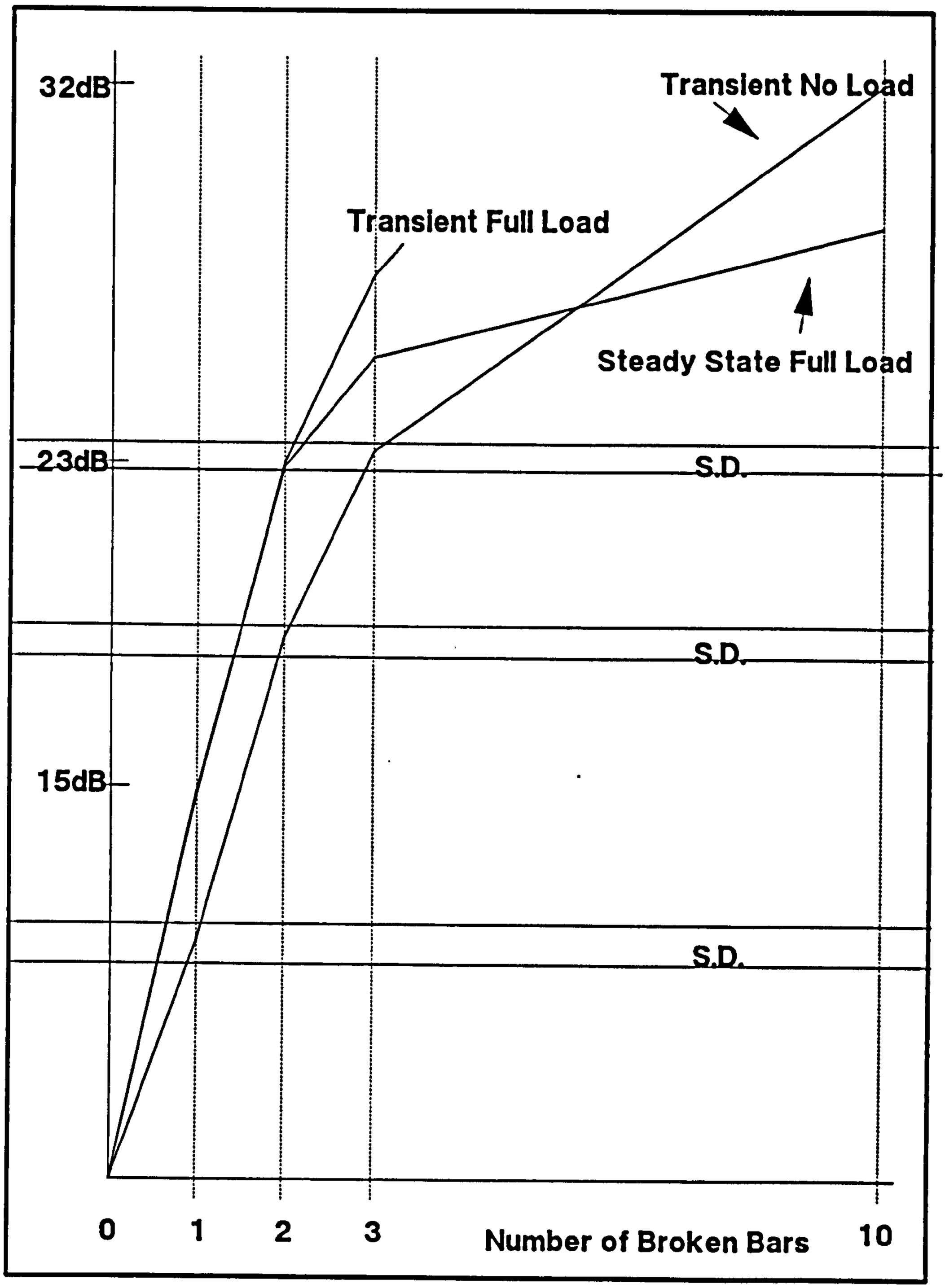

Figure 5.8: Change in amplitude of LSB versus number of broken bars.

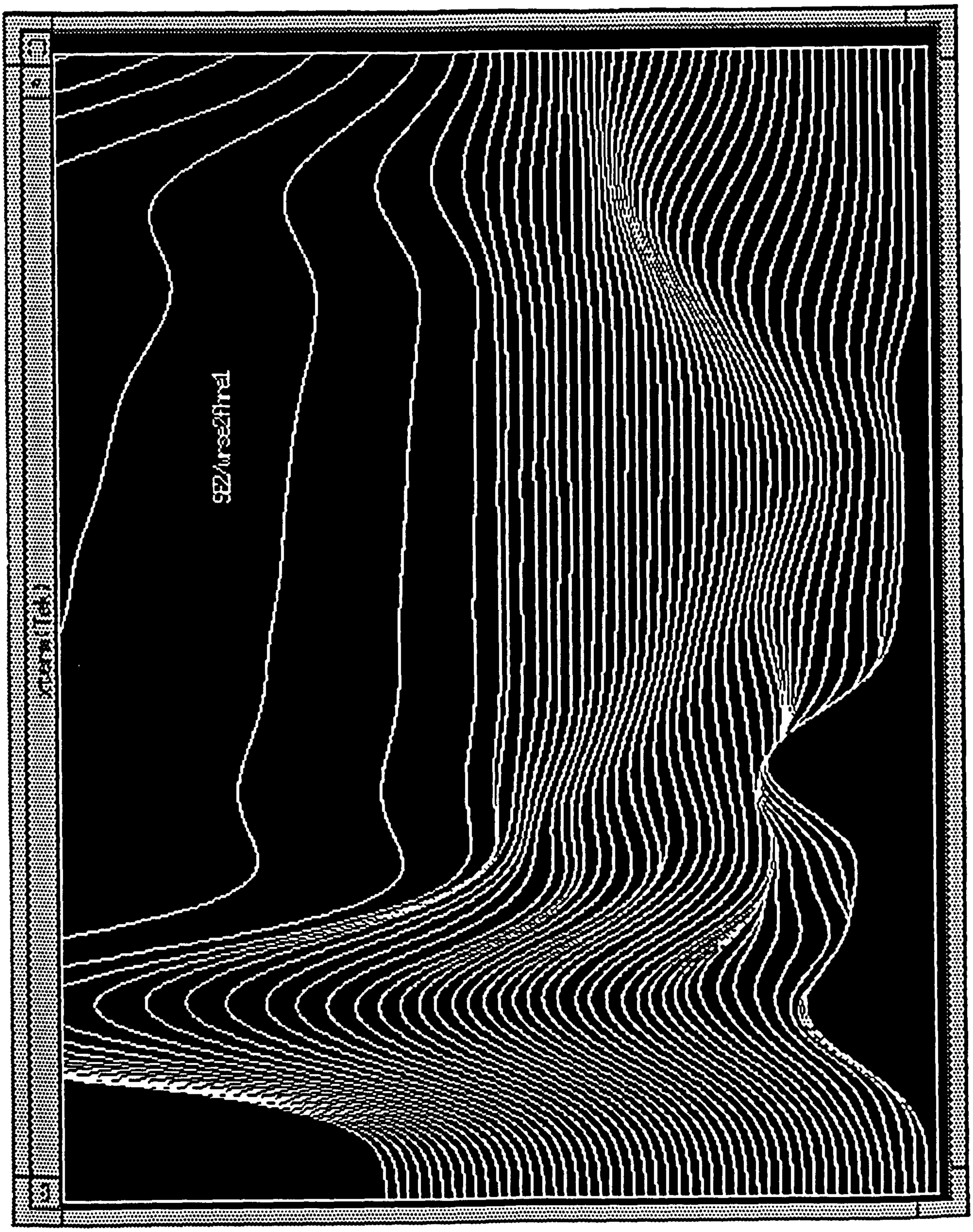

Figure 5.9: FIR plot of line current waveform with high resistance end-ring. Full load.

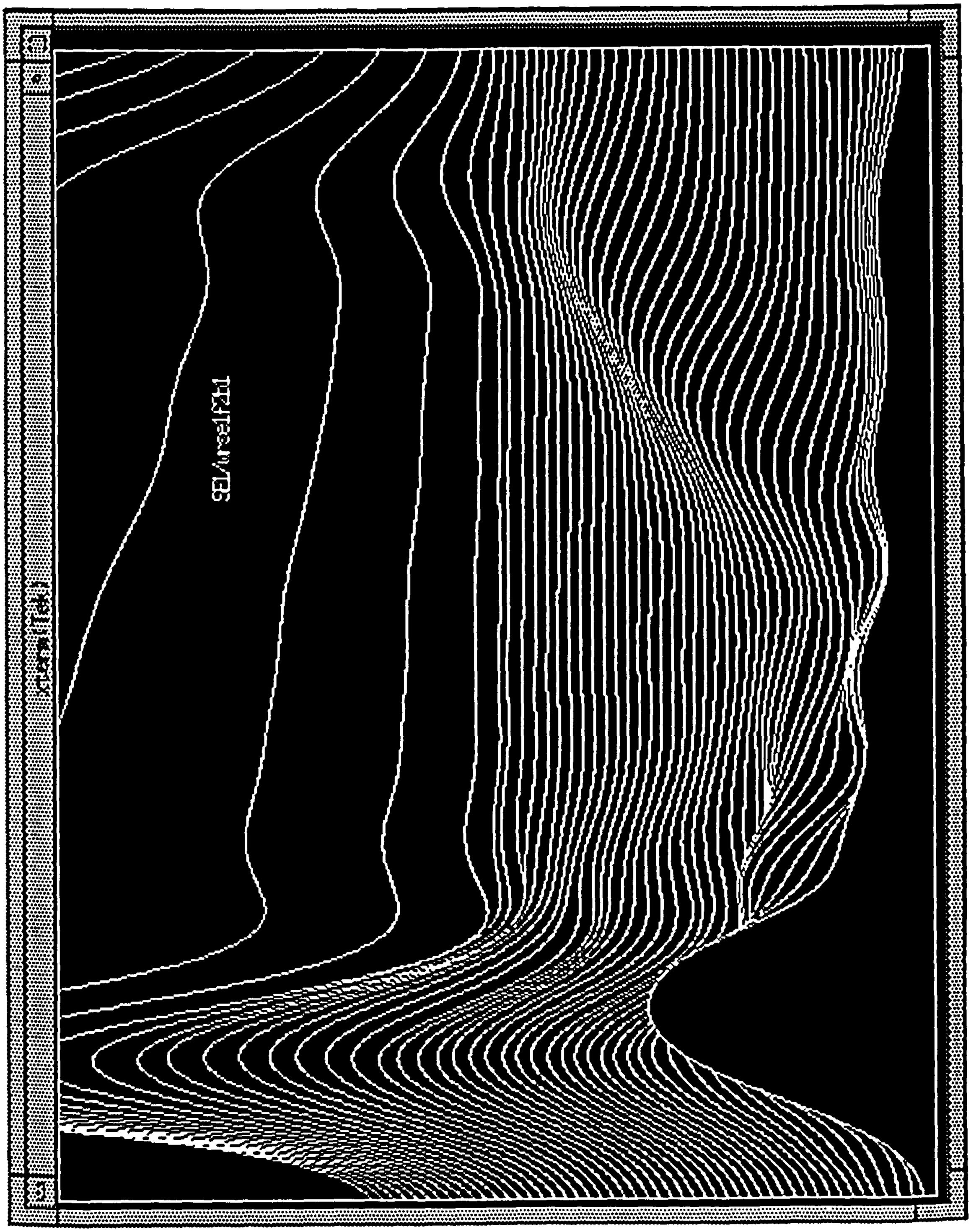

Figure 5.10: FIR plot of line current waveform with 2 broken bars. Full load.

Chapter 6

Machine Parameter Determination

6.1 Introduction

In order to model the induction motor (specifically the test rig) it was necessary to obtain the parameter values by experiment. The experimental procedure used to determine the induction motor's parameter values follows closely that described by Jones [67]. Jones shows that measurements made on individual windings of the three phase machine can be used to obtain the equivalent two phase model parameter values (α/β inductances). These two phase model parameters can also be obtained by arranging the connections of the real machine's windings in various configurations (Alpha/Beta tests). Finally, it is shown that the Standard Locked rotor and Running light tests give rise to the α/β inductances directly and without the complexity of connecting the machine's windings in special configurations.

The parameters required were :-

- magnetisation curve
- leakage saturation curve
- $\alpha\beta$ electrical parameters (2 phase model)
- 3 phase model electrical parameters

- rotor moment of inertia
- friction/windage losses
- core losses

6.2 Wound Rotor Machine Parameters Obtained by Experiment

6.2.1 Magnetisation Curve

The experimental data and calculated results are shown on Tables [6.1] and [6.2]. The rotor was deliberately left open circuit so that a comparison with the Running Light test could be made. In the Running Light test the rotor is assumed to be open circuit, but in this test the rotor was open circuit. Despite being open circuited the rotor would tend to rotate and had to be locked. The torque developed was only just sufficient to overcome friction and this effect is thought to be due to eddy currents induced within the rotor laminations. It was not possible to apply a sufficiently high voltage to simulate the high current excursions this magnetising reactance experiences during the switching transient.

As expected the core losses are a function of the applied voltage and the value of Magnetising Inductance at the operating voltage (435V Line/250V Phase) is 354 mH, the measured inductance being 366 mH which includes 12mH for leakage.

6.2.2 Leakage Saturation Curve

Two sets of saturation data were obtained as indicated in Tables [6.3] and [6.4]. These were in effect a sequence of Locked Rotor tests performed at different current levels. The results are presented in Table[6.5] where the Leakage Inductance is calculated at a number of current steps upto 15 Amperes, the maximum the supply Variac could deliver. The results show the trend indicated by [67] in that there is an initial increase in leakage inductance, which in this case

occurs for currents upto about 6 Amperes. When the current increases above this level the leakage inductance starts to fall and by 15 Amperes the value has dropped to that obtained at 0.25 Ampere. It was not possible to increase the current above 15 Amperes though this curve was extended by examination of other saturation curves. This intuitive extension amounts to a slowly decreasing value for leakage inductance from 9 mH at 15 Amps to 6mH at 100Amps as indicated in Fig.[6.1]. This data was used to create polynomials which adjust leakage inductance in the simulation programs. The leakage is assumed to be equally apportioned between stator and rotor. These tests were performed on the stator side and hence the rotor leakage is obtained by dividing by the square of the turns ratio (Nsr).

6.2.3 Stator/Stator Inductances

This measurement is primarily to obtain values for the Three Phase Model of the Induction Motor. All the combinations possible of the Stator Inductances were examined by energising the three phases in turn and taking measurements on the other two phases. This allowed the assumption that the stator windings were balanced to be verified. The measurements are indicated in Tables [6.6] to [6.11] and the calculated results are presented in Tables [6.12] to [6.14] for the range of current values. For an ideal machine with uniformly distributed windings and no leakage, the mutual coupling between stator phases (Mss) would be cos(120°) (i.e. -0.5) times the Self Inductance (Lss) of a stator phase due to the angular displacement of the stator coils. Thus the theoretical value expected for the mutual coupling (Mss) is -$\frac{1}{2}$Lss which gives the values of 124.5 mH and 127 mH for the averaged 1 and 3 Ampere cases. The leakage is therefore the difference between the expected and measured values of Mss. This results in values of 11.5 mH (124.5 - 113) and 11mH (127 - 116) for the leakage at 3 and 1 Amperes respectively.

Average values at 3 Amps
Lss = 249 mH
Mss = -113 mH
Average values at 1 Amp
Lss = 254 mH

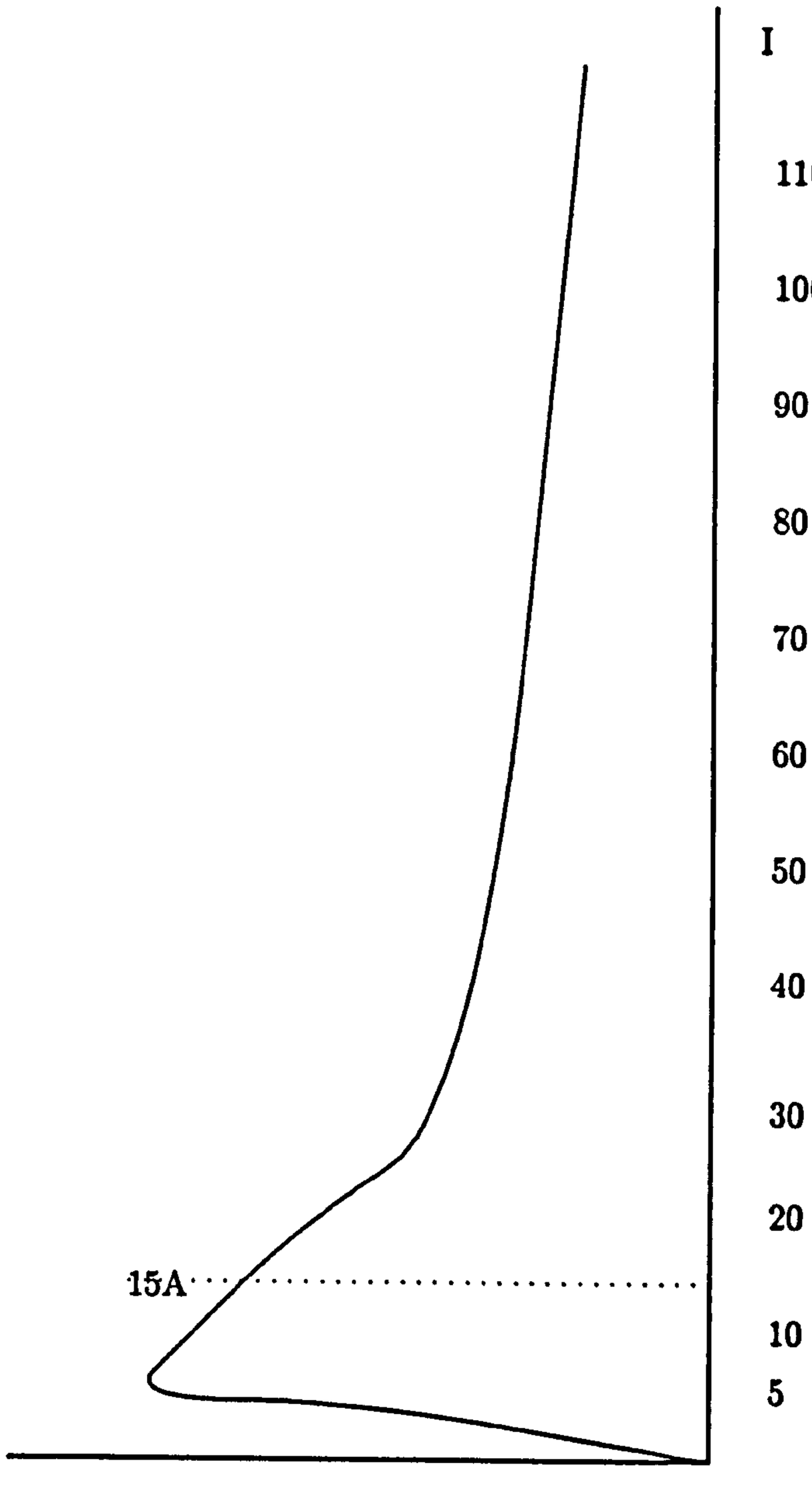

Figure 6.1: Leakage inductance versus phase current

Mss = -116 mH

L1α = Lss - Mss

At 1 Amp L1α = 370 mH

At 3 Amps L1α = 362 mH

Subtracting the stator/stator mutual inductance from the self inductance (Lss - Mss) results in the Alpha and Beta inductances [67]. Thus the 1 and 3 Ampere averages give a value of 370 mH (254 + 116) and 362 mH (249 + 113) for the stator alpha inductance. This alpha inductance should agree with the self inductance obtained using the standard Locked Rotor / Running Light tests when using the single phase equivalent circuit representations in the calculation.

The measurement of stator/stator inductances gave the following approximated results:-

Lss = 249 mH

Mss = -113 mH

Lα = 362 mH

Stator/stator turns ratio (Nss) = 2.2

Stator Leakage inductance = l_1 = 11.5 mH

6.2.4 Alpha Beta Winding Tests

The Alpha Beta values of inductance may also be determined directly by connecting the stator and rotor windings in various configurations [67]. The excitation can be applied on either stator or rotor to determine the self and mutual inductances. The experimental results are shown in Tables[6.15] to [6.19] along with the particular winding configuration indicated in Fig.[6.2]. For the excited winding the quantities of voltage, current and power (V1,I1,W1) were measured. On the secondary the voltage (V2) was measured and in addition a second wattmeter (W12) reading is taken with its current coil in the primary circuit (I1) and its voltage coil connected across the secondary terminals (V2). The value read on wattmeter W12 represents the iron loss.

In all cases the rotor was manually rotated until the voltage reading of V2 was at a maximum. The tests performed on these circuits, result in a mutual and self

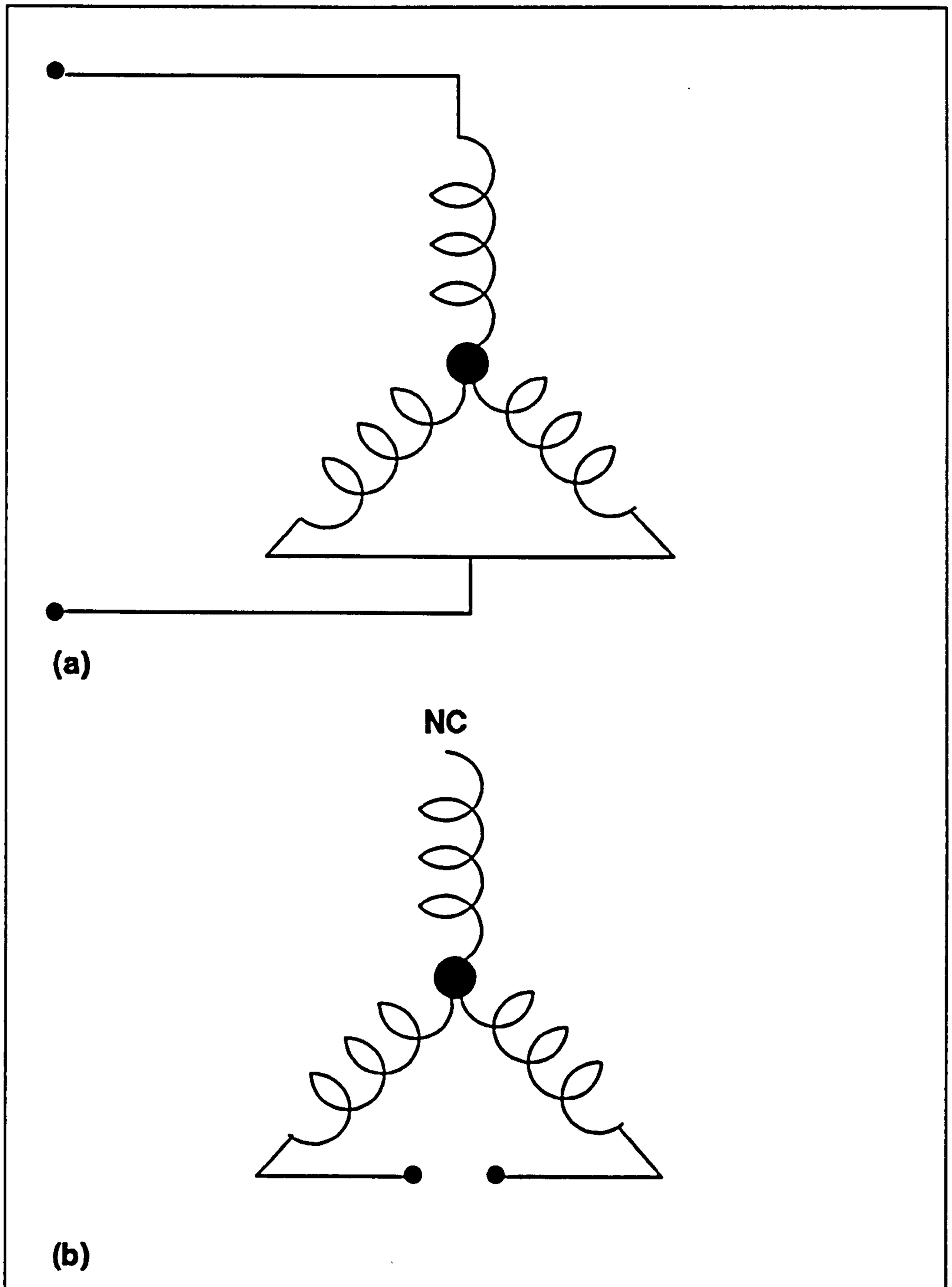

Figure 6.2: $\alpha\beta$ winding configurations

inductance which then has to be scaled by a factor dictated by the particular circuit configuration. Only the first set of results from each batch in Tables [6.15] and [6.19] are used to obtain the average values presented.

A typical calculation proceeds as follows:-
Taking the first result from the experimental data obtained with Stator excited, yellow and blue phases connected, red phase supplied, see Table [6.15]. Initially a wattmeter (W12) was used so that iron losses could be taken into account [67], however this added procedure made little difference to the calculated results and the power readings were either omitted from the calculation or latterly not obtained.

These results were acquired with the stator configured as in circuit (a) and rotor as in (b), these circuits are indicated in Fig.[6.2]. The impedances measured at the terminals of these two circuits are simple multiples of the $\alpha\beta$ impedances and as such have to be scaled to take this into account.

V1 = 425; I1 = 2.5; V2 = 193;
The self inductance is given by :-
L1 = V1/ωI1 = 425/100π 2.5 = 541 mH
The Stator scaling factor for this circuit configuration is 2/3
therefore Lα = $\frac{2}{3}$ L1 = 360 mH
For the mutual inductance :-
M1 = V2/ωI1 = 193/100π 2.5 = 246 mH
This calculation uses parameters from both the Stator and Rotor circuits (I1,V2) and the factor required is the geometric mean of both the circuits factors.
Therefore, factor = $\sqrt{\frac{2}{3}\frac{1}{2}} = \frac{1}{\sqrt{3}}$.
This gives Mα =$\frac{1}{\sqrt{3}}$ 246mH = 142mH.

The α/β tests gave the following averaged results:-

- Rotor/Stator turns ratio (Nsr) = 2.45
- L1α = 362.5 mH
- L2α = 59.0 mH
- Mα = 141.0 mH

Referring these to the Stator circuit results in :-

- $L1\alpha = 362.5$ mH
- $L2'\alpha = L2\alpha\ N_{sr}^2 = 354.2$ mH
- $M'\alpha = M\alpha\ N_{sr} = 345.5$ mH

Since $L1\alpha = M'\alpha + l_1$
Therefore the stator leakage is = 362.5 - 345.5 = 17 mH
and likewise the rotor leakage is = 354.2 - 345.5 = 8.7 mH
It is interest to note that the total leakage inductance is given by 17.0 + 8.7 = 25.7 mH .

6.2.5 Standard Locked Rotor and Running Light Tests

This information is available from the Running Light test indicated in Table[6.20] and from the saturation curve tests results shown in Table[6.21]. The Running light tests have been solved assuming that the leakage reactances are negligible and that the rotor is effectively open circuit.

This results in a magnetising inductance of 361.0 mH at operational voltage and is larger than values obtained by other means. This arises because the circuit is over simplified and a more thorough method was used to evaluate the equivalent single phase circuit [78]. The leakage inductances are obtained from the results shown in Table[6.5] at the chosen current level of 10 Amperes.

From the Running Light test data
V = 251 Volts ; W/ph = 103.4 Watts ; Il = 2.19 Amps
therefore

$$R_o = W_{ph}/I_{ph}^2 = 103.4/(2.19)^2 = 21.56$$

$$Z_o = V_{ph}/I_{ph} = 251/2.19 = 114.6$$

$$X_o = \sqrt{Z_o^2 - R_o^2} = 112.6$$

From the Locked rotor test at Il = 10 Amps
V = 76 Volts ; Il = 10 Amps ; W/ph = 315 ;
this gives

$$R_{eq} = 315/(10)^2 = 3.15\Omega$$

$$Z_{eq} = 76/10 = 7.6\Omega$$

$$X_{eq} = \sqrt{Z_{eq}^2 - R_{eq}^2} = 6.92\Omega$$

X_{eq} is assumed to be equally apportioned to the rotor and stator circuits which results in :-

$$X_{l1} = X'_{l2} = \frac{X_{eq}}{2} = 3.46\Omega$$

The magnetising reactance is given by :-

$$X_m = X_o - X_{l1} = 112.6 - 3.46 = 109.14\Omega$$

this results in a Mutual Inductance of M = 347.4 mH , which compares favourably with the value of 345.5 mH obtained by the Alpha/Beta methods.

The total leakage Inductance is 22.0 mH and this is very similar to the results from other tests.

The Stator (R1) and Rotor (R2) D.C. resistance have been measured as 1.34 Ω and 0.23 Ω respectively. The rotor resistance is difficult to obtain accurately since there is an inherent contact resistance between the slip-ring and the brush which changes with rotor position.

Calculating the rotor resistance from the exact method [78] proceeds as follows :-

$$R'_2 = (R_{eq} - R_1)(\frac{X_o}{Xm})$$

$$= (3.15 - 1.34)\frac{112.6}{109.14}$$

$$R'_2 = 1.86\Omega$$

this must be referred to the rotor circuit

$$R_2 = \frac{R'_2}{Nsr^2}$$

$$= 1.86/6$$

$$R_2 = 0.31\Omega$$

The Standard LR/RL tests gave the following results ;-

- $R_1 = 1.34\Omega$
- $M = 347.4mH$
- $L_1 = M + l_1 = 347.4 + 11 = 358.4mH$
- $L'_2 = 358.4mH$
- $R'_2 = 1.86\Omega$

6.2.6 Discussion on Running Light Test

It is of interest to compare the results from the magnetisation curve experiment and those of the running light test. In the magnetisation curve experiment the rotor was open circuited, whereas in the running light test the rotor is assumed to be open circuited. The calculations are based on data for $V_{ph} = 250$Volts and for the exact equivalent circuit method [78] the leakage inductance is obtained from the leakage saturation test at a similar value of current I = 2.25 Amperes.

- Running Light Po = 103.4W, Io = 2.45A, V= 251V
- Magnetisation Curve Po = 90W, Io= 2.2A, V = 250V
- Saturation Curve I=2.25A, l_l=12mH

From inspection it is clear that more power is dissipated in the running light test which would be expected since friction and windage losses will demand power.

Two methods of calculation were used, in the first case the stator leakage reactance is ignored and in the second the exact equivalent circuit method was used to account for leakage reactance. The results are presented below:-

Approximate method :-

Magnetisation Curve M = 366.7mH

Running Light = 361mH

Exact Method :-

Magnetisation Curve M = 357mH

Running Light M = 349mH

Comparison of the results obtained by any one method shows a difference of approximately 3%, thus the assumption that the rotor is open circuit during the running light test does not introduce a large error.

A comparison can also be made between the approximate and exact methods which give rise to differences of again approximately 3%.

6.2.7 Discussion on the Three Phase Model Parameters

The Stator self (Lss) and Stator/Stator Mutuals (Mss) have already been obtained along with the Alpha/Beta Mutual inductance ($M\alpha$). The magnitude

of the Rotor/Stator Mutual Inductance can be obtained from the Alpha/Beta Mutual Inductance Mα as follows:-

$$M\alpha = \frac{3}{2} Msr$$

giving

$$Msr = \frac{2}{3} 141mH = 94mH$$

The only remaining unknown inductances are the Rotor Self (Lrr) and Rotor/Rotor Mutual (Mrr) Inductances. It was not possible to perform the same test procedure as used to determine the Stator/Stator parameters since there is no access to the rotor neutral point. However data has been obtained on the rotor from the Alpha/Beta tests and using the assumption that the Rotor/Rotor turns ratio is the same as the Stator/Stator turns ratio it is possible to obtain estimated values for these parameters as follows :-

Assumed rotor/rotor turns ratio (Nrr) = 2.2

L2α = 59 mH

where L2α = Lrr - Mrr

but Mrr = -Lrr / Nrr

therefore Lrr(1 -(1/Nrr)) = 59 mH

this results in the values of :-

Lrr = 40.6 mH

Mrr = -18.4 mH

The Inductance parameters for the 3 Phase model of the slip ring rotor machine are listed below :-

- Lss = 249.0 mH
- Mss = -113.0 mH
- Msr = 94.0 mH function of rotor position
- Lrr = 40.6 mH
- Mrr = -18.4 mH

6.3 Squirrel Cage Rotor Parameters

Standard Running Light and Locked Rotor tests were performed on the 51 bar squirrel cage rotor. The Locked rotor tests were carried out over an extended range, so that the leakage saturation of the machine could be assessed. The experimental results are tabulated in Tables [6.22] and [6.23].

The calculation proceeds as follows :-

From the Running Light Test:-

$$R_o = W_{ph}/I_{ph}^2 = 145/(3.15)^2 = 14.6\Omega$$

$$Z_o = V_{ph}/I_{ph} = 250/3.15 = 79.3\Omega$$

$$X_o = \sqrt{Z_o^2 - R_o^2} = 77.9\Omega$$

From the Locked rotor test at I_{ph} =15 Amps. :-

$$R_{eq} = W_{ph}/I_{ph}^2 = 700/15^2 = 3.1\Omega$$

$$Z_{eq} = V_{ph}/I_{ph} = 73.5/15 = 4.9\Omega$$

$$X_{eq} = \sqrt{Z_{eq}^2 - R_{eq}^2} = 3.79\Omega$$

Assuming an even distribution of leakage reactance between the rotor and stator results in :-

$$Xl_1 = Xl_2 = Xl_{eq}/2 = 1.895\Omega$$

and since

$$Xl_1 = \omega\, l_1$$

$$l_1 = 6mH$$

$$X_m = X_o - Xl_1 = 77.9 - 1.895 = 76\Omega$$

and this gives

$$M = X_m/\omega = 242mH$$

and

$$L1 = M + l_1 = 242 + 6 = 248mH$$

The referred rotor resistance is given by :-

$$R_2' = (R_{eq} - R_1)\frac{X_o}{X_m} = (3.1 - 1.34)77.9/76 = 1.8\Omega$$

De-referring the rotor resistance gives :-

$$R_2 = R_2'/Nsr^2 = 1.8/6 = 0.3\Omega$$

The stator leakage inductance was calculated for all values of I_{ph} and these are shown in Table [6.24]. It can be seen that little change in leakage inductance occurs due to saturation upto 15A.

6.3.1 Three Phase Model Parameters for 51 Bar Rotor

From the LR/RL tests it is possible to calculate the three phase model parameters as follows :-

The assumption that leakage inductance is equally apportioned between the rotor and stator circuits is made thus :-

$$l_1 = l_2 = 6mH$$

Given that

$$L1 = Lss - Mss$$

and

$$Mss = -Lss/2 + l_1$$

with substitution and some re-arrangement:-

$$Lss = \frac{2}{3}(L1 + l_1)$$

=(2/3)(248 + 6) = 169mH

Mss = Lss - L1 = 169 - 248 = -79mH

De-referring L2' = L1 = 248mH

$L2 = L2'/Nsr^2 = 248/6 = 41.3mH$

and likewise de-referring $l'_2 = l_1 = 6mH$ gives

$l_2 = 6/6 = 1mH$

The rotor inductances are given by :-

$$Lrr = \frac{2}{3}(L2 + l_2)$$

= (2/3)(41.3 + 1) = 28.2mH

and

Mrr = Lrr - L2 = 28.2 - 41.3 = -13.1mH

De-referring the mutual inductance obtained from the LR/RL test gives:-

Mde = M/Nsr = 242/2.45 = 98.8mH

Msr = (2/3)Mde = 65.9mH

The Inductance parameters for the 3 Phase model of the 51 bar squirrel cage machine are listed below :-

- Lss = 169.0 mH
- Mss = -79.0 mH
- Msr = 65.9 mH function of rotor position
- Lrr = 28.2 mH
- Mrr = -13.1 mH

6.4 Angular Moment of Inertia of Rotors

The Angular Moment of Inertia of each of four different types of rotor used in the test rig were measured by the method of Trifiliar Suspension [74]. In this technique the object with the unknown moment of inertia is suspended from from a suitable point by three wires Fig.[6.3].

A twisting force is applied to the platform and the rotor, which causes the whole system to oscillate. The time taken for a number (10) of complete cycles is measured and then an estimate is made of the period of oscillation (t_p). The unladen suspension mechanism is also subjected to this test so that its moment of inertia can be accounted for. For error estimation a Bronze cylinder was also subjected to the above test, it could however, due to its simple geometry allow an alternative method of calculating the moment of inertia to be used.

The calculation proceeds as indicated below :-

Length of suspension wires (l) = 2.755 metres

Radius from platform centre to suspension point (r) = 0.21 m

Mass of unladen platform (m_p) = 1.2 Kilograms

The Moment of Inertia is given by :-

$$Io = \frac{t_p^2 m\, g\, r^2}{4\pi^2 l}$$

where g is the acceleration due to gravity

For the Unladen Platform

$Io_{ul} = (2.458)_2(1.2)(9.81)(0.21)^2/(4\pi^2(2.755)) = 0.02948$ Kg m^2

Slip-ring Rotor

$Io_t = (0.951)^2(34.3+1.2).(9.81).(0.21)^2/(4\pi^2(2.755)) = 0.1277$

Io_{ssr} = Io_t - Io_{ul} = 0.1277 - 0.02948 = $0.0982 Kgm^2$

51 Slot Rotor

$Io_t = 1^2(27.9+1.2)(3.9776e\text{-}3) = 0.11575$

$Io_{51} = 0.11575 - 0.02948 = 0.08627 Kgm^2$

Bronze Cylinder

$Io_t = (0.995)^2(28.8+1.2)(3.977e\text{-}3) = 0.118$

Io_c = 0.118 - 0.02948 = $0.0886 Kgm^2$

The angular moment of the bronze cylinder was obtained purely for the purposes of estimating experimental error. The moment of rotational inertia (angular momentum) of a cylinder can be shown to be given by the expression :-

$$Io = mass\, radius^2/2$$

The height and radius of the bronze cylinder are 0.2 metres and 0.0762 metres respectively.

therefore $Io_c = (28.8).(0.0762)^2 / 2$

= 0.0886 Kg m^2

Difference between measured and calculated values is :-

0.0886 - 0.0836 = 0.005

The error w.r.t. the measured value is therefore

(5e-3).(100) / 0.0886 = 5.7 %

The calculated results are tabulated in Table [6.26].

6.5 Windage and Friction losses

In order to estimate the windage and friction losses of the machine set the time taken for the shaft's speed to reduce from no load operating speed (1500rpm) to rest was measured and was found to be 39 seconds.

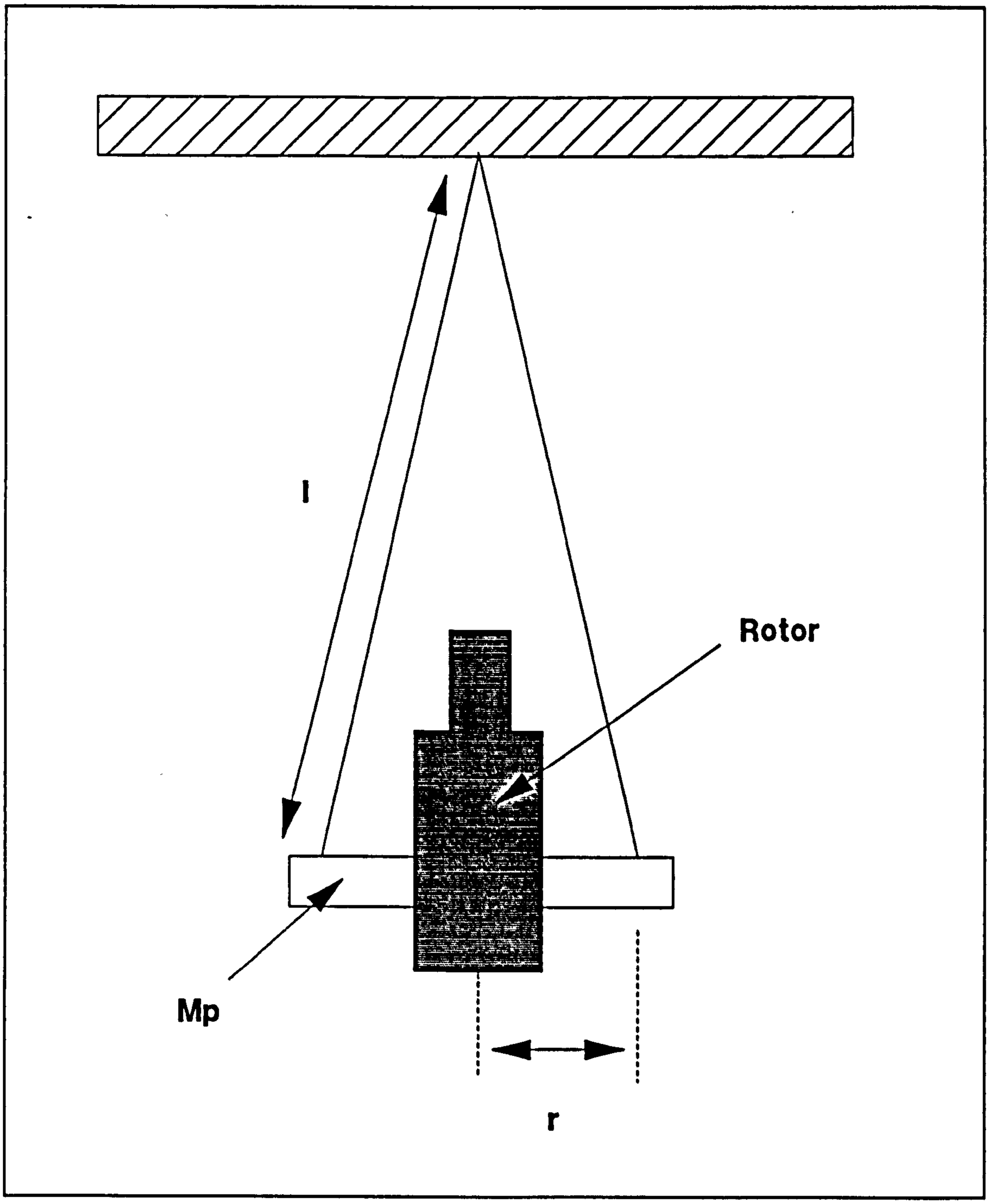

Figure 6.3: Angular Momentum measurement by method of tri-filiar suspension.

Assuming a linear deceleration characteristic, which is certainly not the case, an approximate estimation of these losses can be made :-

$$\frac{d\omega}{dt} = \frac{2\pi 1500}{39\ 60} = 4\, rad\, s^{-2}$$

from this, the average torque can be found :-

$$Torque = J\frac{d\omega}{dt} = 0.8Nm$$

To incorporate this into the model, the torque is made a function of the speed an again a linear characteristic is assumed:-

$$\mathcal{F}(\omega) = \frac{Torque}{\omega}$$

$$\mathcal{F}(\omega) = 0.01Nm/rad\, s^{-1}$$

this gives a maximum windage/friction loss of 1.57 Nm at 1500rpm and zero torque at zero speed. This is a small fraction of the full load steady state torque of 60Nm.

6.6 No-Load Rotational Losses

These losses are comprised of the core loss and friction/windages losses. The laboratory machine is started with the stator windings connected in star and hence the core loss is less than would be obtained for the steady state condition configured in delta. This arises because the core loss can be separated in to eddy current loss and hysteresis loss. Typically hysteresis loss accounts for 80% of the core loss and is proportional to the square of the applied voltage [52].

From the running light test an estimate of this combined loss can be obtained :-

Po = 103.4W, Io = 2.45, V = 251
Core Loss = 3(Po - $(Io)^2$ R1)
= 3(103.4 - $(2.45)^2$ 1.34)
= 286 Watts
It is common practice to represent the core loss of a machine as an extra torque demand added to the load torque. The resultant average load torque over the starting period is calculated for the condition of half speed.

T_{cl} = 286/(157/2) = 3.6 Nm
this also includes the friction windage loss estimated above.

V_ph	W_{ph}	I_o	I_c	I_m
275	21X10X0.5	2.5	0.38	2.47
270	21X10X0.5	2.4	0.38	2.37
260	19X10X0.5	2.3	0.37	2.27
250	18X10X0.5	2.2	0.36	2.17
240	17X10X0.5	2.1	0.35	2.07
230	30X5X0.5	2.0	0.33	1.97
220	28X5X0.5	1.9	0.32	1.87
210	25X5X0.5	1.8	0.30	1.77
200	23X5X0.5	1.7	0.29	1.67
190	21X5X0.5	1.6	0.28	1.57
180	19X5X0.5	1.5	0.26	1.48
150	14X5X0.5	1.25	0.23	1.23
100	35X2.5X0.2	0.85	0.18	0.83
90	29X2.5X0.2	0.84	0.16	0.82
80	23X2.5X0.2	0.74	0.14	0.73
70	19X2.5x0.2	0.65	0.14	0.63
60	14X2.5X0.2	0.56	0.12	0.55
50	29X1X0.2	0.48	0.12	0.46
40	20X1X0.2	0.39	0.1	0.37
30	13X1X0.2	0.31	0.09	0.29
20	12X1X0.1	0.22	0.06	0.21
10	4X1X0.1	0.14	0.04	0.13

Table 6.1: Magnetisation Curve. Rotor open circuit; all three phases energised on Stator.

V_{ph}	I_m	L_m	R_m	θ
275V	2.47A	354mH	720Ω	81.2°
270	2.36	363	689	80.6
260	2.27	364.5	711	80.8
250	2.17	366.6	694	80.6
240	2.07	369	678	80.3
230	1.97	371	705	80.6
220	1.87	374	691	80.4
210	1.77	376	705	80.5
200	1.67	378	696	80.3
190	1.58	384	687	80.0
180	1.48	388	682	79.9
150	1.23	389	628	79.2
100	0.83	383	570	78.1
90	0.82	347	557	78.9
80	0.73	351	564	78.8
70	0.64	351	516	77.9
60	0.55	349	514	77.9
50	0.47	342	431	76.0
40	0.38	338	400	75.1
30	0.3	321	346	73.8
20	0.21	303	329	74.0
10	0.13	237	250	73.4

Table 6.2: Results from Magnetisation Curve.

V_{ph}	I_{ph}	P_{ph}
8.5	1.0	10X0.5
17.0	2.0	31X0.5
25.0	3.0	34
22.2	3.0	25
32.0	4.0	54
42.0	5.0	85
48.0	6.0	119
55.5	7.0	32X5
63.0	8.0	41X5
69.0	9.0	51X5
76.0	10.0	63X5
83.0	11.0	32X5X2.5
89.0	12.0	37X5X2.5
95.0	13.0	44X5X2.5
100.0	14.0	51X5X2.5
105.0	15.0	59X5X2.5

Table 6.3: Saturation Curve1 Rotor locked; all three phases energised on Stator.

V_ph	I_{ph}	P_{ph}
62Volts	8.0 Amps	196Watts
60	7.5	181
57	7.0	157
53	6.5	138
48	6.0	117
45	5.5	99
42	5.0	87
37	4.5	69
34	4.0	57
29	3.5	42
25	3.0	32
21	2.5	22
19	2.25	19
16	2.0	17
14.5	1.75	12
12.5	1.5	9
10.5	1.25	6
8.0	1.0	5
8.5	1.0	20X0.2
7.5	1.0	15X0.2
5.4	0.75	9X0.2
3.6	0.5	5X0.2
1.5	0.25	1X0.1

Table 6.4: Saturation Curve2 Rotor locked; all three phases energised on Stator.

Iph	*Vph*	*Pph*	*Req*	*Zeq*	*Xeq*	l_l
15	105	737.5	3.28	7.0	6.18	9.8mH
14	100	637.5	3.25	7.1	6.36	10.1
13	95	550.0	3.25	7.3	6.54	10.4
12	89	462.5	3.21	7.42	6.68	10.6
11	83	400.0	3.3	7.55	6.78	10.8
10	76	315.0	3.15	7.6	6.92	11.0
9	69	255.0	3.15	7.67	7.0	11.1
8.0	62	196.0	3.06	7.75	7.12	11.3
7.5	60	181.0	3.22	8.0	7.32	11.66
7.0	57	157.0	3.2	8.14	7.48	11.9
6.5	53	138.0	3.27	8.15	7.47	11.89
6.0	48	117.0	3.25	8.0	7.3	11.63
5.5	45	99.0	3.27	8.2	7.52	11.97
5.0	42	87.0	3.48	8.4	7.64	12.16
4.5	37	69.0	3.41	8.2	7.46	11.87
4.0	34	57.0	3.56	8.5	7.7	12.3
3.5	29	42.0	3.43	8.29	7.55	12.0
3.0	25	32.0	3.56	8.3	7.5	11.9
2.5	21	22.0	3.52	8.4	7.6	12.14
2.25	19	19.0	3.75	8.4	7.56	12.04
2.0	16	17.0	4.25	8.0	6.78	10.79
1.75	14.5	12.0	3.92	8.29	7.3	11.63
1.5	12.5	9.0	4.0	8.33	7.3	11.63
1.25	10.5	6.0	3.84	8.4	7.47	11.89
1.0	8.5	4.0	4.0	8.5	7.5	11.9
1.0	7.5	3.0	3.0	7.5	6.87	10.95
0.75	5.4	1.8	3.2	7.2	6.45	10.25
0.5	3.6	1.0	4.0	7.2	5.75	9.14
0.25	1.5	0.1	1.6	6.0	5.78	9.2

Table 6.5: Results of Leakage Inductance calculations from the Saturation Tests.

Vr	Ir	W1	W2	Vyn
47X5	3A	24X5X1	2X20	106
39.25X5	2.5	17X5X1	1.3X20	90
31.7X5	2.0	12X5	1X20	73
24X5	1.5	28X2.5X0.5	12	54
32X2.5	1.0	14X2.5X0.5	3.1X2	36
39.5	0.5	29X0.2	2	17.5

Table 6.6: Stator/Stator Inductances Red-Yellow Phases.

Vr	Ir	W1	W2	Vbn
5X46.5	3A	23X5X1	3.3X5X2.5	107
39X5	2.5	17X5X1	2.4X5X2.5	91
32X5	2.0	12X5X1	1.6X5X2.5	75
48X2.5	1.5	29X2.5X0.5	13	56
32X2.5	1.0	14X2.5X0.5	1.3X5	37
40.5X1	0.5	29X0.2	1X2	18

Table 6.7: Stator/Stator Inductances Red-Blue Phases.

Vb	Ib	W1	W2	Vyn
27X10	3.5	15X10	2X25	125
48X5	3.0	24X5	1.6X25	108
32X5	2.0	23X5X0.5	2X2X5	74
31.7X2.5	1.0	34X2.5X0.2	1.2X5	36

Table 6.8: Stator/Stator Inductances Blue-Yellow Phases.

Vb	Ib	W1	W2	Vrn
27X10	3.5	15X10X1	1X5X10	125
47X5	3.0	24X5	16X2.5X10	107
32X5	2.0	23X5X0.5	1.6X2.5X5	74
32X2.5	1.0	14X2.5X0.5	1.6X4	37

Table 6.9: Stator/Stator Inductances Blue-Red Phases.

Vy	Iy	W1	W2	Vrn
27.25X10	3.5	15X10X1	1X5X10	122
46.5X5	3.0	23X5	0.7X5X10	105
32X5	2.0	23X5X0.5	1.6X2.5X5	73
32.5X2.5	1.0	35X2.5X0.2	3.2X2	36.5

Table 6.10: Stator/Stator Inductances Yellow-Red Phases.

Vy	Iy	W1	W2	Vbn
27.5X10	3.5	16X10	1X5X10	125
47X5	3.0	23X5	1.6X10X2.5	108
32.25X5	2.0	23X5X0.5	2.1X2X5	75
31.6X2.5	1.0	34X2.5X0.2	3.1X2X1	36

Table 6.11: Stator/Stator Inductances Yellow-Blue Phases.

Lss	Mss	Lss	Mss
249 mH	-112.5 mH	246 mH	-113.5 mH
250	-114.6	248.3	-115.8
252	-116.2	254.6	-119.4
254.6	-114.6	254.6	-118.8
254.6	-114.6	254.6	-117.8
251.5	-111.4	257.8	-114.6

Table 6.12: Red-Yellow (left) and Red-Blue Stator Inductances.

Lss	Mss	Lss	Mss
254.5 mH	-113.6 mH	245.5 mH	-113.7 mH
254.6	-114.6	249.3	-113.5
254.6	-117.8	254.6	-117.7
252.27	-114.6	254.6	-117.7

Table 6.13: Blue-Yellow (left) and Blue-Red Stator Inductances.

Lss	Mss	Lss	Mss
247.8 mH	-110.9 mH	250.0 mH	-113.7 mH
246.7	-111.4	249.3	-114.6
254.6	-116.2	256.6	-119.4
258.6	-116.2	251.5	-114.6

Table 6.14: Yellow-Red (left) and Blue-Yellow Stator Inductances.

V1	I1	W1	W12	V2
42.5X10	2.5	17X10X1	2.4X5X5	193
35.6X10	2.0	23X10X0.5	1.7X5X5	160
27X10	1.5	14X10X0.5	1X5X5	122
35.6X5	1.0	34X5X0.2	2.5X2.5X2	81
36.7X2.5	0.5	22X2.5X0.2	0.8X2.5X2	43

Table 6.15: $\alpha\beta$ inductance measurements, Stator Excited Yellow and Blue connected together, Red supplied. Stator factor=2/3, Rotor factor=1/2.

V1	I1	W1	W12	V2
42.6X10	2.5	17X10X1	2.4X5X5	192
37X10	2.0	22X10X0.5	2.3X2.5X5	155
26.5X10	1.5	14X10X0.5	2X2.5X5	120
35.9X5	1.0	34X5X0.2	3.2X2X2	83
36.7X2.5	0.5	22X2.5X0.2	2X1X2	41

Table 6.16: $\alpha\beta$ inductance measurements, Stator Excited Red and Blue connected together, Yellow supplied. Stator factor=2/3, Rotor factor=1/2.

V1	I1	W1	V2
44.5X5	6.125	20X5X2	272X2
37.0X5	4.9	27X5X1	215X2
27.0X5	3.68	16X5X1	162X2
37.3X2.5	2.45	15X2.5	215
45.0	1.23	21X0.5	104

Table 6.17: $\alpha\beta$ inductance measurements, Rotor Excited Yellow and Blue connected together, Red supplied. Stator factor=1/2, Rotor factor=1/2.

V1	I1	W1	V2
45.9X10	2.0	27X10X0.5	179
35X10	1.5	16X10X0.5	136
47.6X5	1.0	40X5X0.2	92
24.5X5	0.5	12X5X0.2	47

Table 6.18: $\alpha\beta$ inductance measurements, Stator Excited, Stator factor=1/2, Rotor factor=1/2.

V1	I1	V2
35X5	6.125	226X2
27X5	4.9	180X2
40.25X2.5	3.68	275
26.7X2.5	2.45	180
32	1.23	86.5

Table 6.19: $\alpha\beta$ inductance measurements, Rotor Excited, Stator factor=1/2, Rotor factor=2/3.

VB_l	IB	IR	WB	-WR	Nr
450	2.3	2.4	700	7.2X50	1495
435	2.19	2.3	630	6.4X50	1495
400	2.0	2.1	550	5.3X50	1495
380	1.9	2.0	500	4.75X50	1495
360	3.55X0.5	1.9	450	3.9X50	1495
340	3.3X0.5	1.75	390	3.1X50	1495
320	3.1X0.5	1.65	69X5	2.6X50	1494
300	2.95X0.5	1.6	64X5	2.3X50	1493
280	2.85X0.5	1.55	58X5	2.0X50	1492
260	2.6X0.5	1.35	50X5	1.4X50	1491
240	2.45X0.5	1.25	44X5	1.0X50	1490
220	2.25X0.5	1.2	39X5	0.8X50	1489
200	2.1X0.5	1.15	70X2.5	0.85X25	1489
180	4.77X0.2	1.1	150.5X5X0.2	0.3X2X5	1485
160	4.74X0.2	1.0	138.0X5X0.2	0.0	1483
140	4.24X0.2	0.94	110.0X5X0.2	0.0	1477
120	4.2X0.2	0.9	98.0X5X0.2	0.0	1470

Table 6.20: Running Light test Two Wattmeter Method. Slip-ring rotor no imbalance.

VB_l	V_{ph}	W_{ph}	L_m	R_m	ψ
450	260	113.4W	338mH	573Ω	79.3°
435	251	103.4	361	609	79.4
400	231	95.0	366	561	78.4
380	219.4	87.5	366	550	78.1
360	207.8	85.0	368	508	77.1
340	196.3	78.3	378	492	76.4
320	185	73.3	380	466	75.6
300	173	68.3	357	438	74.1
280	161.7	63.3	358	412	74.7
260	150.1	60.0	386	375	72.1
240	138.6	56.7	376	338	70.7
220	127	51.7	372	311	69.4
200	115.5	51.3	365	260	66.2
180	104	49.2	351	219	62.3*
160	92.4	46.0	353	186	59.1
140	80.8	36.7	336	177	59.3
120	69.3	32.7	294	147	57.2

Table 6.21: Results of Running Light test, Slip-ring rotor no imbalance: * Experimental error.

V_ph	W_{ph}	I_{ph}
29.4x2.5	56x2.5x5	15
28x2.5	50x2.5x5	14
26.2x2.5	44x2.5x5	13
24.4x2.5	38x2.5x5	12
22.6x2.5	31x2.5x5	11
20.5x2.5	26x2.5x5	10
46x1	136x2	9
41x1	106x2	8
36.3x1	82x2	7
30.5x1	59x2	6
25.4x1	40.5x2	5
20.5x1	27x2	4
15.0x1	15x2	3
10.0	6.5x2	2

Table 6.22: Locked Rotor tests on 51 bar cage rotor.

V_{ph}	W_{ph}	I_{ph}
250	29x5	3.15

Table 6.23: Running Light test on 51 bar cage rotor.

I_{ph}	l_l	I_{ph}	l_l
15A	6.04mH	8	6.22mH
14	6.13	7	6.3
13	6.12	6	6.18
12	6.15	5	6.23
11	6.35	4	6.14
10	6.3	3	5.93
9	6.13	2	6.04

Table 6.24: Leakage inductance l_1 versus I_{ph} for the 51 bar cage rotor.

Suspended Object	Period (10 samples)	Mass
Slip-Ring +P	0.951 sec	34.3 Kg
28 Slot +P	0.986	28.2
51 Slot +P	1.000	27.9
Special 51 +P	1.028	30.3
Unladen Platform	2.485	1.2
Bronze Cylinder +P	0.995	28.8

Table 6.25: Experimental data from tri-filiar test.

Rotor Type	Moment of Inertia
Slip-Ring	0.0982 Kgm^2
28 Slot	0.0842
51 Slot	0.0863
Special 51	0.1029

Table 6.26: Experimentally obtained angular momentum; The estimated error is about 6%.

Chapter 7

Induction Motor Modelling

7.1 Reasons for Modelling

There were two reasons which prompted the development of an Induction Motor simulator (model). In the first instance, it would provide a mathematical description of phenomena observed in the real machine, specifically the frequency content of the line current waveforms. Secondly, it could be used to predict the response of a general induction motor that may well have parameter values substantially different from those of the 11kW test rig machine.

Differential equations describing the operation of the Induction Motor (IM) have been derived by Stanley [14] and are depicted in Equation 7.1. These differential equations have non-constant co-efficients, since speed ($p\theta$) is a function of time, and as such cannot be solved in closed form.

$$\begin{pmatrix} Va \\ Vb \\ Vc \\ Ve \\ Vf \\ Vg \end{pmatrix} = \begin{pmatrix} R1+L1p & pMab & pMac & pMae & pMaf & pMag \\ pMab & R1+L1p & pMbc & pMbe & pMbf & pMbg \\ pMac & pMbc & R1+L1p & pMce & pMcf & pMcg \\ pMae & pMbe & pMce & R2+L2p & pMef & pMeg \\ pMaf & pMbf & pMcf & pMef & R2+L2p & pMfg \\ pMag & pMbg & pMcg & pMeg & pMfg & R2+L2p \end{pmatrix} \begin{pmatrix} Ia \\ Ib \\ Ic \\ Ie \\ If \\ Ig \end{pmatrix} \tag{7.1}$$

where p is the differential operator d/dt

If speed is made constant, then equation 7.1 can be solved by use of Laplace

Transforms to give rise to the analytical equations commonly used in the single phase equivalent circuit of the IM [52,67,79].

However by its very nature the starting transient cannot have a constant speed so that for this condition equation 7.1 must be solved by use of a differential analyser or a numerical integration technique.

The 3 phase IM equations may be transformed to a two phase equivalent system which greatly simplifies the solution as can be seen in equation 7.2.

$$\begin{pmatrix} Vds \\ Vqs \\ Vdr \\ Vqr \end{pmatrix} = \begin{pmatrix} Rs + Lsp & 0 & Mp & 0 \\ 0 & Rs + Lsp & 0 & Mp \\ Mp & Mp\theta & Rr + Lrp & Lrp\theta \\ -Mp\theta & Mp & -Lrp\theta & Rr + Lrp \end{pmatrix} \begin{pmatrix} Ids \\ Iqs \\ Idr \\ Iqr \end{pmatrix} \tag{7.2}$$

Thus the 3 phase IM can be represented by a two phase IM with two orthogonal currents in both the stator and rotor, namely, Ids, Idq and Idr, Iqr. The mathematical development of these 2 phase equations from the 3 phase equations is presented in Appendix A.

Equation 7.2 can be conveniently expressed in the form of equation 7.3, where the inductance matrix $[L]$, the matrix of rotational inductance terms $[G]$ and the resistance matrix $[R]$ can be separated.

$$[V] = ([R] + [L]p + [G] \cdot \omega_r) \cdot [I] \tag{7.3}$$

where $\omega_r = p\theta$ the rotor angular velocity

Equation 7.3 may be rearranged in terms of the derivatives of the four currents Ids, Iqs, Idr and Iqr

$$p[I] = [L]^{-1} \cdot [V] - ([R] + [G] \cdot \omega_r) \cdot [I] \tag{7.4}$$

A further equation is required which relates the torque and speed of the shaft and from this the derivative of the angular velocity $(p\omega)$ may be obtained as shown in equation 7.5.

$$p\omega = ((polepairs)^2 \cdot M \cdot (Ids \cdot Iqr - Iqs \cdot Idr) - \mathcal{F}(\omega))/J \tag{7.5}$$

It is numerically efficient to solve the models with the rotor's angular velocity

expressed in terms of electrical radians/sec. Thus :-

$$p\omega = polepairs\, p\omega_m \;\; (elect.rads/sec)$$

The 2 phase model equations have now been arranged in terms of five derivatives, which can be integrated numerically provided that initial conditions are specified. For the starting transient the initial conditions were that of zero value for all five variables, though transients during dynamic operation were also simulated from pure curiosity.

7.2 Numerical Integration

If a differential equation represents the rate of change of a variable with, say time, then to calculate the value of that variable at some future time, the slope (derivative) is projected forward to estimate this future value. The assumption is of course, that the derivative does not change substantially over this period. Referring to Fig.[7.1], it can be seen that the estimate at time $t1$ is correct, however the estimate at time $t2$ is incorrect. Numerical integration can only be performed if the step in time is sufficiently small so that the derivative can be assumed to remain constant over that time interval.

If a very small fixed step in time is used the solution may well be correct, but the penalty is a large computing time. If the step size is too small, numerical rounding errors can arise and may accumulate. There are therefore two constraints on the choice of step size in that it must not be too large nor too small. A further disadvantage of using a fixed step size is that the error in the estimate is not controlled and can vary throughout the solution. Though fixed step methods have been successfully used by other researchers [27,74], in neither case did they require to apply signal processing to the results. This error in the estimate can be viewed as the background noise level caused by spurious signals which will ultimately determine the smallest signal component that can be observed. Obviously control of this error (background noise) is desirable so that frequency components of small amplitude are not obscured.

A large variety of numerical integration techniques are available but can be broadly separated into Single-Step methods such as the Runge-Kutta type and

Multi-Step methods such as the Predictor-Corrector type [66,80]. As discussed in Chapter 2, Humpage [25] applied a variety of these techniques to the solution of power system transients primarily for the purpose of reducing the computing time.

A comparison was made between a DQ model solved by the single-step RKF45 method and by the Adams-Moulton multi-step method. No significant difference was observed between the two solutions. The Adams-Moulton method was not self starting as is the case for many predictor-corrector techniques and required a single-step method to provide the solutions for the first four steps. In view of these considerations the single-step RKF45 method was adopted.

7.3 Error Control

Error control can be effected by using two methods of estimation. If the two estimates agree to within a specific tolerance then the future value of the variable is accepted and the calculation proceeds to the next step. If not, the step length is reduced and estimates are performed again.

Each estimate is obtained by an update formulae which is a weighted sequence of stages (factors $K0 to K5$). Each stage is itself calculated by a weighted sequence of sub-step calculations and previous stage results.

The resulting method is often referred to as the RKF45 Method after Runge-Kutta-Fehlberg and having a 4^{th} and 5^{th} order estimates. A detailed derivation of this method can be found in [81,80].

7.4 RKF45 Method

This numerical integration technique uses six stages for its calculation of its two estimates. The six stages are calculated by the following equations :-

$$K_0 = \mathcal{F}(t_0, y_0)$$

$$K_1 = \mathcal{F}(t_0 + \frac{h}{4}, y_0 + \frac{h}{4}K_0)$$

$$K_2 = \mathcal{F}(t_0 + \frac{3h}{8}, y_0 + h\left(\frac{3}{32}K_0 + \frac{9}{32}K_1\right)$$

$$K_3 = \mathcal{F}(t_0 + \frac{12h}{13}, y_0 + h\left(\frac{1932}{2197}K_0 - \frac{7200}{2197}K_1 + \frac{7296}{2197}K_2\right))$$

$$K_4 = \mathcal{F}(t_0 + h, y_0 + h\left(\frac{439}{216}K_0 - 8K_1 + \frac{3680}{513}K_2 - \frac{845}{4104}K_3\right))$$

$$K_5 = \mathcal{F}(y_0 + \frac{h}{2}, y_0 + h\left(-\frac{8}{27}K_0 + 2K_1 - \frac{3544}{2565}K_2 + \frac{1859}{4104}K_3 - \frac{11}{40}K_4\right))$$

where h is the step in time and y_0 the initial condition.

After the six stages have been calculated for the differential equation $\mathcal{F}(t_0, y_0)$ the fourth and fifth order updates (estimates) are calculated as follows:-

The fourth order update is given by :-

$$y_1 = y_0 + h\left(\frac{25}{216}K_0 + \frac{1408}{2565}K_2 + \frac{2197}{4104}K_3 - \frac{1}{5}K_4\right)$$

and the fifth order formula is :-

$$y_1' = y_0 + h\left(\frac{16}{135}K_0 + \frac{6656}{12825}K_2 + \frac{28561}{56437}K_3 - \frac{9}{50}K_4 + \frac{2}{55}K_5\right)$$

The difference between the fourth and fifth order estimates gives the local truncation error ϵ :-

$$\epsilon = y_1' - y_1 = h\left(\frac{1}{360}K_0 - \frac{128}{4275}K_2 - \frac{2197}{75240}K_3 + \frac{1}{50}K_4 + \frac{2}{55}K_5\right)$$

A flow chart of the error controlled integration procedure is shown in Fig.[7.2].

Referring to Fig.[7.2], from the initial conditions a step is taken forward in time. After some calculation an estimate of the error is obtained. If the error is too large, the step length h is halved and the calculation is performed again with the new smaller step. If the error is within tolerance,the 4^{th} order estimate of the variable is accepted and becomes the initial conditions for the next step in the calculation. A check is also incorporated to ensure that the error is not too small since this will lead to excessive steps being taken with penalties in time of computation and possible truncation error accumulation. If the error is too small, the time step h is doubled for the next stage in the calculation.

For the 2 Phase model, the above calculations must be performed for each of the five derivatives at every step/sub-step during the calculation. In this manner a period of induction motor performance may be simulated from a given set of initial conditions.

7.5 Sampling of the Variables

A problem which arises by use of an error control algorithm, is that the step size is variable. Though this step size variation in fundamental to the operation of the error control it presents a problem for any subsequent signal processing. Though signal processing techniques do exist for data sampled randomly [71,82], these tend to be highly numerically intensive and are to be avoided unless a constant sampling rate is unachievable.

There is thus, one further level of control required for the IM model in that the variables must be sampled at a uniform rate. This is achieved by forcing a step to fall on all the desired sample points. For example, if the desired sampling rate is 1ms then as the solution nears an integer millisecond point, the step is forced to fall on that millisecond point. This forced step is always less than or equal to the optimal step chosen by the error control algorithm. The net effect is that the solution proceeds with variable step lengths but only those falling on the sample points are stored for subsequent processing. The intermediate results obtained between sample points, having served their purpose in error control, can then be discarded.

7.6 The 2 Phase Model

7.6.1 Initial Work

Both the models of Edwards [83] and Slater [74] were implemented as a first stage in model developments. Edward's model dealt with plugging and dynamic braking, but the integration technique (Trapeziodal Method) was not sufficiently stable to allow study of the starting transient. Slater's modelling was mainly to deduce and reduce the large torque oscillations during the initial starting period. This model allowed non-simultaneous switching of the supply lines so that the torque oscillations could be minimised. The effects of switching any two phases at an angle α, then the third line at angle β are shown in Figs. [7.3,7.4] for minimum and maximum torque oscillation.

7.6.2 Imbalance in a 2 Phase Model

The equivalent two phase machine of the imbalanced three phase machine may be obtained by replacing rotor resistances $R2$ in equation 7.1 with three individual resistances, R_{ra}, R_{rb} and R_{rc}.

The next step in the development of the 2 phase model is to choose the frame of reference. Krause [21] provides a convenient means of applying the desired transform with a generalised transform from 3 phase to 2 phase with an arbitrary reference frame ω.

$$\begin{pmatrix} C_3 \end{pmatrix} = \begin{pmatrix} C_s & C_r^t \\ C_r & C_s^t \end{pmatrix}$$

where

$$\begin{pmatrix} C_s^t \end{pmatrix} = \begin{pmatrix} \sqrt{2/3} \end{pmatrix} \begin{pmatrix} cos(\theta) & cos(\theta - 2\pi/3) & cos(\theta + 2\pi/3) \\ sin(\theta) & sin(\theta - 2\pi/3) & sin(\theta + 2\pi/3) \\ 1/\sqrt{2} & 1/\sqrt{2} & 1/\sqrt{2} \end{pmatrix}$$

and

$$\begin{pmatrix} C_r^t \end{pmatrix} = \begin{pmatrix} \sqrt{2/3} \end{pmatrix} \begin{pmatrix} cos(\beta) & cos(\beta - 2\pi/3) & cos(\beta + 2\pi/3) \\ sin(\beta) & sin(\beta - 2\pi/3) & sin(\beta + 2\pi/3) \\ 1/\sqrt{2} & 1/\sqrt{2} & 1/\sqrt{2} \end{pmatrix}$$

where $\theta = \omega\, t$, $\beta = \theta - \theta_r$ and $\theta_r = \omega_r\, t$.

The selection of the reference frame is obtained by substituting :-

1) $\omega = \omega_e$ for a synchronously rotating reference frame.

2) $\omega = \omega_r$ for a reference frame fixed on the rotor.

3) $\omega = 0$ for a reference frame fixed on the stator.

Selecting $\omega = 0$ for a reference frame fixed on the stator gives :-

$$\theta = \omega t = 0$$

$$\theta_r = \omega_r t$$

and

$$\beta = \theta - \theta_r = -\theta_r$$

Substituting $\beta = -\theta_r$ into the generalised transform and applying it to the 3 phase quantities will result in the appropriate 2 phase equations.

Considering only the rotor circuit, with the three individual rotor resistances R_{ra}, R_{rb} and R_{rc} results in the two phase equivalent of the unbalanced machine.

$$\begin{pmatrix} C_r^t \end{pmatrix} = \begin{pmatrix} \sqrt{2/3} \end{pmatrix} \begin{pmatrix} cos(-\theta_r) & cos(-\theta_r - 2\pi/3) & cos(-\theta_r + 2\pi/3) \\ sin(-\theta_r) & sin(-\theta_r - 2\pi/3) & sin(-\theta_r + 2\pi/3) \\ 1/\sqrt{2} & 1/\sqrt{2} & 1/\sqrt{2} \end{pmatrix}$$

The transformed rotor resistance matrix is given by :-

$$[R_{2phase}] = [C_r]^t [R_{3phase}][C_r]$$

This results in four resistive terms in the rotor circuit given by R_{11}, R_{12}, R_{21} and R_{22} where :-

$$R_{11} = \frac{2}{3}\left[R_{ra}cos^2(\theta_r) + R_{rb}cos^2(\theta_r + \frac{2\pi}{3}) + R_{rc}cos^2(-\theta_r + \frac{2\pi}{3})\right]$$

$$R_{12} = R_{21} = \frac{2}{3}\left[-\frac{R_{ra}}{2}sin(2\theta_r) - \frac{R_{rb}}{2}sin(2[\theta_r + \frac{2\pi}{3}]) + \frac{R_{rc}}{2}sin(2[-\theta_r + \frac{2\pi}{3}])\right]$$

$$R_{22} = \frac{2}{3}\left[R_{ra}sin^2(\theta_r) + R_{rb}sin^2(\theta_r + \frac{2\pi}{3}) + R_{rc}sin^2(-\theta_r + \frac{2\pi}{3})\right]$$

For the balanced 3 phase machine $R_{ra} = R_{rb} = R_{rc} = R2$ so that :-

$$R_{11} = R2$$

$$R_{12} = R_{21} = 0$$

$$R_{22} = R2$$

as was previously derived for the balanced machine in Appendix [A].

Thus for an unbalanced 2 phase machine with the reference frame fixed on the stator, time varying resistances appear in the solution. These time varying resistances may have been avoided by choosing a reference frame stationary with respect to the rotor [21]. However this does not reduce the complexity of the model as the frequency of the supply voltages will then be a function of slip.

7.7 The 3 Phase Model

7.7.1 Introduction

An improved 3 Phase simulation has been developed by direct solution of the induction motor equations [36]. Though more difficult to program and a heavier

computational burden it does not have the same constraints as the d-q-0 model such as the inability to represent supply harmonics and the requirement for either the stator or rotor to be balanced [79].

With this 3 phase model it is possible to apply saturation to individual circuits within the rotor and stator. Imbalance on both stator and rotor windings is permissible as is the application of supply voltages with realistic harmonic components. Furthermore this 3 phase model was a first step to expanding the model to represent the individual rotor bars. The representation of each rotor bar within a 51 bar rotor was expected to result in a more accurate model of the test rig. This expanded model may also have been suitable, with some modification, to predict the response of an arbitrary machine from the name-plate data.

Another advantage of the direct three phase representation is that the variables involved are the actual physical quantities of the motor. They are not transformed to any other reference frame for solution.

7.7.2 Theoretical Development

The relationship between terminal voltage e, the current i, resistance R and flux linkage ψ is given by Maxwell's circuit equation :-

$$e = p\psi + Ri \tag{7.6}$$

where $p = d/dt$

This equation may be applied to each phase of a 3 phase machine as shown generally by equation 7.7.

$$e_1 = Ri_{11} + p[L_{11}i_1 + M_{12}i_2 + M_{13}i_3 \cdots M_{16}i_6] \tag{7.7}$$

Application of equation 7.7 for all six phases will result in the matrix representation of equation 7.1.

For the three phase model, it is more convenient to retain the flux linkage terms, so each winding is represented as shown below :-

$$e_{sa} = p\psi_{sa} + R_s i_{sa}$$

$$e_{sb} = p\psi_{sb} + R_s i_{sb}$$

$$e_{sc} = p\psi_{sc} + R_s i_{sc}$$

$$e_{ra} = p\psi_{ra} + R_r i_{ra}$$

$$e_{rb} = p\psi_{rb} + R_r i_{rb}$$

$$e_{rc} = p\psi_{rc} + R_r i_{rc}$$

where subscripts s and r represent the stator and rotor respectively and subscripts a, b and c represent the three windings of both stator and rotor.
These voltage equations may be expressed in matrix form as :-

$$[e] = p[\psi] + [R][i] \tag{7.8}$$

Equation 7.8 may be re-arranged in terms of flux derivatives :-

$$p[\psi] = [e] - [R][i] \tag{7.9}$$

The relationship between the phase flux linkages $[\psi]$ and the phase currents $[i]$ may be expressed as :-

$$[\psi] = [L][i] \tag{7.10}$$

where

$$[\psi] = [\psi_{sa}, \psi_{sb}, \psi_{sc}, \psi_{ra}, \psi_{rb}, \psi_{rc}]^t$$

$$[i] = [i_{sa}, i_{sb}, i_{sc}, i_{ra}, i_{rb}, i_{rc}]^t$$

and the inductance $[L]$ matrix is :-

$$\begin{pmatrix} Lss & Mss & Mss & Msr\cos(\theta) & Msr\cos(\phi) & Msr\cos(\rho) \\ Mss & Lss & Mss & Msr\cos(\rho) & Msr\cos(\theta) & Msr\cos(\phi) \\ Mss & Mss & Lss & Msr\cos(\phi) & Msr\cos(\rho) & Msr\cos(\theta) \\ Msr\cos(\theta) & Msr\cos(\rho) & Msr\cos(\phi) & Lrr & Mrr & Mrr \\ Msr\cos(\phi) & Msr\cos(\theta) & Msr\cos(\rho) & Mrr & Lrr & Mrr \\ Msr\cos(\rho) & Msr\cos(\phi) & Msr\cos(\theta) & Mrr & Mrr & Lrr \end{pmatrix}$$

where $\phi = \theta + 2\pi/3$, $\rho = \theta - 2\pi/3$

Equation 7.10 may be rearranged in terms of currents :-

$$[i] = [L]^{-1}[\psi] \tag{7.11}$$

The matrix $[L]$ is dependent on the rotor electrical angle θ, which is known from initial conditions or from a previously calculated value. By inverting $[L]$ and

using equation 7.11, the current vector [i] may be evaluated. The values of the current vector [i] may then be used to calculate the electrical torque Te by use of equation 7.12.

$$\begin{aligned} Te = -polepairs[&(i_{sa}i_{ra} + i_{sb}i_{rb} + i_{sc}i_{rc})\, sin(\theta) + \\ &+(i_{sa}i_{rb} + i_{sb}i_{rc} + i_{sc}i_{ra})\, sin(\theta + \frac{2\pi}{3}) + \\ &+(i_{sa}i_{rc} + i_{sb}i_{ra} + i_{sc}i_{rb})\, sin(\theta - \frac{2\pi}{3})]M_{sr} \end{aligned} \tag{7.12}$$

The rotor electrical angle θ required for forming the inductance matrix [L] can be found by integrating the speed equation :-

$$J\frac{d^2\theta_m}{dt^2} + \mathcal{F}\frac{d\theta_m}{dt} + T_m = T_e \tag{7.13}$$

This speed equation is second order and may be separated into two first order differential equations as shown below :-

$$\frac{d\omega_m}{dt} = \frac{1}{J}(T_e - T_m - \mathcal{F}(\omega_m)) \tag{7.14}$$

and

$$\frac{d\theta_m}{dt} = \omega_m \tag{7.15}$$

where

$$\theta_m = \theta / polepairs$$

The three phase model therefore requires the integration of six flux linkage derivatives. It also requires both the derivative of the speed (acceleration) and the derivative of the rotor angle (speed) to be integrated. Numerical integration of the eight differential equations is achieved in the same manner as with the 2 phase models.

7.7.3 Inversion of Inductance Matrix

In order to obtain the currents [i] from equation 7.11, it is necessary to invert the inductance matrix [L] at every step and sub-step of the solution. In general the co-efficients of the inductance matrix [L], being self and mutual inductances of the motor are small; hence the value of the determinant $det[L]$ will be quite

small. Since $det[L]$ is a denominator in the calculation of $[L]^{-1}$, care must be taken to preserve the numerical accuracy of the inverted matrix. Several matrix inversion methods were tried but only the Jacobian, back substitution with partial pivot method [66] was sufficiently accurate. The less accurate methods caused numerical instability of the solution. This Jacobian inversion method was iterative in nature and was thus numerically intensive.

7.7.4 Calculation Procedure

The diagrammatic representation of the solution of the 3 phase model is shown in Fig.[7.5]. The procedure of the solution is as follows :-

Set the initial conditions, which in the case of the starting transient results in all derivatives of the variables and the variables themselves to be of zero value. Using the values of supply voltage, calculate the derivatives. Integrate each to obtain the flux linkage, speed and rotor angle. The error control algorithm will determine if these values fall within tolerance and take the appropriate action as described in the 2 phase modelling section 7.3.

From the rotor electrical angle just obtained, form matrix $[L]$ and invert it to obtain $[L]^{-1}$. It is now possible to calculate the current vector $[i]$ and hence the electrical torque Te. If any load torque or friction/ windage losses are modelled then these must be subtracted from the electrical torque. At this point all variables have been estimated and the solution proceeds for the next time step. In this manner the response of a 3 phase IM can be simulated from a given set of initial conditions.

7.8 Results of 2 Phase DQ Modelling

Initially fixed values of parameters obtained from the standard RL/LR tests were used in the model. As can be seen from Fig. [7.6] the model takes considerably longer to accelerate to speed than the 400ms of the real unloaded machine. However several non-linearities had yet to be incorporated into this model. The effect on the response of the 2 phase model by various parameter changes was observed. This was performed so that the results of previous

studies [26] could be confirmed and also to assess the experimental accuracy required for parameter measurement.

The phenomena observed were :-

- Mutual Inductance saturation
- Leakage Inductance saturation
- Apportioning of leakage reactance between Stator/Rotor
- Skin effect

7.8.1 Mutual Inductance Saturation

From the experimentally derived Mutual Inductance curve, polynomials were generated which related the current flowing in the windings to the value of mutual inductance as shown in Fig.[7.7]. The application of mutual inductance saturation made little change to the model's response though the initial current peaks were slightly larger than that obtained with a fixed value of mutual inductance. As found by Slater [74] the induction motor's response is particularly insensitive to changes in the mutual inductance. Smith [33] found that mutual inductance saturation was of little significance during the starting of an electrically inert machine and was in fact only of significance in the two cases of Plugging and that of the capacitor excited induction generator. Furthermore, the component indicative of rotor faults was known from experiment to occur at the latter stages of the starting transient whereas the saturation of the mutual inductances has greatest effect at the initial stages of the starting transient due to the flux doubling effect. Figure [7.8] shows the variation of the mutual inductance throughout the starting period where the flux doubling effect can be clearly observed. There is also a slight decrease in mutual inductance as the machine reaches operational speed since the current and hence volt drop across the stator leakage reactance and resistance has decreased impinging a slightly larger voltage on the mutual inductance.

7.8.2 Leakage Inductance Saturation

From experimentally derived data obtained by a sequence of locked rotor tests, the relationship between winding current and leakage inductance was obtained. These experiments could only be performed upto a current level of 15A and the shape of the leakage saturation characteristic was intuitively extended from this point by examination of curves from literature [52,67]. The leakage saturation characteristic of the wound rotor machine is shown in Fig. [7.9] where the initial rise and then fall of leakage inductance can be clearly seen. During the starting period, the line current peaks of the real wound rotor machine have initial values in the region of 80A and do not decrease to 15A until the latter stages of the transient. The machine therefore spends considerable time in the upper current levels of the leakage saturation characteristic for which there is no experimental data. A number of "tails" for this characteristic were tried (dotted lines of Fig.[7.9]) and finally the bold line characteristic was accepted since it brought the model's response close to that of the real machine as can be seen in Fig.[7.10].

The simulation of the leakage saturation was achieved by altering the leakage inductance of both rotor and stator as a function of the rms d and q currents in a manner similar to that used by Lipo [24]. The resulting rms saturation current for both rotor and stator was obtained using the following formula :-

$$il_{sat} = \sqrt{id^2 + iq^2} \tag{7.16}$$

The value of il_{sat} is then used in a polynomial approximation of the leakage inductance versus current characteristic obtained experimentally, resulting in a value of leakage inductance for that particular point in time. Representing this characteristic with only one polynomial required that the polynomial be of 33^{rd} order for a reasonable approximation. This increased the computation time significantly and was cumbersome to program. A better method was to use two 3^{rd} order polynomials, one representing the characteristic upto a current level of 7.5A, and the other from this point upto the maximum value of current. On obtaining the present value of the current the software would choose the appropriate polynomial to evaluate the value of leakage inductance. A smooth change over between polynomials was ensured by using a large number of data

points either side of 7.5A in their creation, forcing them both to have the same shape in this region. The coefficients of both 3^{rd} order polynomials are listed below:-

Sat0 = 8.73761e-3
Sat1 = 2.39525e-3
Sat2 = -4.89567e-4
Sat3 = 2.82875e-5

Sat4 = 1.35776e-2
Sat5 = -3.20418e-4
Sat6 = 3.75331e-6
Sat7 = -1.41959e-8

For current levels of 7.5A and below the leakage inductance was calculated with the following expression:-

$$ls = Sat0 + Sat1(il_{sat}) + Sat2(il_{sat})^2 + Sat3(il_{sat})^3$$

and for currents above 7.5A :-

$$ls = Sat4 + Sat5(il_{sat}) + Sat6(il_{sat})^2 + Sat7(il_{sat})^3$$

Though the calculation of il_{sat} and subsequent use in the above polynomials was a very approximate method, it did make the leakage inductance vary with the current level and improve the model's response.

The saturation curve represented by polynomials was incorporated into the model. Several characteristics appeared in the signal spectra of the simulation due to leakage inductance saturation and these could also be observed in the real machine spectra. The most notable was the introduction of the notches throughout the spectrum, when saturation was modelled. These can be observed in the real data as can be seen in Fig.[7.11] and in the simulation as shown in Fig.[4.4]. One other characteristic observed in the simulations was the increase in both the amplitude and frequency of the "13Hz" component. This can easily

be explained since saturation will cause larger currents to flow and hence results in a larger D.C. component induced in the rotor circuits at switch on [18]. As the machine speeds up the D.C. component is decaying at a rate dependent on the L/R time constant of the rotor circuit. This results in a synchronous machine action during start-up which induces an increasing frequency component in the stator windings with an amplitude that decays exponentially as discussed in Chapter 4. It was therefore possible with the use of this simulation to identify components in the real spectra. One notable failing of this application of leakage saturation was that no 3^{rd} harmonic at 150Hz was generated, as is known to be the case for the non-linearity of saturation [52]. No further work was undertaken to resolve this problem since the 3 phase model was under development which would allow leakage saturation to be modelled on an individual phase basis.

7.8.3 Apportioning Leakage Inductance

In the derivation of the equivalent circuit it is usual to equally apportion the leakage inductance between the rotor and stator windings. The model was run using quite substantial re-distributions of the parameter which had little effect on the response. However if the total leakage inductance were changed by a small percentage then a substantial change in the machines response could be observed as shown in Fig.[7.12] which results in a 10% change in the nominal value of 10mH.

It is worth considering whether the leakage inductance can be measured to this accuracy. The AVOs used in experimentation are calibrated to measure rms values for sinusoidal waveforms. The line current waveform during the locked rotor test, if viewed on an oscilloscope, is most definitely not a pure sinusoid, having a prominent 3^{rd} harmonic and possibly higher order harmonics.

7.8.4 Skin Effect

No experimental data was obtained for variation in rotor leakage reactance and resistance due to skin effect. However, Cameron [3], who had previously used the test rig applied a method developed by Liwschitz-Garik [84,85] to calculate the variations in these two parameters.

The Skin Effect arises because the flux linkage in the lower conductor sections in the rotor bar due to leakage flux is greater that the flux linkage in the upper sections. This results in a higher emf induced in the lower sections of the rotor bar which leads to the current density reducing from the top to the bottom of the conductor. The skin effect tends to increase the resistance and reduce the reactance of the bar, hence model parameters R2 and l_2 are affected. Both values for these parameters are obtained from the locked rotor test in which the rotor currents are at a frequency of 50Hz.

Expressions for the change of R2 and l_2 due to skin effect have been developed for a bar with rectangular cross-sectional area [84]. A further calculation is required to account for non-rectangular bar shapes [85]. The procedure developed was applied by Cameron [3] to the 51 bar rotor of the laboratory test rig. This procedure involves calculating the effective bar height h of the non-rectangular rotor. Thus a rotor bar with any cross-sectional shape may be represented by a bar of rectangular cross section with an effective height h.

The following expressions were implemented in the DQ model :-

$$R2_{(50Hz)} = R2_{(fr)}\xi\frac{sinh(2\xi)+sin(2\xi)}{cosh(2\xi)-cos(2\xi)}$$

$$l_{2(50Hz)} = l_{2(fr)}\frac{3}{2\xi}\frac{sinh(2\xi)-sin(2\xi)}{cosh(2\xi)-cos(2\xi)}$$

where

$$\xi = \sqrt{\frac{\omega_{rc}\mu_o h^2}{2\rho}}$$

and

ω_{rc} = angular frequency of rotor currents

h = effective bar height

ρ = resistivity of bar metal (Ω m)

μ_o = permeability of free space

For the laboratory machine ξ is given by the expression :-

$$\xi = 0.034\sqrt{\omega_{rc}}$$

Variation of these two parameters could then be incorporated into the numerical solution. In this particular case the rotor resistance decreased by 1% and the leakage inductance increased by 0.3% over the starting period. The DQ model

using the 51 bar rotor parameter values showed no observable change in response due to skin effect. Previous research [86,87] has indicated that skin effect has little influence on low power motors, however, this will not be the case if large industrial machines are to be modelled [52]. Figure [7.13] shows a typical skin effect characteristic for a large machine.

7.8.5 Results from Imbalance in the 2 Phase Model

Using the DQ model with the reference frame fixed on the stator the value of the rotor phase resistance Ra was increased to simulate a high resistance winding. The results from the DQ model are best illustrated by performing spectral analysis via FFT on the line current waveform as shown in Fig.[7.14]. As with the real machine a noticeable undulation appears in the line current spectra between the 0 to 50Hz range due to imbalance in the rotor as shown in Fig.[7.11].

7.8.6 Problems with the DQ Models

As previously indicated the DQ models may be developed with frames of reference that are fixed with respect to, the stator, the rotor and the synchronous field. Krause [21] who originally developed the 2 phase equivalent models did simulate imbalance during the starting transient. Krause indicated that any reference frame may be used though to avoid sinusoidal rotor resistances it is more convenient to develop the model with a reference frame fixed on the rotor. Hancock [79] on the other hand argues that for the machine with an imbalanced rotor only the DQ model with a reference frame fixed on the rotor is applicable.

In this research project only the DQ model with reference frame fixed on the stator was stable throughout the starting transient. The DQ model with reference frame fixed on the rotor was stable upto the peak of the torque characteristic and the DQ model with reference frame fixed to the synchronously rotating field was unstable after a few tens of milliseconds of simulated time.

The development of these DQ models were double checked and found to be correct. This suggested that the integration routine may not have been suit-

able for the two unstable models. To check the integration routine, both the unstable models were re-written in FORTRAN so that access could be gained to the NAG numerical recipes library which contained a range of integration routines. It was suspected that the stiffness of the differential equations in these reference frames may have been the cause of the instability. Stiffness is a measure of the difference in magnitude of the derivatives. Differential equations with a high degree of stiffness require specialist integration routines for stable solutions. Grear's method, particularly suited to stiff equations was used as the integration routine. This method also calculated a stiffness factor for the set of equations which was found to be low for both cases, indicating that stiffness was not the problem. The solution by library integration routine progressed as with the the RKF45 method and were both unstable. These problems were unfortunately never resolved and by this time the direct three phase simulation was operative. This direct three phase simulation was more representative, in that, the variables related to parameters observed in the real machine, e.g. line current, furthermore less simplifying transformations were involved.

7.9 Results from 3 Phase Modelling

The three phase model was firstly operated using parameter values obtained from the wound rotor machine. Experimental work on the wound rotor machine had only been carried out under full load starts as the signal processing method at that time was not sufficiently refined to detect components indicative of rotor faults under no load starts. In view of this, all wound rotor modelling was carried out under full load so that meaningful comparisons could be made between real and simulated data. The response of the three phase model was identical to the equivalent two phase model's response for a given set of parameter values. The response of the model bore a close resemblance to that of the real machine, if leakage saturation were modelled. Leakage saturation was modelled in an identical fashion to that of the dq model except that the actual phase currents were used in the polynomials. As with the two phase model, experimental error in obtaining critical parameters such as the leakage inductance is thought to account for most of the discrepancy between the response of the real and simulated machine.

The implementation of leakage saturation was now based on a per phase basis. At each step/sub-step of the calculation, the currents of all three rotor and stator phases would be used to evaluate the leakage inductance value of that phase. The application of leakage inductance saturation brought about a similar improvement in response as with the DQ model, however in the 3 phase model, third harmonics and higher frequency odd harmonics were generated. There was of course, an increase in the computation required and hence the time of the simulation.

7.9.1 3 Phase Model in Steady State Operation

In order to check the spectrum of the simulated line currents, the three phase model was operated in steady-state since the spectrum of the real line current waveforms was well known [4,7]. In steady state the real machine is connected in delta and this was taken into account in the model so that direct comparisons could be made to the measurements of the real machine. The amplitude spectrum of the simulated steady-state line current waveform for the unbalanced case had side bands as with the real machine. These side bands $\mp$2sf,and their multiples $\mp n2sf$ are shown in Fig.[7.15]. The application of leakage inductance saturation did not affect the the amplitude of the LSB but increased the USB for reasons discussed in section 7.9.4. Figure [7.16] depicts the change in amplitude for both side bands for increasing rotor imbalance. As with the real machine these two sidebands increase in amplitude with increasing imbalance and their rate of increase reduces at higher fault levels. A comparison is presented in Table [7.1] between the change in side band amplitudes for a sequence of increasing fault levels from both the simulated and real machine. The absolute magnitude of the side bands with respect to the 50Hz component is substantially larger for the simulation than with the real machine being typically 20dB larger for the highest value of external resistance. This disparity was obviously due to the nature of the model itself in that it may be oversimplified or possibly omit some interaction within the real machine.

Despite the difference in absolute magnitude of the sidebands, the model's response in steady-state was found to be similar to that of the real machine and in particular the frequency of the sidebands for a given rotor speed had exact

correlation.

Resistance	Real LSB	Real USB	Sim'.LSB	Sim'. USB
0.3	0dB	0dB	0dB	0dB
0.33	5	6	28	25
0.36	11.4	12.4	32	31
0.39	12.1	13.1	35	35
0.42	13.6	14.6	37	37
0.45	14.6	15.6	38	38

Table 7.1: Increase of side band components in steady state for real and simulated wound rotor machine under full load.

7.9.2 3 Phase Model in Transient State

The response of the 3 phase model during the starting transient under full load starting conditions is shown in Figs.[7.17,7.18,7.19].

It was observed that under full load starts, that the real machine (in star configuration), would reach a pseudo-steady state period prior to the starter configuring the stator windings in delta. The speed and torque were noted as 1345 rpm (281 elec.rad s^{-1}) and 55Nm respectively. Using a load torque of 55Nm for the model resulted in the diagrams of Figs.[7.17,7.18,7.19] where it can be seen that the model reaches a speed of 275 elec.rad s^{-1}, showing close agreement to the response of the real machine. The line current waveforms for phases a and b are shown in Fig.[7.18] and have initial current peaks that are similar to the 80A current peaks of the real machine. Two rotor current waveforms are shown in Fig.[7.19]. As would be expected the rotor currents change their frequency as the machine accelerates to speed.

7.9.3 Imbalance During Transient State

A comparison was performed between the results obtained from the real and simulated wound rotor machine with increasing levels of rotor imbalance during the starting period under full load. These line current waveforms were processed with the 21Hz FIR method and the change in the LSB for increasing fault level

are shown in Table [7.2]. As with the steady state results the magnitude of the LSB components from the simulation are larger than that of the real machine though the difference has reduced to 10dB. The change in the LSB has however better correlation between real and simulated conditions and both have the same shape of characteristic, with smaller increases in LSB amplitude for increasing fault level as shown in Fig.[7.20].

Resistance	Real LSB	Sim'.LSB
0.316	0dB	0dB
0.342	4.2	7.4
0.362	6.4	10.9
0.378	8.1	12.9
0.40	9.8	14.6
0.42	10.9	16.3
0.44	12.0	17.2
0.454	12.9	17.7

Table 7.2: Increase of side band components through 21Hz filter for the real and simulated wound rotor machine during the starting period, full load.

7.9.4 The Upper Sideband (USB)

Line current waveforms from the three phase model during the starting transient for various condition of rotor imbalance were passed to the phase vocoder for analysis. The spectograms for the conditions of no imbalance, 58% imbalance with and without leakage saturation modelling are shown in Figs.[7.21,7.22,7.23] where they can be seen to be similar to those for the equivalent condition of the real machine depicted in Chapter[4]. The enhancement of the upper side band (USB) when leakage saturation was modelled agreed with the predicted response from steady-state theory [2]. The argument is as follows :-

The supply voltages applied to the stator windings result in a forward rotating field in the air-gap. This rotating field induces slip frequency EMFs in the rotor circuits. The air-gap field set up by the rotor circuits will therefore include a fundamentally distributed component which rotates at slip speed in the forward direction with respect to the rotor, and one of equal amplitude which rotates in the backward direction. With a symmetrical rotor, the backwards rotating

components can be shown to cancel, whereas for an unsymmetrical rotor the resultant is non zero. This field, which rotates at slip speed backwards with respect to the rotor, rotates forward at $(1-2s)$ times the synchronous speed with respect to the stator. It therefore induces EMFs of frequency $\mid 2s-1 \mid f$ in the stator windings. The stator current now consists of the normal mains frequency component, together with a component of $\mid 2s-1 \mid f$ times the mains frequency [1]. If the 3^{rd} time harmonic (3f) of the fundamental supply voltage is considered as an other source (due to saturation effects or imbalance of the supply) then, by argument a component of flux will exist in the airgap field at a frequency of $(2s_3-1)f_3$ Hz [2].

But $s_3 = (3\omega_s - \omega_r)/3\omega_s$

where w_s = synchronous speed and ω_r = shaft speed

therefore $s_3 = (3-\omega_r/\omega_s)/3$

$= (2+(1-\omega_r/\omega_s))/3$

$= (2+s)/3$

The third harmonic can also be expressed as

$f_3 = 3f$

and substituting gives

$(2s_3-1)f_3 = (\frac{2}{3}(2+s)-1)3f$

$= (2s+1)f$ i.e. the frequency of the upper side band.

The enhancement of the USB during steady state simulation (due to leakage inductance saturation) was less than that observed during starting transient. This is due to the large differences of current flowing which affects the magnitude of the harmonics produced by the leakage inductance characteristic. In the early experimental work, the USB was eliminated as a suitable feature for reliable diagnosis because of its high variance for a given fault condition. This variance is thought to be related to the generation of harmonics and their subsequent dependence on switching angle.

7.9.5 Supply Harmonics

The 3^{rd} harmonic of the mains supply voltage was modelled at 2% of the amplitude of the fundamental 50Hz component. This level of harmonic was considered to be representative of the maximum permissible in the supply. The three phase

model's supply voltages were changed to incorporate this harmonic. This made little change to the model's response. One of the advantages of the three phase model over the two phase models is that unequal supply voltages could be used. This would allow future studies of simultaneous stator and rotor faults plus the response of the inverter supplied machine. Inverter supplies are often rich in harmonic content.

7.9.6 Switching Angle of Voltage Supply

Slater [74] had shown that for simultaneous switching of the three supply lines, to a balanced machine, that the torque transient was independent of the switching angle. This is not the case for the three line currents which exhibit the same type of response as that obtained from energisation of a transformer [52] and observed in the early transformer experiments of this project. If the switching angle is adjusted to minimise the current transient on one phase of the machine, the other two phases (120° apart), exhibit an increase in their current transient. The combined effect is that the transient currents at starting under the conditions of simultaneous switching give rise to an identical total asymmetrical flux and hence torque transient. This could easily be verified by the use of the models.

It was of interest to determine what possible effect the point on wave switching had on the lower side band component and whether this could affect the diagnosis of rotor faults. The laboratory machine was not subjected to point on wave switching control since any diagnostic technique should not require this constraint as it is uncommon in industry.

The three phase model was used to obtain starting transients at a range of switching angles from 0° through to 360°. Using the phase vocoder the amplitude and time for the lower side band maximum to occur on channel 3 (23.44 Hz) was noted.

It was found that the maximum amplitude change for any switching angle was very small (0.04%) and that the time of the maximum varied in a regular fashion with switching angle. If plotted these results trace out a crude sinusoid suggesting that the position of the side band maximum (in time) varies sinu-

soidally with switching angle by a maximum of 4ms. When leakage saturation is modelled the variation resembles a sinusoid with a large 3^{rd} harmonic.

In the balanced machine the asymmetrical flux will act on an arrangement of equally spaced bars around the rotor periphery. Due to the unsymmetrical flux some bars will contribute more torque that others. If this asymmetrical flux is rotated spatially by changing the switching angle of the supply, then the torque contribution from each bar will be changed. However, the net torque generated will be the same, providing the rotor is viewed as a conducting sheet and spaces between bars are ignored.

In the unbalanced case, the spatial arrangement of the asymmetrical flux will influence the net torque generated. Consider if a broken bar is at a position where the asymmetrical flux may have generated a torque maximum if the bar had been whole. Obviously the broken bar cannot generate torque and the total combined torque of the rotor will be different to the case of a balanced rotor.

In the experimental work it was found that the amplitude of the 15Hz component exhibited a larger variance than that of the 21Hz component and this was thought to be due to rotor position and/or switching angle. It was of interest to see if the model exhibited this same phenomenon. With leakage saturation modelled the variance of the 15Hz component was found to be double that of the 21Hz component. Interestingly without leakage saturation modelling the opposite was true, though in both cases the variance was smaller than that when saturation was modelled.

7.9.7 Starting Position of Rotor

It was necessary to assess what influence the starting position of the rotor (specifically the position of the faulty bar) had on the measurement of side band amplitude. The three phase model was used to obtain a range of starting transients at a range of rotor starting angles measured with respect to phase *a* of the stator.

The simulated results suggested that for a given fault level the time at which the lower side band is a maximum is independent of the position of the rotor. This contrasts the experimental results that do tend to suggest that initial rotor

starting position does influence the time at which the LSB reaches its maximum.

It is known from experimental work on both cage and wound rotors that rotor imbalance causes the real machine to accelerate to operational speed in a shorter time that that of a balanced machine. This is not observed in the model where increasing imbalance results in a small increase in the run up time. Obviously some aspect of the real machine is not being correctly modelled, though an increase in resistance in all three rotor phases brings about an increase in starting torque as obtained with real machines.

7.9.8 Input Power, Rotor Power, Power Factor

In order to try and correlate the lower side band maximum in the latter section of the transient period other variables of interest were observed using the three phase model. The input power and rotor mechanical power are displayed in Fig.[7.24] for the balanced condition and Fig.[7.25] for the unbalanced case. These along with the torque could be examined to see if their maximums coincided with that of the lower side band. This was not found to be the case for all three variables. All three of the above waveforms could of course be processed by the phase vocoder to obtain their spectograms. This showed that all three variables were primarily composed of a large d.c. term representing the average value, an oscillatory term which started at 100Hz at standstill and decreased to a low frequency (typically 3Hz) at operating speed and a 50Hz component due to the asymmetrical flux during the initial period of the transient.

The power factor of a 3 phase induction motor changes throughout the starting period from an initial value of about 0.4 through a peak of almost 0.9 to its steady state value of 0.7 approximately [78]. The power factor characteristic is similar to that of the torque/speed curve though it peaks at later stage. Both rotor power and torque peaks have not been found to correlate with the LSB peak both occurring at a later time. It seemed reasonable to assume that the decreasing current level coupled with an increasing power factor may have resulted in a maximum that could cause the LSB peak. However calculating the power factor was not as straight forward as in steady state. The power factor will change throughout each single cycle of the supply voltage. An attempt was made using the Fourier Transform to obtain the phase of a line current waveform

and the phase of its supply voltage. Subtraction of the phase characteristics was believed to result in the phase difference and hence power factor at any particular point in time. The method was unsuccessful, and in retrospect it was thought that the inappropriateness of Fourier analysis to determine the spectral amplitude of a non stationary signal must surely apply equally to the determination of the phase angle. Future work in this research project must examine the phase shift between currents and voltages to determine their effect on the sideband components.

7.9.9 Imbalance on Stator

An advantage of the 3 phase model over the two phase DQ models is that imbalance can be implemented on both the rotor and stator. Two conditions of stator imbalance were simulated namely that of a low resistance winding and an imbalanced supply. In both cases, the model, when run in steady state showed a slight increase in the 150Hz component as found by Leonard [2] for real machines. The modelling in the starting transient case showed no components that may have interfered with the diagnosis.

7.9.10 Sidebands in a Balanced Machine

Steady state theory indicates that each rotor phase generates side bands which due to time and angular displacement cancel completely for the balanced machine [1,75]. The three phase model allows this to be observed since any quantity may be stored and displayed. Examination of the calculation of current shows that any stator phase current component is comprised of six terms as indicated below :-

$$Ia = [L^{-1}[1,1]\psi_{sa} + L^{-1}[1,2]\psi_{sb} + L^{-1}[1,3]\psi_{sc} + L^{-1}[1,4]\psi_{ra} + L^{-1}[1,5]\psi_{rb} + L^{-1}[1,6]\psi_{rc}]$$

where $L^{-1}[]$ is an element of the inverse of the inductance matrix.

The first term is the contribution of the phase to its own current. The next two terms are the contributions from the other stator phases. The three last terms are the current contribution from each of the rotor phases. The rotor current

contributions can be seen in Fig.[7.26] and Fig.[7.27] along with the summation of these rotor terms. The summation can be seen to be a sinusoid superimposed with a small low frequency oscillation. Analysis of any of the single rotor terms shows a side band component as found in the line current waveform of a machine with rotor faults. However analysis of the summation of the rotor terms results in the disappearance of the side band by cancellation as stated by steady state theory [1].

7.9.11 Bar Representation in the 3 Phase Model

For the steady state derivation of the single phase equivalent circuit the effective phase resistance may be calculated for a cage rotor [39]. This entails partitioning the end-rings into as many sections as there are rotor bars. The resistance of the two end-ring sections for a particular bar are then appended to the resistance of that bar. This involves the use of a transformation to account for the differences between bar current and end-ring current. This transformation is analogous to the reflection of an impedance from, say a secondary winding to the primary winding of a transformer. Thus the whole rotor is now represented by rotor bars which incorporate their portion of end-ring resistance, suitably transformed. To obtain the equivalent rotor phase resistance one bar's resistance is further transformed taking into account parameters such as the stator winding factor, the total number of bars and the number of series turns per phase, as indicated in equation 7.17.

At first it was thought that reducing the number of bars by one but maintaining the end-ring resistance would be representative of a broken bar as shown below :

$$R2' = (12/(R-B))(k_w T)^2 \left[r_b + (R\, r_{er})/(2\, polepairs^2 \pi^2)\right] \qquad (7.17)$$

R :- number of bars

B :- number of broken bars

T :- number of series turns/phase

k_w :- stator winding factor

r_b :- bar resistance

r_{er} :- end ring resistance

Equivalent values of phase resistances for a given number of broken bars were calculated using equation 7.17. These resistances were used in a single rotor phase in the 3 phase cage model, the other two phase resistances being calculated for a balanced rotor. The number of broken bars and the change in amplitude of the component of interest for the 21Hz filter, for both the real and simulated cases are presented in Table [7.3].

Condition	Real F.L.	Sim'. F.L.	Real N.L.	Sim'. N.L.
Balanced	0dB	0dB	0dB	0dB
1 Broken Bar	15	26	11.5	13.5
2 Broken Bars	23	26.8	18.8	14.3
3 Broken Bars	27.5	27.9	23.3	14.9
10 Broken Bars	-	31.9	32	19

Table 7.3: Increase in side band component measured from computer model of cage rotor machine versus number of broken bars.

The increase between the balanced and single broken bar cases is very large compared to that obtained for the real machine. This is partly due to the lack of background noise which is to all intents and purposes absent from the computer simulation. An other contributory factor is that the balanced condition is truly balanced unlike the real machine where inherent imbalance is always present due to the manufacturing process. Both these factors raise the background noise floor of the real machine and hence the above measurement (whether real or simulated) is in fact from the noise floor to the specific fault level. As with the wound rotor machine simulation the LSB during the starting transient is larger than that of the real machine. The change in the amplitude of the simulated LSB component does increase as the number of broken bars increases as found with the real machine.

One further problem with the 3 phase cage rotor machine simulation was that the leakage inductance had only been measured upto 15A and found to be linear. With the wound rotor machine, the turning point of the leakage saturation curve had been reached and a "tail" had been estimated to obtain the leakage inductance at higher current levels. With the cage rotor machine, the maximum was not known and this meant that the modelling of the leakage inductance would have been even more approximate than that of the wound rotor machine.

In view of this a fixed value of leakage inductance was chosen (4mH) which would cause the machine to accelerate to speed in the same time as that taken by the real machine.

The 3 phase model had shown good agreement for general trends and the spectral components generated by imbalance. However it was clear that the rotor circuit was not being adequately represented for the cage rotor with broken bars.

The apparent rotor phase seen from the stator is not fixed on the rotor (unlike the wound rotor phase), so that as the rotor turns bars enter and exit the apparent phase. A broken bar, thus rotates through all three rotor apparent phases and it is thought that this cannot be realistically represented by a small increase in one of the rotor's phase resistances of the model. One possible solution to this problem was to model all the rotor bars and end-rings and not just lumped phases. This had been under consideration from the onset of the modelling undertaken in this research work. The problem with the present cage rotor representation is that if the end-ring resistances are appended to the appropriate bars then the rotor may be drawn as shown in Fig.[7.28]. In this situation the breaking of a bar suggests that no current will flow through the end-ring sections connected to it. This contradicts work by Williamson [1] and Weichsel [88] who have shown that currents do flow in the end-rings sections associated with broken bars.

Furthermore, despite the general success of the models to represent the faulted induction motor, there was one notable condition in which they failed to respond as with the real machine. It had been observed that a rotor with broken bars would accelerate to operational speed in less time than that with a balanced rotor. This was not the case with the modelling which in general resulted in a small increase in time taken over that of the balanced condition.

If all rotor phase resistances of the model were increased the torque/speed characteristic was shifted to give a larger starting torque as with real machines. It was quite evident that there was some mechanism within the real machine which was not being represented in the model.

The problems with assigning an equivalent phase resistance value to represent broken bars and the limitations of the rotor modelling indicated that a bro-

ken end-ring should manifest itself differently to that of a broken bar. This was known not to be the case in steady state, where broken end-rings generate sidebands as with broken bars. Steady state techniques do not presently differentiate between bar and end-ring faults, instead a measure of the condition of the rotor called the broken bar factor (BBF) is presented. Nevertheless experimentation was carried out using an otherwise healthy rotor which had a small cross section removed. This resulted in a high resistance end-ring section between two bars. These results are presented in Chapter 5 where it is shown that differentiation between end-ring faults and bar faults may be possible, but more importantly the results clearly indicated that the rotor modelling would require improvement for more realistic results.

Extension of the model to represent 51 rotor bars had been considered for some time. A model with three stator phases and six rotor phases had been completed as a first step towards modelling 51 bars as 51 phases. It was now clear that this intended model would not accurately represent the end-rings and hence the rotor as a whole.

7.10 Discussion

The 2 phase DQ modelling had showed that the effects of mutual inductance saturation, skin effect and stator/rotor leakage inductance re-distribution had minor effects on the response of the modelled laboratory machine. Despite the simplicity of the modelling of the leakage inductance saturation characteristic it was clear that this parameter had a significant effect on the response of the machine.

The three phase model allowed implementation of leakage inductance saturation on a per phase basis and as such produced a line current waveform in which the harmonic content was similar to that of the real machine. This model also permitted imbalance on both stator and rotor windings which allowed the effect of line voltage imbalance, a low resistance stator phase and a supply with a realistic third harmonic component. Variation of the initial starting position of the rotor and the switching angle of the supply was also investigated by use of this model.

The effect of a given imbalance on the rotor resulted in a significantly larger side band component in the model during both steady state and starting transient conditions. The change of the LSB however showed better agreement between the the real wound or cage machine and that of its model. The frequency of the side bands was exactly correct for a given rotor speed.

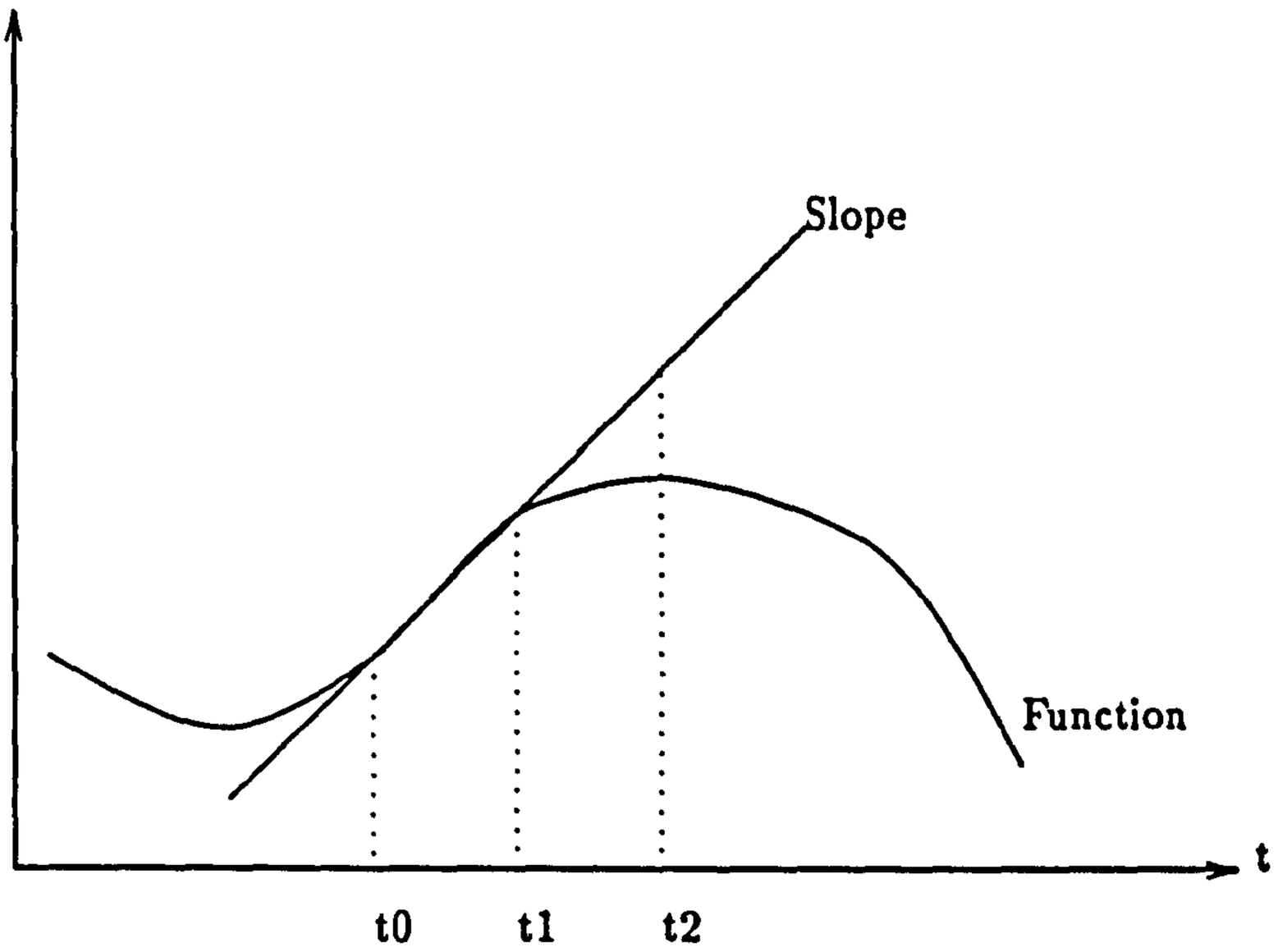

Figure 7.1: Numerical Integration, estimates the next value of the function from the slope at the present value.

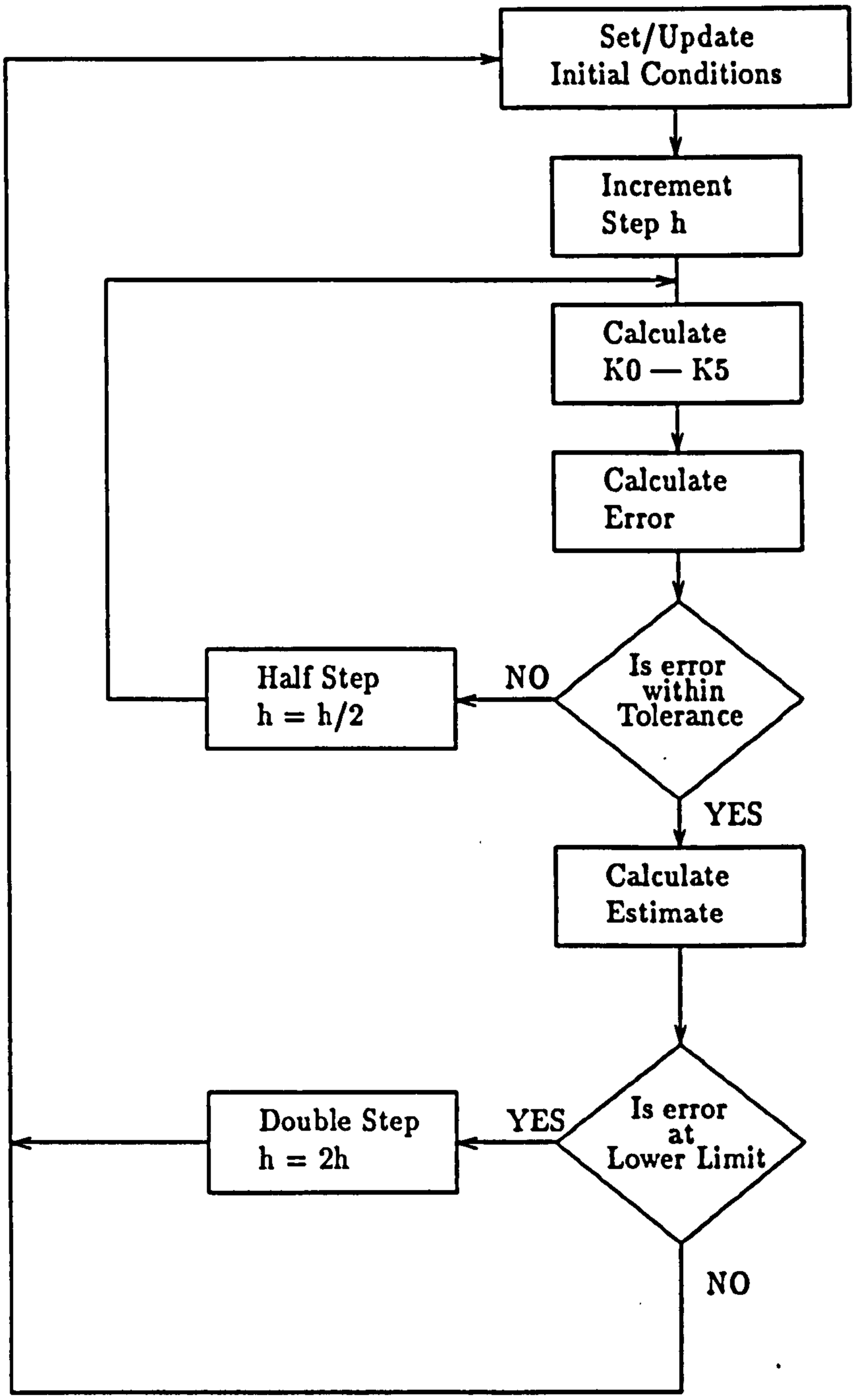

Figure 7.2: Flowchart of error control algorithm

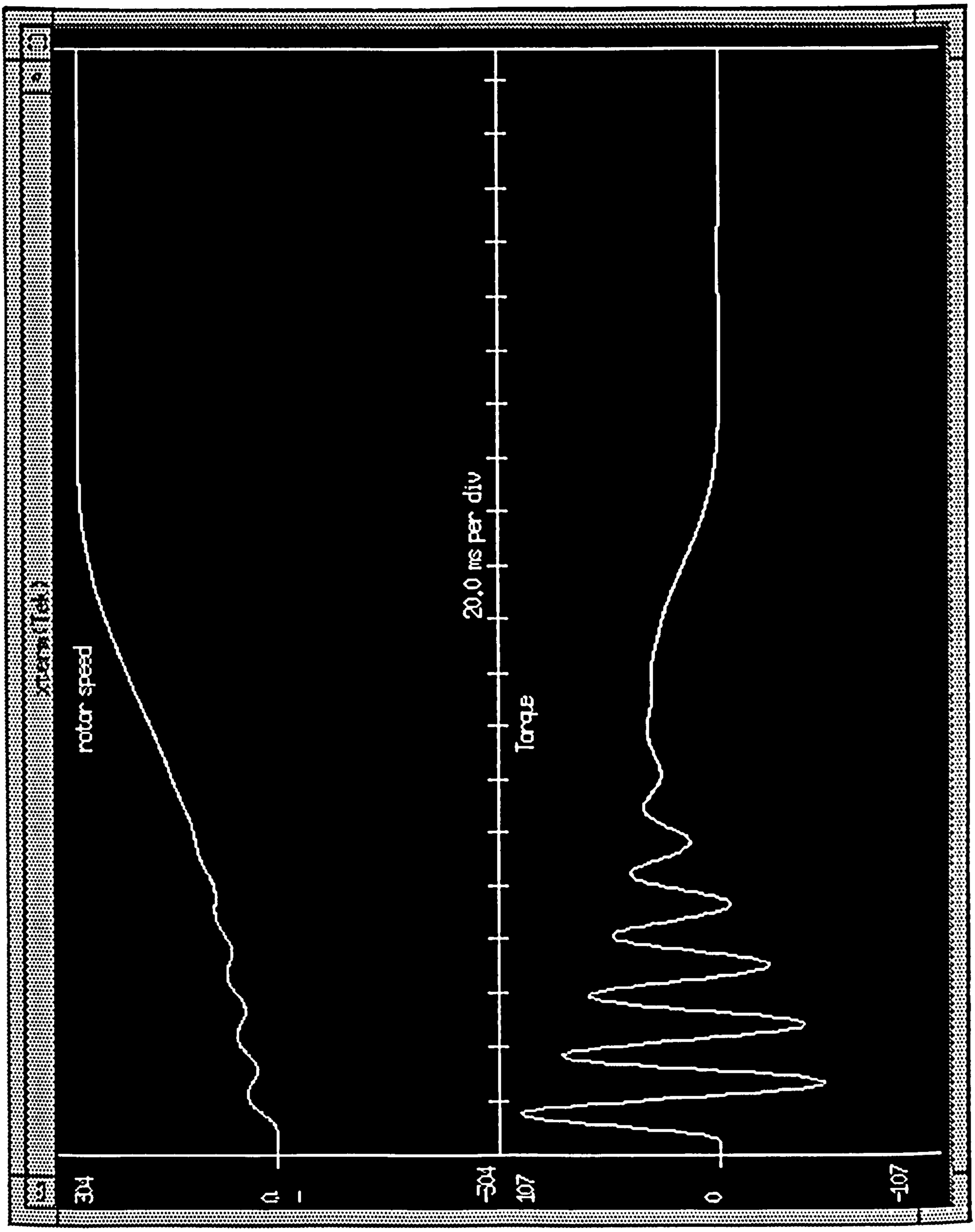

Figure 7.3: Non-simultaneous switching, two lines at $\alpha = 0°, \beta = 90°$

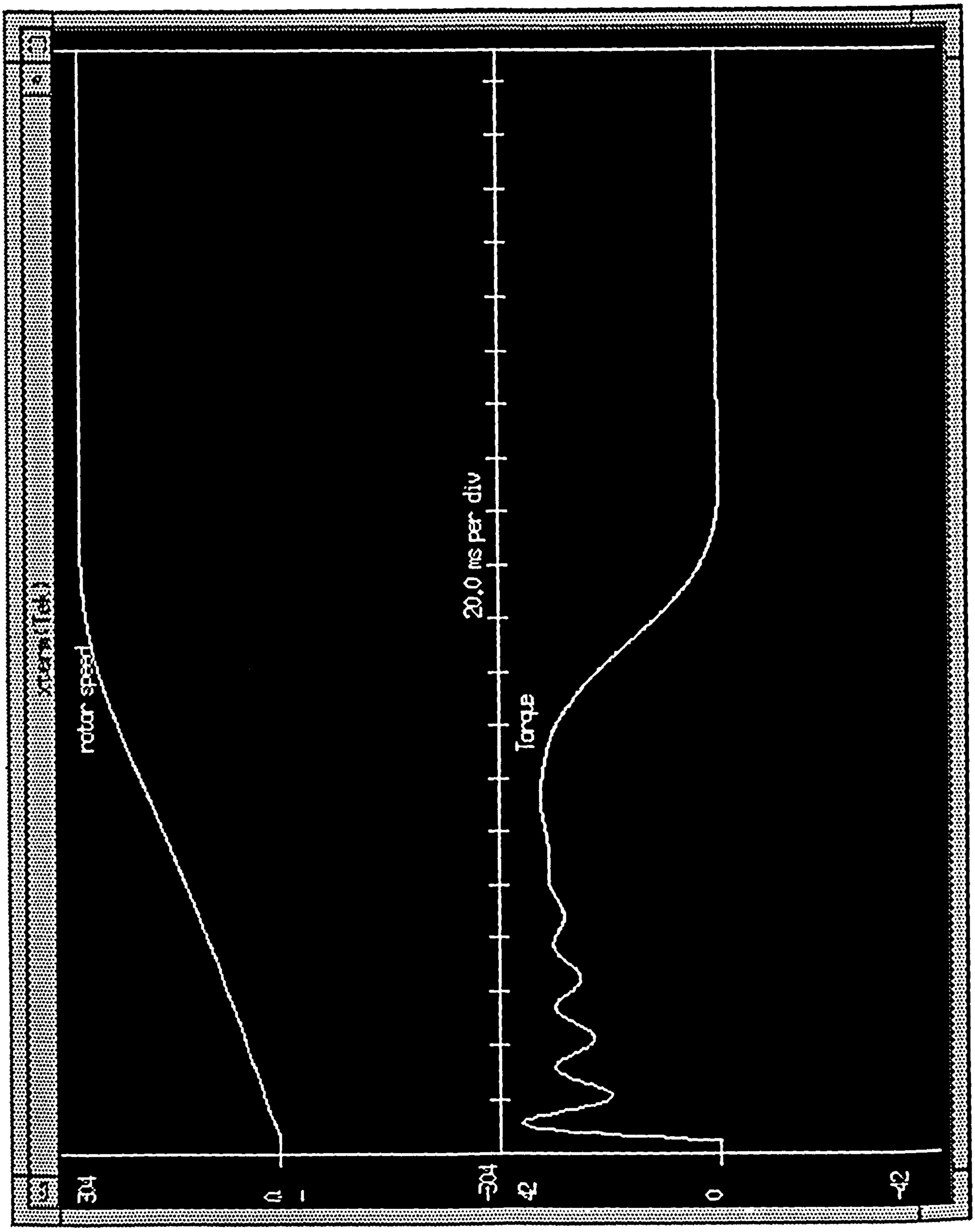

Figure 7.4: Non-simultaneous switching, two lines at $\alpha = 90°, \beta = 90°$.

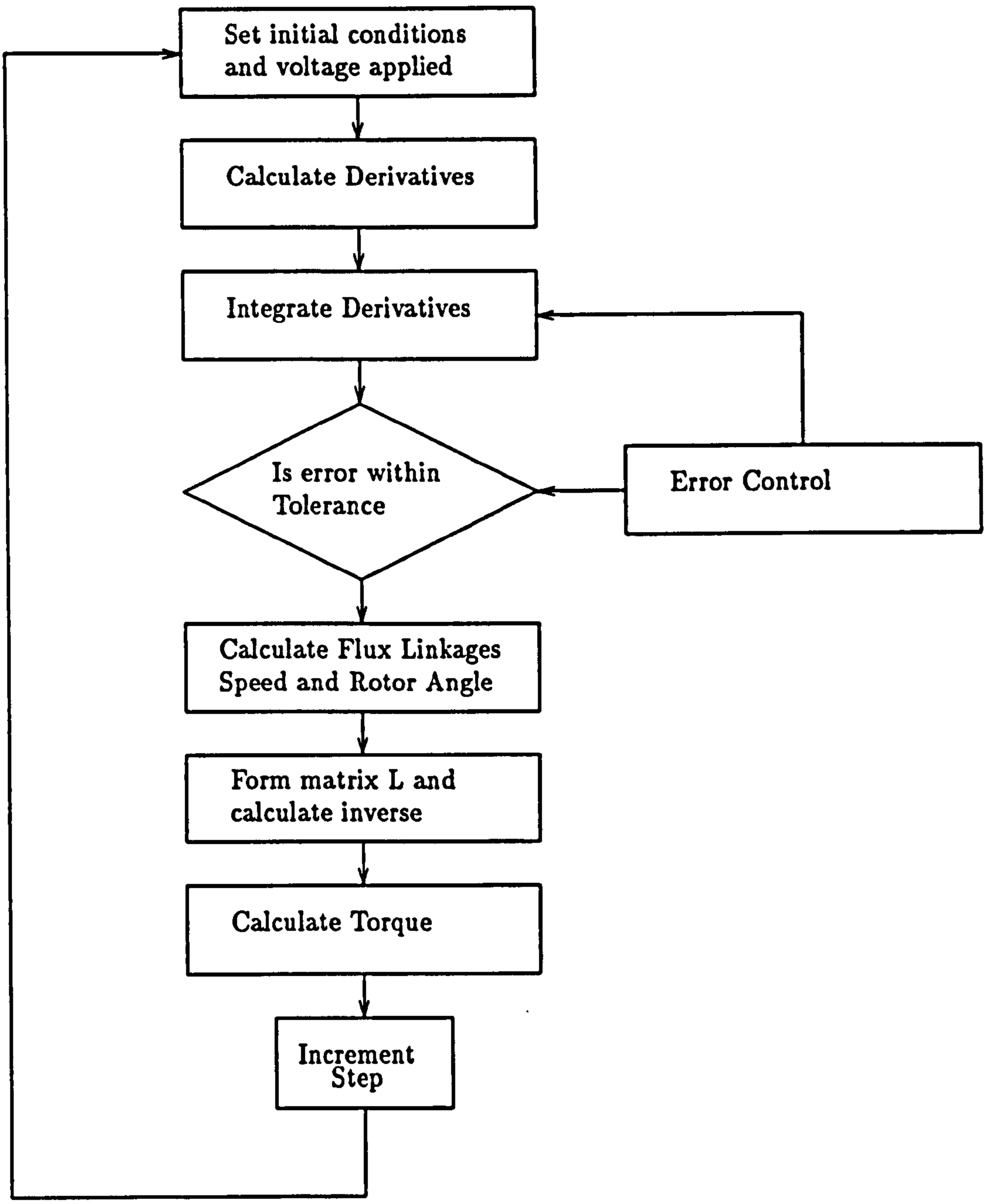

Figure 7.5: Flowchart of 3 Phase Model.

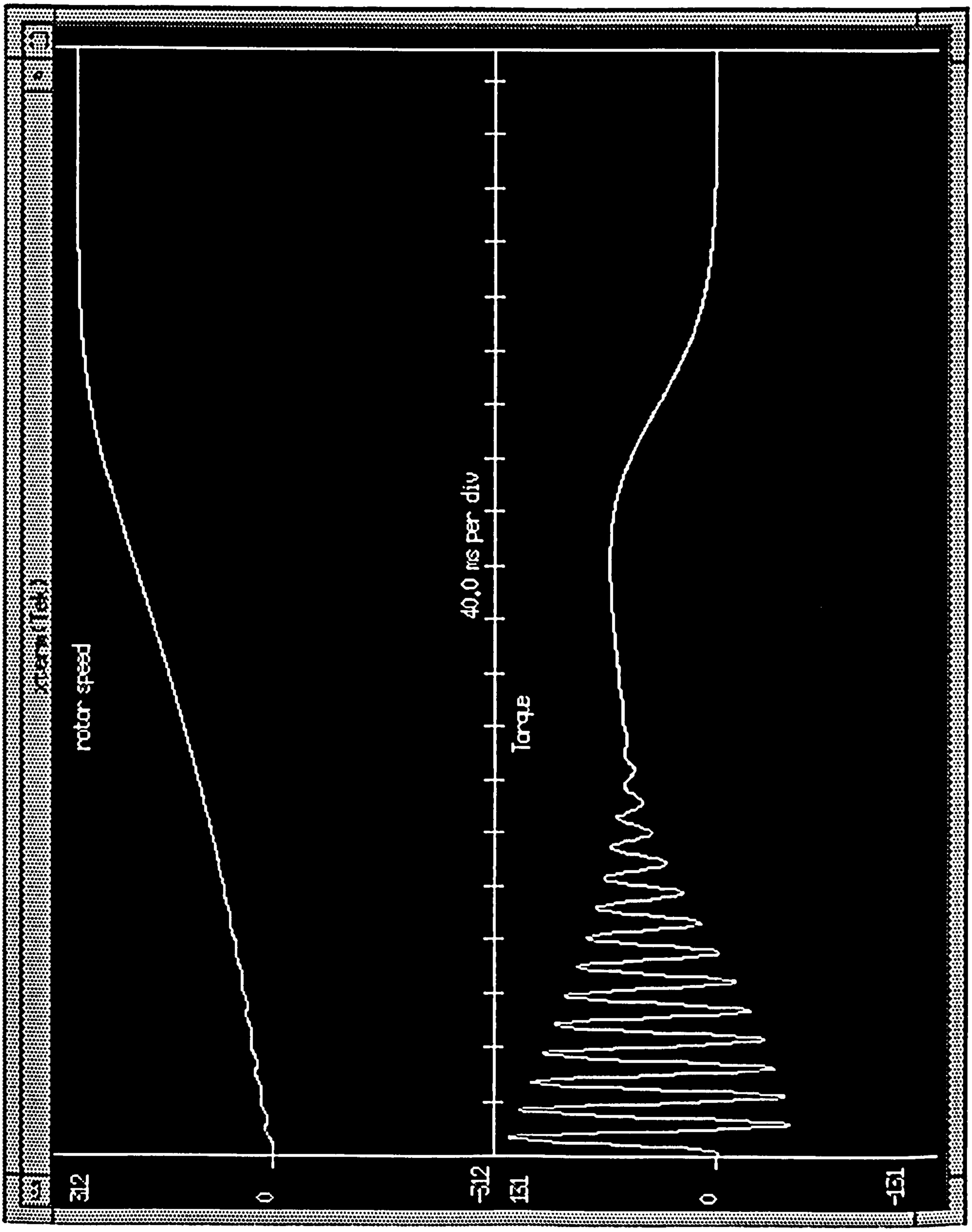

Figure 7.6: Accelerating torque and rotor electrical angular velocity simulation using fixed parameter values from RL/LR tests.

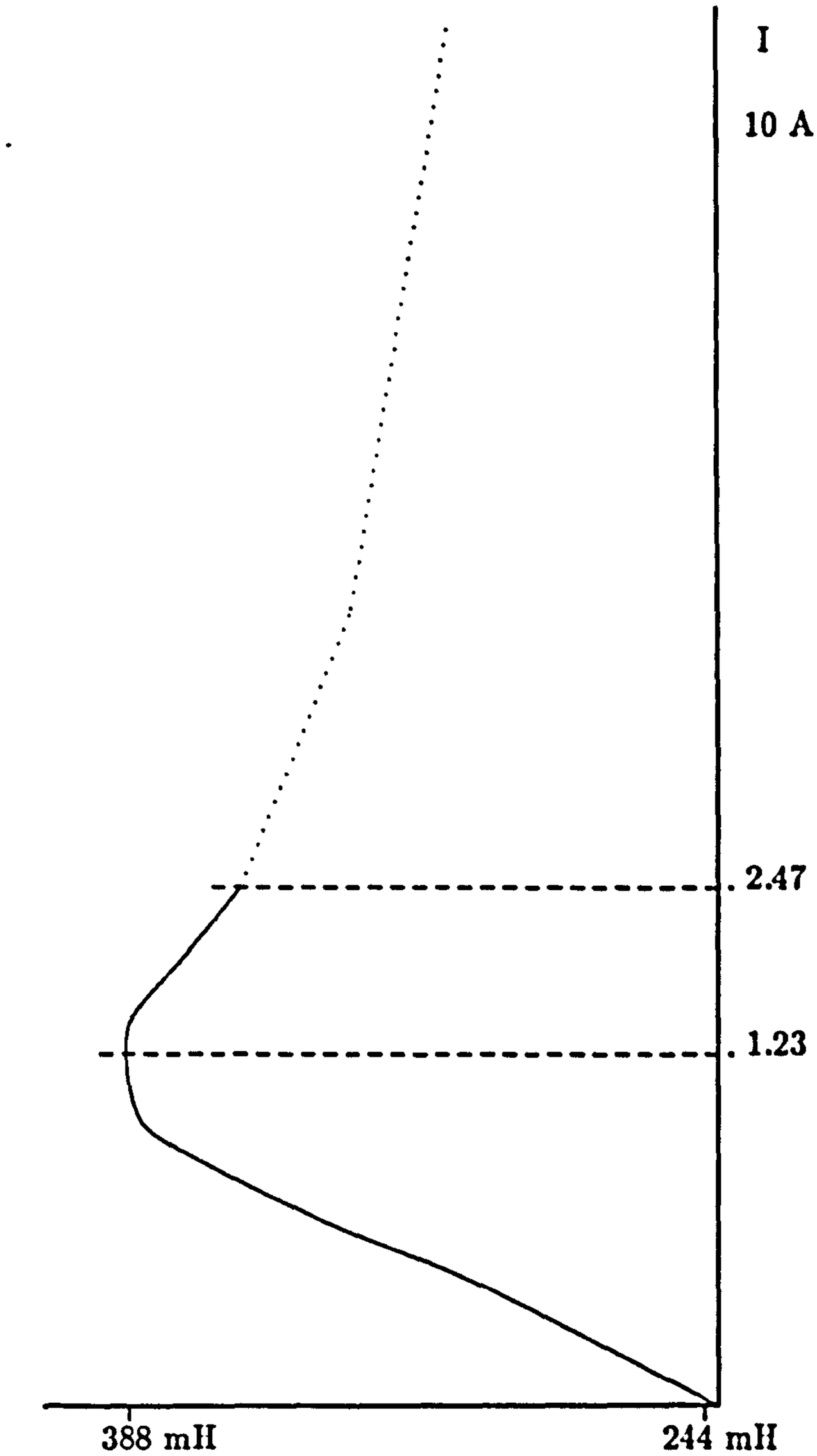

Figure 7.7: Mutual inductance characteristic for the wound rotor machine.

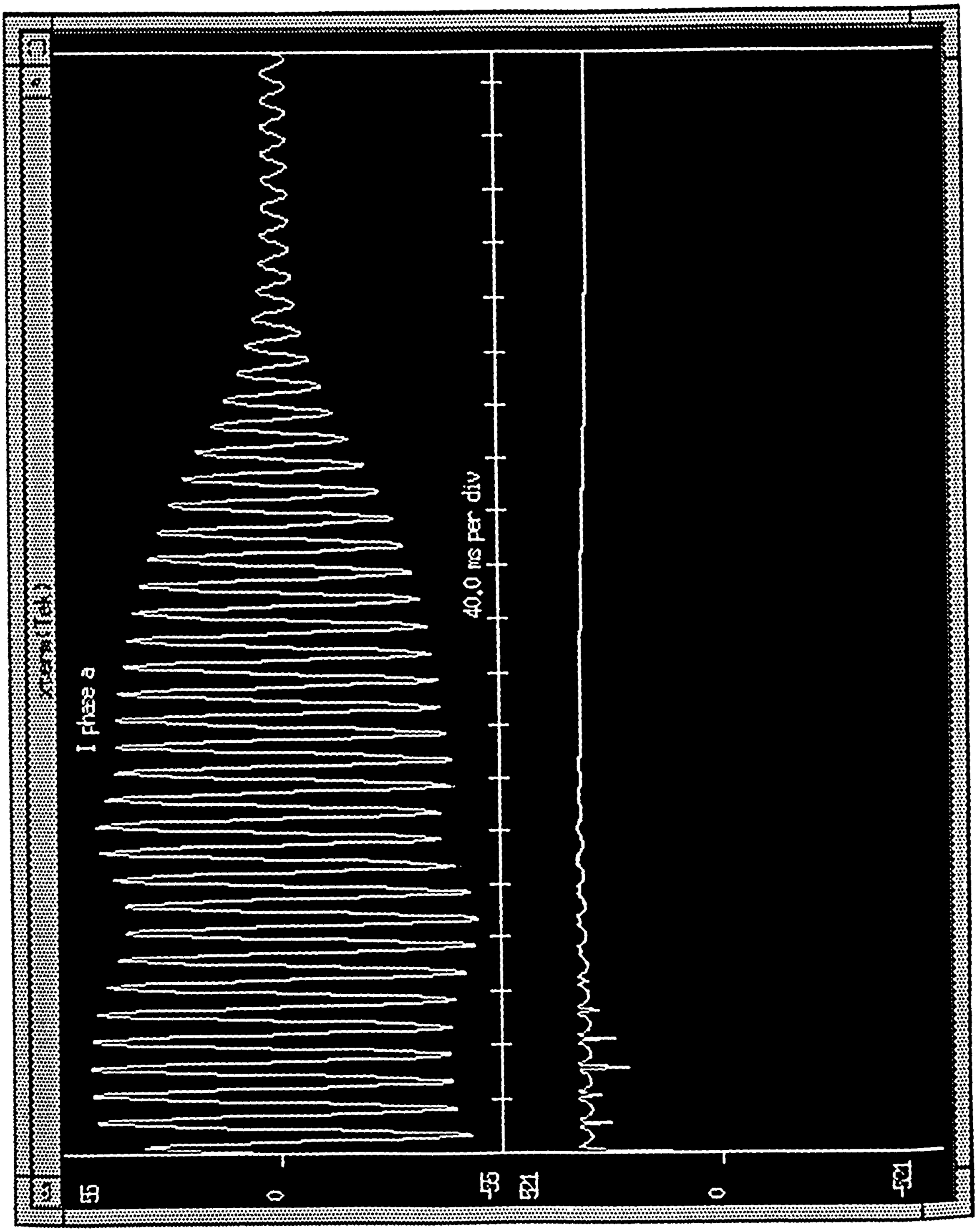

Figure 7.8: Line current and variation of mutual inductance during the starting period.

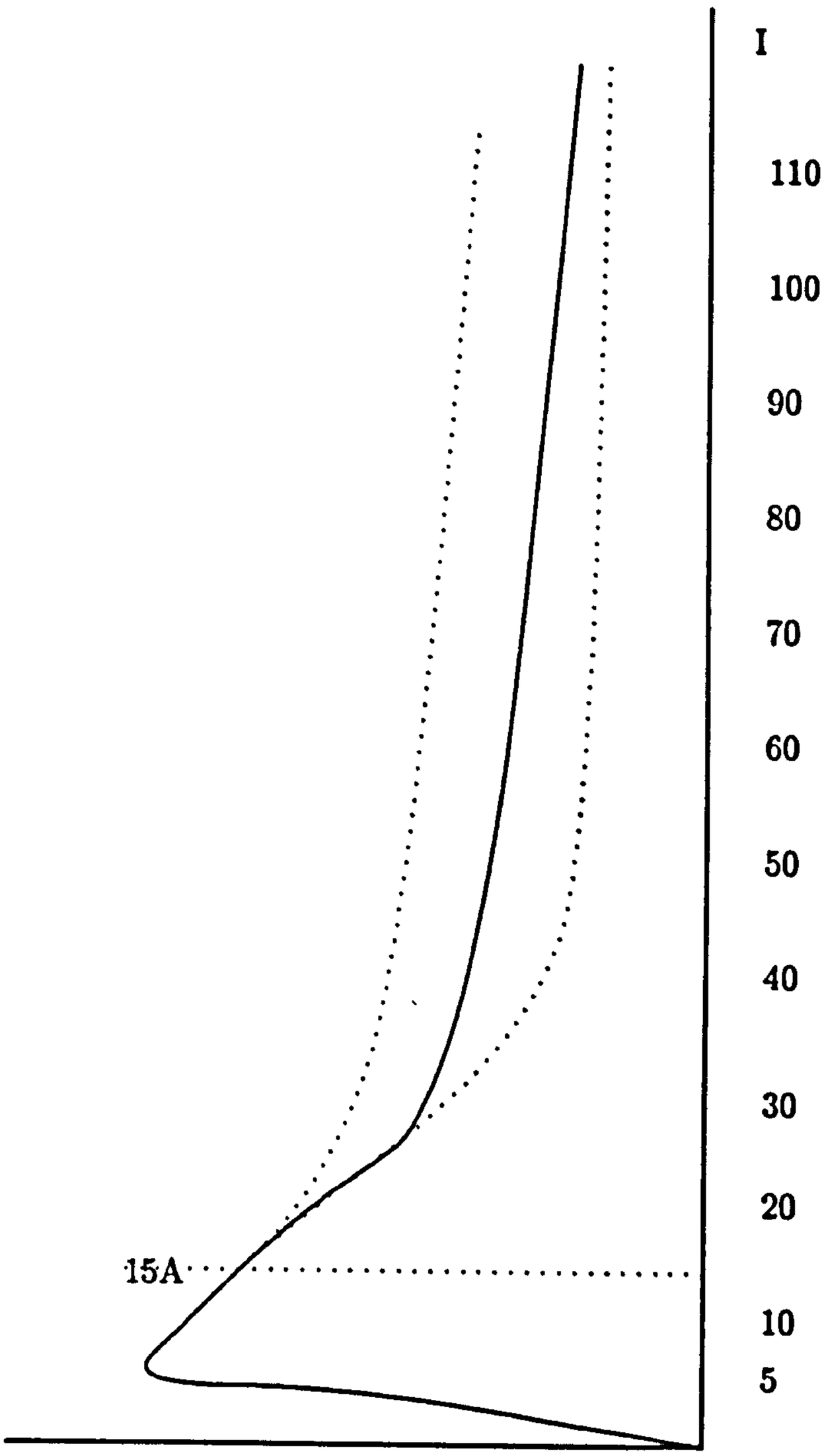

Figure 7.9: Leakage inductance saturation characteristic for the wound rotor machine.

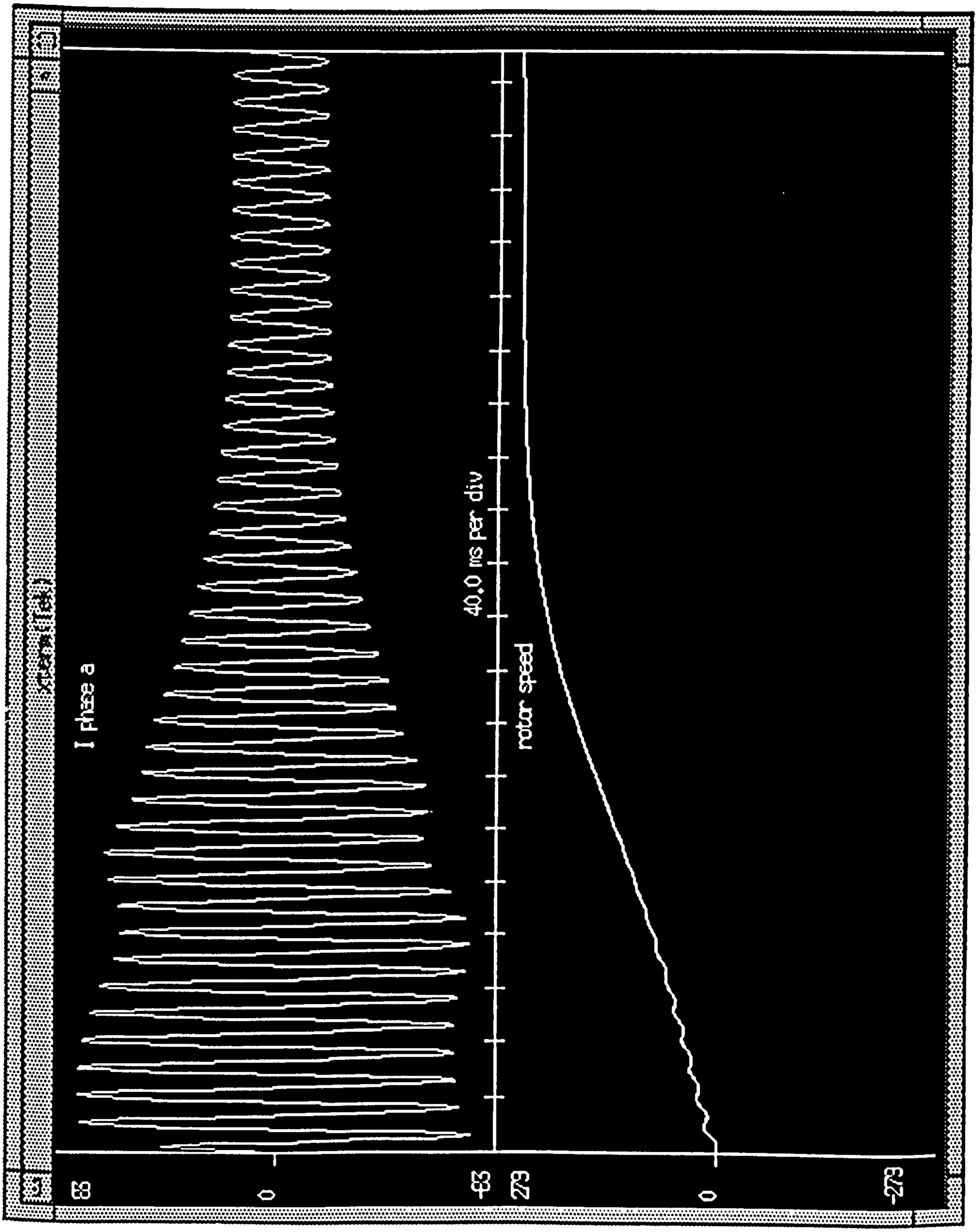

Figure 7.10: Stator current Ia and rotor speed (elec.rad/s) for the wound rotor machine modelling with leakage inductance saturation.

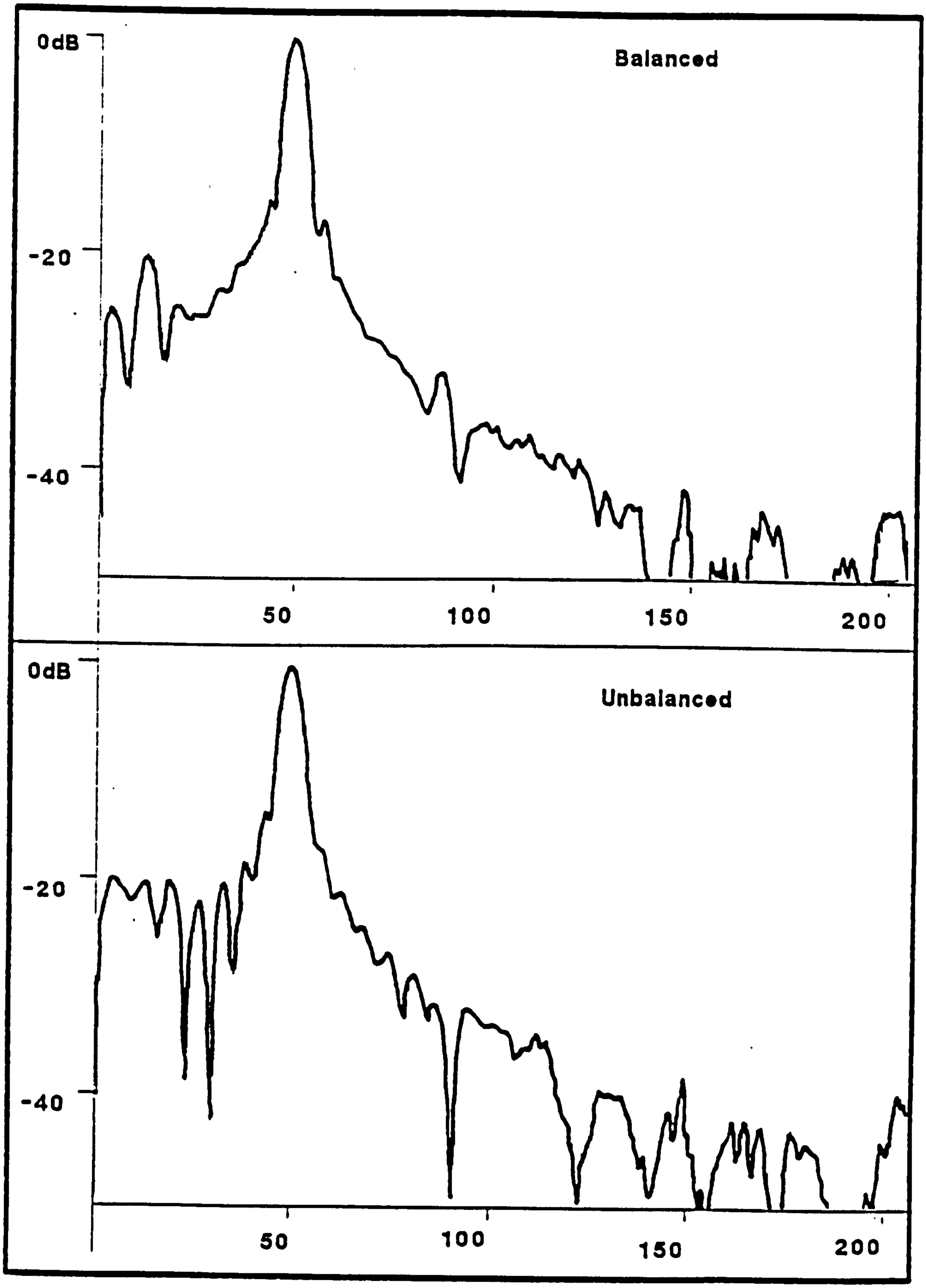

Figure 7.11: Spectrum of real line current waveform showing peak at "13Hz" and undulation in 0-50Hz region due to imbalance on the rotor.

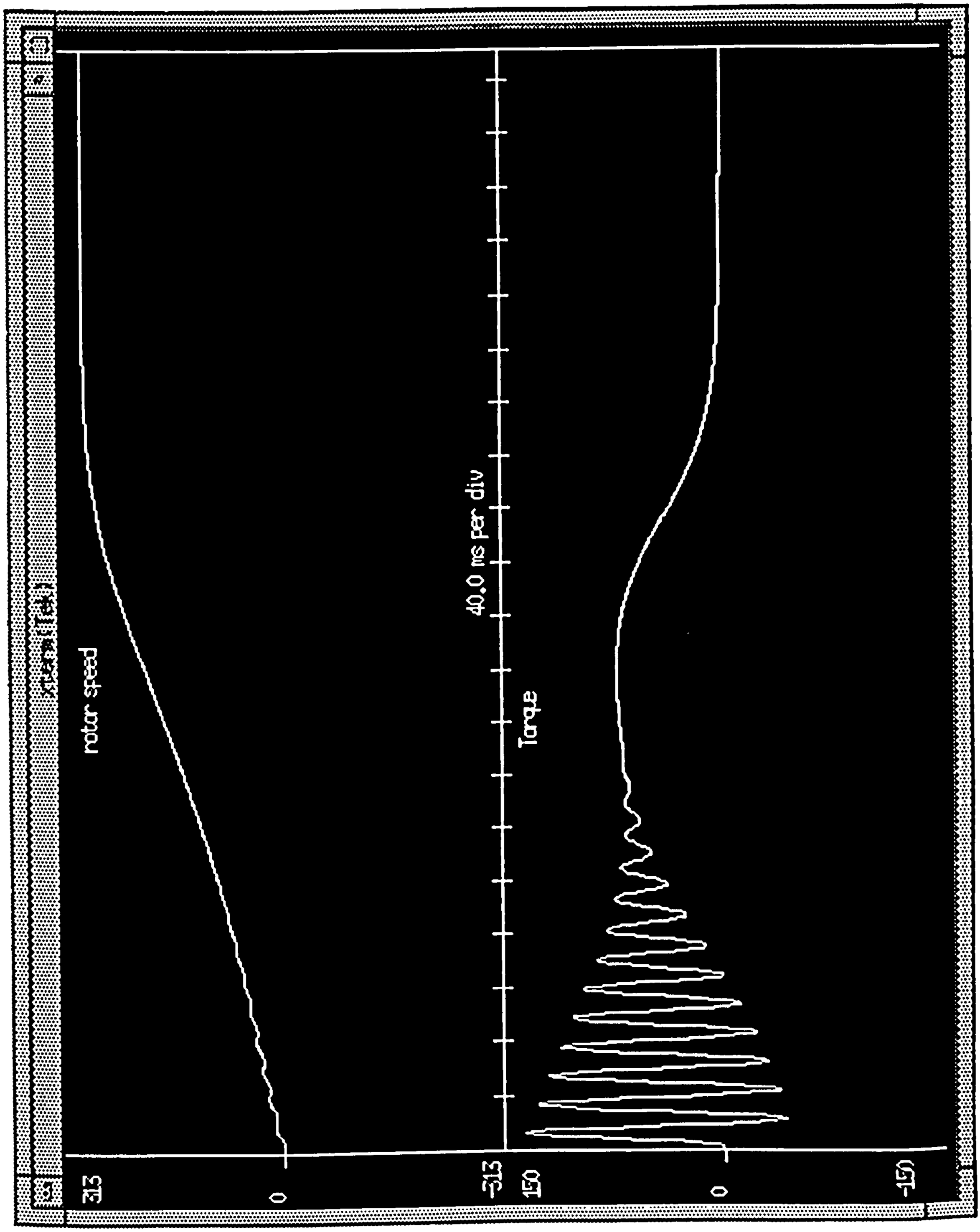

Figure 7.12: Response of model for 10% decrease in leakage inductance over the the case of Fig. 7.6

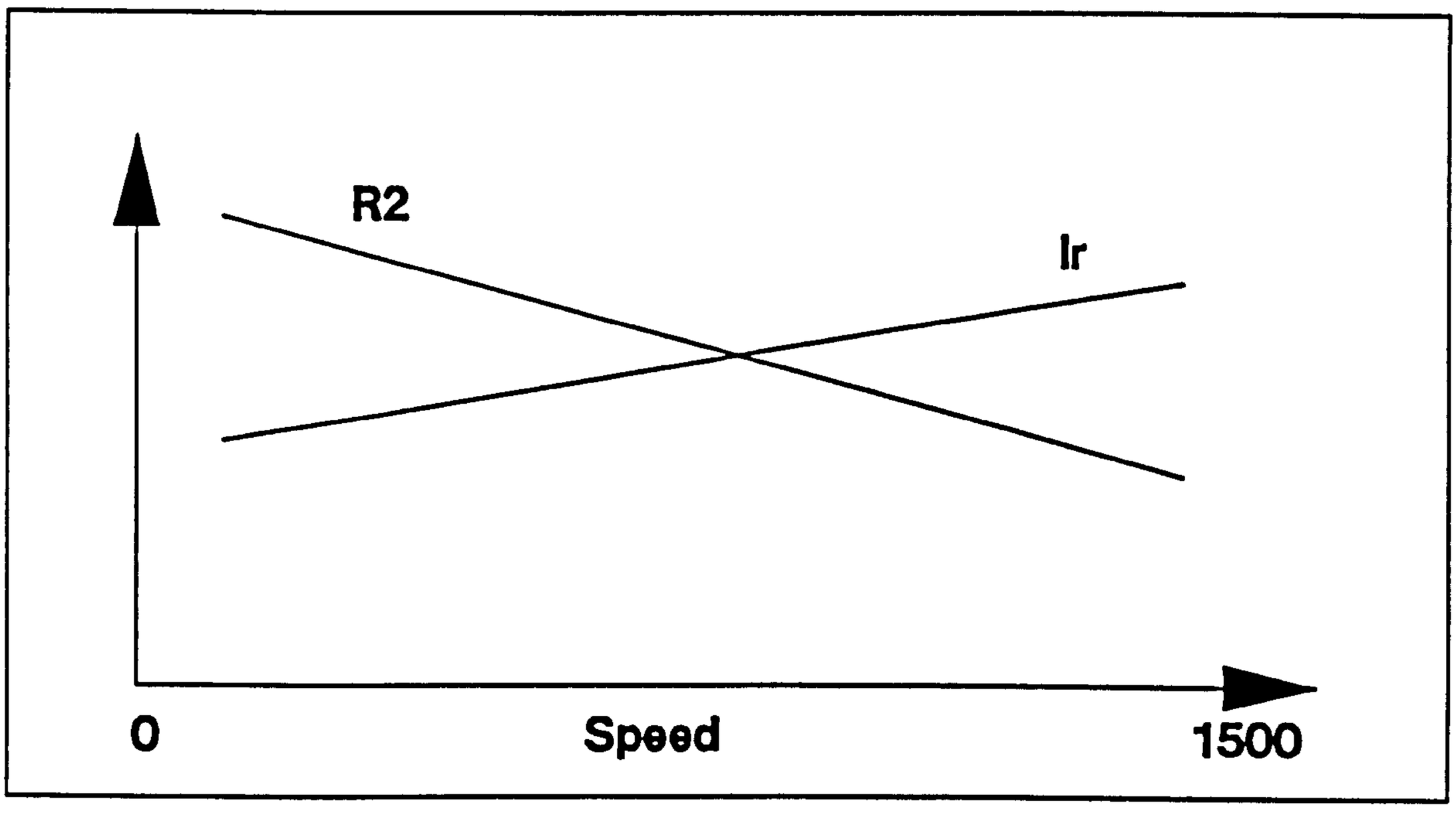

Figure 7.13: Typical changes in l_2 and R_2 due to skin effect.

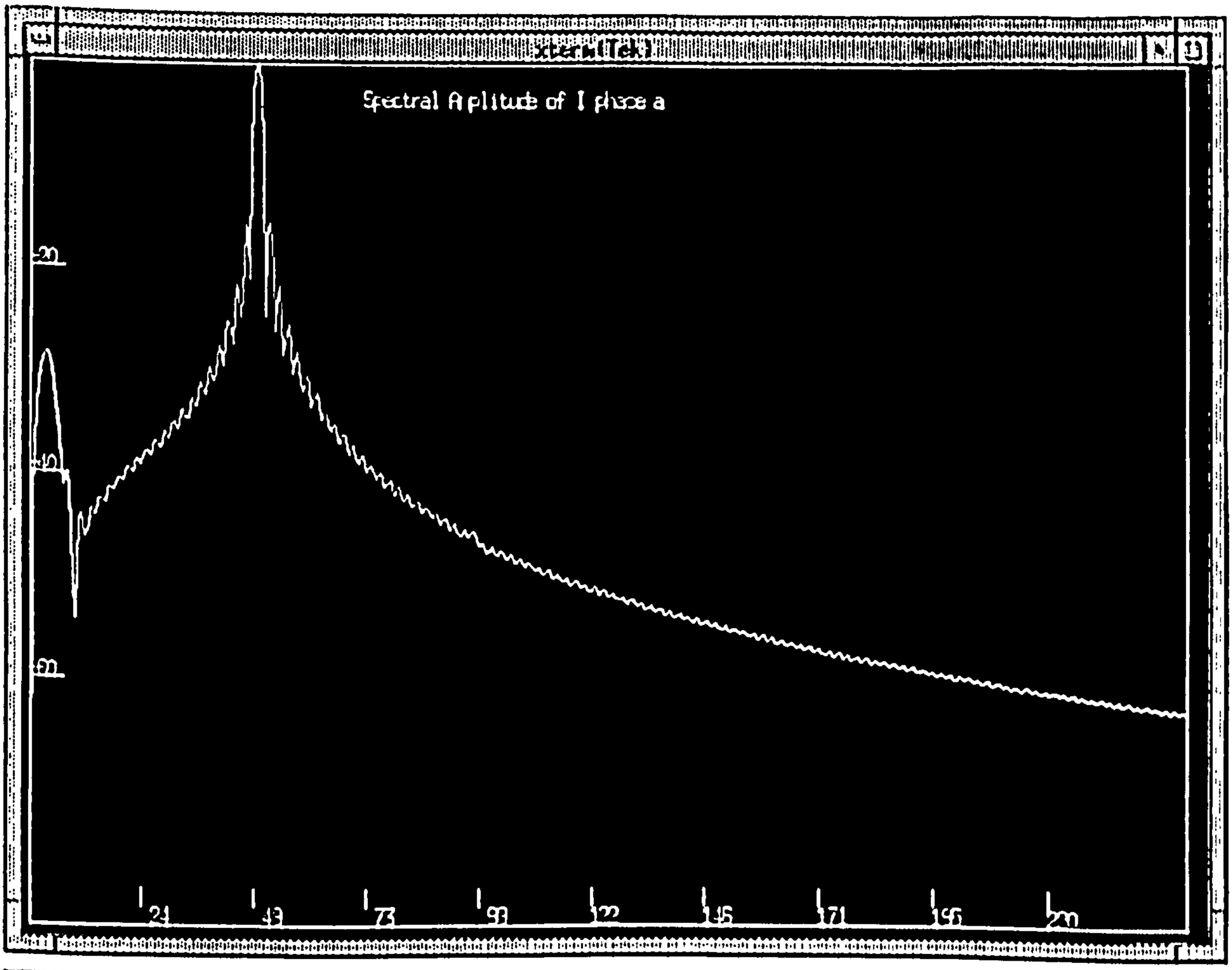

Figure 7.14: Line current spectra from DQ model showing undulation in 0-50Hz region due to imbalance in the rotor.

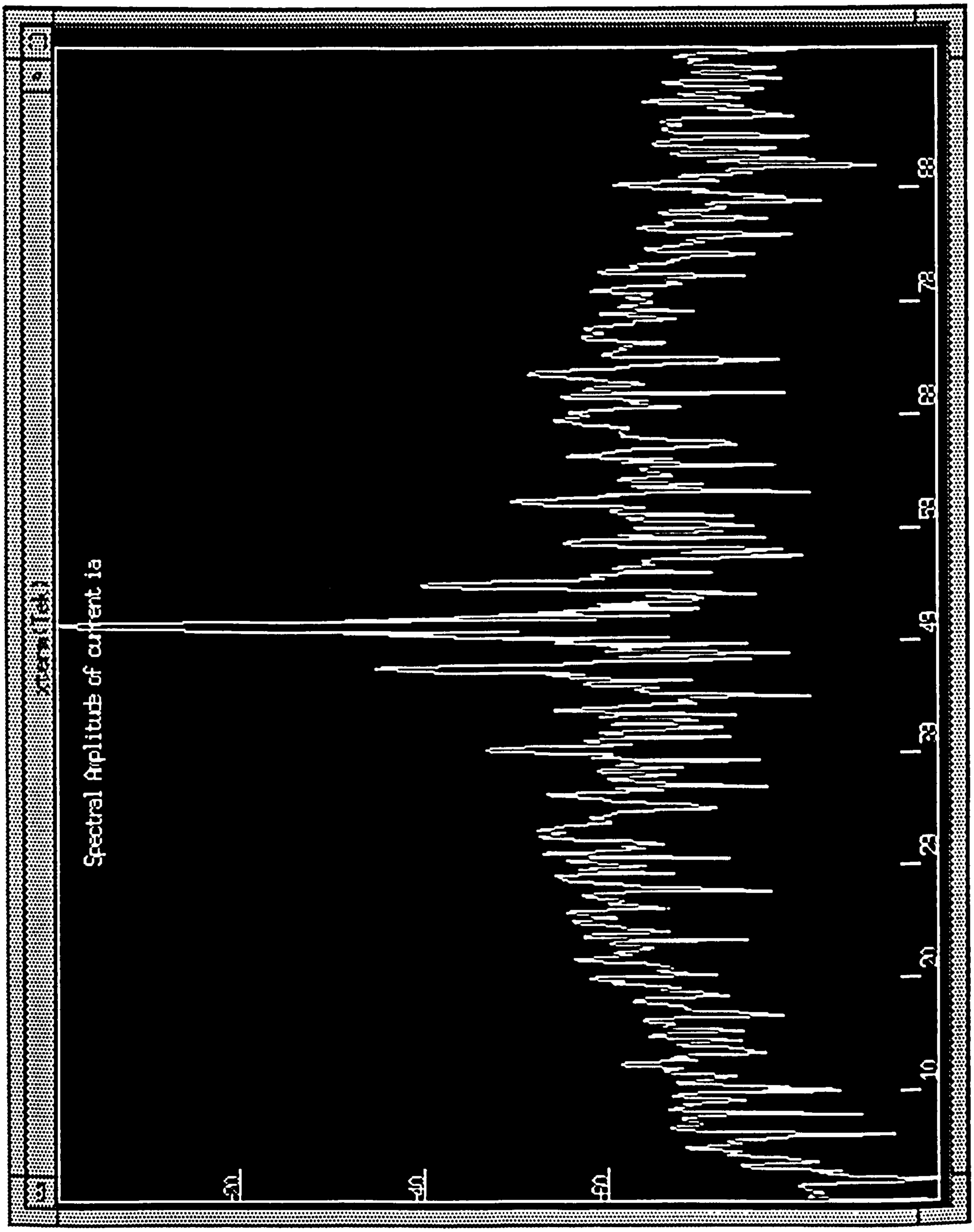

Figure 7.15: Simulated steady state line current spectrum with imbalance and leakage saturation modelling.

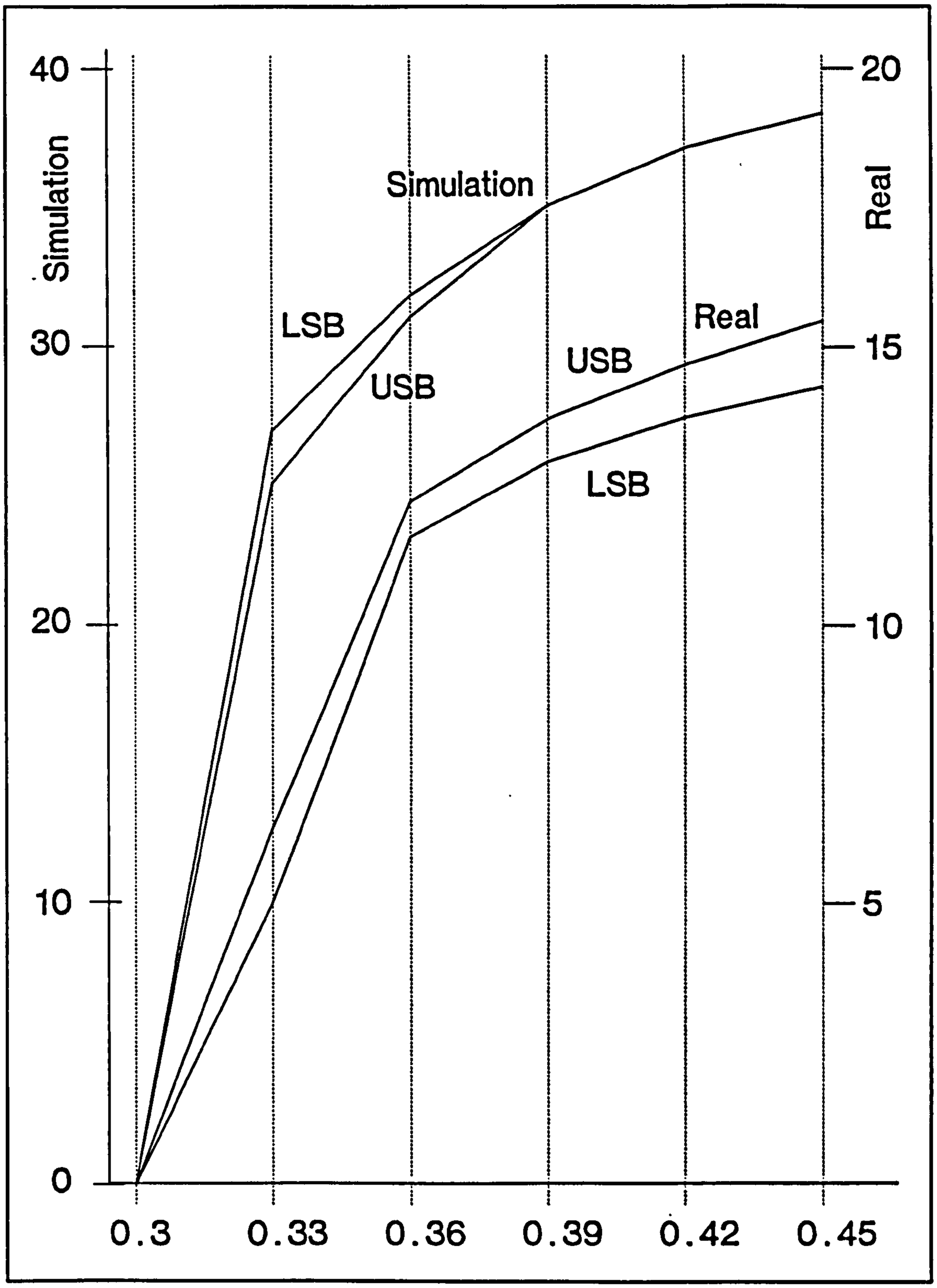

Figure 7.16: Change in both upper and lower side band amplitude over balanced condition for steady state simulation of wound rotor machine.

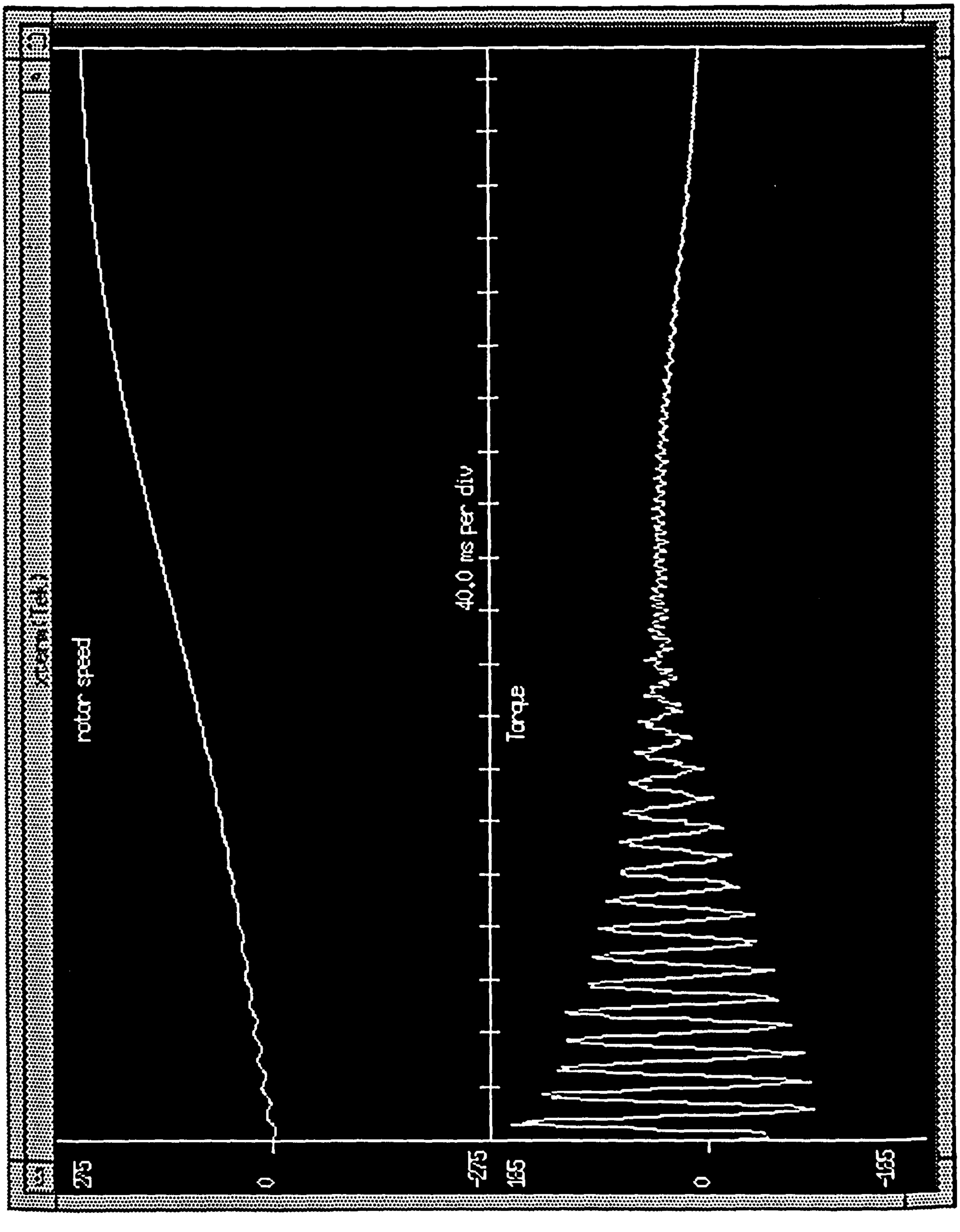

Figure 7.17: Simulated starting transient of wound rotor machine showing accelerating torque and rotor electrical angular velocity.

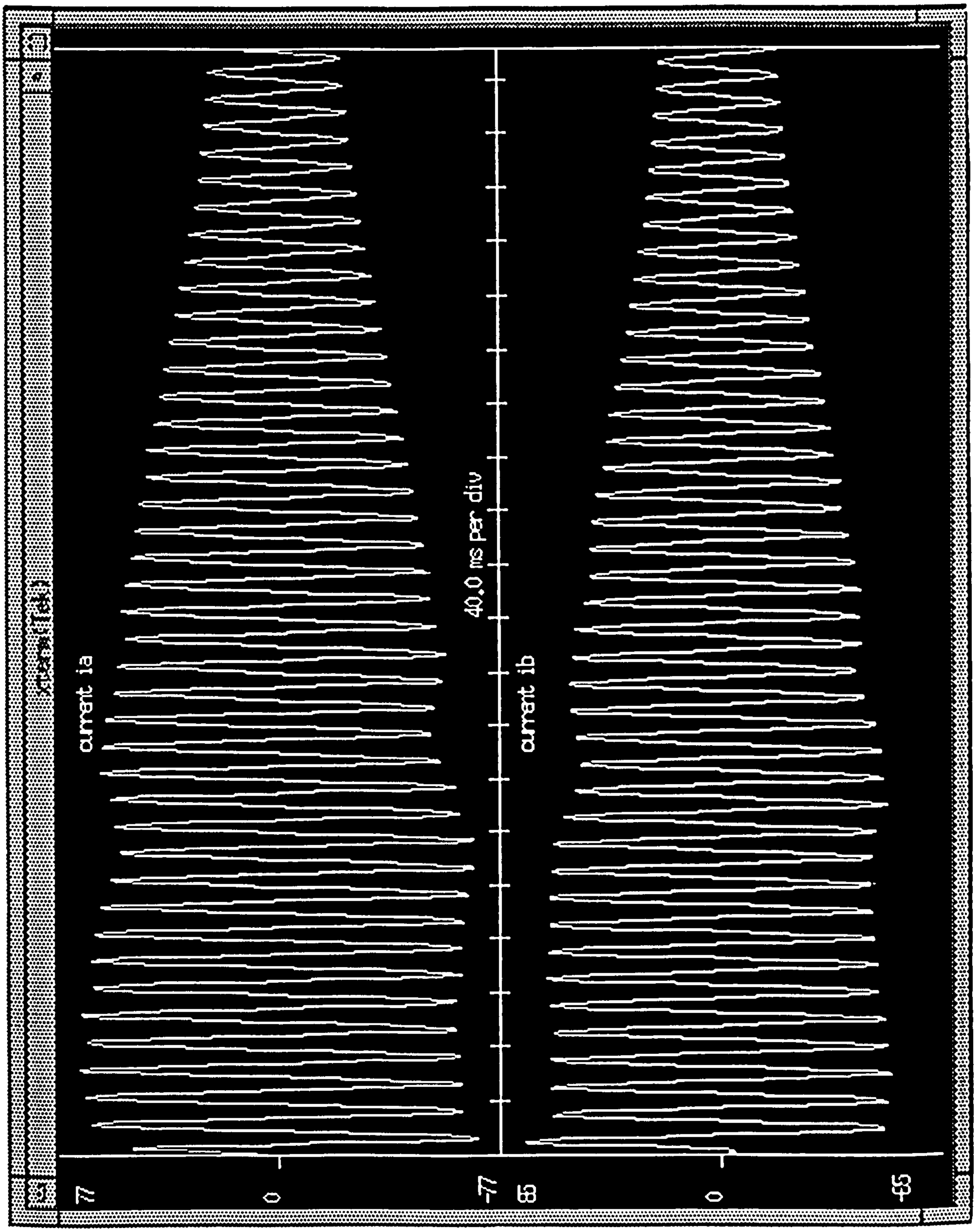

Figure 7.18: Simulated starting transient of wound rotor machine showing stator curent of phases a and b.

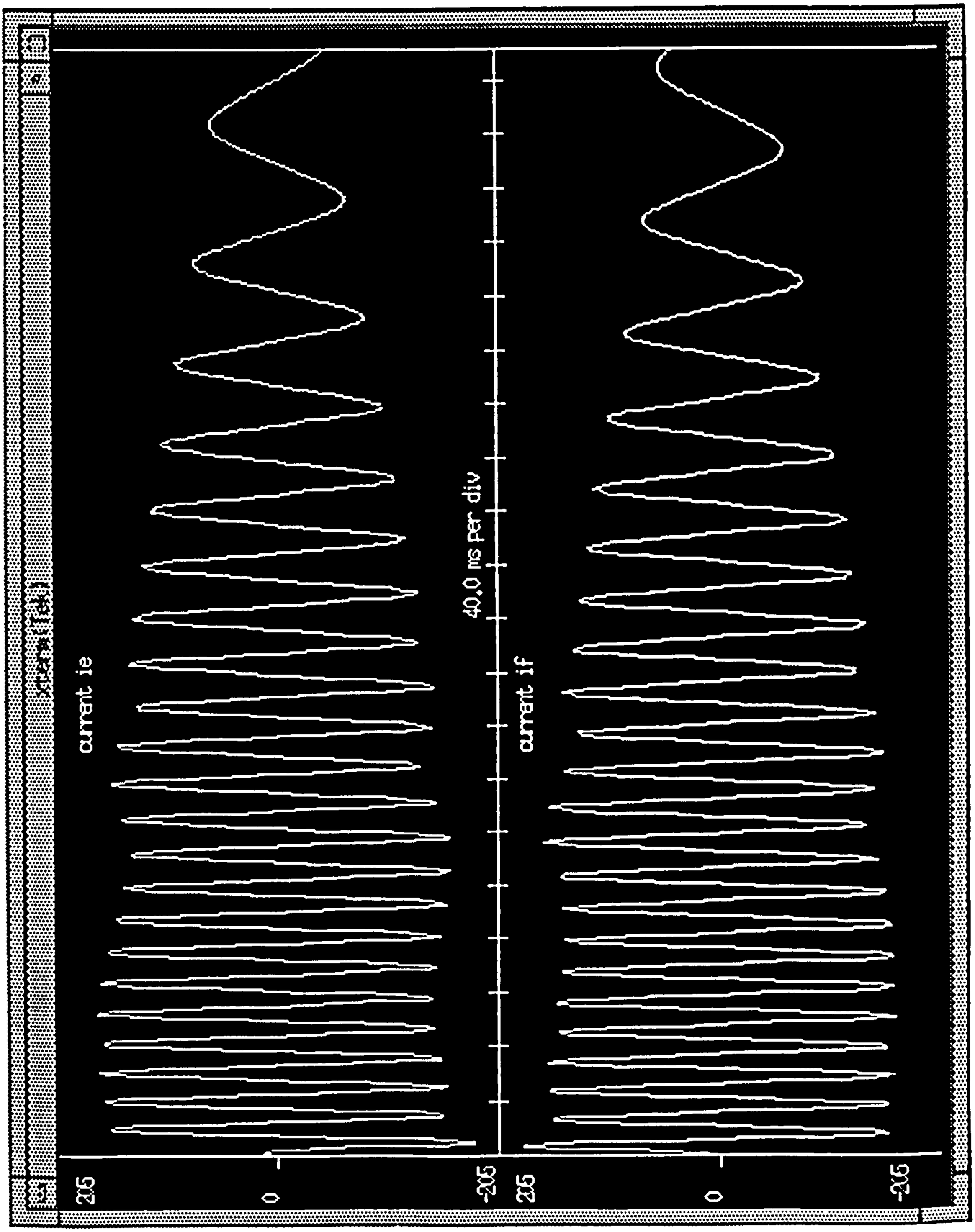

Figure 7.19: Simulated starting transient of wound rotor machine showing rotor current of phases e and f.

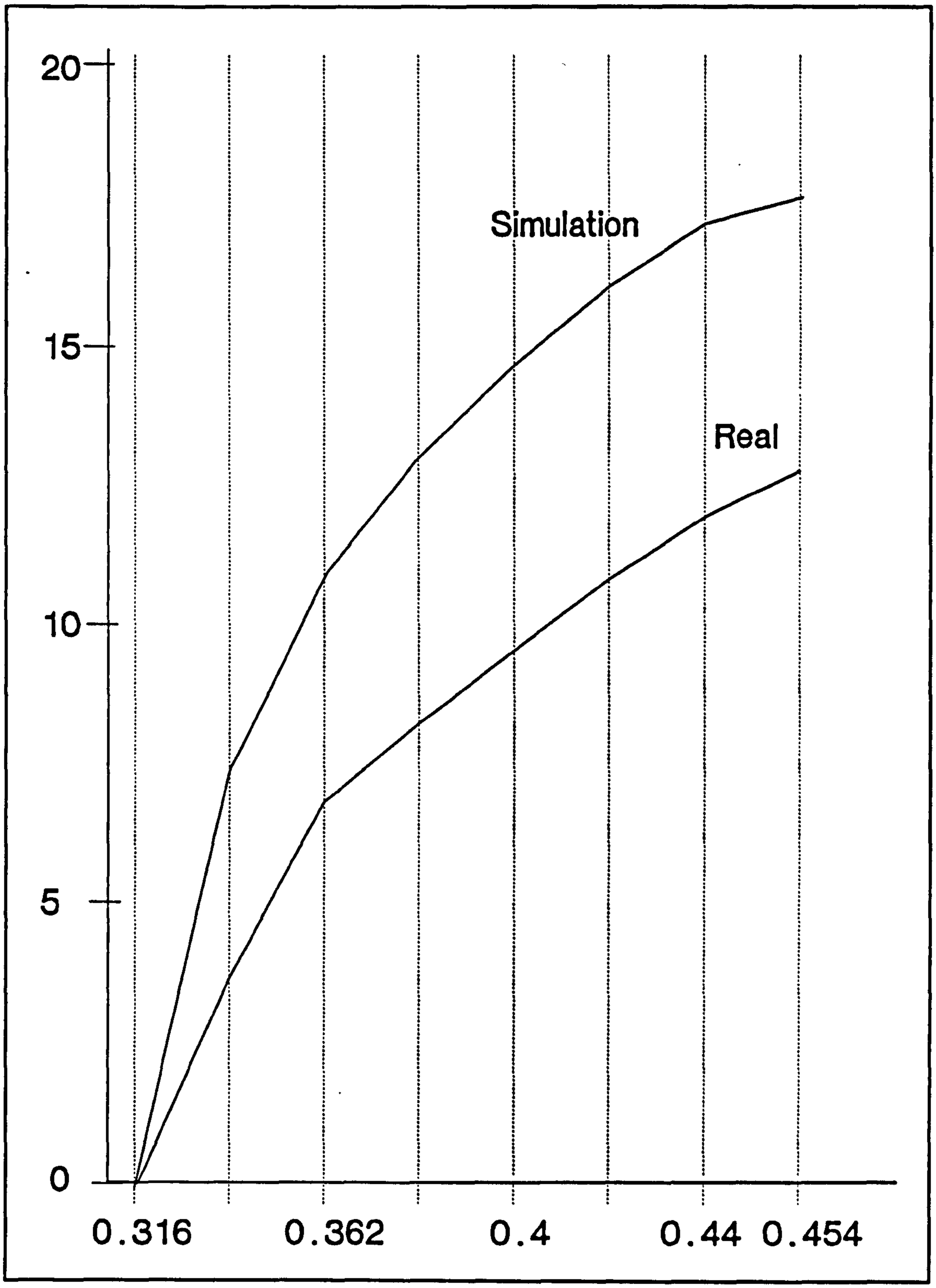

Figure 7.20: Comparison of real and simulated LSB amplitudes of wound rotor machine during the starting transient.

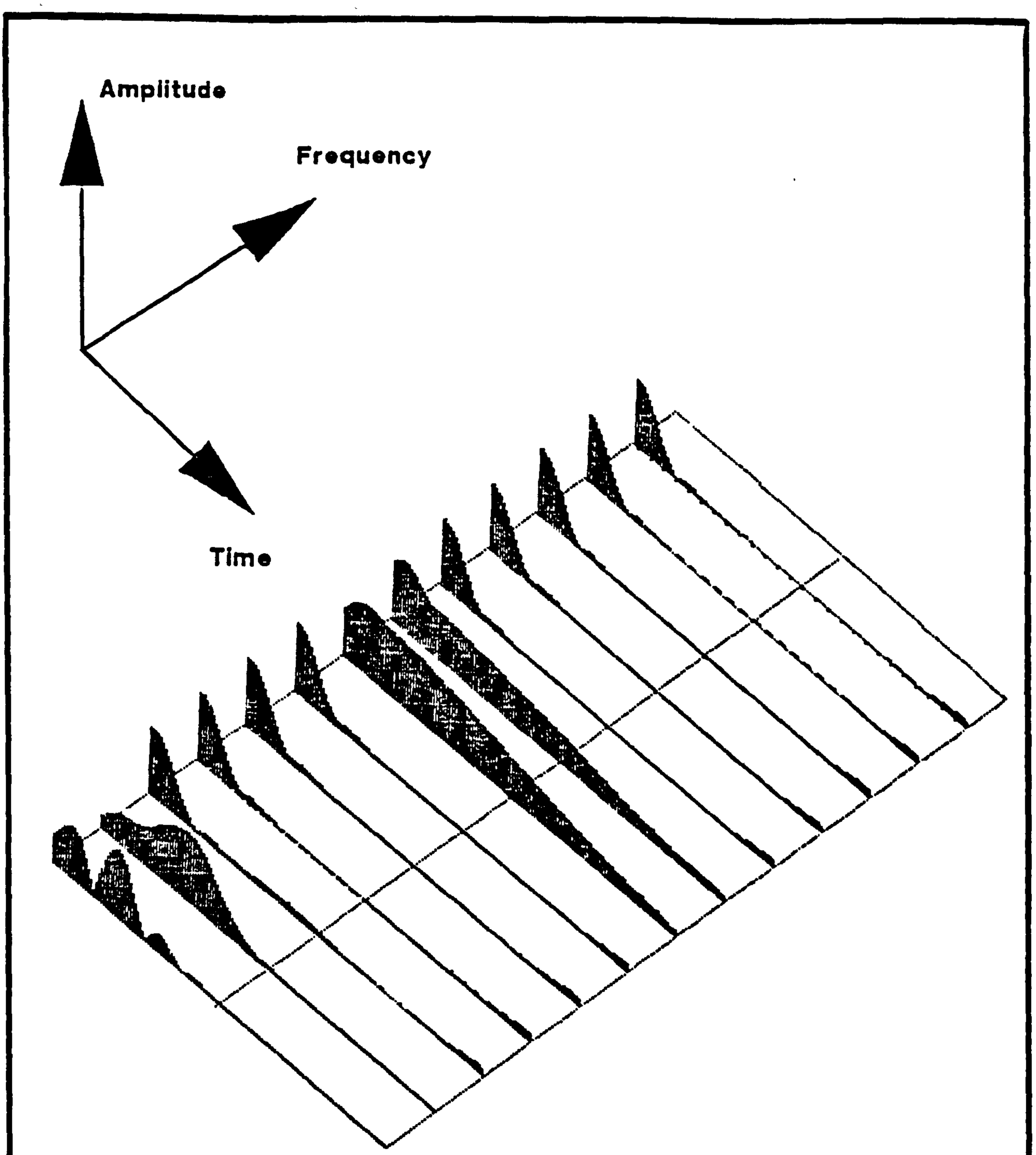

Figure 7.21: Phase vocoder plot of simulated balanced machine.

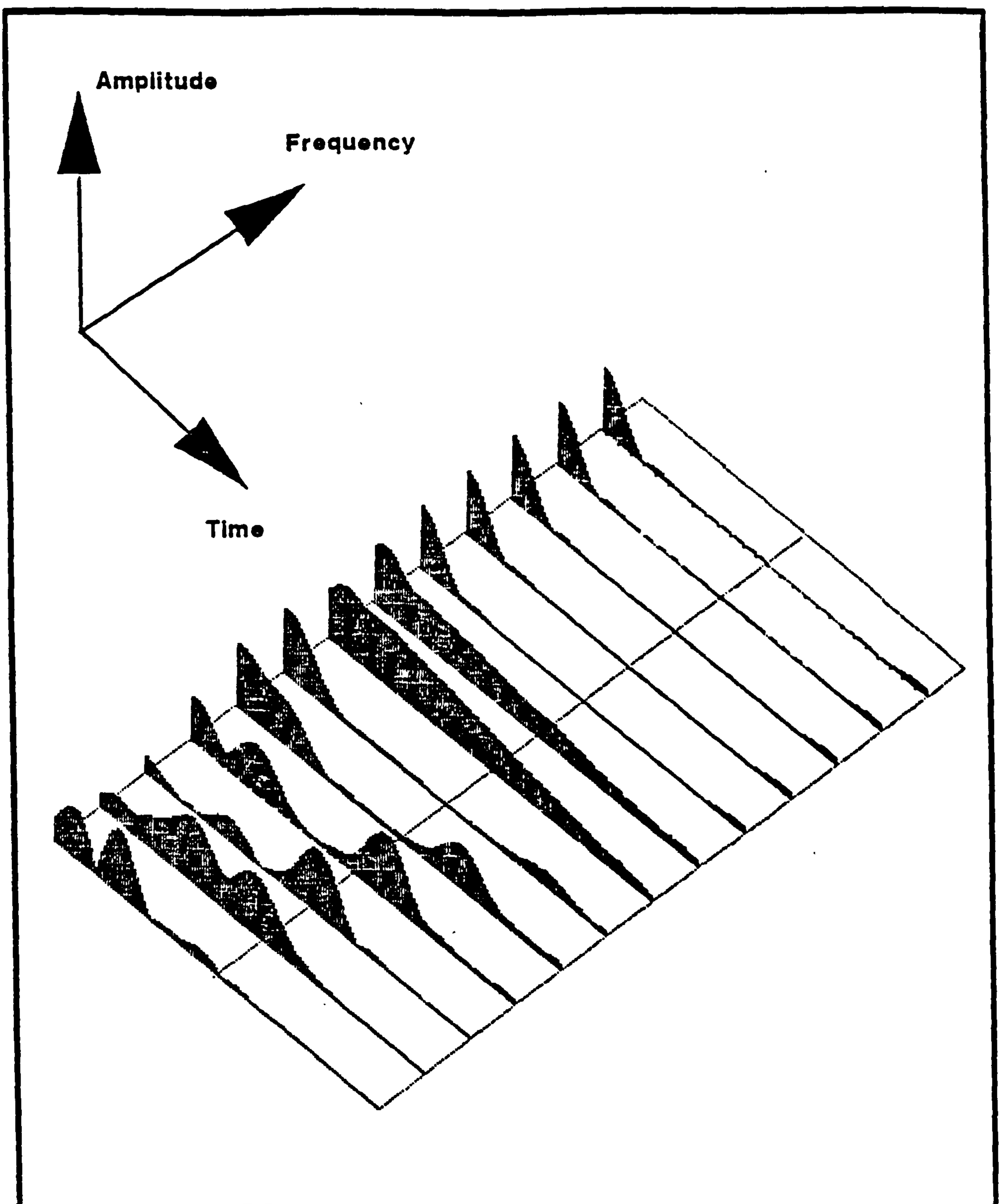

Figure 7.22: Phase vocoder plot of simulated machine with 58% imbalance.

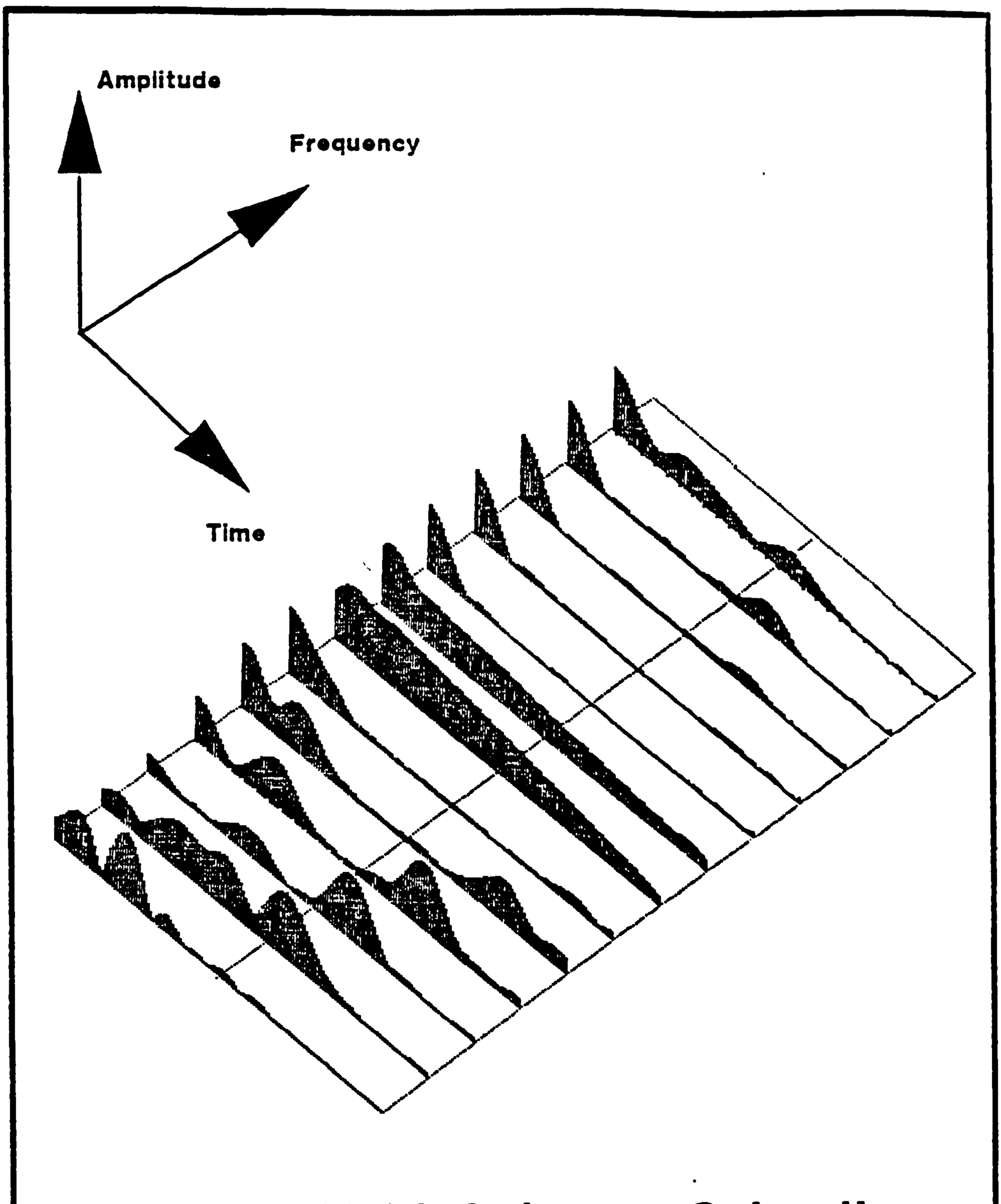

Figure 7.23: Phase vocoder plot of simulated machine with 58% imbalance and leakage saturation modelling.

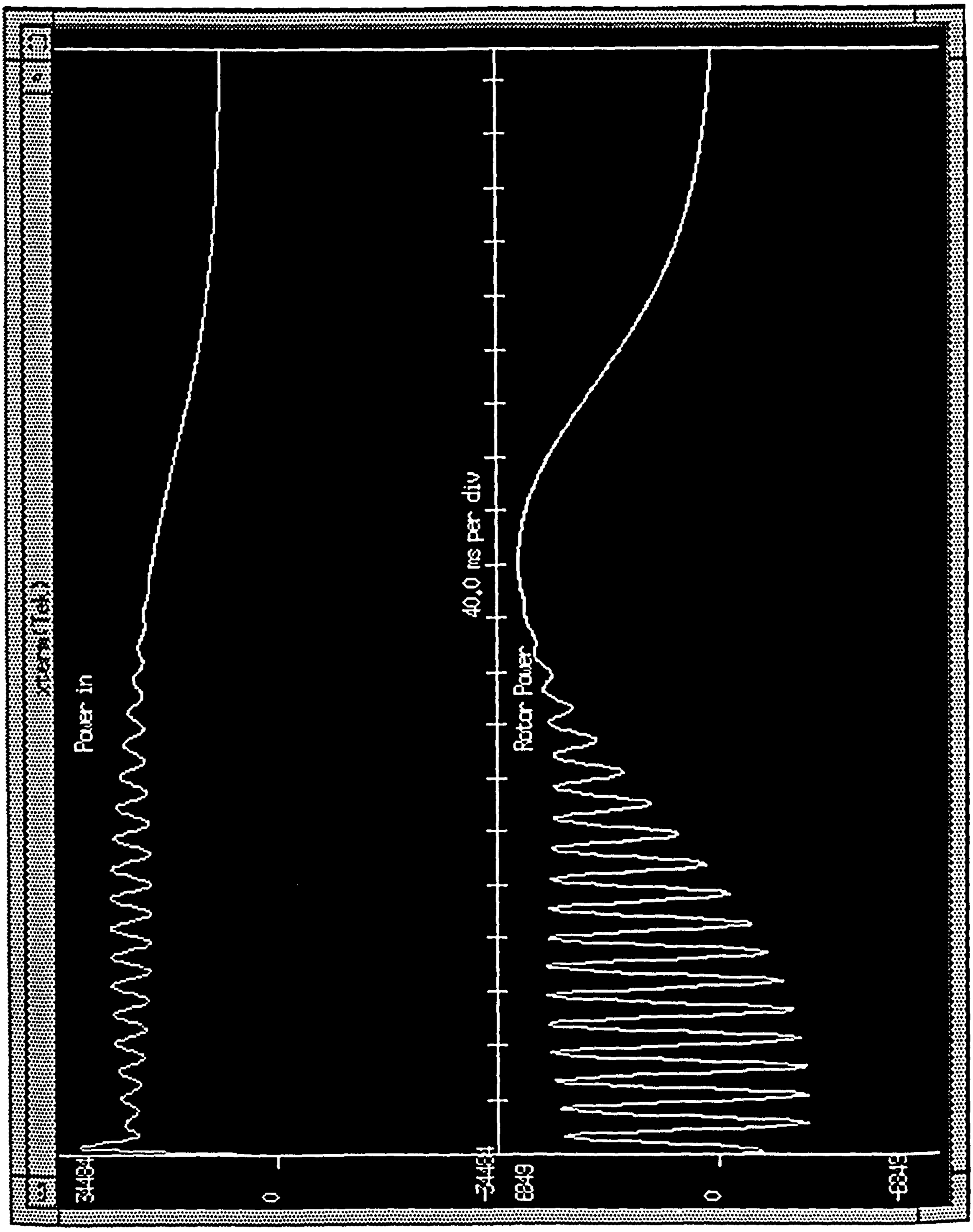

Figure 7.24: Input Power and Rotor Power during the starting transient for a balanced simulated machine.

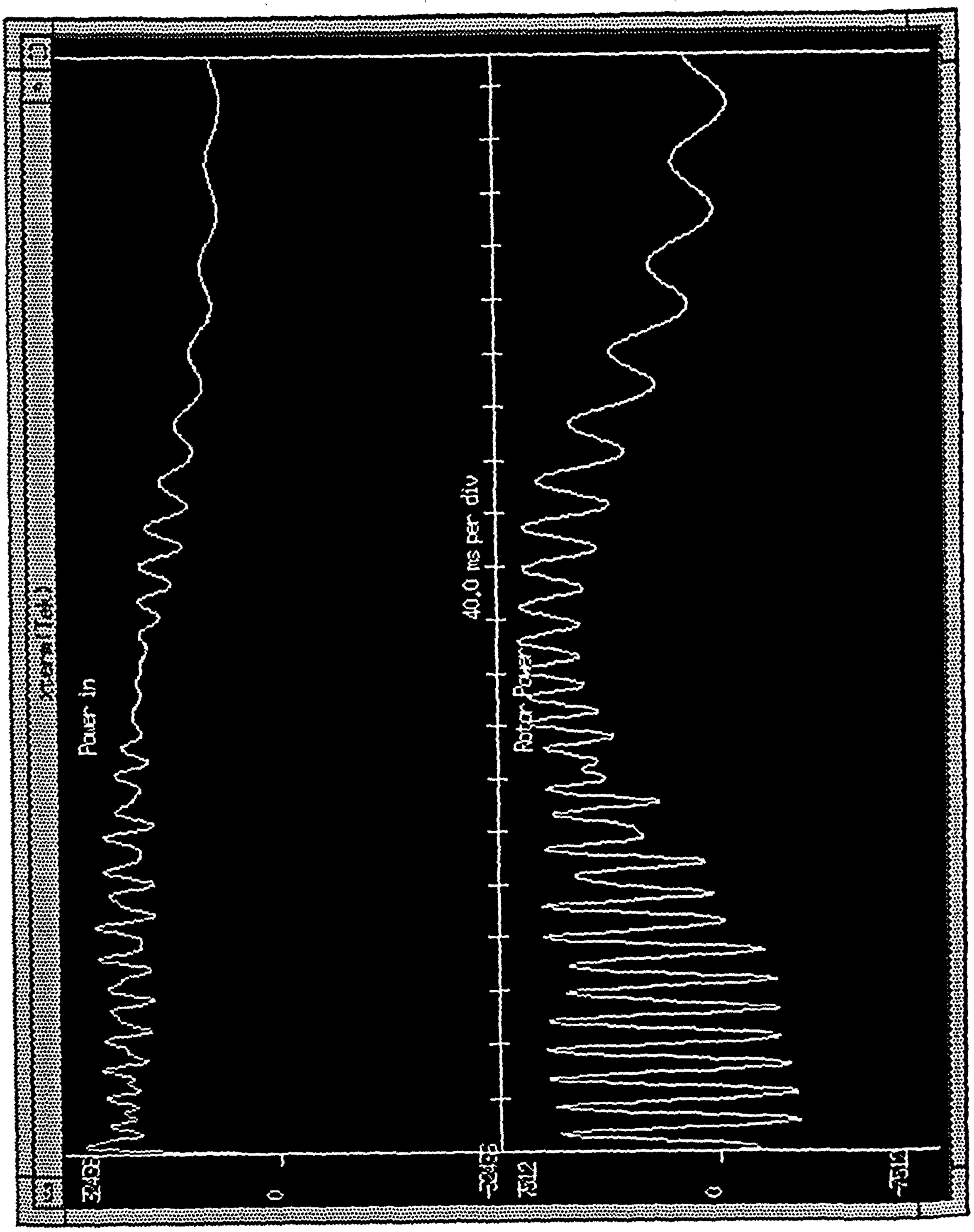

Figure 7.25: Input Power and Rotor Power during the starting transient for a simulated machine with rotor imbalance.

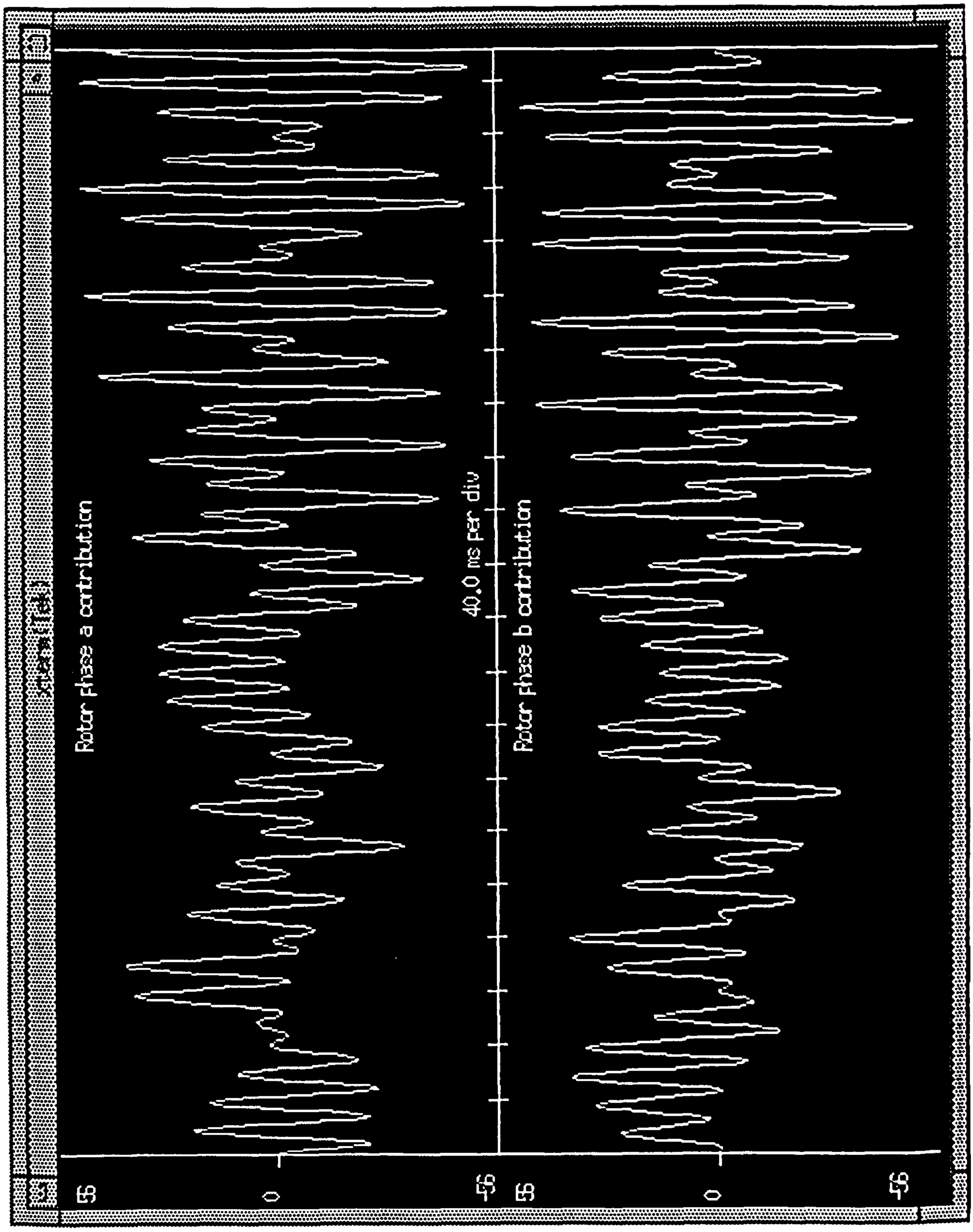

Figure 7.26: Contribution from rotor phases a and b to the current of stator phase a.

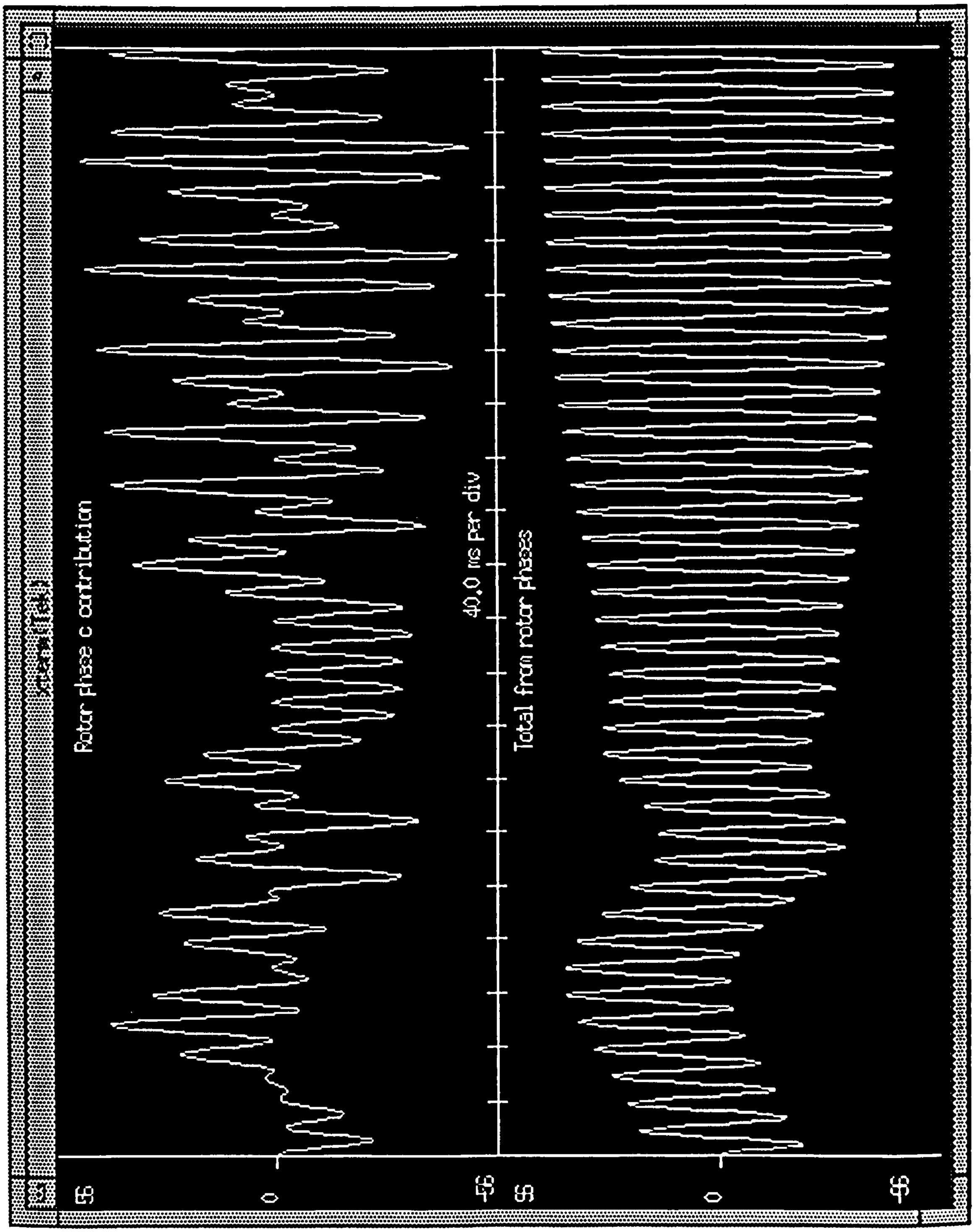

Figure 7.27: Contribution from rotor phase c (top) to stator phase current a. Summation of all rotor contributions to stator phase a current.

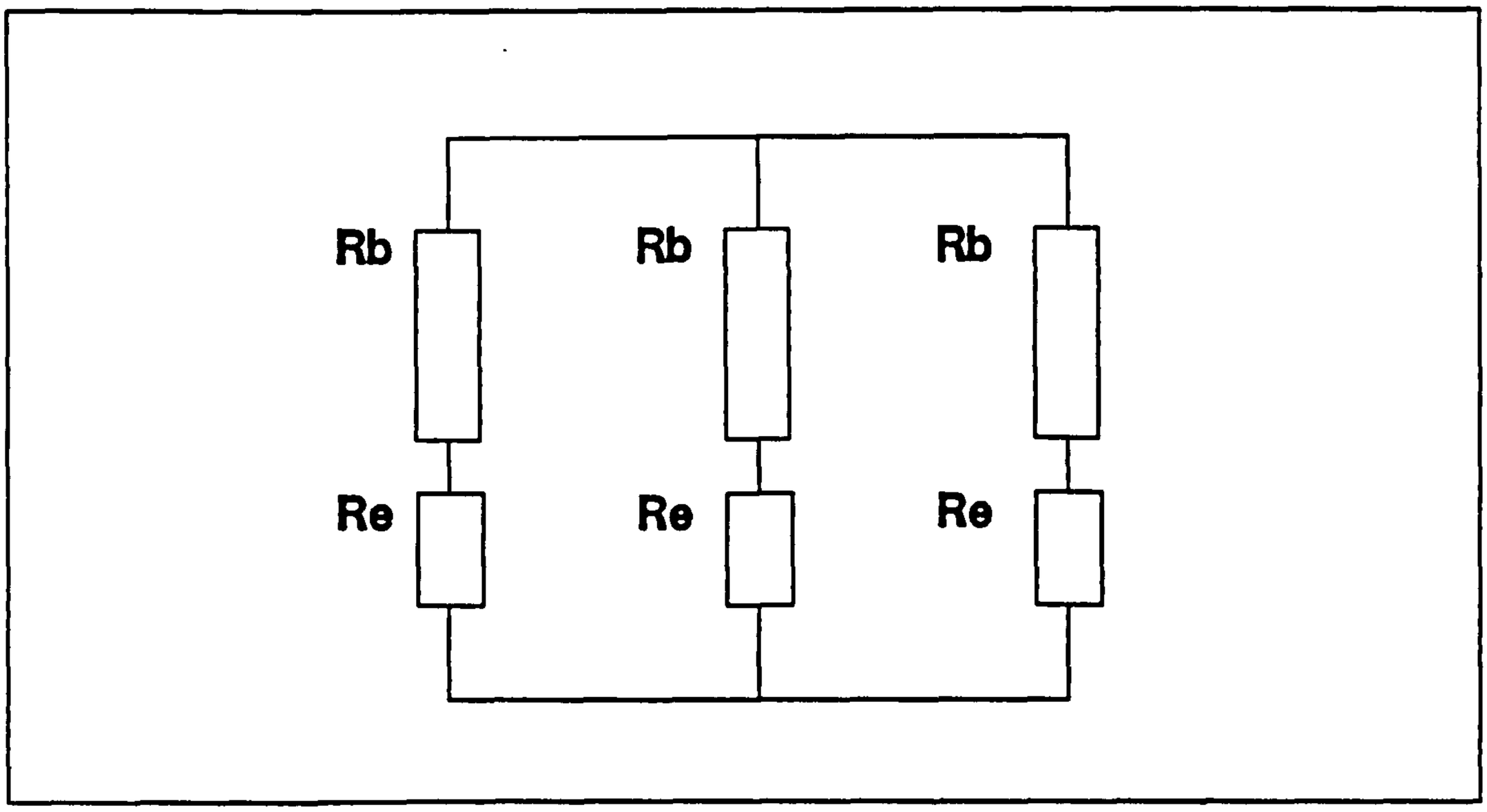

Figure 7.28: Rotor phases, comprising bar resistance and end-ring section

Chapter 8

Conclusion

8.1 Summary of Thesis Content

The principal objective of this project was to investigate whether it was possible to determine rotor faults within a 3 phase induction motor by analysis of the line current waveform during the starting transient. This objective has been met in the laboratory for a small 11kW 3 phase induction motor with a range of fault severity, from a single high resistance bar through to 3 fully broken bars.

Initially, studies were undertaken to review induction motor fault mechanisms and the computer simulation of the induction motor under transient conditions. All literature read describing induction motor fault mechanisms dealt with the steady state theory and analysis. The manifestation of these fault mechanisms under starting conditions was unknown. Previous work in computer simulation had been undertaken primarily to determine the peak torque and current during starting transient and re-switching operations. The purpose of induction motor simulation in this research work was to study a machine with a faulted rotor and to observe the frequency spectra of the resulting line current waveforms for components indicative of that fault.

Initial experimental work concentrated on a similar but simpler device than the induction motor, namely, the single phase transformer. From this work, experience was gained into the response of the switching transient and the application of signal processing to the line current waveform. Spectral analysis of the in-

rush current showed that both even and odd harmonics were of substantially greater amplitude than found in the steady state current. This was anticipated since the abrupt discontinuity at switch-on would generate a wideband spectrum and the large current peaks produced thereafter would be composed of large harmonic components. A comparison of the harmonic amplitude was also performed between the first and second 400ms period after switch-on. This showed that the even harmonics suffer a far greater reduction in amplitude than the odd harmonics as the in-rush current decays to the steady state value. This reduction in even harmonic content is due to the increasing symmetry of the current waveform as it decays to the steady state waveshape. Point on wave switching control was effected to facilitate the study of the switching angle on the harmonic content of the current waveform. As expected from theory the spectral components are larger for the worst case switching conditions of 0° and 180° than that of the best case switching conditions of 90° and 270°. The effect of supply voltage amplitude on harmonic content was also examined where a larger voltage would increase both even and odd harmonics, though the increase in the odd harmonic content was substantially larger than that of the even harmonics. In other words the higher the level of saturation, the more prominent become the odd harmonics and this is due to the shape of the transformer's B/H curve.

Modelling of the transformer's B/H characteristic was also undertaken to simulate the transient current waveform. Though some correlation could be observed between the spectra of real and simulated current waveforms, on the whole correlation was poor. This is now thought due to the use of a static B/H curve in a situation where a dynamic solution would have been more appropriate.

Experimental work on the test rig was initially carried out on a wound rotor with large rotor phase imbalances effected by means of an external resistor connected to a rotor phase via the slip rings. The wound rotor work was carried out almost exclusively on full load starts so that components indicative of faults would be easily observed. The line current waveforms obtained were analysed using an industry standard spectrum analyser and though these large faults could be quantified it was clear that these techniques were not suitable for detecting small faults in a machine under light or no load conditions. This was due to the nature of the line current waveform which had components that varied

their frequency and amplitude during the transient period. This prompted an investigation into alternative signal processing techniques more suited to this application.

The signal processing method selected (which was originally developed for Speech Analysis) was chosen because of the non-stationary nature of both speech and the line current waveforms. This processing method, called the Phase Vocoder was wideband in nature and could produce plots of the amplitude of frequency components as the transient progressed. From these wideband plots, changes in amplitude could be observed between the processed line currents of the test rig with a balanced rotor and a faulted rotor. As in the case of steady state analysis three components showed particular sensitivity to the degree of rotor imbalance, namely, the LSB, USB and PSH. One particular feature of interest noted from the vocoder plots was that of the LSB which experienced an amplitude maximum at a frequency between 15-25Hz. This occurred in the latter part of the starting transient at a slip of about 0.3. The investigation thus concentrated mainly on this large amplitude feature which was sensitive to the degree of rotor imbalance.

On completion of the wound rotor work it was possible to diagnose a small fault level from a full load start. However, to obtain a consistent diagnosis the machine had to be allowed to cool between starts. This effect was due to the fact that the external resistance was maintained at a constant temperature due to it having a large surface area exposed to the air in the laboratory. The windings of the machine however were enclosed in slots and despite the forced cooling provided for the machine, increased in temperature and hence in resistance. This caused the ratio of internal and external resistances to be temperature dependent with subsequent effect on the diagnosis of the fault level.

In parallel with the experimental study, the development of a computer model of the induction motor was under taken. Originally the induction motor model was represented by the two phase dq axis method, which greatly simplified the machine's performance equations. This two phase equivalent model allowed manipulation of variables and the introduction of non linearities, such as skin effect and saturation, so that the effect on the simulated line current and resulting spectrum could be observed. This model proved extremely useful in determin-

ing the sensitivity of the machine's response to parameter variation, particularly the leakage reactance. The dq model, however, had limitations such as the inability to represent supply harmonics and that either the stator or rotor had to be balanced. Furthermore the nature of this model would not allow a phase by phase representation of leakage saturation, though a crude relationship between the dq currents and the level of saturation could be implemented. This allowed the leakage saturation to be modelled and in fact brought the model's response closer to that of the real machine but did not generate a realistic harmonic content. These limitations prompted the development of a three phase model which would be more representative of the real machine.

The experimental study moved to the cage rotor machine where relatively large faults were initially observed to confirm the detection of faults on this type of rotor and also to further refine the signal processing. At this stage both the USB and PSH were shown to be less reliable indicators of rotor imbalance than the LSB. In view of this, experimental work concentrated in the region in which the LSB was known to reach a maximum in amplitude.

The next stage of the study required the purchase of two new cage rotors which allowed not only small fault levels to be studied but more importantly a sequence of increasing fault levels to be implemented. The faults studied varied from a high resistance bar through to three fully broken bars. The study now concentrated on the no-load starts which were shorter in duration and had components of less magnitude than that of full load starts. The analysis by phase vocoder had been reduced to observing the output of only two (23.4 - 31.2Hz) of the sixty four channels available. The wideband nature of the phase vocoder was now no longer required and in fact became an inconvenience due to the processing time taken. A simpler and more versatile processing method based on FIR filters was then developed. This new processing method allowed high resolution plots of amplitude versus frequency versus time to be produced where it could be observed that the LSB reached an amplitude maximum at frequency of about 15Hz. However, for any given fault level it was found that a relatively large variance existed from the results obtained at this frequency. After some experimentation, a suitable compromise between the amplitude and the variance of the observed component was reached with the filtering being performed at 21Hz. In fact, filtering was also performed at 24Hz as a form of control in

case an unexpected result occurred. No unexpected conditions arose and it was clear that some latitude in the filter frequency can be tolerated without loss of information. This may well not be the case in a noisy industrial environment.

Investigations were carried out into conditions which may have brought about erroneous diagnoses of the fault level. These conditions included the initial starting position of the rotor, large degrees of static air-gap eccentricity, the point on wave switching of the supply voltage and the temperature of the machine. The final analysis technique was shown to be unaffected by these four conditions. A suitable rotor for eliminating any possible effect due to dynamic air-gap eccentricity was not available for experimentation.

The case of an otherwise healthy rotor with a high resistance end-ring was also investigated. This study arose because of concerns about the representation of the rotor circuit in the three phase model in which the end- rings' impedances are appended to the phase resistances after appropriate transformation. The end-ring sections are physically different from the rotor bars and as such it was reasoned that faults should manifest themselves differently to that of rotor bar faults. Using the FIR filtering technique it was possible to observe differences between rotor bar and end-ring faults though more work would be required to quantify the results. Interest had been expressed in the ability to differentiate between bar and end-ring problems by engineers in industry, since it is apparently well known that end-ring failures cause less problems that rotor bar failures.

Experimentation was performed on the test rig with a view to determining the induction motor's parameters for use in the computer models. Various different types of test were performed in obtaining the electrical parameters resulting in similar values within the tolerances of experimental error.

The parameters obtained for modelling were :-

- $\alpha\beta$ electrical parameters (2 phase model)
- 3 phase model electrical parameters
- rotor moment of inertia
- magnetisation curve
- leakage saturation curve

- friction/windage losses
- core losses

Finally, a three phase model was developed which allowed implementation of leakage inductance saturation on an individual phase basis, resulting in a line current waveform with a harmonic content similar to that of the real machine. This model was also used to investigate imbalances on both rotor and stator, the effect of the starting position of the rotor and the switching angle of the supply. The effect of switching angle on the model's response showed that no significant change occurred to the amplitude of the LSB maximum though the position in time of the maximum did vary in a regular fashion with the switching angle. This agreed with experimental observations of the real machine.

The model also suggested that the time at which the LSB reached maximum amplitude was independent of the initial starting position of the rotor, which contrasts with the experimental results. One notable failing of the model to represent the real machine was under the conditions of rotor imbalance. It was known from experimental work that a machine with a high resistance phase or broken bars would accelerate to speed in less time than that of the balanced machine. This was not observed to be the case with the model which exhibited a slight increase in the run up time indicating that some aspect of the real machine was not being correctly represented. Nevertheless the general response of the model was similar to that of the real machine in that a LSB component was generated due to rotor imbalance. The LSB component also exhibited the same amplitude maximum in the latter stages of the starting transient as had been observed with the real machine. The application of leakage inductance saturation contributed to the amplitude of the USB component as indicated by steady state theory and was further confirmation that many aspects of this particular model did represent the real machine.

The simulated line current waveform of a no load start, had significantly larger sideband components in both steady state and transient states to that of the real machine, for a given level of imbalance. The change in side band amplitude for change in fault level showed better correlation between simulated and real machines. Relating a specific number of broken rotor bars to an equivalent phase imbalance is thought to be a major source of error in this analysis and

indicates that future modelling should accommodate individual rotor bars and the two end-ring sections.

It was apparent that the accurate modelling of system non linearities, particularly leakage saturation would always be approximate since the physical dimensions of the rotor and stator could not be adequately represented and as such only general trends could be observed by use of the models.

8.2 Recommendations for Future Work

In all, approximately 300 individual starting transients from the laboratory test rig have been obtained over this period of research with a further forty obtained from industrial machines. These records have been stored so that a database can be accrued for future use. To date none of the industrial machines have shown symptoms of rotor faults and in the majority of cases these results were confirmed by MOTORMON[1], a steady state diagnosis package. However, in the case of very large industrial machines (4MW+) the length of time taken to accelerate to speed posed problems for the data acquisition system used. This system consisted of "off the shelf" components and though very useful for the test rig proved to be restrictive for industrial use. For the continuation of this study a system with far greater data acquisition capability will be required, this could be implemented with a dedicated ADC board in a PC.

The ability to implement faults in a controlled manner on the test rig was fundamental to the development of the diagnostic technique. The opportunity to perform similar experimental tests on a large industrial machine would be ideal, however in practice this would require access and use of a fully fitted machine shop with adequate power supplies, lifting equipment and a generous sponsor. The only other alternative would be study machines that were known to have faults and this opportunity does not arise frequently.

The final computer simulation though more realistic than the original dq models does have limitations which may restrict its use in determining the faulted characteristics of large industrial machines. However there are still areas of interest

[1]Trademark of the ENTEK Corporation

to be explored with this model, such as inverter fed machines, double cage machines and the modelling of principal slot harmonics due to air-gap eccentricity. It is clear that a more sophisticated computer model will be required to predict the response of an arbitrary machine with faulted rotor. Recent developments in induction motor modelling using the finite element technique [89] may prove fruitful since the dimensions of the magnetic circuit may be represented and the cost and speed of computation is also decreasing yearly.

Incorporation of the Transient Analysis technique into a dedicated diagnostic instrument as developed by Ratter [90] should be quite straight forward. This instrument has all the necessary signal conditioning stages and a dedicated card for performing FFTs which would leave only the implementation of the FIR filter, a relatively simple task. Furthermore the dedicated instrument utilises sophisticated classifiers which can be trained to determine fault conditions, providing that the experimental data can be obtained. This instrument is designed to monitor a large number of machines in an industrial environment and would be in a favourable position to capture the line current waveform of a faulty machine during the starting period.

One other area in which this technique may find industrial application has been suggested by engineers in industry. Many plant operators and service companies perform steady state condition monitoring of induction motors using MOTOR-MON. One particular machine, which had been subject to condition monitoring for some time, failed to start and inspection of the machine's history showed that there were no indications of developing rotor faults. A more thorough investigation revealed that the outer cage of this double cage machine was in fact damaged. In a double cage machine, only the inner cage of the machine is in use during steady state operation and hence subject to steady state analysis. The outer cage, used for starting, is usually put under more stress than the inner cage particularly for a machine with heavy duty cycle. The starting transient technique developed in this research work, when fully refined for industrial use, should throw some light on the condition of these outer cages.

References

[1] S Williamson and A Smith.
Steady-state analysis of 3-phase motors with rotor-bar and end-ring faults.
Proc IEE, Vol 129, Pt B, No 3, May 1982.

[2] R Leonard.
Induction motor fault recognition.
Master's thesis, (CNAA) RGIT, 1985.

[3] J R Cameron.
Vibration and current monitoring for on-line detection of airgap eccentricity in induction motors.
PhD thesis, (CNAA) RGIT, 1987.

[4] B G Gaydon C Hargis and K Kamash.
The detection of rotor faults in induction motors.
In *IEE Int Conf on Electrical Machines - Design and Applications*, July 1982.

[5] W T Thomson, N D Deans, R A Leonard, and A J Milne.
Condition monitoring of induction motors for availability assessment in offshore installations.
In *4th Euredata Conference*, Venice, Italy, 1983.

[6] B G Gaydon.
An instrument to detect induction motor rotor circuit defects by speed fluctuation measurements.
In *Testmex 79 Conf. Papers*, pages 5–8, 1979.

[7] W T Thomson, R A Leonard, N D Deans, and A J Milne.
Monitoring strategy for discriminating between types of rotor defects in induction motors.
18th UPEC Proc. University of Surrey Guildford, UK , pp 241-246, 1983.

[8] S J Yang.
Low Noise Electric Motors, IEE Monographs in Electrical and Electronic Engineering.
Oxford Science Publications, 1981.

[9] R A Leonard and W T Thomson.
Vibration and stray flux monitoring for unbalanced supply and inter-turn winding fault diagnosis in induction motors.
In *Proc. 1st UK International Conference on Condition Monitoring, Uni. College of Swansea*, April 1984.

[10] W T Thomson, J Penman, R A Leonard, and A J Milne.
Failure identification of offshore induction motor systems using on-line condition monitoring systems.
In *Proc. 4st National Reliability Conference, Birmingham, UK*, April 1983.

[11] J Penman.
Condition monitoring of electrical drives.
Proc IEE, 133 Pt B(3), MAY 1986.

[12] J R Cameron, W T Thomson, and A B Dow.
Vibration and current monitoring for detecting airgap eccentricity in large induction motors.
Proc IEE, 133 Pt B(3), May 1986.

[13] W T Thomson, N D Deans, and D G Edwards et al.
On-Line Fault Diagnosis of Large Induction Motors.
RGIT, 1987.

[14] H C Stanley.
An analysis of the induction machine.
Transaction Amer, Inst Elect Engrs. Vol 57, pp 751-57, 1938.

[15] F Maginniss and N Schultz.
Transient performance of induction motors.
Transactions of AIEE, Vol.63, September 1944.

[16] C Weygandt and S Charp.
Electromechanical transient performance of induction motors.
Transaction of AIEE, Vol. 65, 1946.

[17] M Chidambara and S Ganapathy.
Transient torques in 3-phase induction motors during switching operations.

Trans AIEE, Pt III, 1962.

[18] F M Hughes and A S Aldred.
Transient characteristics and simulation of induction motors.
Proc. IEE, Vol. 111, No. 12, December 1964.

[19] F Fynn W Wood and A Shanmug Asundaram.
Transient torques in induction motors, due to switching of supply.
Proc IEE, Vol 112, No 7, July 1965.

[20] G J Rogers.
Linearised analysis of induction motor transients.
Proc IEE, Vol 112, pp 1917-1926, 1965.

[21] P Krause and C Thomas.
Simulation of symmetrical induction machinery.
IEEE Transactions on Power Apparatus and Systems, Vol PAS-84, November 1965.

[22] W Kaplan N Enslin and J Davies.
Influence of transient switching currents and fluxes on the torque developed by a squirrel-cage induction motor.
Proc IEE, Vol 113, No 6, June 1966.

[23] R Slater and S Wood.
Constant-speed solutions applied to the evaluation of induction-motor transient torque pears.
Proc IEE, Vol 114, No 10, October 1967.

[24] T A Lipo and A Consoli.
Modelling and simulation of induction motors with saturable leakage reactance.
IEEE Industry Applications Society, Annual Meeting Conference Record,pp 527-535, 1981.

[25] W D Humpage and B Stott.
Predictor-corrector methods of numerical integration in digital-computer analyses of power system transient stability.
Proc IEE, Vol 112, No 8, August 1965.

[26] Slater R D, Wood W, Flynn F, and Simpson R.
Digital computing of induction motor transient torque patterns.
Proc. IEE, Vol. 113, No. 5, May 1966.

[27] I Smith and S Sriharan.
Transient performance of the induction motor.
Proc IEE, Vol 113, No 7, July 1966.

[28] H E Jordan.
Digital computer analysis of induction machines in dynamic systems.
IEE Trans. PAS, Vol. Pas-86, No.6, June 1967.

[29] I R Smith and S Shriharan.
Induction motor re-switching transients.
Proc. IEE, Vol. 114, No. 4, April 1967.

[30] B Zorbas V Ramsden and R Booth.
Prediction of induction-motor dynamic performance in power stations.
Proc IEE, Vol 115, No 4, April 1968.

[31] J E Van Ness.
Synchronous machine analogs for use with network analysis.
Trans. Amer. Inst. Elect. Engrs. Vol.73, pp 1054-1060, 1954.

[32] C B Cooper and E D Howells.
The calculation of power system stability with particular reference to the victorian system.
Instn. Engrs. Australia Elect. Engng. Trans., EE1, pp 75-84, 1965.

[33] I Smith and S Sriharan.
Transients in induction machines with terminal capacitors.
Proc IEE, Vol 115, No 4, April 1968.

[34] S D T Robertson and K M Hebbar.
A digital model for three phase induction machines.
IEEE Transactions On Power Apparatus Systems, Vol Pas-88, No 11, November 1969.

[35] G Kron.
Tensors for Circuits.
New York: Dover, 1959.

[36] De Sarkar Asish, K and J Berg Gunnar.
Digital simulation of three phase induction motors.
IEEE Transactions on Power Apparatus and Systems, Vol Pas-89, No 6, July/August 1970.

[37] I R Smith and B Hamill.
Effect of parameter variations on induction motor transients.
Proc IEE, Vol 120, No 12, December 1973.

[38] JE Brown and C Grantham.
Determination of the parameters and parameter variations of a 3 phase induction motor having a current displacement rotor.
Proc IEE Vol 122 No 9, September 1975.

[39] M Kostenko and L Piotrovsky.
Electrical Machines.
MIR Publishers, 1977.

[40] S Sriharan.
Digital simulation of a group of induction motors.
Proc IEE, Vol 122, No 12, December 1975.

[41] T Tsao J R Smith, A F Stronach and K A Goodman.
Prediction of dynamic response of marine systems incorporating induction-motor propulsion drives.
Proc IEE, Vol 127, Pt B, No 5, September 1980.

[42] T E Durrani W D Humpage and V F Carvalno.
Dynamic response analysis of inter-connected synchronous-asychronous machine groups.
Proc IEE, Vol 116, pp 2015-2027, 1969.

[43] J R Smith, J Penman, and Abd Allah.
The simulation of transient response of singly excited electrical machines.
Int. J. Comput. in Elect. Eng. Vol.3, pp 271-279, 1977.

[44] M R Lloyd.
Transient performance of induction motors in electro- mechanical systems.
IEE Conference Publication No 213, 1982.

[45] J R Smith G W Buckley, M R Lloyd and G J Rogers.
Application of induction motor simulation models to power system and industrial applications, 13th universities power engineering conference.
IEE Conference Publication No 213, 1982.

[46] P D Agarwal and P L Alger.
Saturation factors for leakage reactance of induction motors.
Proc IEE, Vol 80, pp 1037-1042, 1961.

[47] P Silvester.
Dynamic resistance and inductance of slot embedded conductors.
IEEE Transactions Power Apparatus And Systems, V87, Pt, Pg 250-256, 1968.

[48] G J Gogers and D S Benaragama.
The piece by piece solution of eigenvalue problems.
Proc. Computmag. SRC Oxford, pp 329-331, 1976.

[49] R Bollini A Godhwani and R Chakraverty.
Digital simulation of unsymmetrical 2-phase induction machines using CSMP.
IEEE Region 5 'Conference Technology For An Efficient Tomorrow'. Illinois Uni., April 1983.

[50] Ghani Sayeed Nural.
Digital computer simulation of three-phase induction machine dynamics - a generalized approach.
IEEE Trans On Industry Applications, Vol 24, No 1, Jan/Feb 1988.

[51] Ghani Sayeed Nurul.
On simulating dynamic behaviour of three phase induction machines with squirrel cage rotor.
Simulation pp 182-193, May 1988.

[52] M G Say.
Alternating Current Machines.
Pitman, 1976.

[53] A A Hudson.
Transformer magnetising inrush current.
The Electrical Research Association, 2020.

[54] T R Specht.
Transformer inrush and rectifier transient currents.
IEEE Trans. on Power App. and Sys., Vol. Pas 88, No. 4, April 1969.

[55] R Yacamini and A Abu-Nasser.
Numerical calculation of inrush current in single phase transformers.
IEE Proc., Vol. 128, Pt. B, No. 6, Nov 1981.

[56] W K MacFadyen et al.
Method of predicting transient current patterns in transformers.

Proc IEE, Vol 120, No 11, November 1973.

[57] Allan Greenwood.
Electrical Transients in Power Systems.
Wiley, 1971.

[58] J A Fleming.
Experimental researches on alternate current transformers.
J. IEE , Vol.21, Sec.8, pp 677-685, 1892.

[59] A R Daniels.
Introduction to Electrical Machines.
MacMillan, 1976.

[60] T R Specht.
Transformer magnetising inrush current.
AIEE , Trans. Vol. 70, pp 323-328, 1951.

[61] J E Holcomb.
Distribution transformer magnetising inrush current.
Proc. IEE Vol.80, Pt.3, pp 697-702, 1961.

[62] W K Macfayden, R S Simpson, R D Slater, and W S Wood.
Representation of magnetising curves by exponential series.
Proc. IEE Vol.120, Pt.8, pp 902-904, 1973.

[63] J Rye.
Measurement of magnetising inrush currents on a 11kv rural system.
Electricity Council Research Report, March 1973.

[64] S Ray.
Digital simulation of B/H excursions for power system studies.
IEE Proc, Vol 135, Pt C, No 3, May 1988.

[65] R D Slater.
Heavy-duty switching angle selector.
Proc IEE, Vol 114, No 1, January 1967.

[66] W Kaplan.
Advanced Mathematics for Engineers.
Addison-Wesley, 1981.

[67] C V Jones.
Unified theory of electrical machines.

Butterworths, 1967.

[68] C Baldwin.
Method of Electrical Measurement.
Blackie and Son Ltd, 1953.

[69] J A Edminster.
Electric Circuits.
McGraw-Hill, 1972.

[70] J Bendat and A Piersol.
Random Data: Analysis and Measurement Procedure.
Wiley and Sons, 1971.

[71] N B Jones.
Digital Signal Processing, IEE Control Series 22.
Peregrinus, 1982.

[72] L R Rabiner.
Techniques for designing finite duration impulse response digital filters.
IEE Trans Comm Tech, Vol COM-19, No 2, April 1971.

[73] D E Newland.
Random Vibrations and Spectral Analysis.
Longman, 1974.

[74] R D Slater.
Transients in Electrical Machines.
PhD thesis, Thesis, University of Strathclyde, 1966.

[75] P L Alger.
The Nature of Polyphase Induction Machines.
Wiley, 1951.

[76] L Flanagan and R M Golden.
Phase vocoder.
Bell Sys Tech J, Vol 45, pp 1493-1509, November 1966.

[77] R W Schafer and L R Rabiner.
Design and simulation of a speech analysis-synthesis system based on short time fourier analysis.
IEEE Transaction on Audio and Electroacoustics AU-21, pp 165-174, June 1973.

[78] Mulukutla S Sarma.
Electrical Machines.
West Publishing Company, 1985.

[79] N N Hancock.
Matrix Analysis of Electrical Machinery.
Pergamon Press, 1974.

[80] R L Burden and J D Faires.
Numerical Analysis.
PWS Publishing Company, Boston, 1987.

[81] E Fehlberg.
Klassische runge-kutta formeln vieter und niedrigerer ordnung mit schrittweiten-kontrolle und ihre anwendung auf warmeleleitungs probleme.
Computing. Vol 6, pp 61-71, 1970.

[82] L R Rabiner and Barnard Gold.
Theory and application of D.S.P.
Prentice Hall, 1975.

[83] J D Edwards.
Electrical Machines.
Macmillan, 1986.

[84] M M Liwschitz-Garik.
Computation of skin effect in bars of squirrel cage motors.
Trans. AIEE, Vol. 74, Part 3, August 1955.

[85] M M Liwschitz-Garik.
Skin effect bars of squirrel cage rotors.
Trans. AIEE, Vol. 73, Part III A, April 1954.

[86] H W Lorenzen.
Der einfluss der stromverdrangung auf die erzwungenen pendelugen von asynchronmaschinen.
ETZ-A, 88, pp 445-451, 1967.

[87] A Meyer.
Influence de l'effet pelliculaire sur le regime stationaire et sur les oscillations forcees de machines asynchrones.
Brown Boveri Rev ,8, pp 500-507, 1976.

[88] H Weichsel.
Squirrel-cage rotors with split resistance rings.
Journal of Amer Inst of Elect Eng, Vol 47, pp 606-610, 1928.

[89] A C Smith, S Williamson, and J R Smith.
Transient currents and torques in wound rotor induction motors using the finite-element method.
IEE Proc, Vol 137, Pt B, No 3, May 1990.

[90] A Ratter.
Development of a Real Time Digital Signal Processing System for Machine Condition Monitoring.
PhD thesis, (CNAA) RGIT, 1991.

[91] O Herrman R E Schafer, RL R Rabiner.
Fir digital filter banks for speech analysis.
Bell Syst. Techn. J Vol 54, pp 531-544, March 1975.

[92] M R Porinoff.
Implementation of the digital phase vocoder using the fast fourier transform.
IEEE Trans on Acoustics, Speech and Signal Processing, Vol ASSP-24, No 3, June 1976.

[93] A J Moorer.
The use of the phase vocoder in computer music applications.
Journal of the Audio Engineering Society, Vol 26, No 1/2, Jan/Feb 1978.

[94] L R Rabiner and C M Rader.
Digital Signal Processing.
IEEE Press, 1972.

Appendix A

Axes Transformations

The transformation from Three phase rotating to Two Phase stationary axes can be separated into two distinct transformations namely Three Phase rotating (a,b,c) to Two Phase rotating (α,β,0) and then Two Phase rotating (α,β,0) to Two Phase Stationary (d,q,0). These transformations are diagrammatically shown in Fig.[A.1].

The basic differential equations for a three phase induction motor can be expressed in matrix form as :-

$$\begin{pmatrix} Va \\ Vb \\ Vc \\ Ve \\ Vf \\ Vg \end{pmatrix} = \begin{pmatrix} R1+L1p & pMab & pMac & pMae & pMaf & pMag \\ pMab & R1+L1p & pMbc & pMbe & pMbf & pMbg \\ pMac & pMbc & R1+L1p & pMce & pMcf & pMcg \\ pMae & pMbe & pMce & R2+L2p & pMef & pMeg \\ pMaf & pMbf & pMcf & pMef & R2+L2p & pMfg \\ pMag & pMbg & pMcg & pMeg & pMfg & R2+L2p \end{pmatrix} \begin{pmatrix} Ia \\ Ib \\ Ic \\ Ie \\ If \\ Ig \end{pmatrix}$$

where p is the differential operator d/dt

$$i.e \qquad [V] = [Z] \cdot [I] \qquad (A.1)$$

where it is assumed that :-

$Mae = Mbf = Mcg = M1cos(\theta)$

$Maf = Mbg = Mce = M1cos(\theta + 2\pi/3)$

$Mag = Mbe = Mcf = M1cos(\theta + 4\pi/3)$

$Mab = Mac = Mbc = Mef = Meg = Mfg = M1cos(2\pi/3) = -M1/2$

$L1 = M1 + l_1 \qquad and \qquad L2 = M1 + l_2$

$M1$ is the mutual inductance between any two windings when coaxial.

These equations are based on the following assumptions:-

a) no core losses

b) inductances are independent of current i.e. no saturation

c) the mutual inductances between a stator winding and a rotor winding vary with the cosine of the angle between their axes. Other inductances are independent of rotor position.

d) stator and rotor slotting, stray capacitance and skin effect are considered negligible.

e) stator and rotor windings are considered balanced.

In their present form the voltage equations A are either non-linear, when θ is unknown, or have variable co- efficients when θ is a known function of time e.g. when speed is constant. In either case only a numerical step-by-step solution can be obtained. By application of the two transformations indicated above, the equations can transformed into a set of stationary axes equations thus reducing the number of equations. If the zero-sequence currents are not present then the number of equations are reduced further. Zero-sequence currents would only flow if there were an external connection to the neutral point of the rotor circuit [67] and this is not normally the case.

The first step is to apply the (a,b,c,α,β,0) transformation which results in the equivalent two phase machine. It should be noted that a condition of these transformations is that power is invariant [79,67].

The transform expressed in matrix form is :-

$$\begin{pmatrix} Ia \\ Ib \\ Ic \\ Ie \\ If \\ Ig \end{pmatrix} = \begin{pmatrix} [C1] & [0] \\ [0] & [C1] \end{pmatrix} \begin{pmatrix} Ids \\ Iqs \\ Io1 \\ I\alpha \\ I\beta \\ Io2 \end{pmatrix}$$

$$i.e. \qquad [I] = [C] \cdot [I]' \qquad (A.2)$$

where C1 is :-

$$\begin{pmatrix} C1 \end{pmatrix} = \begin{pmatrix} \sqrt{2/3} \end{pmatrix} \begin{pmatrix} 1 & 0 & 1/\sqrt{2} \\ -1/2 & \sqrt{3}/2 & 1/\sqrt{2} \\ -1/2 & -\sqrt{3}/2 & 1/\sqrt{2} \end{pmatrix}$$

The 3 phase and 2 phase voltage equations are of course related by the same transformation (C) and the equivalent 2 phase impedance matrix is given by :-

$$[Z]' = [C]^t \cdot [Z] \cdot [C] \tag{A.3}$$

The voltage equations for the equivalent 2 phase motor in the alpha and beta axes are thus :-

$$\begin{pmatrix} Vds \\ Vqs \\ V\alpha \\ V\beta \end{pmatrix} = \begin{pmatrix} Rs+Lsp & 0 & Mpcos(\theta) & Mpsin(\theta) \\ 0 & Rs+Lsp & Mpsin(\theta) & -Mpcos(\theta) \\ Mpcos(\theta & Mpsin(\theta) & Rr+Lrp & 0 \\ Mpsin(\theta & -Mpcos(\theta) & 0 & Rr+Lr \end{pmatrix} \begin{pmatrix} Ids \\ Iqs \\ I\alpha \\ I\beta \end{pmatrix}$$

$$where\ M = (3/2) \cdot M1, \qquad Ls = M + l_1, \qquad Lr = M + l_2$$

The 2 phase rotating axes may now be transformed to the 2 phase stationary axes by the application of the following transformation in which power is invariant.

$$\begin{pmatrix} Ids \\ Idq \\ I\alpha \\ I\beta \end{pmatrix} = \begin{pmatrix} 1 & 0 & 0 & 0 \\ 0 & 1 & 0 & 0 \\ 0 & 0 & cos(\theta) & sin(\theta) \\ 0 & 0 & sin(\theta) & -cos(\theta) \end{pmatrix} \begin{pmatrix} Ids \\ Iqs \\ Idr \\ Iqr \end{pmatrix}$$

$$i.e. \qquad [I] = [C2] \cdot [I]' \tag{A.4}$$

The voltage equations are related by this transformation C2 and the impedance matrix is obtained in a similar way to the operation indicated in equation A.3.

Thus the equivalent voltage equations in the stationary axes may be written :-

$$\begin{pmatrix} Vds \\ Vqs \\ Vdr \\ Vqr \end{pmatrix} = \begin{pmatrix} Rs+Lsp & 0 & Mp & 0 \\ 0 & Rs+Lsp & 0 & Mp \\ Mp & Mp\theta & Rr+Lrp & Lrp\theta \\ -Mp\theta & Mp & -Lrp\theta & Rr+Lrp \end{pmatrix} \begin{pmatrix} Ids \\ Iqs \\ Idr \\ Iqr \end{pmatrix}$$

$$i.e. \qquad [Vdq] = [Zdq] \cdot [Idq] \tag{A.5}$$

For the staring transient case the speed is a variable quantity and as can be seen from the expanded form of equation A.5 there will therefore be four equations and five unknowns. A further equation is thus required and this is obtained from the mechanical system relating the torque and acceleration of the shaft.

$$Torque = (J/polepairs) \cdot p\omega + f(\omega) \tag{A.6}$$

where J is the total inertia of the motor's rotor plus that of any mechanical load and f(ω) is the load torque expressed as a function of speed, including the mechanical losses of the motor.

The electromagnetic torque can be shown [79,67] to be given by :-

$$Te = polepairs \cdot M \cdot (Ids \cdot Iqr - Iqs \cdot Idr) \tag{A.7}$$

Equations A.6 and A.7 can be combined to give :-

$$p\omega_r = ((polepairs)^2 \cdot M \cdot (Ids \cdot Iqr - Iqs \cdot Idr) - f(\omega_r))/J \tag{A.8}$$

To solve for the four currents of this 2 phase model it is necessary to rearrange the matrix of equations A.5 in terms of derivatives of the required currents, This is achieved as follows :-

Equation A.5 may be re-written as follows:-

$$[V] = ([R] + [L]p + [G] \cdot \omega_r) \cdot [I] \tag{A.9}$$

where $\omega_r = p\theta$ the rotor angular velocity

Equation A.9 can be rearranged so that an expression is obtained for the derivatives of currents:-

$$p[I] = [L]^{-1} \cdot [V] - ([R] + [G] \cdot \omega_r) \cdot [I] \tag{A.10}$$

The individual matrices of this equation are expanded below :-

The inductance matrix L is :-

$$[\,L\,] = \begin{pmatrix} Ls & 0 & M & 0 \\ 0 & Ls & 0 & M \\ M & 0 & Lr & 0 \\ 0 & M & 0 & Lr \end{pmatrix}$$

and the inverse of this inductance matrix is :-

$$\left[L \right]^{-1} = \begin{pmatrix} Lr/D & 0 & -M/D & 0 \\ 0 & Lr/D & 0 & -M/D \\ -M/D & 0 & Ls/D & 0 \\ 0 & -M/D & 0 & Ls/D \end{pmatrix}$$

where $D = Ls.Lr - M^2$

The resistance matrix R is:-

$$\left[R \right] = \begin{pmatrix} Rs & 0 & 0 & 0 \\ 0 & Rs & 0 & 0 \\ 0 & 0 & Rr & 0 \\ 0 & 0 & 0 & Rr \end{pmatrix}$$

The matrix of rotational inductance terms G is:-

$$\left[G \right] = \begin{pmatrix} 0 & 0 & 0 & 0 \\ 0 & 0 & 0 & 0 \\ 0 & M & 0 & L \\ -M & 0 & -L & 0 \end{pmatrix}$$

Thus equation A.10 represent the derivatives of the four currents Ids and Iqs in the stator, Idr and Iqr in the rotor and equation A.8 represents the derivative of the rotor speed. These five equations can be solved by step by step numerical techniques and are the basis of the 2 phase simulation presented in this work. It should be noted that these equations have been derived with the reference frame fixed in the stator and that similar groups of equations can be derived in other reference frames [79,21].

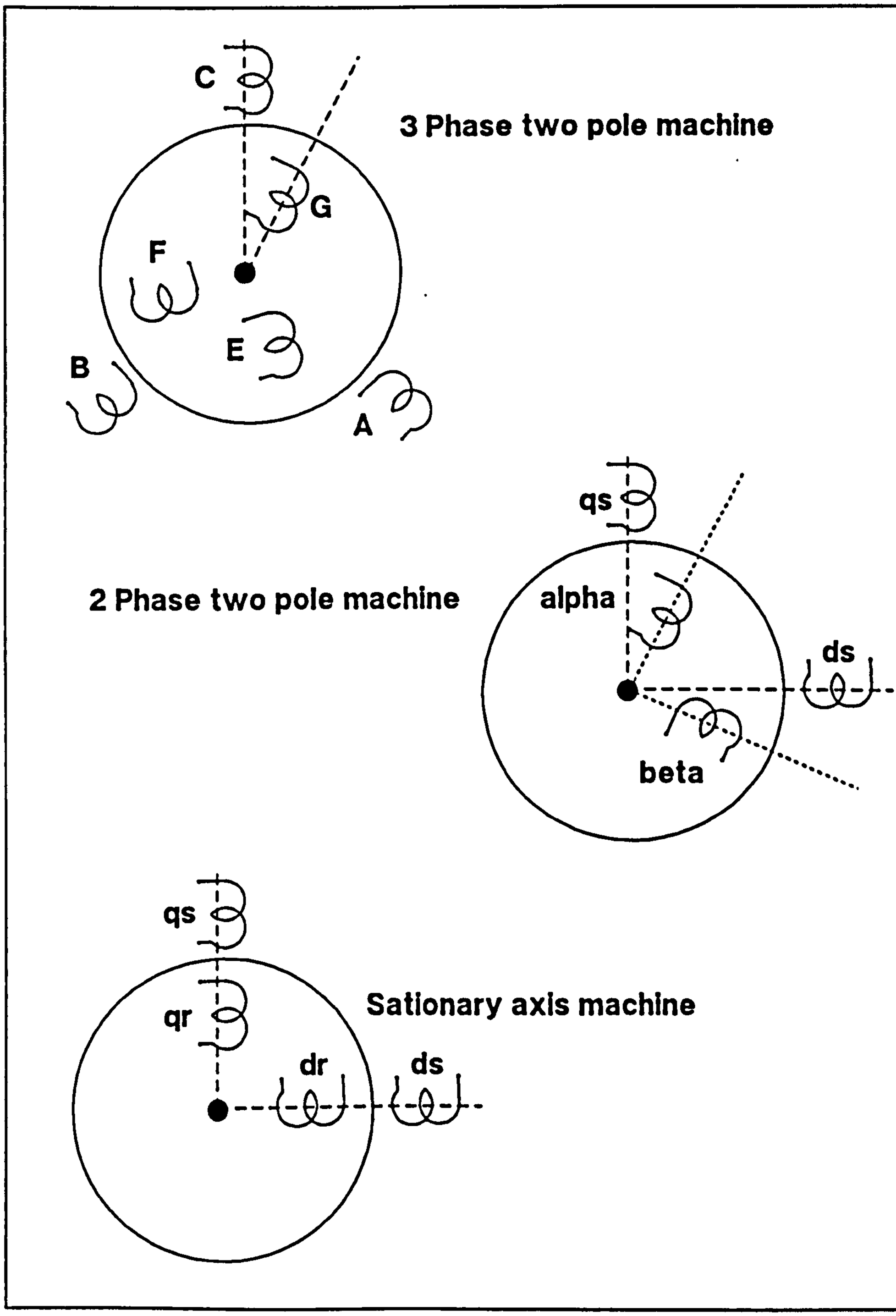

Figure A.1: Diagrammatic representation of 3 phase to 2 phase to Stationary axes machine.

Appendix B

The Phase Vocoder

B.1 Introduction

The Phase Vocoder has been traditionally used to analyse Speech waveforms mainly as a means of data rate reduction and for manipulating the the basic speech parameters. The parameters obtained from this Short Time Fourier Transform (STFT) of these speech waveforms have been the magnitude and phase (or phase derivative), hence PHASE vocoder. The Phase Vocoder can be thought of as a bank of bandpass filters to which the signal of interest is fed. The amplitude of any particular component can be measured at the output of the appropriate filter (Fig.[B.1a]). When the magnitude components of these filters are displayed together the graph is often referred to as a Spectogram or Waterfall diagram and represents the change in spectral amplitudes with time. The original vocoders consisted of banks of suitably tuned analog bandpass filters whose output was usually fed to a paper recorder that represented amplitude by the darkness of the trace plotted. Thus a signal with a non-stationary spectrum could be captured as a group of amplitude changes with time.

The analog method was not particularly versatile and changes of filter parameters and the method of data output could be inconvenient. Flanagan and Golden[76] of Bell Laboratories presented a method for digital implementation of the Phase Vocoder which would allow the design parameters (centre frequencies, bandwidth etc.) to be varied and thus their effect examined. The difficulty

in implementing such systems in digital form is the rapid rise in the computational burden as the frequency bands are increased. Schafer and Rabiner [77] have shown how to greatly reduce the amount of computation required for the analysis procedure by formulating the system such that most of the computation is performed by the Fast Fourier Transform (FFT). The FFT of any data sequence of length (N) requires approximately ($N.log_2(N)$) operations whereas the direct solution by Discrete Fourier Transform (DFT) requires $(N)^2$ operations. It can be seen that there is considerable reduction in the number of operations for large values of (N) (e.g $N = 2048$) by use of the FFT algorithm.

B.2 Formulation

Let $x(n)$ represent the input waveform. The discrete short- time Fourier transform of $x(n)$ is defined by :-

$$X_k(n) = \sum_{r=-\infty}^{\infty} x(r)\, h(n-r)\, W_N^{-rk} \qquad for\, k = 0, 1, \ldots, N-1, \qquad \text{(B.1)}$$

where $W_N = e^{j(2\pi/N)}$

and $h(n)$ is an appropriately chosen window. $X_k(n)$ may be interpreted as (N) samples of a time varying spectrum with (k) the index associated with frequency and (n) the index associated with time. According to equation B.1, $X_k(n)$ is obtained at each time sample (n) by weighting the sequence $x(r)$ by the window $h(n-r)$ and performing a Fourier transform on the resulting sequence.

It is informative to consider equation B.1 in terms of a bank of digital bandpass filters with contiguous passbands as shown in Fig.[B.1a]. Consider a set of (N) complex bandpass filters $h_k(n)$ with passbands equally spaced about the unit circle and with unit- sample responses.

$$h_k(n) = (1/N)\, h(n)\, W_N^{nk}, \qquad k = 0, 1, \ldots, N-1 \qquad \text{(B.2)}$$

where $h(n)$ is a prototype low-pass filter with real unit sample- response. If these filters are combined to form the structure shown in Fig.[B.1b], then the output of the (k)th filter, denoted by $y_k(n)$, is given by the convolution :-

$$y_k(n) = \sum_{r=-\infty}^{\infty} x(r)\, h_k(n-r)$$

$$= \sum_{r=-\infty}^{\infty} x(r)\,((1/N)\,h(n-r)\,W_N^{(n-r)k})$$

$$= (1/N)\,W_N^{nk} \sum_{r=-\infty}^{\infty} x(r)\,h(n-r)\,W_N^{-rk}$$

$$= (1/N)\,W_N^{nk}\,X_k(n) \qquad \text{(B.3)}$$

where $X_k(n)$ is the discrete short-time Fourier transform of $x(n)$ as given by equation B.1. From equations B.1 and B.3 a single channel of the filter bank is seen to be equivalent to the structure shown in Fig.[B.2a].

It is imperative that no information is lost in the analysis by this digital Phase Vocoder. Thus if all the outputs of the bank of bandpass filters are added together then the resulting waveform should be identical to the input waveform. This summed output can be expressed as :-

$$y(n) = \sum_{k=0}^{N-1} y_k(n)$$

$$= (1/N) \sum_{k=0}^{N-1} X_k(n)\,W_N^{nk}$$

It is therefore necessary for the filter response $h(n)$ to be chosen in such a manner that no information is lost [91]. This results in two conditions for $h(n)$

$$i)\ h(0) = 1$$

$$ii)\ h(n) = 0 \ \ for\ n = \mp N, \mp 2N, \mp 3N, \mp 4N, \cdots \qquad \text{(B.4)}$$

These conditions are equivalent to the statement in the frequency domain that although each $h_k(n)$ is not necessarily an ideal bandpass filter, the sum of their N frequency responses is unity for all frequencies.

The most straight forward approach to designing the proto-type low-pass filter $h(n)$ is by windowing [82]. Specifically the unit sample response

$$h_{ideal}(n) = sin(n\pi/N)/(n\pi/N) \qquad \text{(B.5)}$$

of an ideal low-pass filter with cut off frequencies at $Wc = \mp(\pi.N)$ is multiplied by a smooth, finite duration window (e.g. Hamming, Kaiser etc.) to obtain $h(n)$. The precise specifications of $h(n)$ are determined by the length and shape of the window. Any $h(n)$ designed in this manner will fulfil the criteria in equations B.4.

B.3 Implementation of the Phase Vocoder Using the FFT Algorithm

If the number of frequency bands (N) is chosen to be a highly composite number (usually an integer power of 2) then the FFT algorithm can be employed to compute efficiently the short-time Fourier transform $X_k(n)$ defined by equation [B.1]. It can be seen that equation B.1 does not have the form of a DFT and, therefore, cannot be computed directly with the FFT algorithm. The limits on the summation are given as infinite, but in practice are finite and determined by the length of $h(n)$. By recognising $X_k(n)$ as samples, equally spaced in frequency, of the (continuous-valued) Fourier transform of $x(r)\,h(r-n), X_k(n)$ can be expressed as the DFT of an (N) point sequence obtained by time domain aliasing of $x(r).h(n-r)$. Substituting $s = r - n$ into equation B.1 gives :-

$$X_k(n) = \sum_{s=-\infty}^{\infty} x(n+s)\,h(-s)\,W_N^{-(n+s)k}$$

$$X_k(n) = W_N^{-nk} \sum_{s=-\infty}^{\infty} x(n+s)\,h(-s)\,W_N^{-sk}$$

which can be written as

$$X_k(n) = W_N^{-nk} \sum_{l=-\infty}^{\infty} \sum_{m=0}^{N-1} x(n+lN+m)\,h(-lN-m)\,W_N^{-(lN+m)k}$$

by taking

$s = lN + m \;\; for\, m = 0, 1, \ldots, N-1$

and $l = -\infty, \ldots, -1, 0, +1, \ldots, +\infty.$

Interchanging the orders of summation and using $W_N^N = 1$ gives :-

$$X_k(n) = W_N^{-nk} \sum_{m=0}^{N-1} \sum_{l=-\infty}^{\infty} x(n+lN+m)\,h(-lN-m)\,W_N^{-mk}$$

which can be expressed

$$X_k(n) = W_N^{-nk} \sum_{m=0}^{N-1} z_m(n)\,W_N^{-mk} \tag{B.6}$$

where

$$z_m(n) = \sum_{l=-\infty}^{\infty} x(n+lN+m)\,h(-lN-m) \tag{B.7}$$

The expression

$$Z_k(n) = \sum_{m=0}^{N-1} z_m(n)\, W_N^{-mk}$$

can be recognised as the DFT of the (N) point (in m) sequence $z_m(n)$ for fixed (n) and, can therefore, be computed directly with the FFT algorithm once $z_m(n)$ has been formed. In addition to the computational savings gained by computing the short-time Fourier transform using the FFT , further savings may be gained by avoiding the complex multiplications by W_N^{-nk} in equation B.6. It can can be seen that $X_k(n)$ is given by :-

$$X_k(n) = W_N^{-nk}\, Z_k(n)$$

where $Z_k(n)$ is the DFT of $z_m(n)$. A property of the DFT is that a circular shift in one domain (time) corresponds to a multiplication by a complex exponential in the other domain (frequency). This property can be exploited by performing a circular shift of $z_m(n)$ prior to computing its DFT, thus the multiplications by W_N^{-nk} are avoided. Equation B.6 can be re-written as :-

$$X_k(n) = \sum_{m=0}^{N-1} z_{(m-n)N}(n)\, W_N^{-mk}$$

or

$$X_k(n) = \sum_{m=0}^{N-1} x_m(n)\, W_N^{-mk} \tag{B.8}$$

where

$$x_m(n) = z_{(m-n)N}(n)$$

The procedure for computing the discrete short-time Fourier transform coefficients $X_k(n)$ at a particular value of (n) based on the preceding analysis is the following. Referring to Fig.[B.3b], the input data sequence which is considered as a function of the dummy index variable (r) is multiplied by the window $h(n-r)$ (in practice $h(n)$ is often zero phase, in which case $h(n-r) = h(r-n)$). It is assumed that $h(n)$ is of infinite duration and, in fact, is chosen to have a length equal to an even multiple of (N), plus one. The resulting weighted sequence is partitioned into sections each of length (N) such that $x(r)|_{r=n}$ is the zeroth sample of one of the sections. The resulting N-point subsequences denoted by $x_m^{(l)}(n)$ for $0 \leq m \leq N-1$ are then added together to form :-

$$z_m(n) = \sum_l x_m^{(l)}(n), \qquad m = 0, 1, \ldots, N-1$$

$z_m(n)$ is circularly shifted (in m) by (n) samples to obtain

$$x_m(n) = z_{(m-n)N}(n) \ ,$$

and its DFT is computed by means of the FFT algorithm to give the desired $X_k(n)$, i.e. ,

$$X_k(n) = \sum_{m=0}^{N-1} x_m(n)\, W_N^{-(nk)} \qquad k = 0, 1, 2, \ldots, N-1.$$

B.4 Magnitude-Frequency Conversion

If we again consider this system to be a bank of band-pass filters, it can be seen that what is present at the output are the real and imaginary parts of the input signal in each of the (N) equally spaced frequency bands. The amplitude of the output component from any channel can be obtained by taking the square root of the sum of squares of the real and imaginary parts. The frequency of a component in an output channel may be obtained by taking the derivative of the phase angle as defined by the arctangent of the imaginary part over the real part [92]. This frequency is the difference between the actual frequency and the centre frequency of the corresponding band-pass filter. To depict this in formulas, let $a_k(n)$ be the real part of the output of the (k)th channel and $b_k(n)$ be the imaginary part of the (k)th output channel.

$$A_k(n) = sqrt(a_k(n)^2 + b_k(n)^2) \tag{B.9}$$

$$\theta_k(n) = arctan(b_k(n)/a_k(n)) \tag{B.10}$$

$$d\theta/dt = C1/C2 \tag{B.11}$$

where

$$C1 = a_k(n)\, d(b_k(n)/dt) - b_k(n)\, d(a_k(n)/dt)$$

and

$$C2 = a_k(n)^2 + b_k(n)^2$$

Equation B.11 can be simplified by a trigonometric expansion :-

$$sin\{\theta_k(n) - \theta_k(n-1)\} = sin\{\theta_k(n)\}\, cos\{\theta_k(n-1)\} - cos\{\theta_k(n)\}\, sin\{\theta_k(n-1)\}$$

$$= b_k(n)\, a_k(n-1) - a_k\,(n) b_k(n-1) \tag{B.12}$$

likewise

$$cos\{\theta_k(n) - \theta_k(n-1)\} = cos\{\theta_k(n)\}\, cos\{\theta_k(n-1)\} + sin\{\theta_k(n)\}\, sin\{\theta_k(n-1)\}$$

$$= a_k(n)\, a_k(n-1) + b_k(n)\, b_k(n-1) \qquad \text{(B.13)}$$

$$d\theta_k(n) = arctan[(sin\{\theta_k(n) - \theta_k(n-1)\}/(cos\{\theta_k(n) - \theta_k(n-1)\}] \qquad \text{(B.14)}$$

with the initial conditions $\theta_k(0) = 0$, $a_k(0) = 1$, $b_k(0) = 0$.

The operations above are graphically depicted in Fig.[B.2b]

Thus with the above equations it is possible to implement the Phase Vocoder in software in which the amplitude and frequency changes with time can be obtained. The phase derivative allows a component's frequency at any time to be measured and allows mapping of time varying spectral components at all frequencies whereas the band-pass filters must be restricted to discrete frequencies dictated by the inverse of the length of the partitioned data sequence discussed above [93]. In practice however, use of the phase derivative to determine component frequency could only be achieved for very large fault levels.

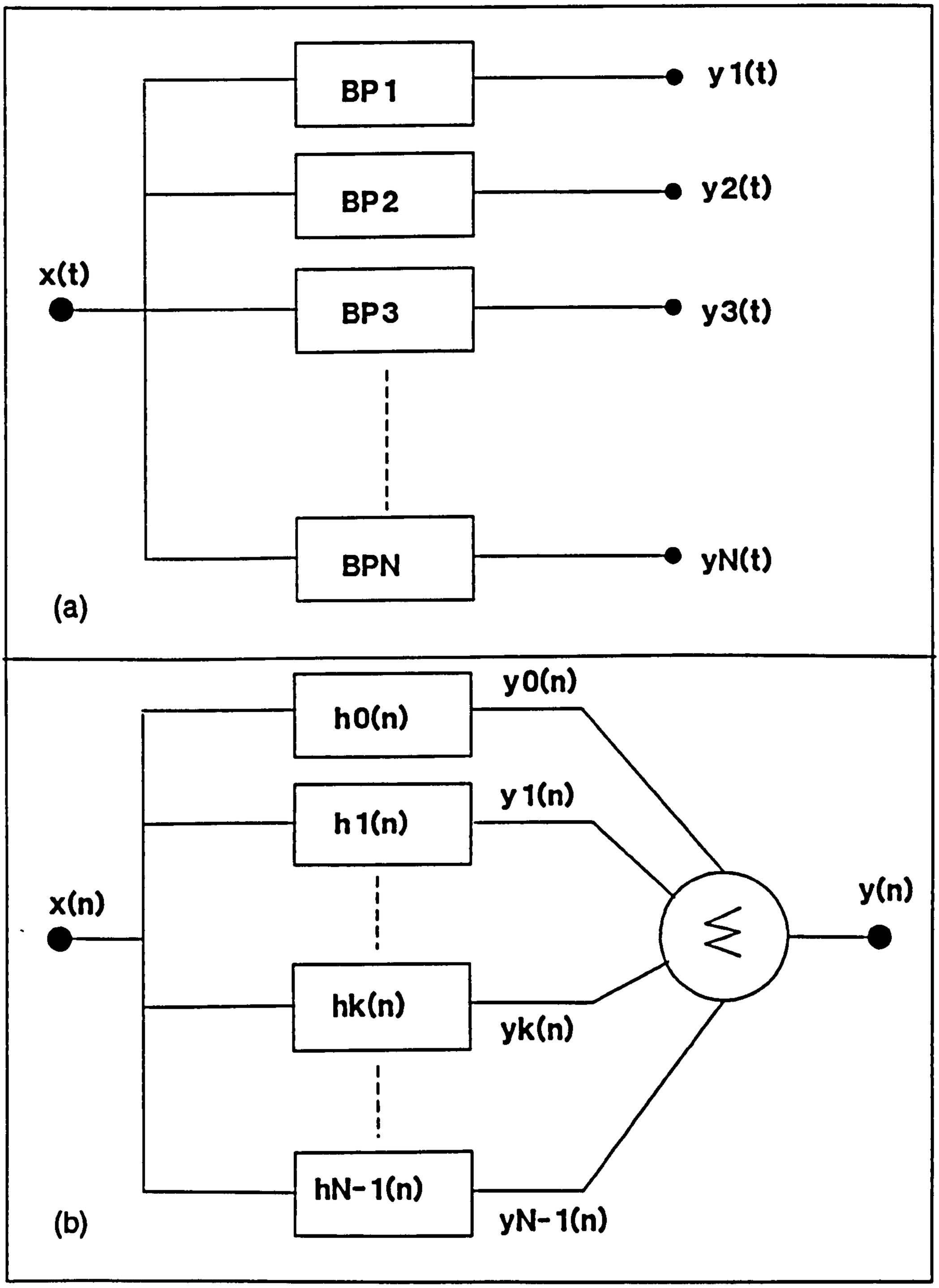

Figure B.1: a) Phase vocoder represented as a bank of bandpass filters. b) Structure of proto-type low pass filters.

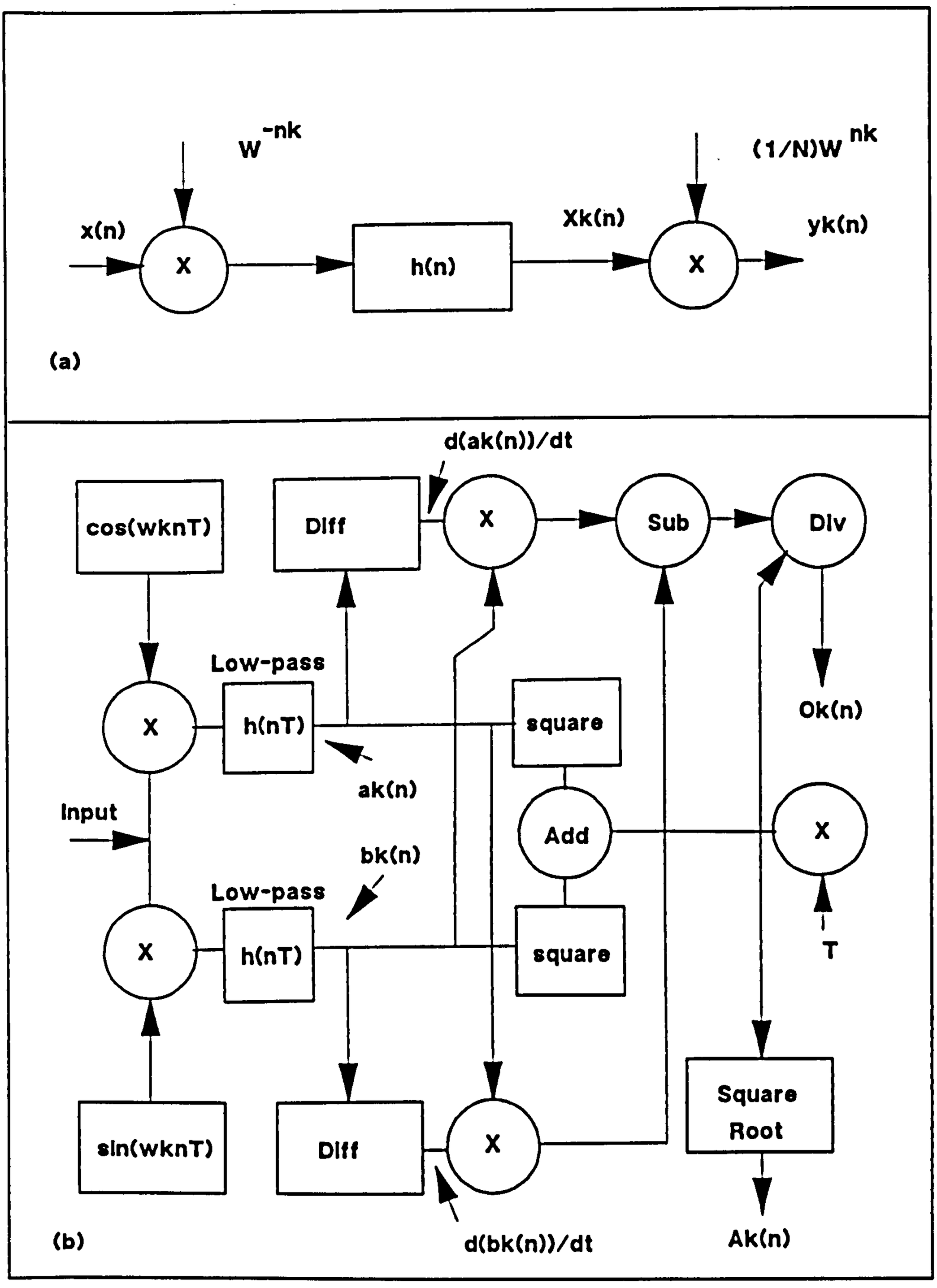

Figure B.2: a) A single channel of the filter bank. b) Diagrammatic representation of phase vocoder operation.

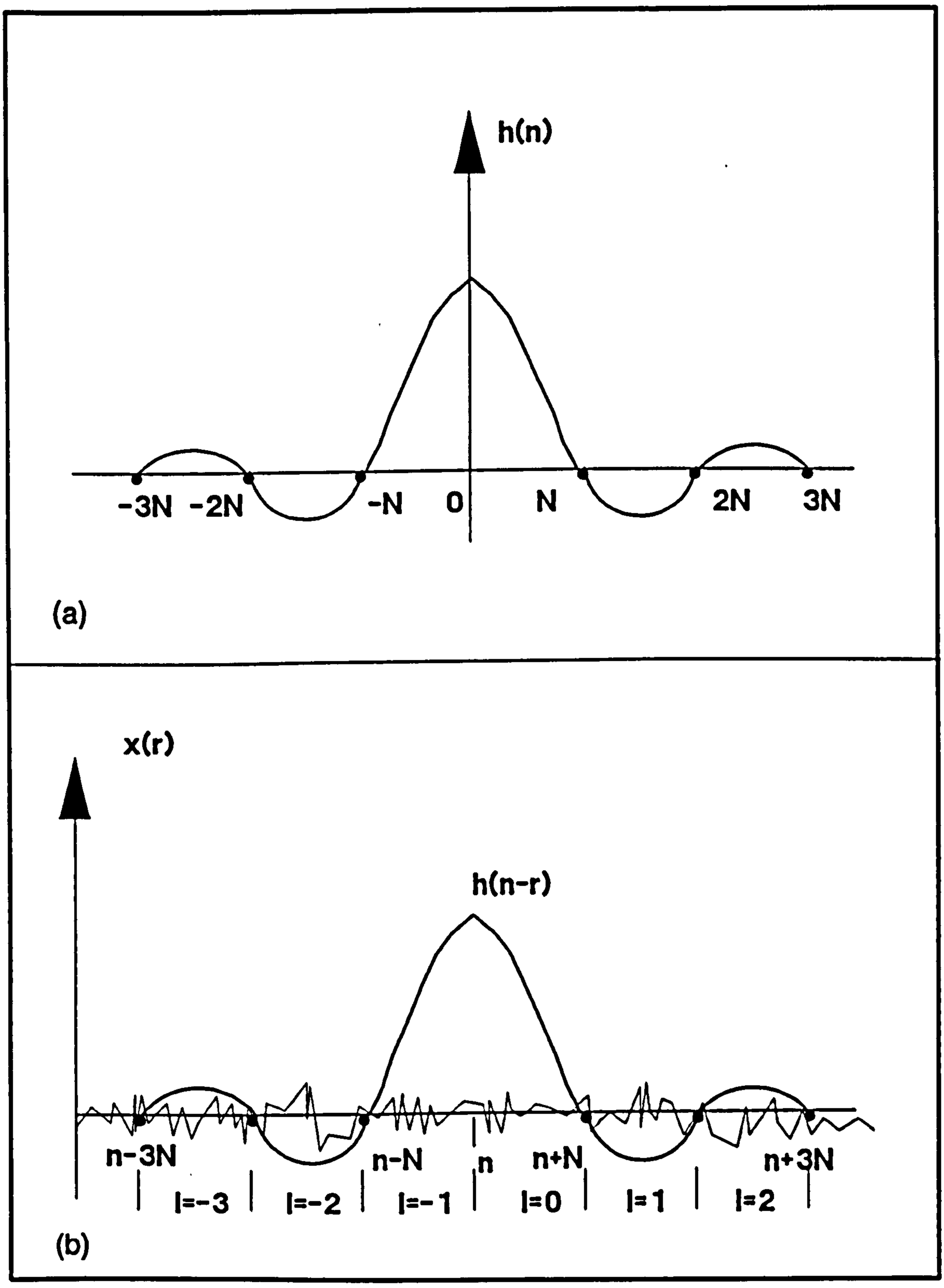

Figure B.3: a) Window type filter operator. b) Partitioned sub-sequences of numerically applied vocoder.

Appendix C

FIR Filter Design by the Windowing Method

C.1 Introduction

There are essentially three well known classes of design techniques for linear phase Finite Impulse Response (FIR) filters, namely, the Window Method, the Frequency Sampling and Optimal filter design methods [82,94]. Since there are many factors that determine which class of filters will be used in a particular application, it is difficult to recommend one class of design to the exclusion of all others.

One advantage of FIR filters is that they can be designed with exactly linear phase so that frequency dispersion will not corrupt the data. This finds particular application in areas where the signals are non-stationary, such as Speech Processing and in this case the transitory line current waveforms of an induction motor. Both the Phase Vocoder and the final signal processing method make use of FIR filters designed by the Window method.

C.2 Theoretical Development

The frequency response of any digital filter ($He^{j\omega}$) is periodic in frequency and as such can be expanded in a Fourier Series. The resultant series is of the form :-

$$H(e^{j\omega}) = \sum_{n=-\infty}^{\infty} h(n)e^{-j\omega n} \tag{C.1}$$

where

$$h(n) = \frac{1}{2\pi}\int_0^{2\pi} H(e^{j\omega n})\, e^{j\omega n}\, d\omega$$

The co-efficients of the Fourier series are identical to the impulse response of the filter.

There are two difficulties with the representation of equation C.1 for designing FIR filters. Firstly the filter impulse response is infinite in duration and secondly it is unrealizable because the impulse response begins at $-\infty$; i.e. no finite amount of delay can make the impulse response realizable.

One possible way of obtaining an FIR filter that approximates $H(e^{j\omega})$ would be to truncate the infinite Fourier series at $n = \mp M$. Direct truncation of the series leads to the well known Gibb's phenomenon, which manifests itself as an overshoot or ripple in the desired frequency response.

A more successful way of obtaining an FIR filter is to use a finite weighting sequence $w(n)$, called a window, to modify the Fourier co-efficients $h(n)$ in equation C.1 to control the convergence of the Fourier series.

Thus the design of a realizable low-pass filter requires that the impulse response of the proto-type low-pass filter given by :-

$$h1(n) = \frac{sin(Bn\pi)}{n\pi} \tag{C.2}$$

where B is the normalised bandwidth
should be multiplied by a weighting function selected from Tables [C.1],[C.2] to give the desired result. The application of the window will however change the desired filter characteristics slightly and is often referred to as blurring of the frequency response.

If a filter other than low-pass is required, then this realizable low-pass filter must be appropriately transformed [82]. For the particular case of a band-pass

filter this involves multiplying the window-ed low-pass impulse response by a factor of :-

$$2cos(2\pi F_c n)$$

where F_c is the desired normalised centre frequency.

The final band-pass filter's impulse response is thus given by :-

$$h3(n) = \frac{sin(Bn\pi)}{n\pi}\,(0.5 + 0.5\,cos(\frac{2n\pi}{N})\,)2\,cos(2n\pi F_c)$$

where

$$n = \frac{-N}{2} \cdots -1, 0, 1 \cdots \frac{+N}{2}$$

C.3 Filter Application

To implement the FIR filter it is necessary to convolve the impulse response $h3(n)$ of $N1$ points with the data $x(n)$ of $N2$ points. This can easily be achieved by direct convolution, given by :-

$$y(n) = \sum_{m=o}^{n} h3(n)\,x(n-m)$$

where

$$0 \leq n \leq N1 + N2 - 1$$

Though simple to program, this direct convolution (also known as slow convolution), requires that $(N1 + N2)^2$ multiplications be performed.

This convolution can however be implemented much more efficiently by use of an FFT algorithm. Firstly both the filter $h3(n)$ and the data sequence $x(n)$ must be of the same length. This eliminates the wrap round difficulties inherent in circular convolution and results in a linear convolution as obtained by direct convolution. To achieve this result, both the filter and data sequences are appended with the appropriate number of zero-valued samples to make them both $(N1 + N2 - 1)$ point sequences.

The next step is to take the FFT of both the data and filter sequences. The two transformed results are then multiplied. This multiplication is in fact filtering

in the frequency domain. Having applied the filtering, it only remains to transform the filtered data back into the time domain by use of the Inverse Fourier Transform (IFT).

The implementation of an FIR Window filter by convolution can thus be easily applied with high computational efficiency by use of an FFT algorithm.

C.4 Processing Sequence

From experimental data it has been observed that the LSB component, as it passes through 21Hz in the latter part of the starting transient, has both a large amplitude and a relatively low variance. In Fig.[C.1] is shown the application of fast convolution to a line current waveform and the impulse response of a bandpass filter with a centre frequency of 21Hz.

The resulting filtered line current waveform is of course a 21Hz sinewave, since the BP filter's centre frequency is at 21Hz. However this waveform is not simply a 21Hz sinewave since it can be seen to be heavily amplitude modulated. It is the amplitude modulation that contains the information that is required. To recover the modulating signal the standard AM recovery techniques are applied, namely, rectification and subsequent low-pass filtering. The complete processing method is shown in Fig.[C.2] where it can be seen that the final waveform contains two peaks. The first peak is due to the abrupt discontinuity when the machine is switched on, the second (if present) is the component that indicates the fault level. In this particular example the machine had a single broken bar and experienced a no-load start. For larger numbers of broken bars this second peak will increase and can thus be used for diagnosis. In the case of full-load starts, three peaks are observed since the LSB is of sufficient amplitude to be observed at 21Hz in the pre-half speed region.

C.5 Implementation

Though the original FIR signal processing software was implemented on a mainframe computer, the final version has been written for an IBM compatible PC.

The purchase of a maths co-processor to speed up floating point operations has reduced the diagnosis time to 49 seconds. Having obtained data from the laboratory machine with various fault conditions it was thus possible to diagnose the condition of the machine by analysing the line current waveform during the starting period.

Weighting Function	Mainlobe Width	StopBand Attenuation
Rectangular	2/N	21dB
Bartlett	4/N	25
Hanning	4/N	44
Hamming	4/N	53
Blackman	6/N	74

Table C.1: FIR Window filter Bandwidth and Attenuation. N :- number of filter co-efficients.

Name	Function
Rectangular	1
Bartlett	1-2 | n |/N
Hanning	$0.5 + 0.5cos(2\pi n/N)$
Hamming	$0.54 + 0.46cos(2\pi n/N)$
Blackman	$0.42 + 0.5cos(2\pi n/N) + 0.08cos(4\pi n/N)$

Table C.2: FIR filter design table, indicating some common Window functions.

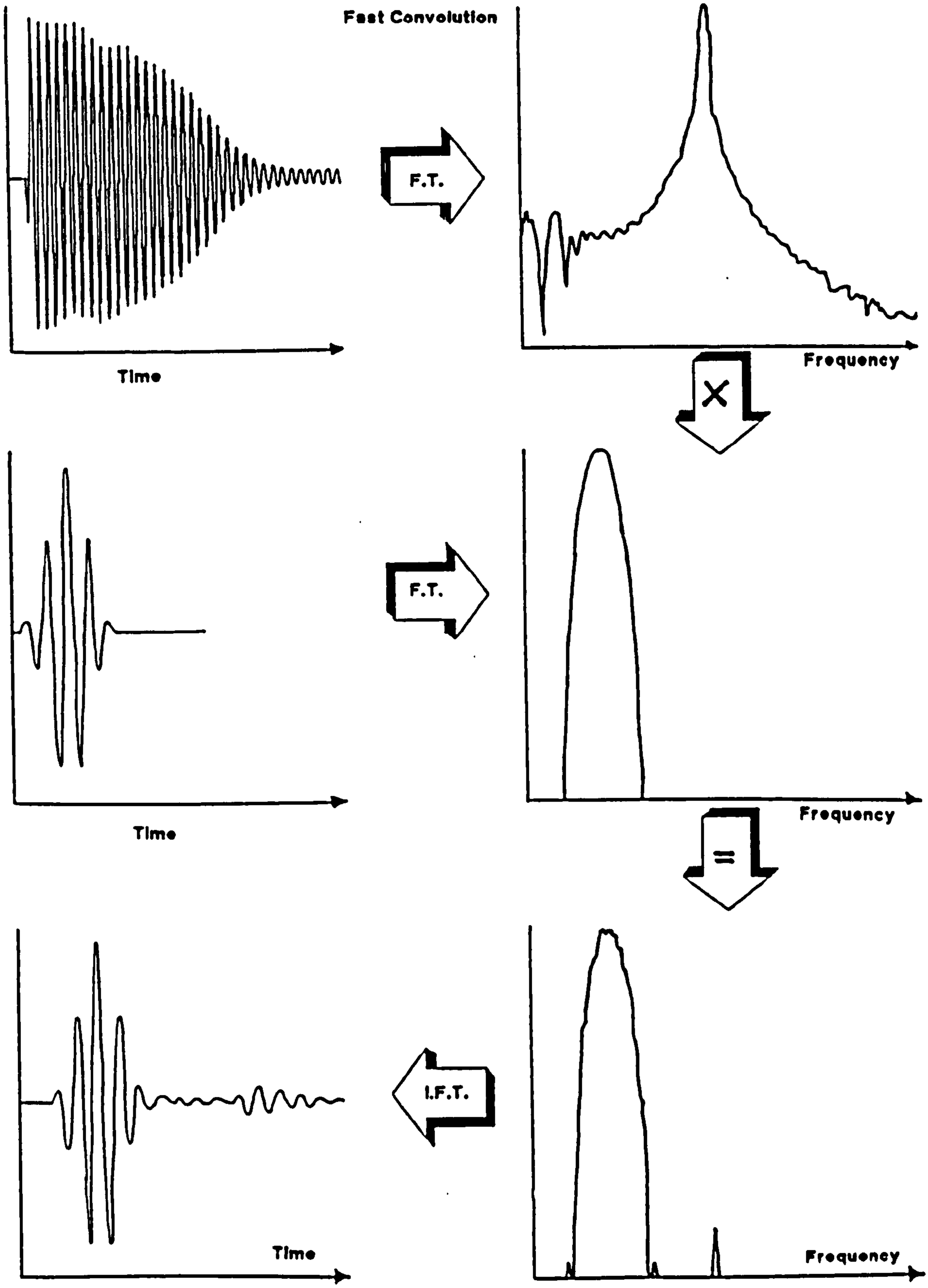

Figure C.1: Application of 21Hz bandpass filter by convolution to the line current waveform.

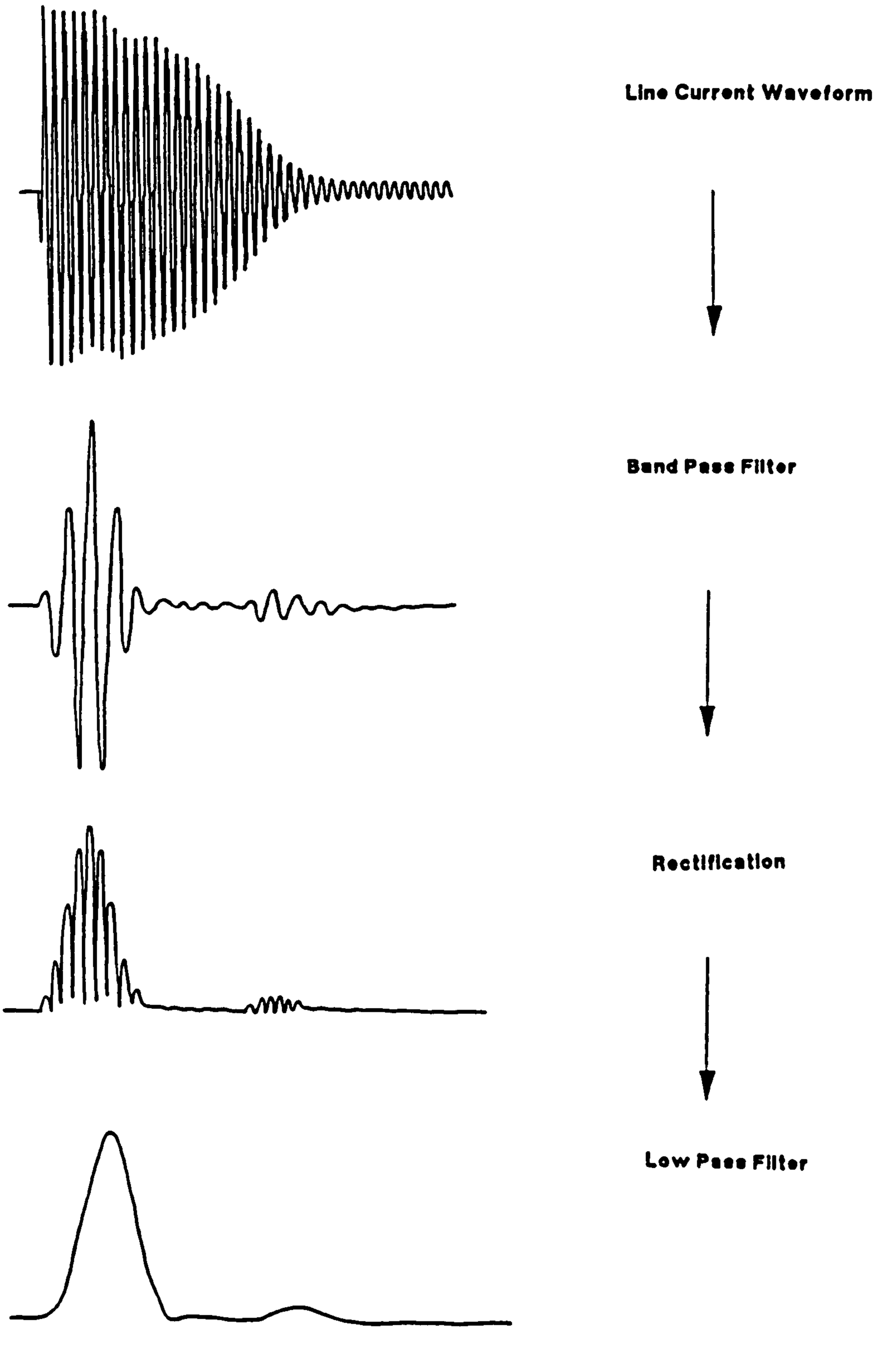

Figure C.2: Final FIR processing showing bandpass filtering, rectification and lowpass filtering.

Appendix D

Published Papers

ICEM 89

UPEC 89

UPEC 90

FAULT DETECTION IN INDUCTION MOTORS AS A RESULT OF TRANSIENT ANALYSIS

S Elder, J F Watson and W T Thomson

Robert Gordon's Institute of Technology, Aberdeen

INTRODUCTION

A variety of faults can occur within 3 phase Induction Motors during normal operation. Several, such as cage rotor malfunctions, rotor-stator eccentricity or inter-turn insulation breakdown can result in a potentially catastrophic failure of the machine if they progress undetected. [1,2,3,4]

Over the last few years a variety of Condition Monitoring techniques has been developed which monitor the health of the motor and can be used to detect the onset of such fault conditions. These techniques are most useful if they can be implemented on-line and planned maintenance can then prevent plant failures.

A variety of machine parameters have been monitored; vibration [2], leakage flux [5] and line current [3] being the most prominent. Line current is probably the most useful of the three since in an industrial environment it is the most accessible parameter and it can be measured using standard techniques in a position remote from the motor under investigation. The monitoring of line current forms the basis of the work presented in this paper.

The vast majority of the work to date has been concerned with monitoring the machine under steady state conditions and many of the existing techniques require that the motor in question be under load before reliable diagnoses can be carried out.

Throughout the starting transient period however, (particularly if started Direct On Line), large currents flow in the motor, even under no-load conditions. During this short period the machine is under conditions of severe electrical and mechanical stress and the purpose of the work described in this paper is to determine whether, under these conditions, machine faults such as high resistance or broken rotor bars could be detected at a much earlier stage in their development. It is also hoped that any inherent stator-rotor eccentricity can also be detected during the starting transient since any unbalanced magnetic pull (U.M.P.) is a maximum at starting.

Furthermore, there are certain situations where it is either impractical or undesirable to test a machine under loaded conditions and under these circumstarces it would be beneficial to have a condition monitoring technique which could be applied to the starting transient.

Approach Adopted

The research has been conducted in two parallel paths. One path involves the capture of the line current waveforms from a purpose-built laboratory test rig which allows implementation of a variety of known fault conditions. Several such condition monioring test rigs are available within the Machine Condition Monitoring Centre at RGIT. These are essentially 11 kW industrial motors within which specific faults such as static and dynamic eccentricity and/or a variety of rotor malfunctions can be introduced. Initial work was carried out on a wound rotor machine where specific phase imbalances could be introduced by means of external resistors.

The signal capture and analysis system is shown in Fig. 1. A Hall effect current sensor monitors the current in one phase. The voltage output from the sensor is fed to a 300 KHz digital oscilloscope which is interfaced to a standard personal computer. The p.c. itself is interfaced to an HP 9840 mainframe computer. In this way real data can be stored on the mainframe and be accessible to the processing programs. At present the mainframe is essential for the signal processing and analysis although it is anticipated that this will not be necessary in the future.

The current waveforms have been examined in the time domain and processed by both spectral and cepstral analysis on industry standard analysers. The signal processing has been extended to the use of Speech Processing algorithms which have proved particularly useful and it is in this area that software development for fault recognition is currently taking place.

The other parallel path is in Induction Motor simulation on a mainframe computer. This model of the induction motor produces waveforms (line current etc) which can be processed as with the real motor. A reasonably accurate model is extremely useful in understanding the very complex real machine transients. It can be used to determine the influence of individual parameter variations on the resulting line current waveforms, but perhaps more importantly it has been used to indicate particular aspects of the transient waveform of the real machine which merit further detailed investigation.

Four waveforms are depicted in Fig. 2 which show the effect that a 50% imbalance in the rotor resistance of one phase has on the transient current patterns. Figs. 2a) and b) are produced from the test rig and 2c) and d) from the computer simulation.

The simulation model used in this case is a 3 phase generalised model although the effects of saturation have not been included. Nontheless, close examination of the waveforms reveals that differences do exist in the transient patterns obtained with and without rotor imbalance, although it is obviously difficult to analyse or quantify these effects in the time domain as shown.

Analysis Techniques and Results

There are several reasons why the analysis of transient waveforms is more complex than their steady state counterparts. Those most relevant to this investigation are outlined below.

A transient waveform as shown in Fig. 2 is not statistically stationary as is assumed to be the case in the analysis of steady state waveforms.

In steady state analysis the variance of a line current waveform is minimised by averaging a large number of blocks (frames) of data, the listening time is extended until an acceptable number of frames have been processed. In transient analysis extending the listening will only increase the noise since the transient will usually be of fixed length. To minimise the variance of transient waveforms a number of transients must be recorded and their spectra averaged. [6]

The resolution of a Fourier Transform in the frequency domain is inversely proportional to the record length. In steady state analysis the record length can theoretically be infinite but is practically limited to the memory size of the analyser, nevertheless, it is still possible to resolve frequencies to milli-Hertz. In transient analysis the record length is fixed and in the case of the unloaded test rig will be in the order of 250 ms giving a theoretical frequency resolution of 4 Hz.

It has been shown that sidebands associated with rotor bar faults in steady state conditions are also present during the starting transient, but of course they are changing in frequency with time. [4] At a normal operating slip(s) of say 3% sidebands are situated at + 2sf and - 2sf around the 50 Hz component namely at 47 Hz and 53 Hz. However at the beginning of the starting transient the rotor is stationary and hence the slip is unity. This places these two components at 150 Hz and - 50 Hz respectively. The -50 Hz component is a phase shifted 50 Hz component w.r.t. the fundamental 50 Hz wave. As the rotor accelerates these components change in amplitude and frequency and at half speed (i.e. slip = 0.5) the lower component is at 0 Hz and the upper at 100 Hz. This sequence is depicted in Fig. 3.

Performing a spectral analysis on both balanced and unbalanced rotor starting currents gives rise to the spectral amplitudes shown in Fig. 4. It can be clearly seen that a substantial change takes place in the region from 10 to 45 Hz and it is possible to quantify gross rotor imbalances of 50% or more with this data. However this form of spectral analysis produces a summation of all events within the transient period so that no indication is given as to when these various spectral components contributed to the total spectrum.

These transient waveforms have a changing spectrum with time and it is in this respect that they are similar to human speech. It seemed reasonable that methods used to extract the frequency and amplitude content of speech would prove useful in extracting data from a line current transient waveform.

The Phase Vocoder is a technique whereby signals with time-varying spectra can be analysed. It has been in use for many years in Speech Processing and it can be represented as a bank of band-pass filters. [7] As components change their frequency they will pass through different filters and their amplitude can be measured. These bandpass filters must be phase invariant so that all frequencies are delayed by equal amounts. This technique can be implemented in software where it can be readily altered if required. [8] The output from a phase vocoder is referred to as a Spectrogram and is a plot of Frequency versus time versus Amplitude. This three dimensional representation allows filtering in two dimensions to be performed so that the amplitude of a frequency component at a particular time may be evaluated.

Figs. 5 and 6 show plots of the output from the first thirteen channels of the phase vocoder. Fig. 5 relates to the test rig in a nominally balanced condition whereas Fig. 6 represents a rotor resistance imbalance of 50% The amplitudes of the thirteen bandpass filters can be seen to change with time, and clear and significant differences can be observed between the two cases shown. Using this technique it is possible to detect rotor imbalances of 5% from a single transient whereas previously imbalances of only 25-30% could be detected from the average of ten or more spectra.

Though impractical to display in this paper, the output of the phase vocoder usually consists of sixty four channels with a channel separation of approximately 8 Hz. The spectrograms have therefore yielded a mass of data which is currently being investigated to extract features indicative of fault conditions. Both real and simulated data have revealed similar trends and patterns.

In Figs. 5 and 6 the two sidebands associated with rotor imbalance can be clearly observed to be changing with time as theory predicts. The amplitude of these components in the unbalanced rotor case is significantly larger. It is in this area that current work is progressing to quantify the severity of the fault and the whole spectrogram is being examined to extract other features representative of different fault conditions.

Computer Simulation

The original simulation was performed using the equivalent two axis D-Q model because of its simpler set of resultant equations. [9] The two phase currents i_D and i_Q of the stator were then transformed back to the three line currents i_a, i_b and i_c.

Saturation was approximated by varying the leakage inductance in both stator and rotor from a saturation characteristic curve derived from tests on the machine. [10] Though simple, this addition to the basic model improved the resulting simulated line current spectra and indicated that saturation was the

cause of certain characteristics in the spectra of the real machine. In this way it was possible to change parameters associated with the machine and observe the effect in the simulation and to related this to the real machine.

The limitations of the two axis D-Q model are that a balanced magnetic circuit is necessary and that at least one winding must be completely balanced. [11] In the stationary reference frame imbalance in the rotor phase resistances results in sinusoidally varying resistances in the machine equations. [12]

A three phase model has now been developed as a first step to a more accurate representation of an induction motor. [13] Though more complicated in implementation it will accommodate localised saturation and imbalance in both the stator and rotor windings if required. The feasibility of extending this model to represent individual rotor bars is under investigation.

As with the D-Q model the non-linear differential equations produced must be numerically solved using an iterative technique unless gross assumptions such as constant speed are introduced. A Runge-Kutta iterative technique with error control is used in the simulation software.

Machine parameters may be obtained from standard tests. [14] Harmonics in the supply voltage, saturation, skin effect and thermal effects will alter these values and are to be investigated further. Rotor position and switching angle both effect the transient waveform and their influence must be taken into account.

The question arises as to how much effort should be afforded towards exact simulation (if at all possible) since the remit of this research is to determine faults and to quantify them. Pragmatically it is anticipated that the final results will show general trends indicative of faults within classes of machines rather than exact solutions.

Conclusions

A technique is being developed which will allow the detection and identification of specific faults within 3 phase Induction motors during the starting transient.

Work to date has concentrated on a wound rotor laboratory machine and the analysis techniques developed allow 5% imbalances in the rotor phase resistances to be detected. Current work is progressing on Squirrel Cage and industrial machines with a view to extending the fault recognition algorithms.

The transient process is very complex and it would be extremely difficult to analytically predict the occurrence of specific frequency components and their variation under known fault conditions. The thrust of the work to date has concentrated on the identification of patterns and trends which are representative of specific faults and to eventually establish a knowledge base on which diagnoses can be made. It is in this respect that the computer simulation of the machine has proved most useful.

At present a very detailed and complex analysis is used to detect faults requiring the use of a mainframe computer. It is anticipated that once sufficient test data has been obtained this analysis will be dramatically reduced, allowing a stand alone instrument to be designed.

References

[1] Hargis, C, Gaydon, B G and Kamash, K, Proc. EMDA, Conf., 1982, pp 216-220.

[2] Leonard, R, MPhil Thesis, CNAA 1985.

[3] Cameron, J, Thomson, W T and Dow, A B, Proc. IEE, Vol 133, Pt B, No 3, May 1986.

[4] Williamson, S and Smith, A, Proc IEE, Vol 129, Pt B, No 3, May 1982.

[5] Penman, J, Hadwick, J G, Barker, B, 3rd Int. Conf. Elec. Mach., Brussels, 1978.

[6] Random Data: Analysis and Measurement Procedure, Bendat, J and Piersol, A, 1971, Wiley & Sons.

[7] Flanagan, L and Golden, R M, Bell Sys. Tech. J, Vol, 45, pp 1493-1509, November 1966.

[8] Schafer, R W and Rabiner, L R, IEEE Trans. AU 21, June 1973, pp 165-174.

[9] Slater, R D, PhD Thesis, University of Strathclyde, 1966.

[10] Lipo, T A and Consoli, A, IEEE Trans. on Ind. App., 1981, pp 527-35.

[11] Matrix Analysis of Electrical Machinery, Hancock, N N, MacMillan, 1974.

[12] Krause and Thomas, C, IEEE Trans. PAS 84, November 1965, pp 1038-1053.

[13] Asish De Sarkar, K and Berg, J, IEEE Trans. PAS 89, No 6, July/August 1970, pp 1031-1037.

[14] The Unified theory of Electrical Machines, Jones, Charles V, Butterworth, 1967.

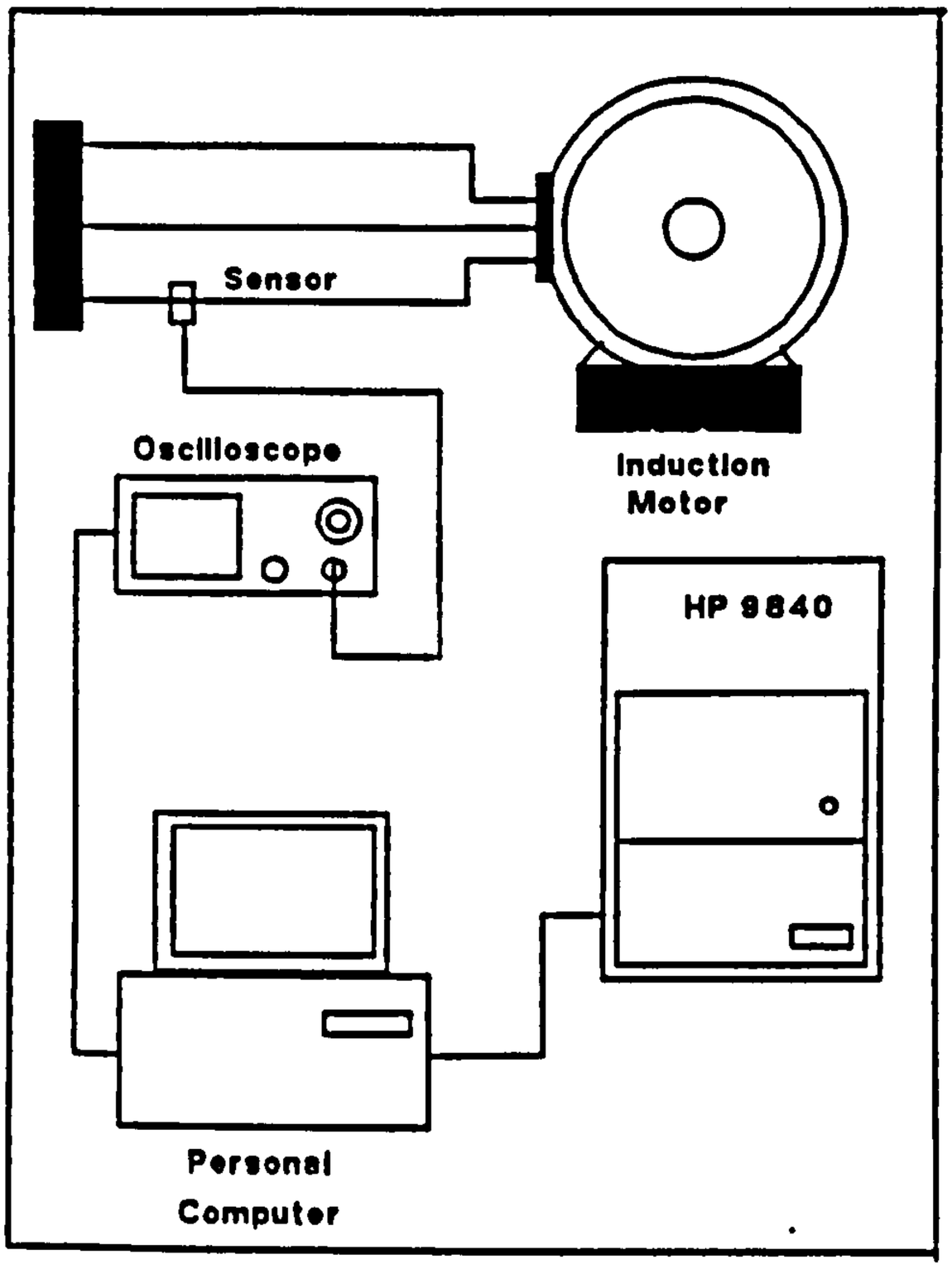

Fig. 1 System Layout

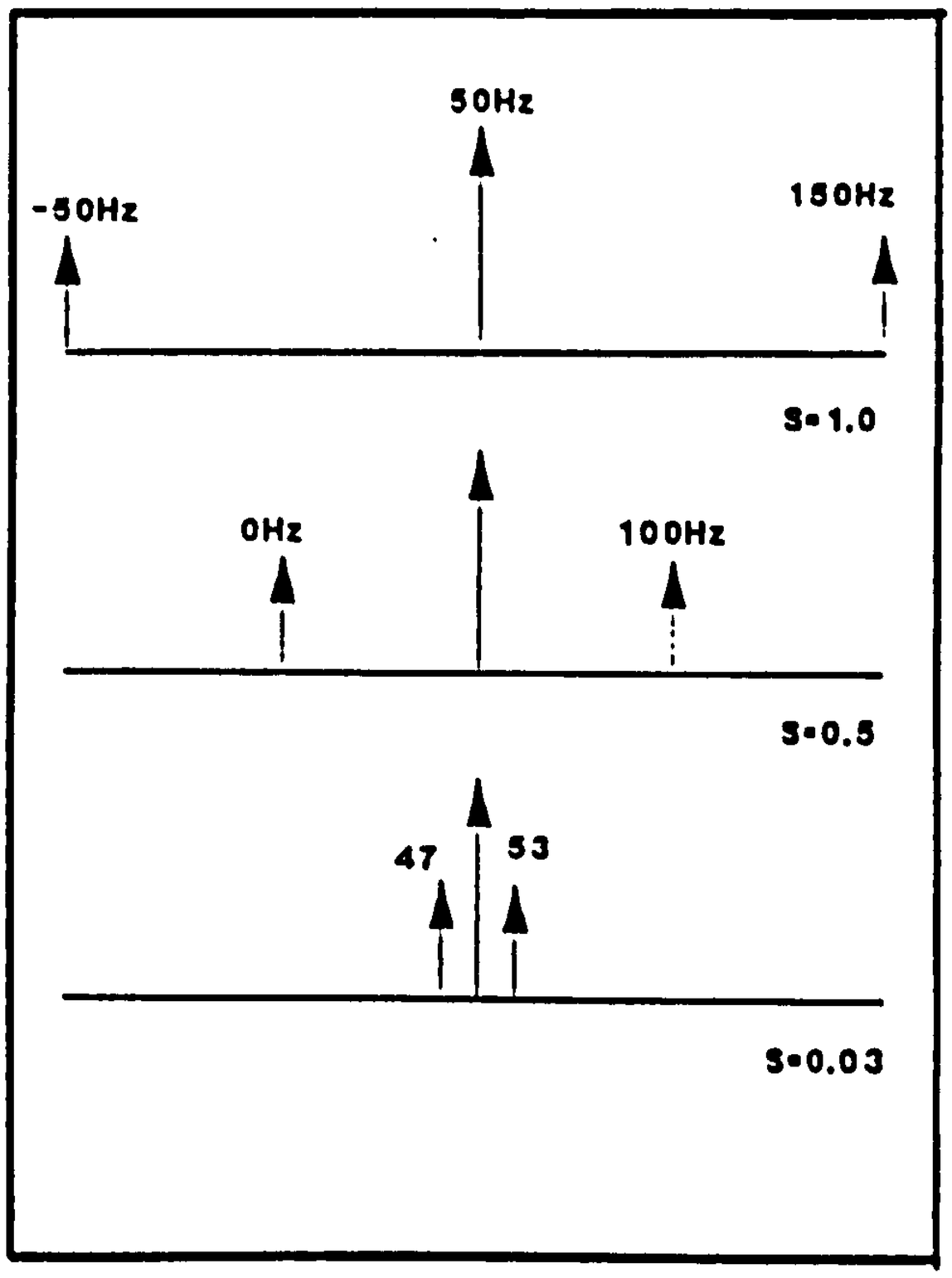

Fig. 3 Sideband frequency variation with slip

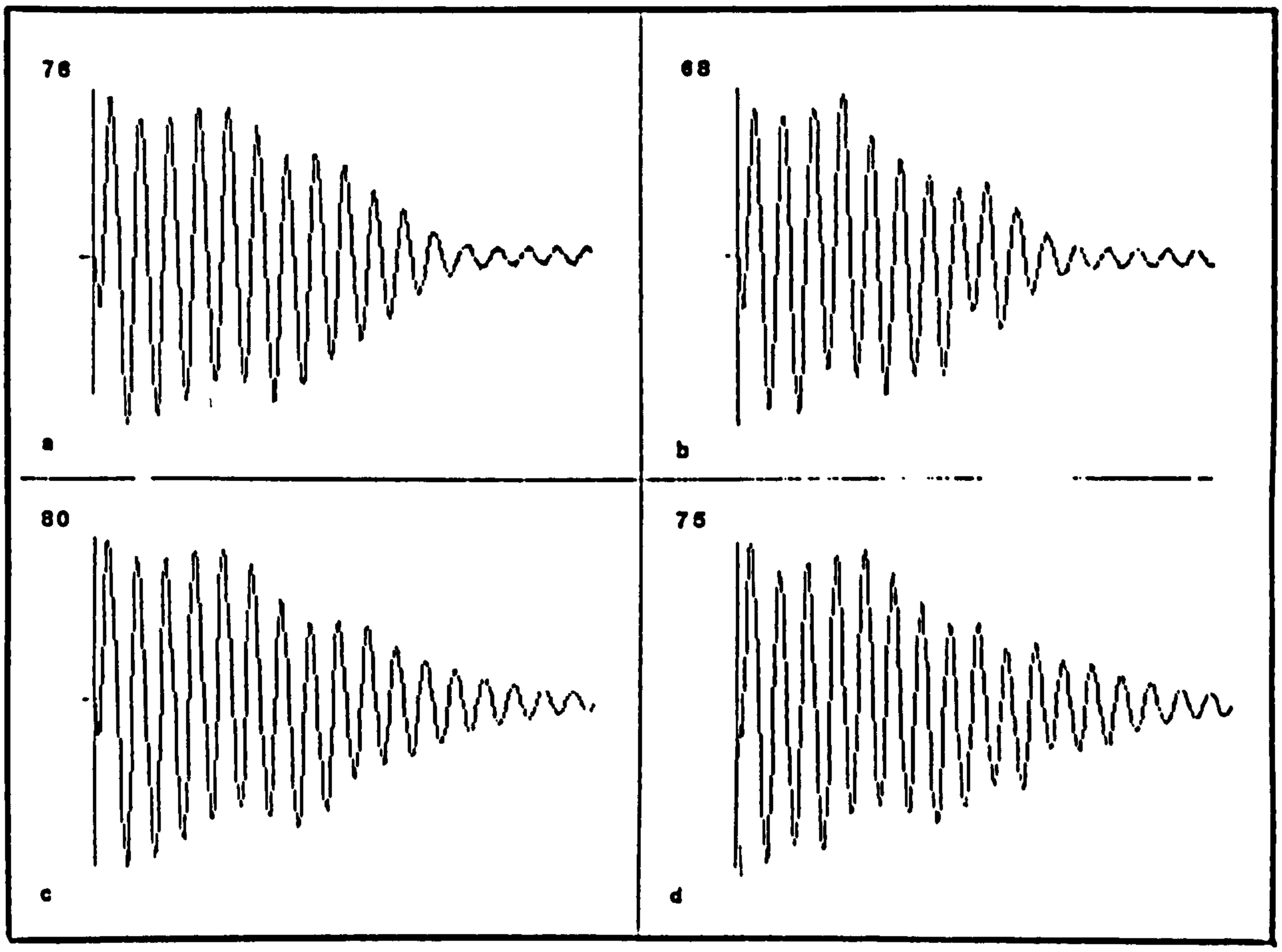

Fig. 2 Typical Starting Transients
a) Real machine - balanced
b) Real machine - unbalanced
c) Simulation - balanced
d) Simulation - unbalanced

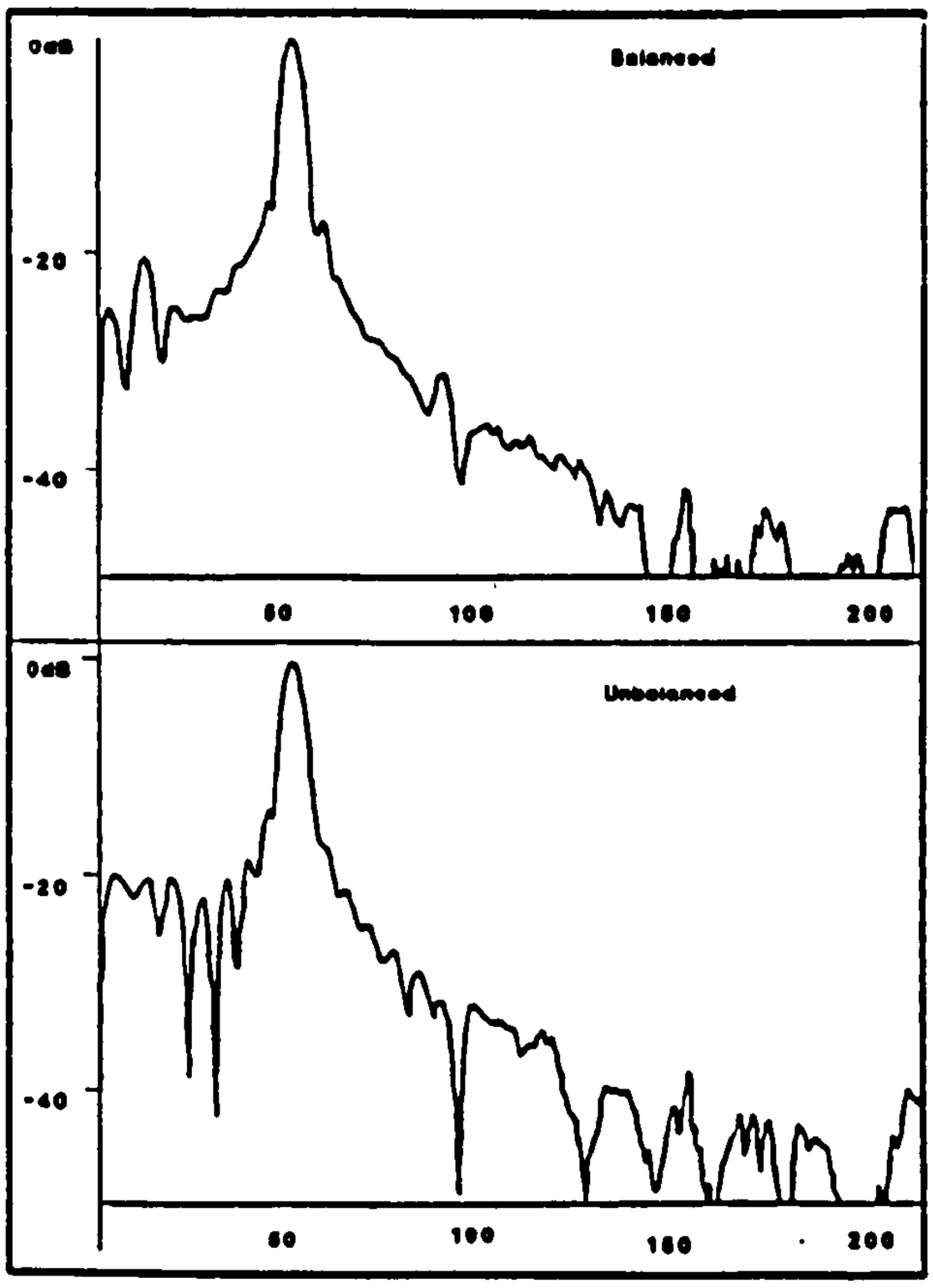

Fig. 4 Typical Spectra of Line current during starting transient

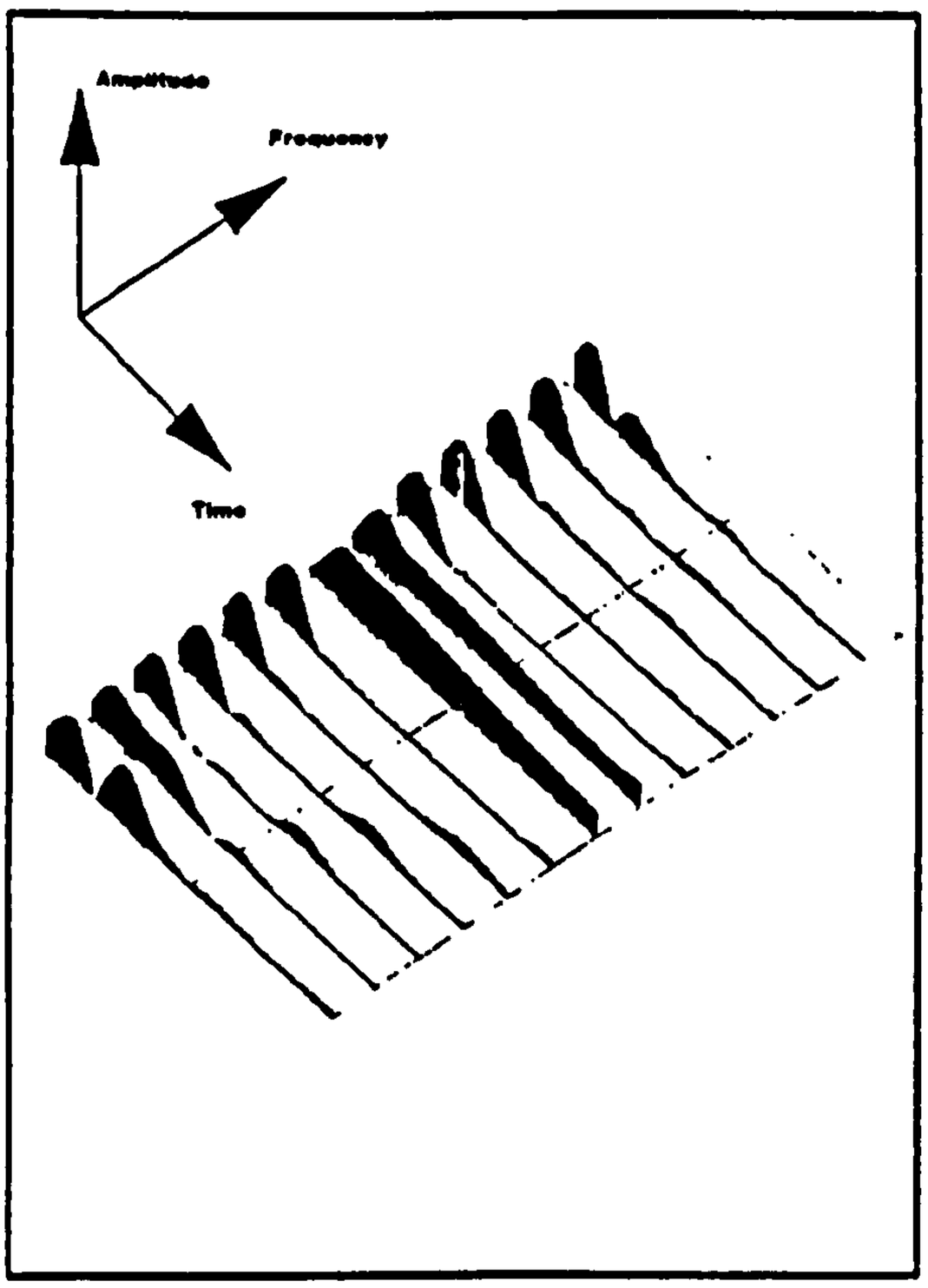

Fig. 5 Phase Vocoder output - Real machine - nominally balanced

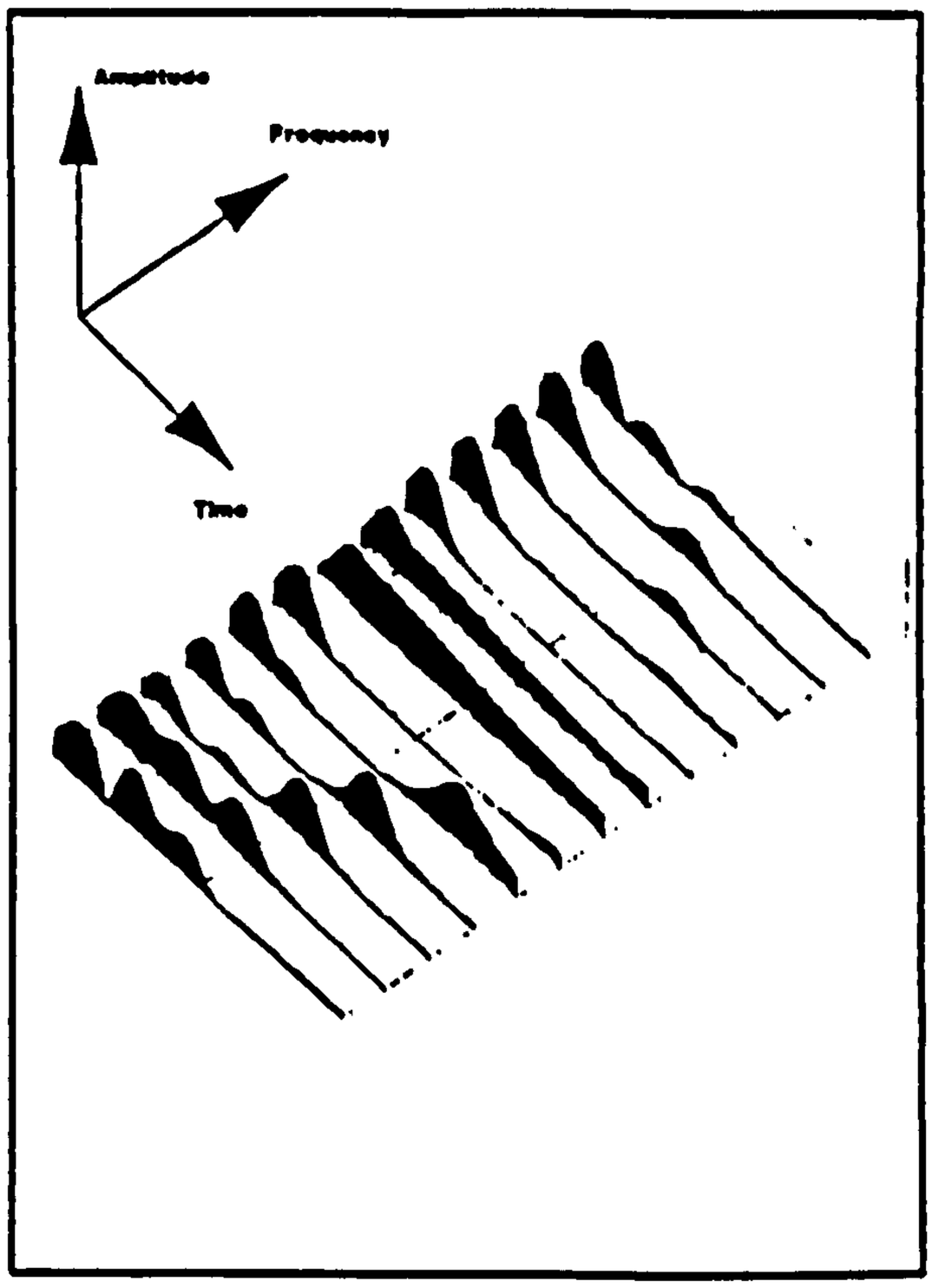

Fig. 6 Phase Vocoder output - Real machine - 50% Rotor Resistance imbalance

THE MONITORING AND ANALYSIS OF TRANSIENT CURRENTS FOR THE PURPOSE OF FAULT DETECTION IN INDUCTION MOTORS

S Elder, J F Watson and W T Thomson

Robert Gordon's Institute of Technology, Aberdeen

INTRODUCTION

A variety of possible faults can occur within a 3 phase Induction Motor during normal operation. Several such as broken rotor bars or rotor-stator eccentricity can result in a potentially catastrophic failure of the machine if they progress undetected. [1,2,3,4] Consequently, a number of Condition Monitoring techniques have been developed over the last few years, with a view to detecting these faults at an early stage in their development. Planned maintenance can then prevent unexpected plant failures.

A variety of machine parameters have been monitored; vibration [2], leakage flux [5] and line current [3] being the most prominent. Line current is probably the most useful of the three since in an industrial environment it is the most accessible parameter and it can be measured using standard techniques in a position remote from the motor under investigation. The monitoring of line current forms the basis of the work presented in this paper.

The vast majority of the work to date has been concerned with monitoring the machine under steady state conditions and many of the existing techniques require that the motor in question be under load before reliable diagnoses can be carried out.

Throughout the starting transient period however, (particularly if started Direct On Line), large currents flow in the motor, even under no-load conditions. During this short period the machine is under conditions of severe electrical and mechanical stress and the purpose of the work described in this paper is to determine whether, under these conditions, machine faults such as high resistance or broken rotor bars could be detected at a much earlier stage in their development. It is also hoped that any inherent stator-rotor eccentricity can also be detected during the starting transient since any unbalanced magnetic pull (U.M.P.) is a maximum at starting.

There are also certain situations where it is either impractical or undesirable to test a machine under loaded conditions. Under these circumstances it would be beneficial to have a condition monitoring technique which could be applied to the starting transient.

Developed Technique

This work has been developed along two parallel paths. One path involves the capture of the line current waveforms from a purpose-built laboratory test rig which allows implementation of a variety of known fault conditions. Several such condition monioring test rigs are available within the Machine Condition Monitoring Centre at RGIT. These are essentially 11 kW industrial motors within which specific faults such as static and dynamic eccentricity and/or a variety of rotor malfunctions can be introduced. Initial work was carried out on a wound rotor machine where specific phase imbalances could be introduced by means of external resistors.

A Hall effect current sensor monitors the current in one phase. The voltage output from the sensor is fed to a 300 KHz digital oscilloscope which is interfaced to a standard personal computer. The p.c. itself is interfaced to an HP 9840 mainframe computer. In this way real data can be stored on the mainframe and be accessible to the processing programs. At present the mainframe is essential for the signal processing and analysis although it is anticipated that this will not be necessary in the future.

The current waveforms have been examined in the time domain and processed by both spectral and cepstral analysis on industry standard analysers. The signal processing has been extended to the use of Speech Processing algorithms which have proved particularly useful and it is in this area that software development for fault recognition is currently taking place.

The other parallel path is in Induction Motor simulation on a mainframe computer. This model of the induction motor produces waveforms (line current etc) which can be processed as with the real motor. A reasonably accurate model is extremely useful in understanding the very complex real machine transients. It can be used to determine the influence of individual parameter variations on the resulting line current waveforms, but perhaps more importantly it has been used to indicate particular aspects of the transient waveform of the real machine which merit further detailed investigation.

Typical starting transient current waveforms obtained from the laboratory test machine are shown in Fig. 1. Fig. 1 a) represents the machine in a nominally balanced condition whereas in Fig. 1 b) a 50% imbalance in the resistance of one rotor phase has been introduced. Close examination does reveal that differences between the two waveforms do exist although it is obviously difficult to analyse or quantify these effects in the straightforward time domain as shown.

Analysis Techniques and Results

There are several reasons why the analysis of transient waveforms is more complex than their steady state counterparts. Those most relevant to this investigation are outlined below.

A transient waveform as shown in Fig. 1 is not statistically stationary as is assumed to

be the case in the analysis of steady state waveforms.

In steady state analysis the variance of a line current waveform is minimised by averaging a large number of blocks (frames) of data, the listening time is extended until an acceptable number of frames have been processed. In transient analysis extending the listening will only increase the noise since the transient will usually be of fixed length. To minimise the variance of transient waveforms a number of transients must be recorded and their spectra averaged. [6]

The resolution of a Fourier Transform in the frequency domain is inversely proportional to the record length. In steady state analysis the record length can theoretically be infinite but is practically limited to the memory size of the analyser, nevertheless, it is still possible to resolve frequencies to milli-Hertz. In transient analysis the record length is fixed and in the case of the unloaded test rig will be in the order of 250 ms giving a theoretical frequency resolution of 4 Hz.

It has been shown that sidebands associated with rotor bar faults in steady state conditions are also present during the starting transient, but of course they are changing in frequency with time. [4] At a normal operating slip(s) of say 3% sidebands are situated at + 2sf and - 2sf around the 50 Hz component namely at 47 Hz and 53 Hz. However at the beginning of the starting transient the rotor is stationary and hence the slip is unity. This places these two components at 150 Hz and - 50 Hz respectively. The -50 Hz component is a phase shifted 50 Hz component w.r.t. the fundamental 50 Hz wave. As the rotor accelerates these components change in amplitude and frequency and at half speed (i.e. slip = 0.5) the lower component is at 0 Hz and the upper at 100 Hz.

Performing a spectral analysis on both balanced and unbalanced rotor starting currents gives rise to the spectral amplitudes shown in Fig. 2. It can be clearly seen that a substantial change takes place in the region from 10 to 45 Hz and it is possible to quantify gross rotor imbalances of 50% or more with this data. However this form of spectral analysis produces a summation of all events within the transient period so that no indication is given as to when these various spectral components contributed to the total spectrum.

These transient waveforms have a changing spectrum with time and it is in this respect that they are similar to human speech. It seemed reasonable that methods used to extract the frequency and amplitude content of speech would prove useful in extracting data from a line current transient waveform.

The Phase Vocoder is a technique whereby signals with time-varying spectra can be analysed. It has been in use for many years in Speech Processing and it can be represented as a bank of band-pass filters. [7] As components change their frequency they will pass through different filters and their amplitude can be measured. These bandpass filters must be phase invariant so that all frequencies are delayed by equal amounts. This technique can be implemented in software where it can be readily altered if required. [8] The output from a phase vocoder is referred to as a Spectogram and is a plot of Frequency versus time versus Amplitude. This three dimensional representation allows filtering in two dimensions to be performed so that the amplitude of a frequency component at a particular time may be evaluated.

Figs. 3 to 8 show plots of the output from the first thirteen channels of the phase vocoder. Figs. 3, 4 and 5 are the vocoder outputs from the line current starting transients on the real laboratory machine with progressively increasing imbalance in the resistance of one rotor phase.

At point (a) on all records a ridge can be seen to start. This ridge increases in frequency as time progresses and ends at point b. This is the - 2 sf component as it tracks from half speed (slip = 0.5) to a speed near synchronous speed.

It can clearly be seen that the amplitude of this component is larger with greater rotor imbalance. Meanwhile the + 2sf component is moving from 100 Hz to 50 Hz (points c to d) over this same period and though substantially smaller than the - 2sf component it can also be seen to increase with rotor imbalance.

Figs. 6 to 8 represent the response of the phase vocoder to the computer simulated machine.

Fig. 6 is the output with the simulated, balanced machine and it can be clearly seen that no side-bands exist. Comparison with Fig. 3 leads to the inference that the real machine can only reach a nominally "balanced" condition since these components are still present when no external resistance is added. Such behaviour could probably be anticipated from the wound rotor laboratory machine.

Fig. 7 shows the vocoder output for the simulated machine with the same degree of imbalance as with the real machine in Fig. 5. Again the lower side-band components are clearly visible though the upper sideband components appear not to exist.

The upper sideband components are present but are so small that they are outwith the dynamic range of the display. Furthermore the upper-sideband component is enhanced in the real machine by the third harmonic of slip [2,4]. In this simulation the harmonics of the supply voltage have been neglected and in this particular figure no attempt has been made to represent saturation which usually has a negative half-wave characteristic which will generate odd harmonics.

Fig. 8 shows the simulated result with the same degree of imbalance as with Fig. 7 but in this case saturation of the leakage reactances has been implemented from data obtained from the real machine. It can be seen that the upper side-band components are now of similar magnitude to that of the real machine.

Though impractical to display in this paper, the output of the phase vocoder usually consists of sixty four channels with a channel separation of appoximately 8 Hz. The spectrograms have therefore yielded a mass of

data which is currently being investigated to extract further features indicative of fault conditions.

Computer Simulation

The original simulation was performed using the equivalent two axis D-Q model because of its simpler set of resultant equations. [9] The two phase currents i_D and i_Q of the stator were then transformed back to the three line currents i_a, i_b and i_c.

Saturation was approximated by varying the leakage inductance in both stator and rotor from a saturation characteristic curve derived from tests on the machine. [10] Though simple, this addition to the basic model improved the resulting simulated line current spectra and indicated that saturation was the cause of certain characteristics in the spectra of the real machine. In this way it was possible to change parameters associated with the machine and observe the effect in the simulation and to related this to the real machine.

The limitations of the two axis D-Q model are that a balanced magnetic circuit is necessary and that at least one winding must be completely balanced. [11] In the stationary reference frame imbalance in the rotor phase resistances results in sinusoidally varying resistances in the machine equations. [12]

A three phase model has now been developed as a first step to a more accurate representation of an induction motor. [13] Though more complicated in implementation it will accommodate localised saturation and imbalance in both the stator and rotor windings if required. The feasibility of extending this model to represent individual rotor bars is under investigation.

As with the D-Q model the non-linear differential equations produced must be numerically solved using an iterative technique unless gross assumptions such as constant speed are introduced. A Runge-Kutta iterative technique with error control is used in the simulation software.

Machine parameters may be obtained from standard tests. [14] Harmonics in the supply voltage, saturation, skin effect and thermal effects will alter these values and are to be investigated further. Rotor position and switching angle both effect the transient waveform and their influence must be taken into account.

The question arises as to how much effort should be afforded towards exact simulation (if at all possible) since the remit of this research is to determine faults and to quantify them. Pragmatically it is anticipated that the final results will show general trends indicative of faults within classes of machines rather than exact solutions.

Conclusions

A technique is being developed which will allow the detection and identification of specific faults within 3 phase Induction motors during the starting transient.

Work to date has concentrated on a wound rotor laboratory machine. Spectogram analysis of the transients in this machine has indicated the existence of features and patterns which are representative of specific machine faults. Further work is in progress which will hopefully allow the severity of a specific fault to be quantified in terms of the magnitude of components within the phase vocoder output. Investigations are continuing on Squirrel Cage laboratory and industrial machines with a view to extending the fault recognition algorithms.

The transient process is very complex and it would be extremely difficult to analytically predict the occurrence of specific frequency components and their variation under known fault conditions. The thrust of the work to date has concentrated on the identification of patterns and trends which are representative of specific faults and to eventually establish a knowledge base on which diagnoses can be made. It is in this respect that the computer simulation of the machine has proved most useful.

At present a very detailed and complex analysis is used to detect faults requiring the use of a mainframe computer. It is anticipated that once sufficient test data has been obtained this analysis will be dramatically reduced, allowing a stand alone instrument to be designed.

References

[1] Hargis, C, Gaydon, B G and Kamash, K, Proc. EMDA, Conf., 1982, pp 216-220.

[2] Leonard, R, MPhil Thesis, CNAA 1985.

[3] Cameron, J, Thomson, W T and Dow, A B, Proc. IEE, Vol 133, Pt B, No 3, May 1986.

[4] Williamson, S and Smith, A, Proc IEE, Vol 129, Pt B, No 3, May 1982.

[5] Penman, J, Hadwick, J G, Barker, B, 3rd Int. Conf. Elec. Mach., Brussels, 1978.

[6] Random Data: Analysis and Measurement Procedure, Bendat, J and Piersol, A, 1971, Wiley & Sons.

[7] Flanagan, L and Golden, R M, Bell Sys. Tech. J, Vol. 45, pp 1493-1509, November 1966.

[8] Schafer, R W and Rabiner, L R, IEEE Trans. AU 21, June 1973, pp 165-174.

[9] Slater, R D, PhD Thesis, University of Strathclyde, 1966.

[10] Lipo, T A and Consoli, A, IEEE Trans. on Ind. App., 1981, pp 527-35.

[11] Matrix Analysis of Electrical Machinery, Hancock, N N, MacMillan, 1974.

[12] Krause and Thomas, C, IEEE Trans. PAS 84, November 1965, pp 1038-1053.

[13] Asish De Sarkar, K and Berg, J, IEEE Trans. PAS 89, No 6, July/August 1970, pp 1031-1037.

[14] The Unified theory of Electrical Machines, Jones, Charles V, Butterworth, 1967

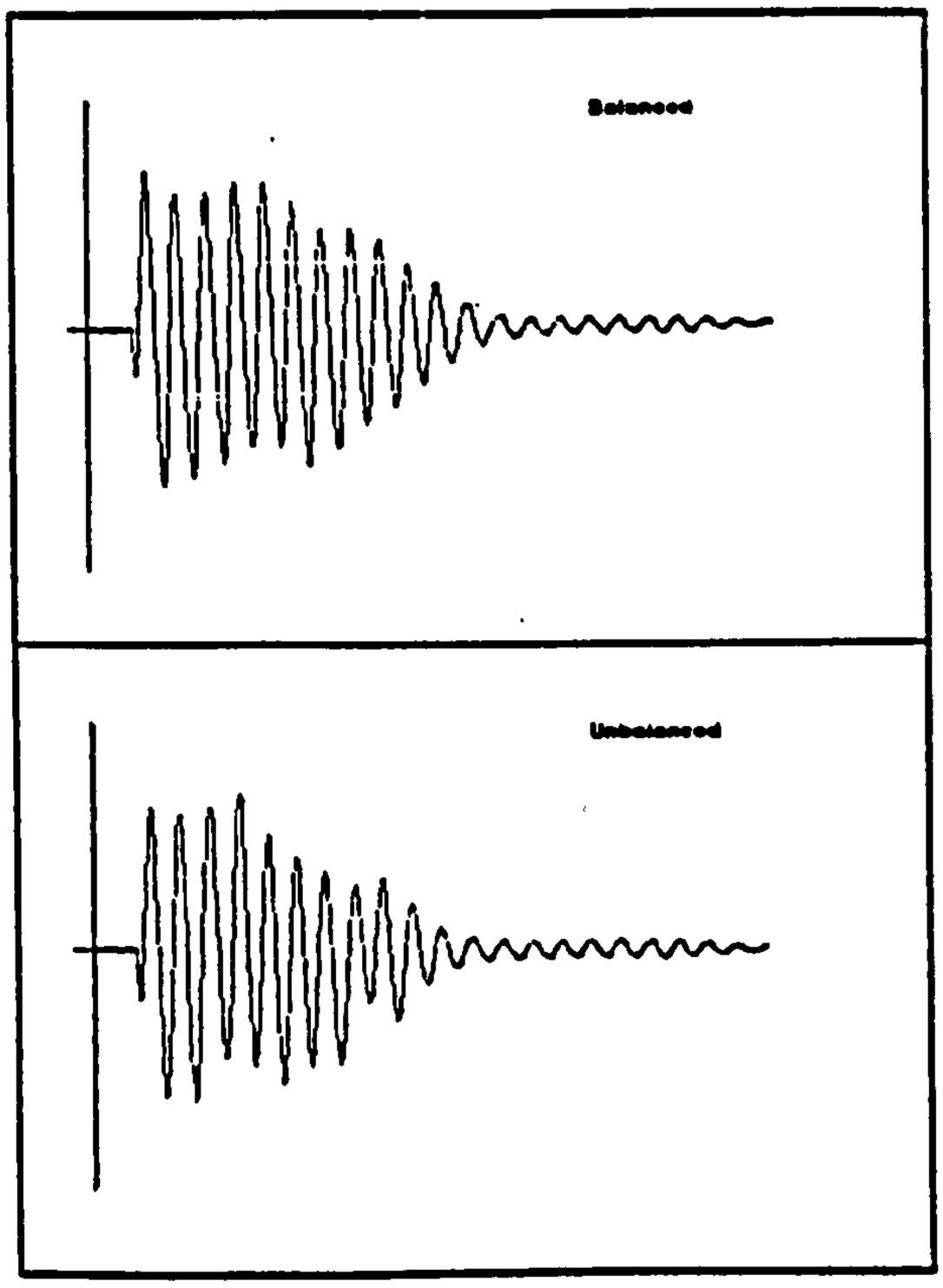

Fig. 1 Typical Line Current Starting Transients

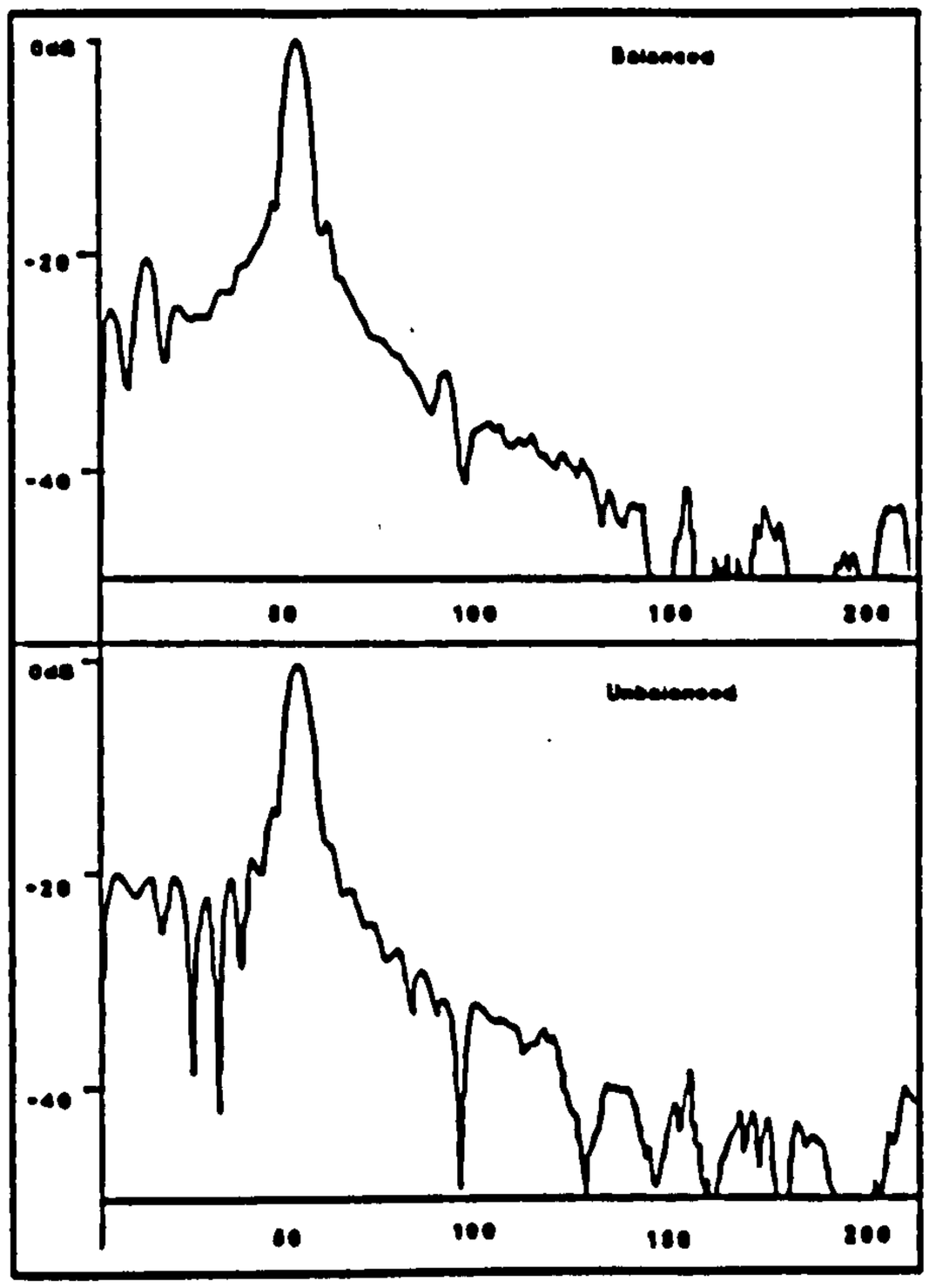

Fig. 2 Spectral Analysis of Transients of Fig. 1

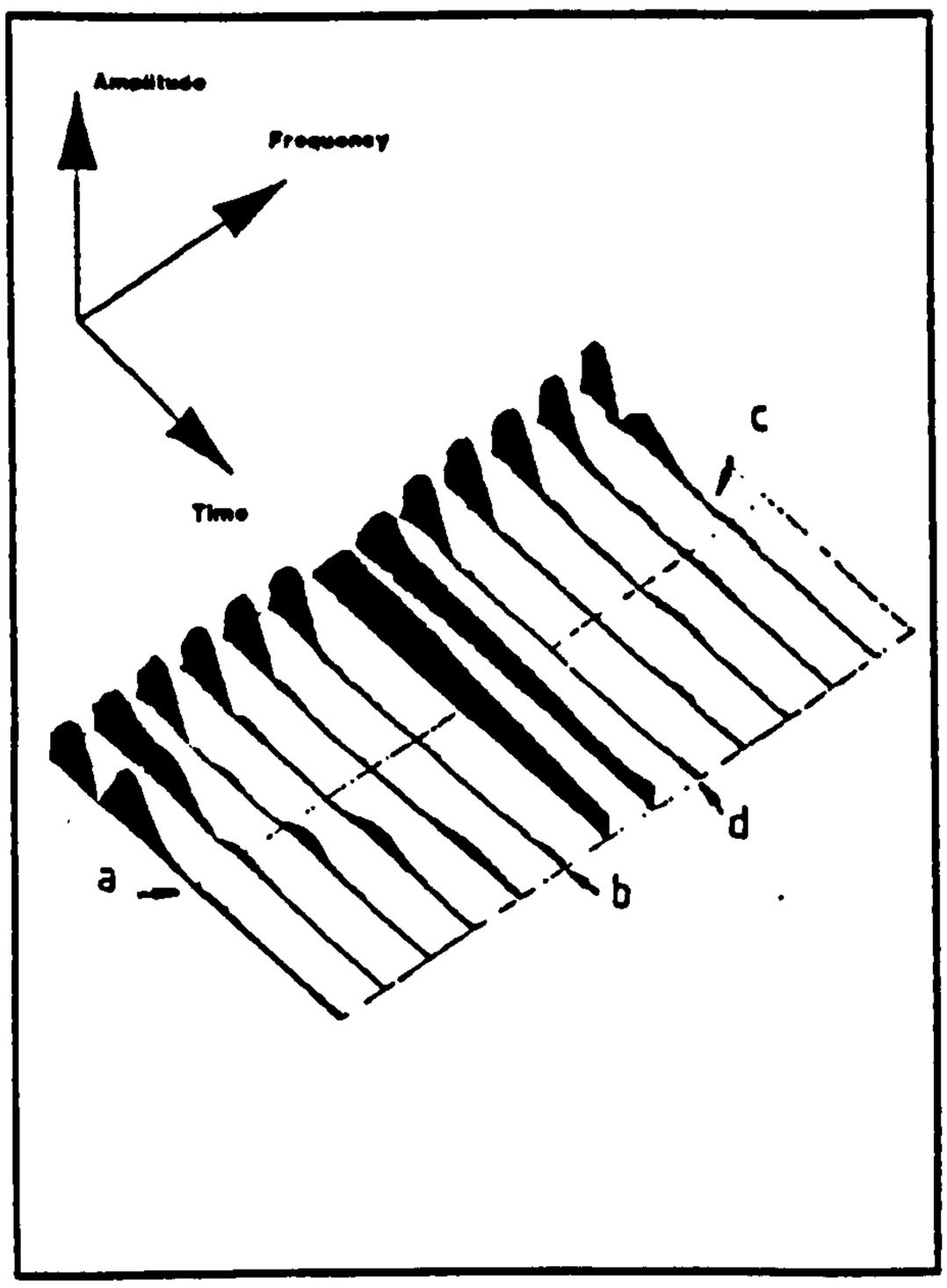

Fig. 3 Spectrogram - Real Machine. Normally Balanced

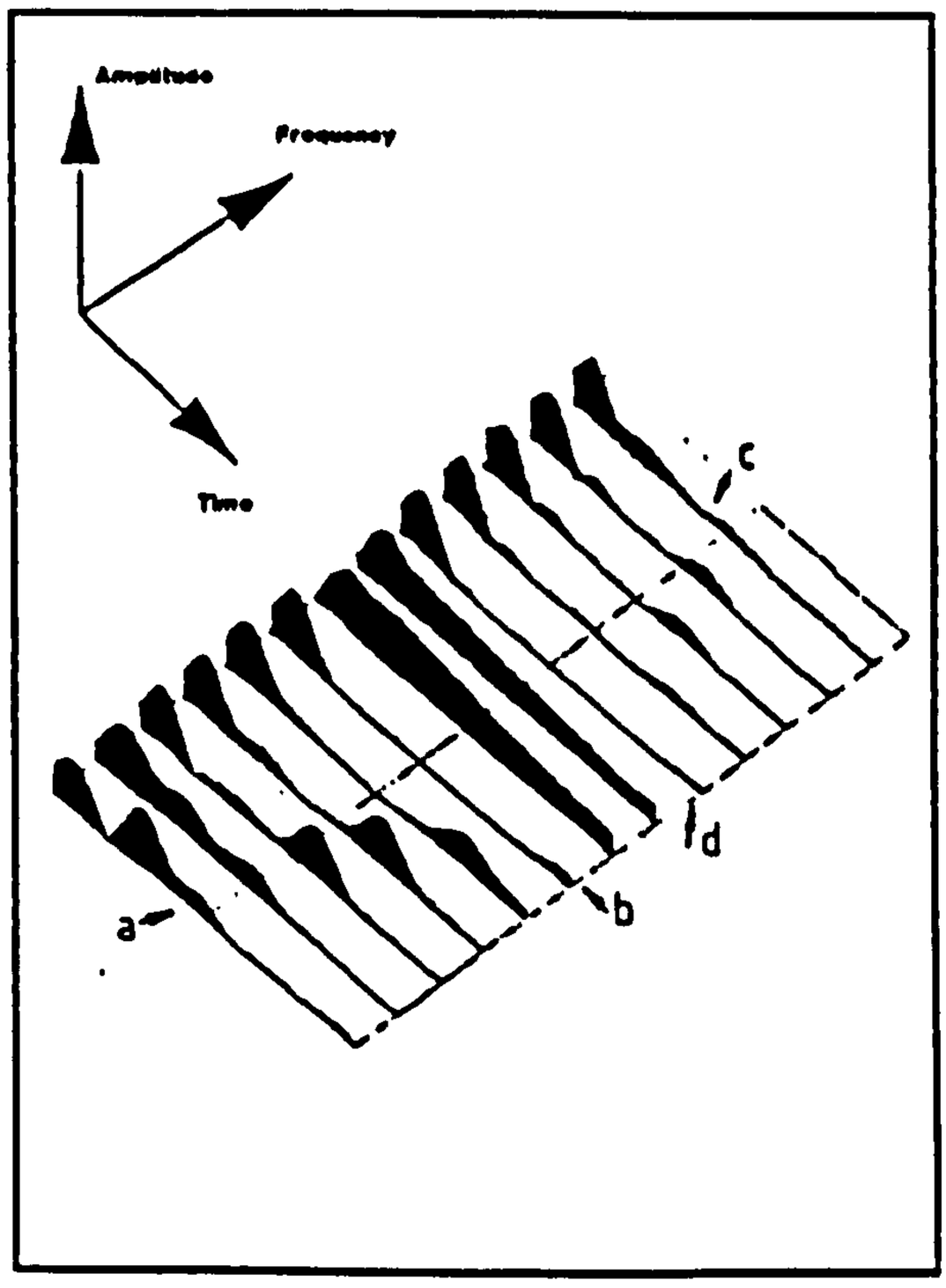

Fig. 4 Spectrogram - Real Machine 20% increase in one rotor phase resistance

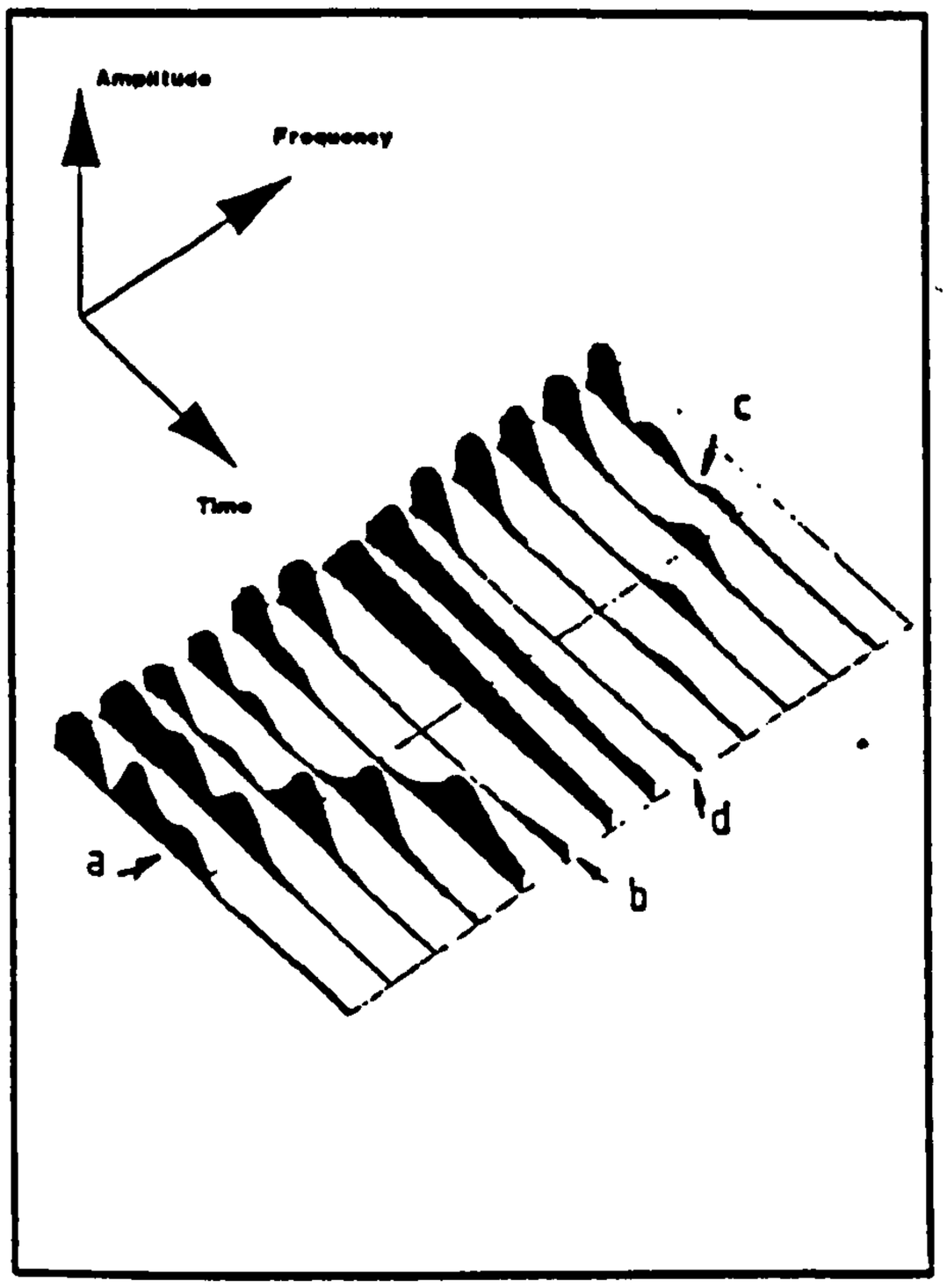

Fig. 5 Spectrogram - Real Machine
58% imbalance

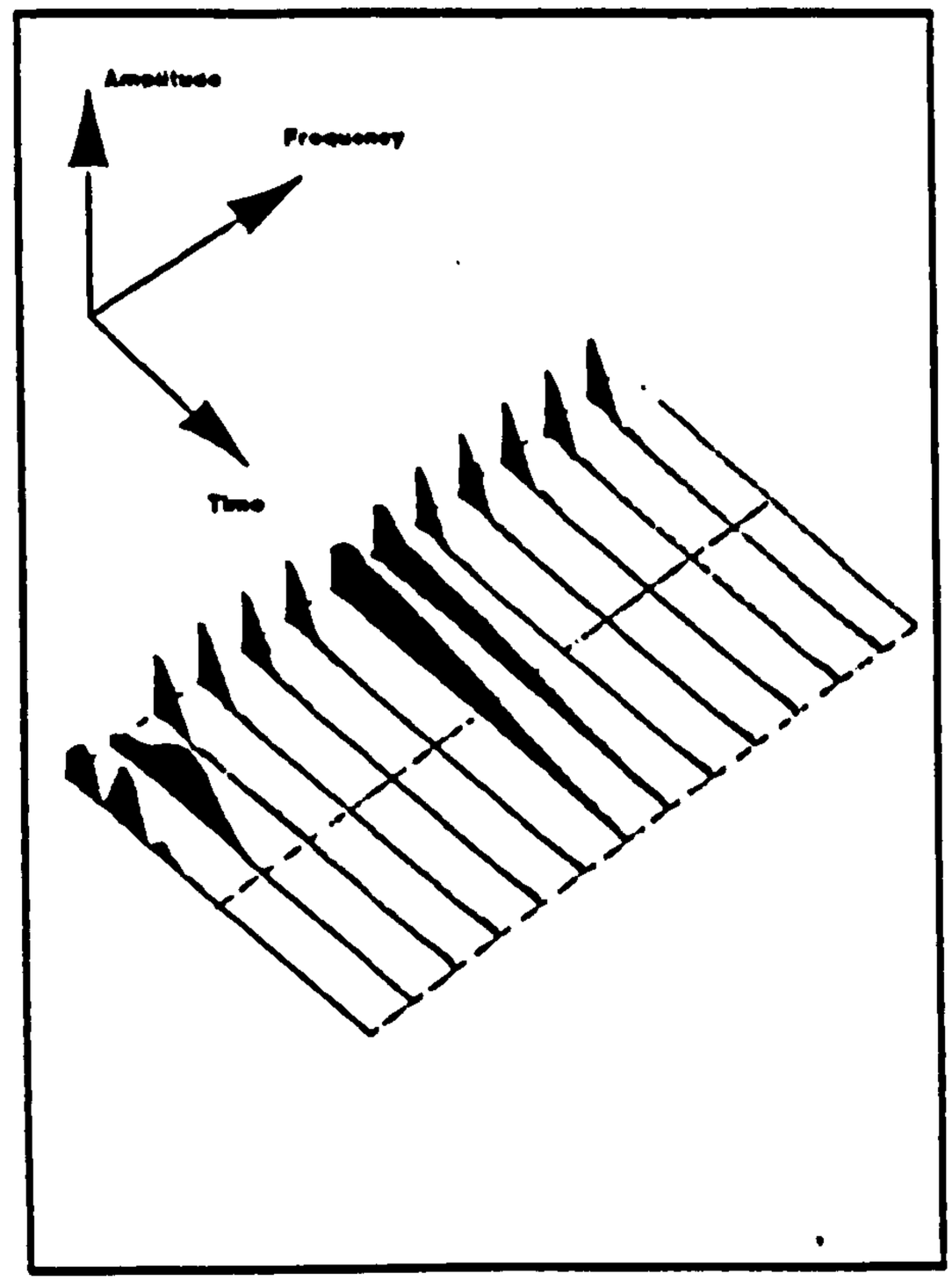

Eg. 6 Spectrogram - Simulated Machine
Balanced

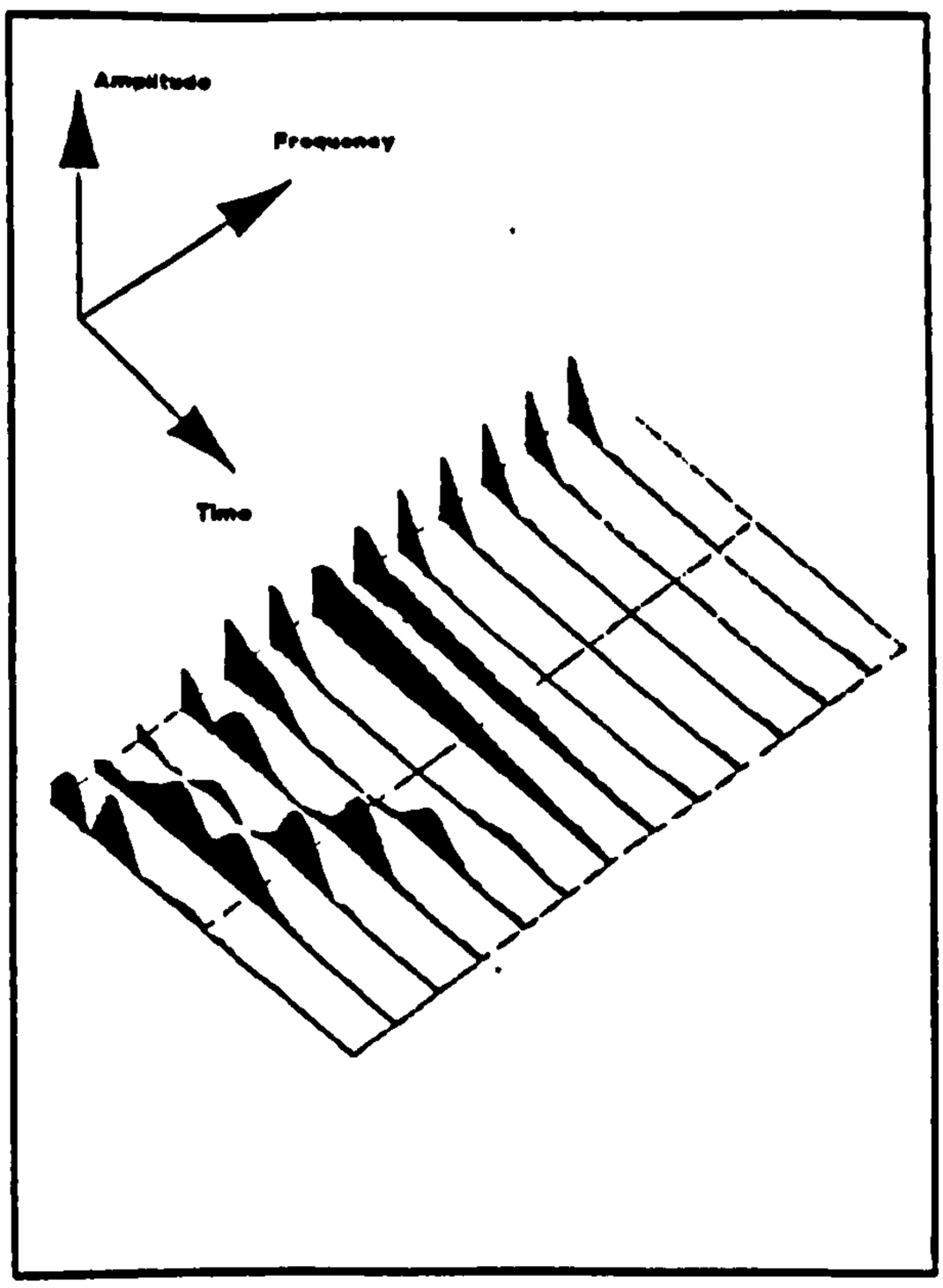

Fig. 7 Spectrogram - Simulated Machine
58% imbalance

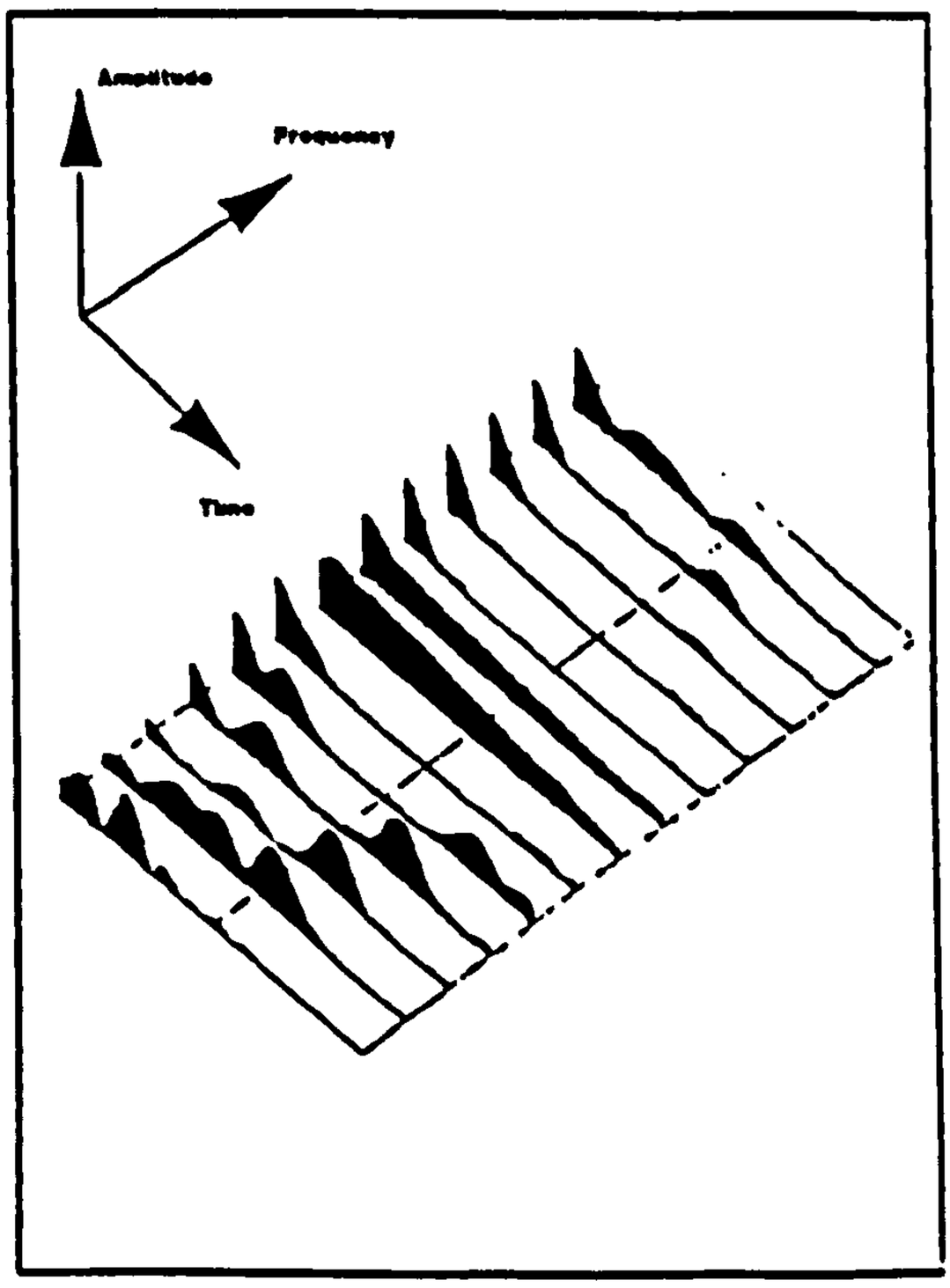

Eg. 8 -Spectrogram - Simulated Machine
58% imbalance and Saturation

THE ANALYSIS OF TRANSIENT CURRENTS IN INDUCTION MOTORS FOR THE PURPOSE OF DETECTING ROTOR FAULTS

S Elder, J F Watson and W T Thomson

Robert Gordon's Institute of Technology, Aberdeen, UK

List of Symbols

f = supply frequency (50 Hz)
s = p.u. slip

INTRODUCTION

The technique described in this paper allows an assessment to be made concerning the condition of the rotor of a 3 phase Induction Motor by performing a single start with the machine on no load.

The vast majority of the work to date concerned with the condition monitoring of I.M's has required that the motor be operating under steady state conditions and that the motor in question be under load before reliable diagnosis can be carried out [1,2,3,4].

There are certain situations where it is either impractical or undesirable to test a machine under loaded conditions. In these circumstances it would be beneficial to have a condition monitoring technique which could be applied to a no load start, and which utilised the most readily available parameter for analysis, ie the line current.

Initial work on this analysis utilized a 11 kW wound rotor machine where large rotor phase imbalances could be implemented by use of an external resistance connected to a rotor phase through the slip rings. The analysis techniques used at this time were broad band and computationally intensive. Components indicative of broken bars were clearly identified [5,6].

This work has now been extended to squirrel cage rotors for faults of varying degrees of severity and the signal processing has been drastically reduced so that the analysis and diagnosis can be easily implemented by a standard personal computer.

The analysis technique is currently being applied to large industrial machines with a view to broadening its application.

It is the results from the work on a laboratory machine having a 51 slot squirrel cage rotor and the application of the signal processing that is presented in this paper.

Frequency component indicative of rotor faults

It has been shown that sidebands associated with rotor bar faults in steady state condition monitoring are also present during the starting period, but of course they are changing in frequency with time [7]. At a normal operating slip of say 3% sidebands are situated at + 2 sf and - 2 sf around the 50 Hz component, namely 47 and 53 Hz. However at the beginning of the starting transient the rotor is stationary and hence the slip is unity.

This places these two sideband components at 150 Hz and - 50 Hz respectively. The - 50 Hz component is a phase shifted 50 Hz component with respect to the fundamental 50 Hz wave or if preferred is a negative sequence 50 Hz component. As the rotor accelerates these sidebands change in amplitude and frequency and at half speed (ie slip = 0.5) the lower sideband (1 - 2 s)f is at 0 Hz and the upper sideband (1 + 2 s)f is at 100 Hz. Evenutually the machine reaches its operating speed and the sidebands occupy their positions as used in the steady state diagnosis. This change in frequency is depicted in Fig. 1 for the cases of slip equal to 0, 0.5 and 0.03 p.u.

As with the steady state analysis of line current waveforms the lower sideband has been found to be a good indicator of the number of broken bars, though it is by no means the only spectral component whose amplitude is influenced by the rotor condition.

Method of analysis

The lower sideband changes in frequency from - 50 Hz through 0 Hz and finally reaches approximately 50 Hz over the run up period. If phase is ignored, then this component can be seen to decrease from 50 Hz to 0 Hz during the standstill to half speed period. From half speed to operating speed the lower sideband increases from 0 Hz to approximately 50 Hz. It has been observed that when a fault is present the amplitude of the lower sideband between half speed and operating speed increases to a significant peak before decaying to its steady state value.

The amplitude of the lower sideband between standstill and half speed is significantly less in amplitude than that in the second half of the transient and this may be partly due to the impedance of the supply to this negative sequence component. Computer simulation of this I.M. with phase imbalance on the rotor also results in a significant difference in lower sideband amplitude between standstill to half speed and half speed to operating speed.

This lower sideband component may be observed by passing the line current waveform, real or simulated, through a bank of bandpass filters. These bandpass filters have their centre frequencies 1 Hz apart throughout the 50 Hz range and as the lower sideband changes in frequency it passes through different filters. These results are displayed for the cases of no broken bars and three broken bars in Figs. 3 and 4 respectively.

These diagrams are a plot of amplitude, frequency and time throughout the starting period. The difference can be clearly seen between the unfaulted and faulted cases. The elongated mound on the right hand side of Fig. 3 is the lower sideband moving from 0 to approximately 50 Hz. It can be seen that the amplitude of this component is not constant, increasing sharply just after half speed, reaching a maximum and then slowly decaying as the motor approaches operating speed.

Though these diagrams were necessary to observe the component of interest it is quite clear that a single bandpass filter chosen to intercept the sideband at its maximum would be all that is required for a diagnosis. The output waveform from a single bandpass filter with centre frequency at 21 Hz and subsequent demodulation is shown in Fig. 2 corresponding to the faulted and unfaulted conditions.

Choice of Bandpass filter centre frequency

It has been shown that during the starting period of an I.M., a transient component is generated whose action is analogous to that of a synchronous machine

[8]. The frequency of this component is the rotor's speed which is increasing and its amplitude is decreasing.

The amplitude of this component is highly dependent on the switching angle and collides with the lower sideband component in the region just after half speed. Since the control over switching angle is to be avoided because of cost and added complexity to the diagnosis technique, it is necessary to select the centre frequency of the bandpass filter well away from this region so that phase switching does not adversely affect the diagnosis.

The lower sideband component decreases in amplitude as it approaches 50 Hz at operating speed and two factors must be considered. Firstly the 50 Hz supply current component is very large compared to the sideband and given that any filter has a finite rejection ratio the closer the chosen centre frequency is to 50 Hz the more 50 Hz noise will be passed through the filter. Secondly, the amplitude of the lower sideband is also decreasing in the later part of the transient and due consideration must be given to observing this component when its amplitude is large. There are therefore two constraints on the choice of the centre frequency:

a) As high a frequency as possible to avoid the phase switching noise.

b) As low a frequency as possible to avoid the supply 50 Hz component and to intercept the lower sideband while its amplitude is still large.

It has been found experimentally for the laboratory motor, that a centre frequency of 21 Hz is the optimal choice. This is expected to be a machine dependent selection though a large change in the centre frequency is not anticipated.

Rotor position at start

Experiments have been carried out to observe the effect of the rotor starting position on the amplitude of the lower sideband component. The rotor was moved to a range of starting positions and the results from the laboratory machine indicate that no significant change in amplitude occurs. It is of interest to note that the time at which the lower sideband passes through the 21 Hz bandpass filter is highly dependent on rotor starting position and the implication from this is that the location of a damaged rotor bar with respect to an arbitary reference point on the shaft, could be extracted. The situation is further complicated however, since the switching angle of the supply also affects the result.

Temperature of machine

Tests were performed on the I.M. with a rotor having three broken bars, firstly at room temperature and then after the machine had been running at full load for an hour and had reached a temperature of 85 degrees celcius. Results for the laboratory machine indicate that no significant change occurs in the sideband amplitude due to temperature.

Eccentricity and broken bars

It was necessary to investigate whether any inherent eccentricity in the rotor could lead to an erroneous diagnosis of the number of broken bars. A level of 60% static eccentricity was introduced into the laboratory machine in which a rotor with one broken bar was installed. No significant change in sideband amplitude was observed.

The possibility of detecting static eccentricity during the starting transient has also been investigated. The components of interest are sidebands of the principal slot harmonics which are not only of very small amplitude, but increase in frequency extremely rapidly making their detection and quantification very difficult. These components are to be investigated more thoroughly in the future.

No rotor with broken bars and dynamic eccentricity was available for testing.

High Resistance Endring

A small section was removed from the endring of an otherwise healthy 51 slot rotor. This did not result in a fully open circuited endring but served to increase the resistance of the endring section between two adjacent bars. The results were similar to that obtained for the case of two broken bars except that the lower sideband's amplitude during its negative sequence phase (s = 1 to 0.5) was substantially larger than in the two broken bars case.

Signal Processing

The signal processing sequence applied to the line current waveform is depicted in Fig. 5.

Firstly the signal is passed through a bandpass filter with a centre frequency of 21 Hz. The resulting waveform contains two packets of energy. The initial peak is due to the connection of the motor to the supply, this abrupt change in line current generates a wide band spectra some of which passes through the bandpass filter. The second peak, if present, indicates rotor imbalance. It is clear that the output of the bandpass filter is an amplitude modulated 21 Hz sinewave and in view of this the standard methods for amplitude recovery may be performed, namely, rectification and low pass filtering.

The processing has been implemented in software since it is more convenient to change any of the parameters, though if required could easily be performed by hardware.

An elementary diagnosis program has been developed on a standard IBM compatible PC, which will correctly indicate the four conditions of 0, 1, 2 and 3 broken bars for the laboratory machine.

The application of this technique to other machines is under way, however, no conclusive results are available as yet.

Result of Tests on a 51 Slot SC Rotor

A series of tests have been carried out for various fault levels on the laboratory machine under the conditions of, steady state full load, transient state full load and transient state no load. In each case the amplitude of the lower sideband was measured and a comparison of the increase in amplitude in this component with the number of broken bars is presented in Fig. 6. It can be seen that both the steady state and full load start give similar results from 0 to 2 broken bars. The case of no load start has a similar shape to that for full load start though the change in side band amplitude is not so large. Nevertheless, the changes in the no load case are still sufficiently large so that no ambiguity can exist between the fault levels.

The results of transients presented in this paper are averages from ten measurements of any one condition. The variance of the results was investigated by firstly performing ten starts with a rotor having 3 broken bars, the average and standard deviation were then calculated. A further twenty starts were then performed and the average and standard deviation for the whole data set of thirty records was then calculated. There was found to be only a very small difference between the averages and standard deviation and on this basis it is not expected that the amplitude of the lower sideband from any single start will fall outwith the range obtained from a set of ten starts.

The standard deviation (s.d) for the no load starts is indicated on Fig. 6 the full load results are omitted for clarity. If the particular cases of 2 and 3 broken bars is examined, it can be seen that the upper limit of the s.d. for the 2 broken bars case and the lower limit of the s.d. for the 3 broken bars case are still clearly separated.

CONCLUSION

A technique has been developed which will allow diagnosis of the condition of the rotor within a laboratory 3 phase I.M. by analysing the line current waveform during a no load starting transient.

The work to date has progressed from large imbalances implemented in a wound rotor machine to broken and high resistance bars in a 51 slot squirrel cage machine. The case of a damaged endring has also been detected by this technique.

The signal processing, originally utilising speech analysis techniques has since been simplified so that it can easily be implemented in either software or hardware.

Future work will concentrate on the application of this analysis technique to large industrial machines with a view of developing a diagnostic instrument.

REFERENCES

1. Hargis, C, Gaydon, B G and Kamash, K, Proc. EMDA, Conf, 1982, pp 216-220

2. Leonard, R, MPhil Thesis, CNAA 1985

3. Cameron, J, Thomson, W T and Dow, A B, Proc. IEE, Vol 133, Pt B, No 3, May 1986

4. Penman, J, Hadwick, J G, Barker, B, 3rd Int. Conf. Elect. Mach., Brussels, 1978

5. Elder, S, Watson, J F and Thomson, W T, 4th Int. Conf. Elect. Mach., London, 1989

6. Elder, S, Watson, J F and Thomson, W T, UPEC Conf, Belfast, 1989

7. Williamson, S and Smith, A, Proc. IEE, Vol 129, Pt B, No 3, May 1982

8. Hughes, F M and Aldred, S, Proc. IEE, Vol 111, No 12, Dec 1964

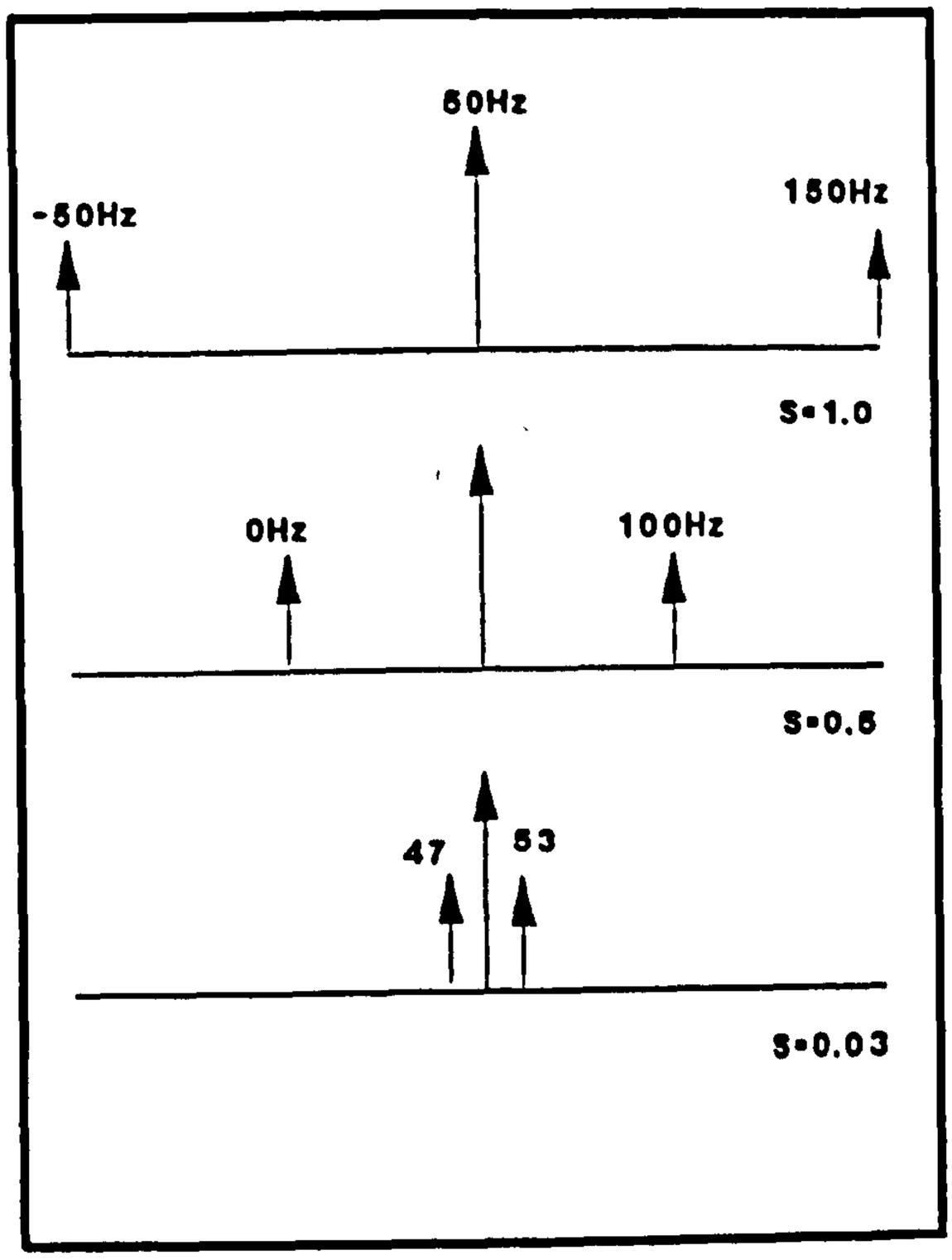

Figure 1 Change in frequency of 2 sf sidebands with slips

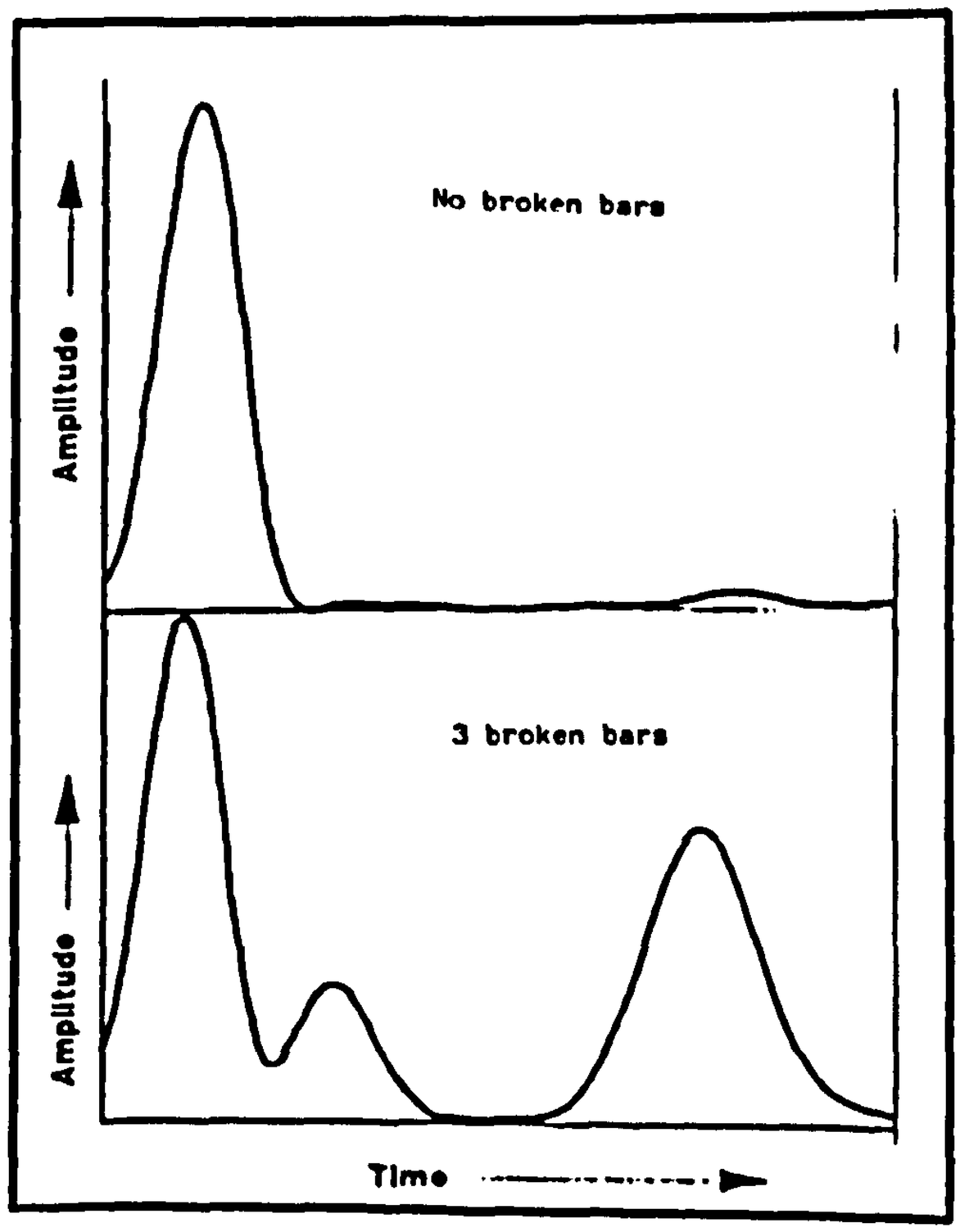

Figure 2 Demodulated output of a 21 Hz B.P. filter

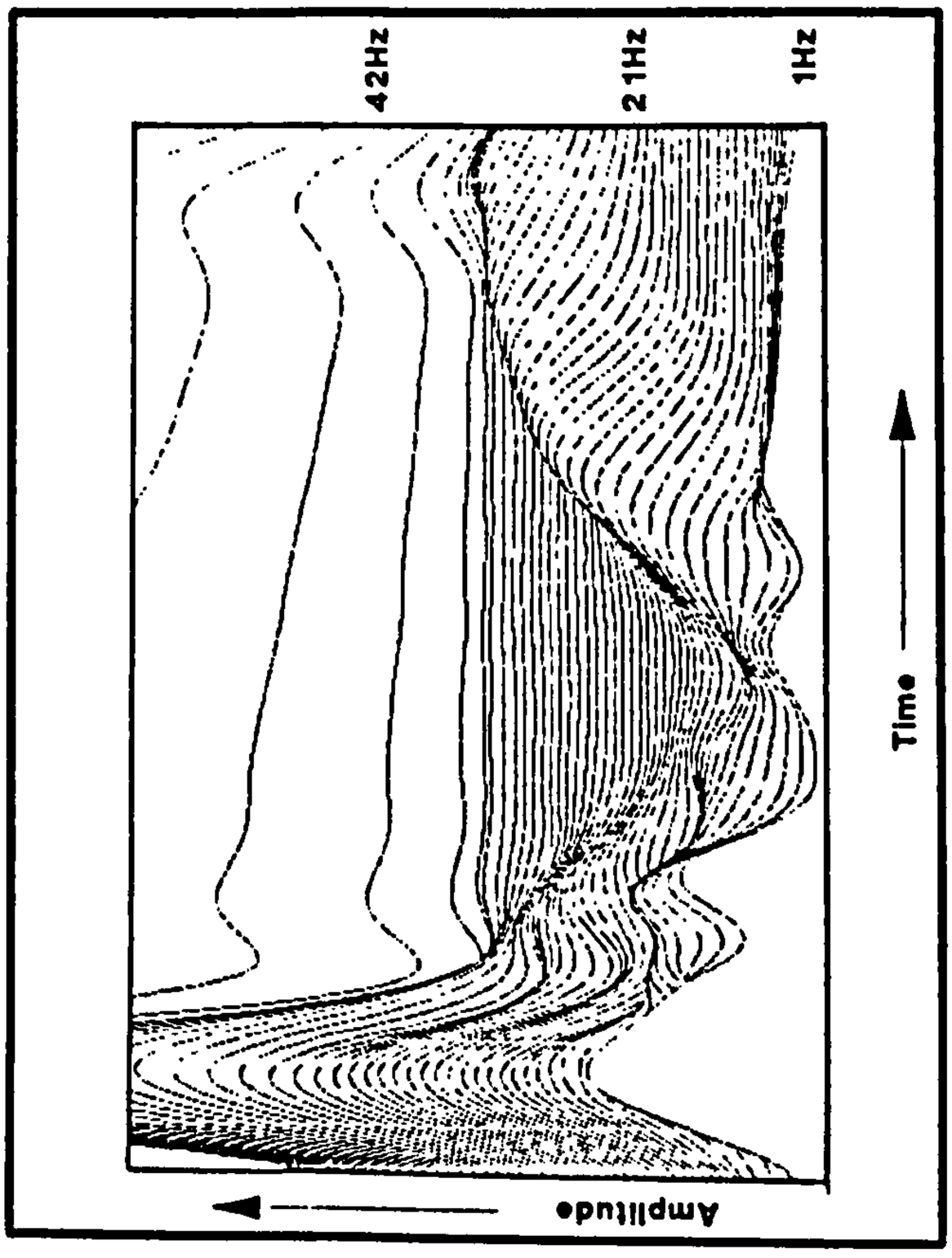

Figure 4 Time-Amplitude-Frequency plot of transient current - 3 broken bars

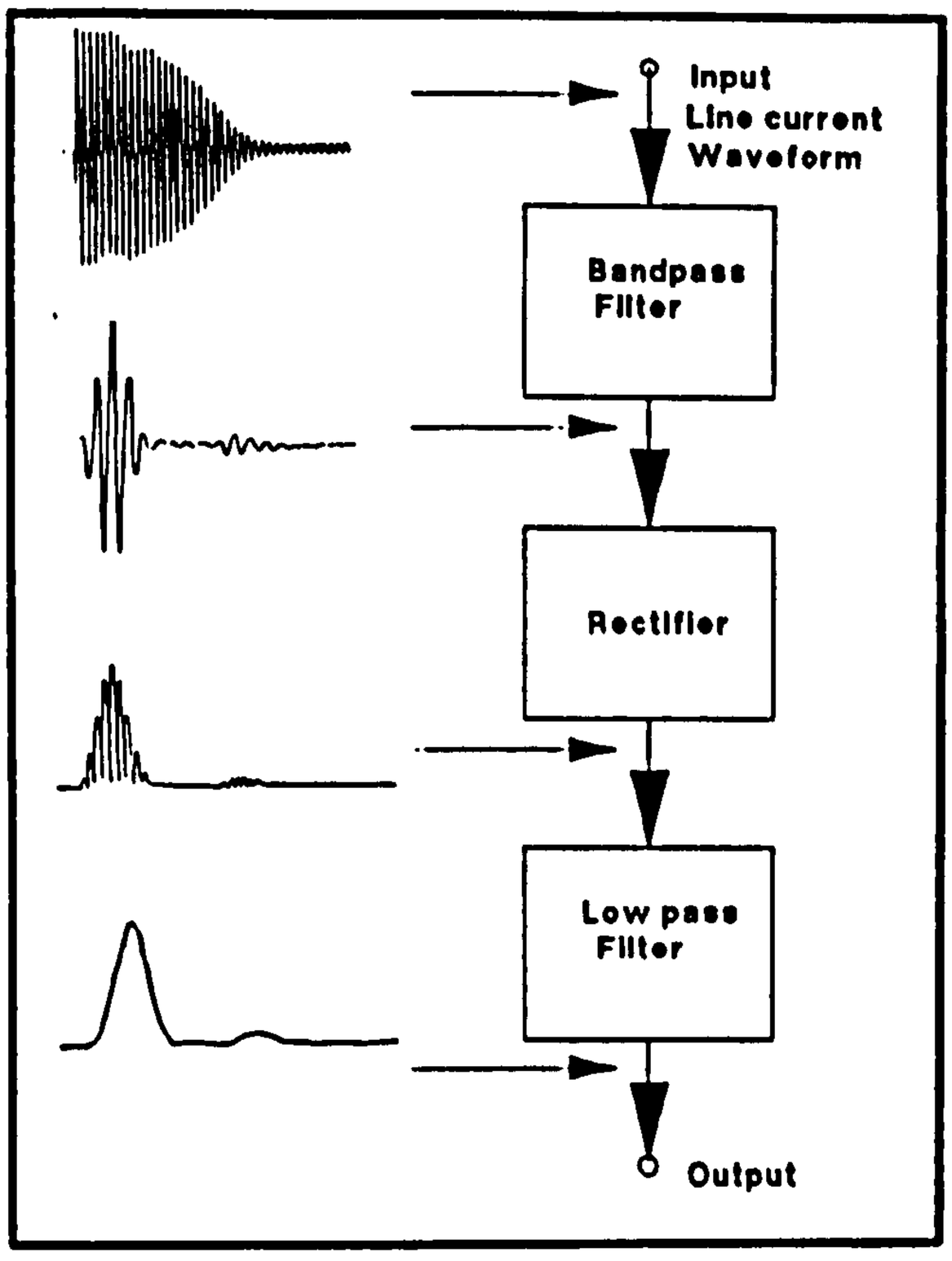

Figure 5 Signal processing sequence

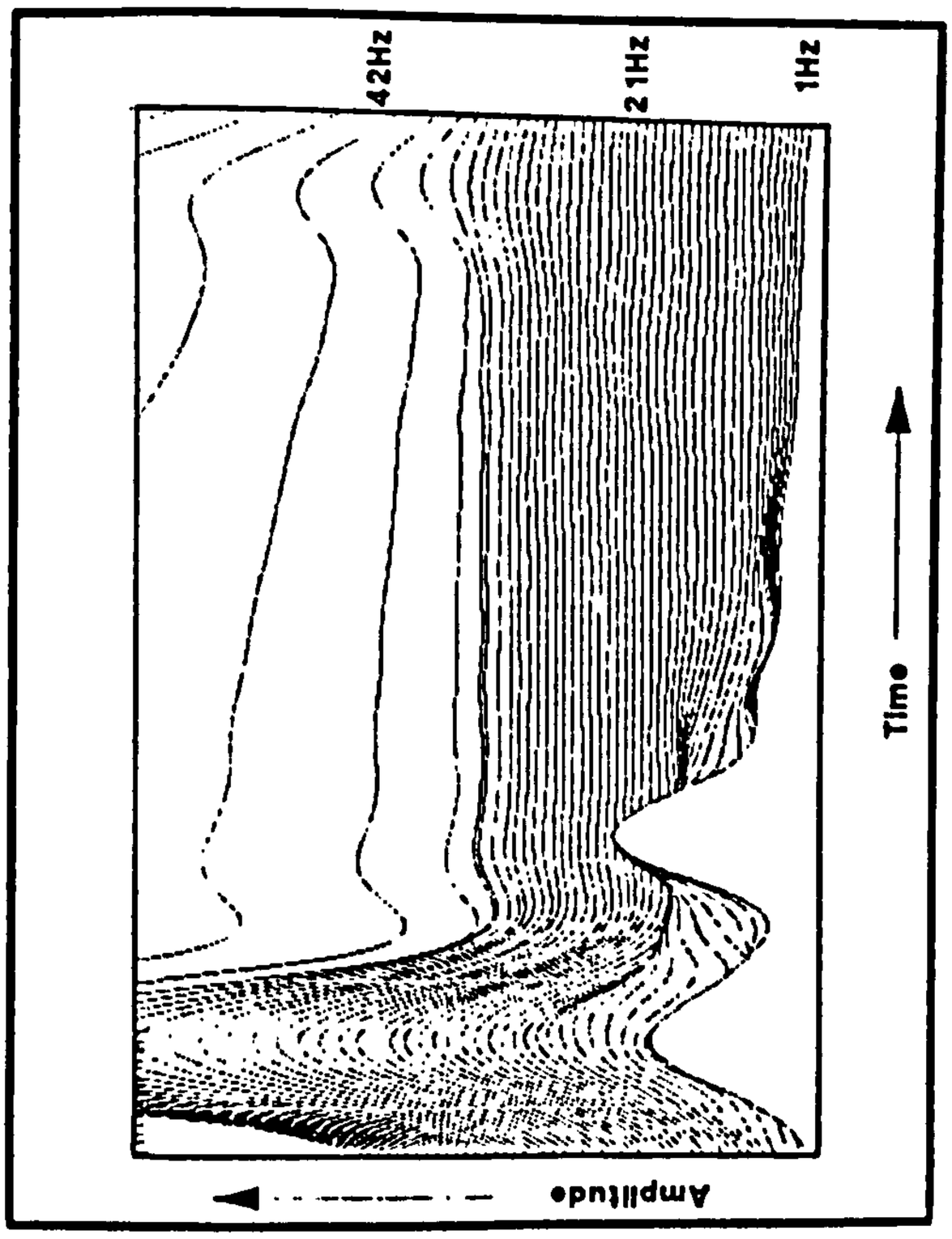

Figure 3 Time-Amplitude-Frequency plot of transient current - no broken bars

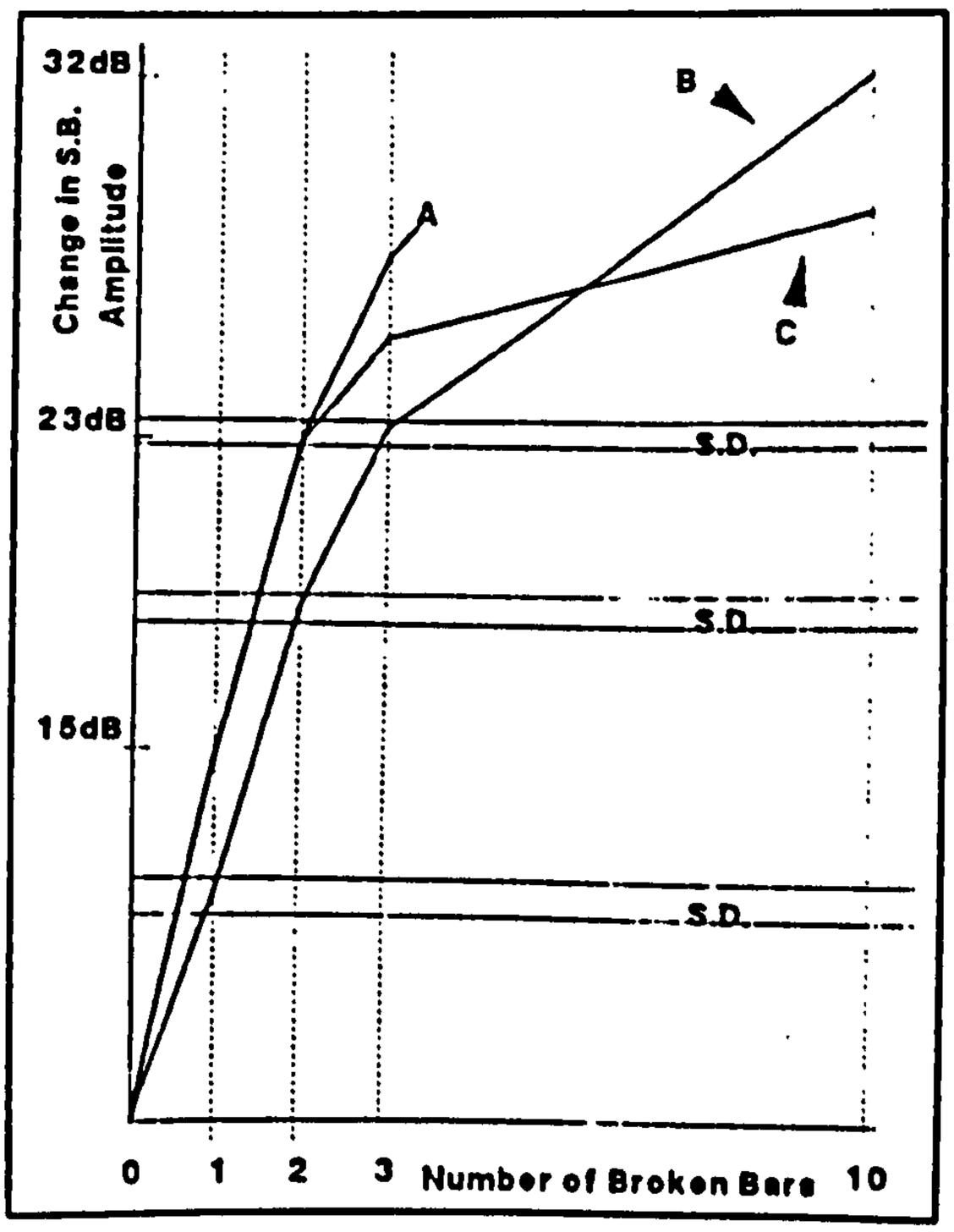

Figure 6 Change in S.B. Amplitude v Broken Bars
a) Transient Full Load b) Transient No-Load
c) Steady State Full Load

[1]Typeset in LaTeXwith PiCTeXmacros, printed on HP Laserjet Series II